Okinawa Institute of Science and Technology Graduate University

Thesis submitted for the degree

Doctor of Philosophy

Banp Regulates DNA Damage response and Chromosome Segregation to Promote Cell-cycle Progression and Cell Survival in Zebrafish Retina

---

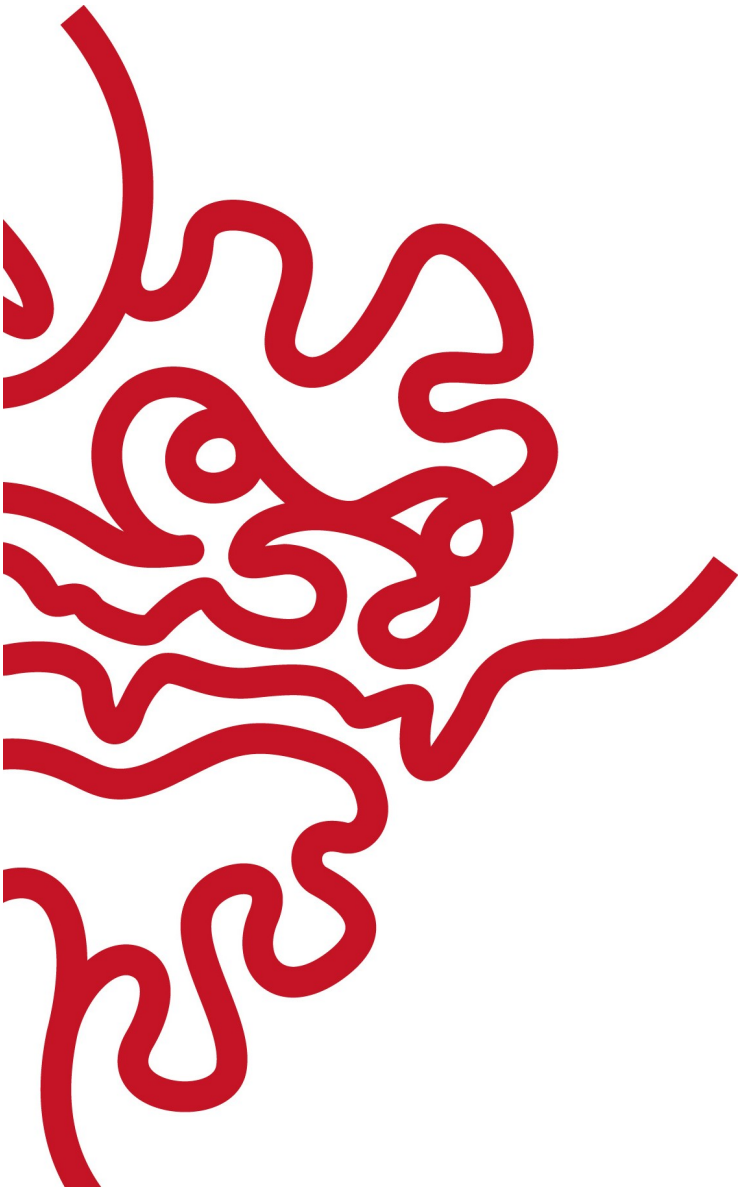

By

Swathy Babu

Supervisor: Ichiro Masai

March 2022

Declaration of Original and Sole Authorship

I, Swathy Babu, declare that this thesis entitled “Banp regulates DNA damage response and chromosome segregation to promote cell-cycle progression and cell survival in zebrafish retina”, and the data presented in it are original and my own work.

I confirm that:

1. No part of this work has previously been submitted for a degree at this or any other university.
2. References to the work of others have been clearly acknowledged. Quotations from the work of others have been clearly indicated and attributed to them.
3. In cases where others have contributed to part of this work, such contribution has been clearly acknowledged and distinguished from my own work.
4. None of this work has been previously published elsewhere.

Date: March 2022

Signature: 

Abstract

Btg3 associated nuclear protein (Banp) was initially identified as a nuclear matrix associated protein and is a tumor suppressor. Recently it was reported that Banp binds to the CGCG element containing motif enriched near the transcription initiation site of CpG island promoters, namely Banp motif, promotes the transcription in a DNA methylation dependent manner, and controls metabolic genes in pluripotent stem and differentiated neuronal cells. However, cellular roles of Banp in embryonic development remains to be elucidated. Here we report a novel role of Banp in cell-cycle progression and cell survival of zebrafish retinal progenitor cells (RPCs). In zebrafish *banp*^{rw337} mutants, retinal progenitor cells showed mitotic cell accumulation and subsequent apoptosis. DNA replication stress and *tp53*-dependent DNA damage response were activated in *banp*^{rw337} mutants. Inhibition of Tp53 significantly rescued apoptosis but not mitotic defect and DNA double strand break accumulation, suggesting that Banp is required for maintaining integrity of DNA during segregation and replication. Furthermore, live imaging of mitosis in *banp* morphant retinas revealed that chromosome segregation was not smoothly processed from prometaphase to anaphase, leading to prolonged M-phase. Bulk RNA-seq analysis show that mRNA expression of two chromosomal segregation regulators, *cenpt* and *ncapg*, were decreased in *banp*^{rw337} mutants. Furthermore, ATAC-seq analysis showed that chromatin near their transcription start site was closed in *banp*^{rw337} mutants and indeed Banp motif was found in this chromatin-closed region, suggesting that Banp directly regulates *cenpt* and *ncapg* transcription via Banp motif to promote chromosome segregation during mitosis. Our findings reveal that Banp is required for cell-cycle progression and cell survival by regulating replicative DNA damage response and mitotic chromosome segregation.

Acknowledgement

First, I would like to express heartfelt gratitude to Prof. Ichiro Masai for allowing me to pursue a Ph.D. under his supervision. I believe the principles I learned from him are applicable throughout my life.

I am grateful to my Ph.D. thesis committee members, Prof. Mitsuhiro Yanagida and Prof. Matthias Wolf, for their continuous support and suggestions throughout my Ph.D. years.
I am extremely grateful to Prof. Peter Gruss and Prof. Tim Hunt for taking out their valuable time for occasional meetings throughout my Ph.D.. Their suggestions, encouragement and kind words have given me immense motivation to pursue my work.

I would like to express my appreciation to all members of the developmental neurobiology unit for their help and co-operation, especially Dr. Mamoru Fujiwara for his assistance with histology and Dr. Tetsuya Harakuni for his assistance with genotyping. I would like to thank four former lab members, Masahiro Yamaguchi, Noriko Tonou-Fujimori, Yukihiro Yoshimura, Eri Oguri for supporting the initial phase of mapping and cloning of *rw337* at Masai lab. Thank you so much to Dr. Nishtha Ranawat and Mai Omar for being the best colleagues anyone could ask for. Their constant encouragement, advice, and discussions aided me in pursuing my Ph.D. both professionally and personally.

I am thankful to the OIST sequencing section (SQC), imaging section, and mass spectrometry facility members for providing all the assistance to perform my experiments in time. I would like to thank Dr. Yuki Takeuchi and Dr. Hemanta Sharama for their valuable help and teaching data analysis (RNA -seq and ATAC-seq).

Finally, I would like to express my gratitude to my family and friends. I am fortunate to have Latha Babu, Sandra Babu, NK Babu and Jibin Sadasivan, as supporting pillars of my life. They provided me the strength to overcome the odds and a pandemic to complete my Ph.D. I would like to express my heartfelt gratitude to my friends Manana Kutsia, Jigyasa Arora, Afshan Jamshaid, Soumen Jana, Dr. Ivan Mbogo, Leya Lopez and Anju Ajanthakumar for being there for me as a family.

Abbreviations

AO	Acridine Orange
ATAC-seq	Assay for Transposase-Accessible Chromatin with high-throughput sequencing
atm	Ataxia telangiectasia mutated
atr	Ataxia telangiectasia mutated and rad3 related
banp	BTG3 Associated Nuclear Protein
BAX	Bcl-2 Associated X-protein
BrdU	Bromodeoxyuridine / 5-bromo-2'-deoxyuridine
CNS	central nervous system
CRISPER	Clustered Regularly Interspaced Short Palindromic Repeats
dpf	days post fertilization
DSB	double-strand DNA break
EGFP	enhanced green fluorescent protein
ENU	N-Nitroso-N-methylurea
fgf	fibroblast growth factors
GS	glutamine synthetase
HDAC	histone deacetylase
Hh	Hedgehog
hpf	hours post fertilization
INL	Inner nuclear layer
IPL	Inner plexiform layer
MO	morpholino
OPL	outer plexiform layer
PBS	phosphate buffer saline
pH3	phospho-histone H3 (serine- 10)
PKM	pyruvate kinase muscle
PR	photoreceptor
PUMA	p53 upregulated modulator of apoptosis
RGL	retinal ganglion cell layer
RNA-seq	RNA sequencing
RPCs	retinal progenitor cells
smar1	Scaffold/Matrix-Associated Region 1- binding protein
TSS	transcription start site
TUNEL	Terminal deoxynucleotide transferase-mediated dUTP nick-end labeling
WT	Wild type

This thesis is dedicated to NK Babu (father), Latha Babu (mother) and Sandra Babu (sister)
I could not have done this without you!

Table of contents

List of figures

List of tables

CHAPTER 1

Literature review

1.1 General Introduction

The cell cycle process in which one cell divides into two is fundamental and essential for the development, growth, and survival of an organism. The molecular mechanisms determining cell division have gained significant attention since 1983, especially from the classic works of Professor Tim Hunt where he discovered patterns of oscillating proteins called cyclins in sea urchins post-fertilization (Evans, Rosenthal et al. 1983). This work and the discovery of additional cell cycle regulatory factors led to the Nobel prize in 2001. Since then, till to this date, the efforts to understand this fundamental process remain constant. As a result, we know that the cell cycle is controlled by carefully orchestrating multiple proteins and regulatory factors. Every day, studies revealing new regulatory factors or mechanisms are being added to this regulatory network.

1.1.1 Cell cycle: A brief introduction

The general process of cell division is defined to have four phases as G1, S, G2, and M (Figure 1-1). G1 is the preparatory phase for division. S-phase is when replication of genetic material, DNA occurs. In the G2-phase, a cell prepares for the following M-phase. M-phase or mitosis is when the segregation and separation of chromosomes into two daughter cells occurs. It is needless to say that error-free and sequential progress of the cell cycle is necessary. One of the biggest challenges for a cell to attain effortless cell division is intrinsic or extrinsic lesions in DNA during division. To safeguard its daughter cells from carrying such DNA damage, a checkpoint/surveillance mechanism exists in each phase of the cell cycle (Figure 1-1).

During cell division, DNA lesions which occur as a result of DNA replication, cellular metabolism, and environmental stress, continually challenge the integrity of the genome (Thompson and Schild 2002). Enhanced cell proliferation increases the rate of DNA replication errors and subsequently induces DNA strand breaks. In a developing organism, loss of function of factors involved in the process of DNA replication, Chromatin segregation leads to DNA double-strand or single-strand breaks. These DNA breaks, in turn, activate DNA damage repair mechanisms (Magdalou, Lopez et al. 2014, Jegadesan and Branzei 2021). Cell cycle checkpoints make sure to repair the defects or damage occurring during each phase. Such a surveillance mechanism can detect severe defects during the cell cycle and promote cell death by activating apoptosis. This activation of cell death is to avoid accumulation or propagation of further lethal damage. The regulation of this surveillance mechanism involves many factors. *tp53* is one of the most well-known of them. *tp53* is involved in several different regulatory functions.

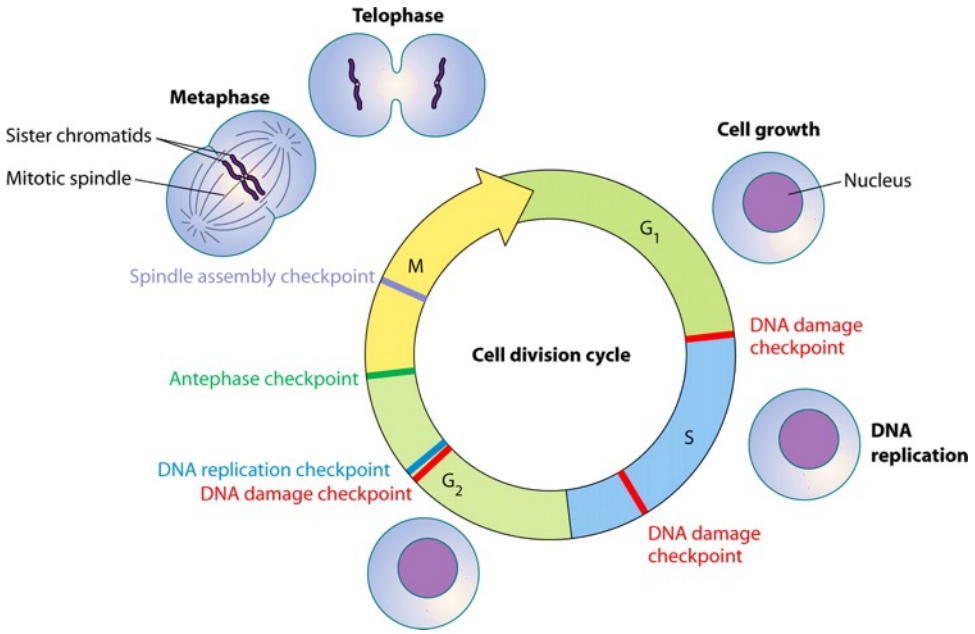

Figure 1-1: A schematic showing the cell cycle and its checkpoint mechanisms.
During cell division cell proceeds from the G1-S-G2-M phase, respectively. Rectangular boxes represent checkpoints in each cell cycle phase. Figure adapted from (Chin and Yeong 2010)

1.1.2 *tp53* has dual functions to induce cell cycle arrest and apoptosis during DNA damage

Tumor suppressor protein Tp53 acts as a significant node in a complex signaling network for DNA damage response, which activates cell-cycle arrest, mediates DNA repair and induces apoptosis in response to various DNA lesions and cellular stress (Figure 1-2). Under normal conditions, Tp53 is generally unstable, and its protein level is low due to rapid degradation by a ubiquitin ligase, namely mouse double minute 2 homolog (*mdm2*) (Kubbutat, Jones et al. 1997). However, when cells suffer from double-stranded DNA breaks or DNA replication stress, PI3-kinase family proteins, ataxia telangiectasia mutated (*atm*), and ataxia telangiectasia mutated and rad3 related (*atr*) are activated, respectively (Shiloh 2003). *atr* and *atm* subsequently activate checkpoint kinase 1 (*chk1*) and checkpoint kinase 2 (*chk2*), respectively. Chk1 inhibits cdc25 phosphatase, which generally promotes *cyclinB1/cdk1*-mediated M phase transition. Chk1 also activates *wee1*, which generally inhibits *cyclinB1/cdk1*-mediated M phase transition (O'Connell, Raleigh et al. 1997) (Figure 1-2, green pathway). Therefore, *chk1* inhibits M phase entry and prevents mitosis-mediated chromosomal catastrophe during DNA repair. On the other hand, *chk2* cooperates with *atm* to phosphorylate N-terminal serine residues (Ser-15 and Ser-20) of *tp53*. This phosphorylated *tp53* loses affinity of *mdm2* and is thereby released from *mdm2*-mediated degradation and becomes stabilized (Blackford and Jackson 2017).

tp53 is a transcription factor, which activates many downstream targets linked to cell-cycle arrest and apoptosis. In the initial and mild DNA damage condition, Tp53 binds to its promoter and promotes transcription of its N-terminal truncated isoform, Δ*113p53*, which preferentially activates transcription of cell-cycle arrest genes cdk inhibitor *p21(cdkn1a)* (Chen, Ng et al. 2009). *p21*(*cdkn1a*) interacts with *cyclinD/cdk4/6*, which arrests G1-S phase transition and facilitates DNA repair and cell survival (Figure 1-2, red pathway). On the other hand, in the

case of chronic and severe DNA damage, full length Tp53 protein are stabilized and preferentially promotes transcription of pro-apoptotic genes including BH3 only proteins such as *puma* and *noxa*, tumor suppressor *pten*, and *bax*, and then induces cell death. In general, activating BH3 only proteins is crucial for induction of apoptosis; BH3 only proteins interact with anti-apoptotic Bcl2 proteins, such as Bcl2 and Bcl-XL, and release Bax from Bcl2-mediated inhibition. As a result, Bax proteins are activated and translocated into the mitochondria outer membrane, forming an oligomeric complex, which functions as a large channel. From this Bax channel, cytochrome C (also called Apaf2) is released and forms the protein complex with Apaf1 and Caspase9 called apoptosome. Apoptosome subsequently activates effector caspases, leading to apoptosis (Shen and White 2001) (Figure 1-2). Thus, *tp53* has dual functions to promote either cell survival or apoptosis. It is imperative to understand how two opposite *tp53* functions are differentially regulated during DNA damage response.

Previous biochemical studies on *tp53* have identified posttranslational chemical modifications on *tp53*, which promote *tp53* transcriptional activity. Most of them activate transcription of *tp53* target genes linked to both cell-cycle arrest and apoptosis. However, there is one exciting modification. Acetylation of lysine 120 (K120) in the *tp53* DNA binding domain rapidly occurs after DNA damage, and this acetylated-K120 *tp53* isoform is preferentially accumulated at pro-apoptotic target genes. Loss of its acetylation selectively inhibits the transcription of pro-apoptotic genes such as *bax* and *puma* without affecting cell-cycle arrest target transcription, suggesting that acetylated-K120 *tp53* isoform preferentially induces apoptosis (Tang, Luo et al. 2006, Sykes, Stanek et al. 2009). However, it remains to be elucidated how such modification is regulated.

Thus, it is essential to elucidate the repertoire of proteins involved in biasing the balance between cell-cycle arrest and apoptosis. The exact mechanism of how a cell decides whether to undergo apoptosis or arrest under different circumstances is unclear. *tp53* is one of the major players in DNA damage response. Several regulatory factors are being added to this network. I propose that one of the new components that can potentially contribute to regulate these networks is a btg3-associated nuclear protein (*banp*).

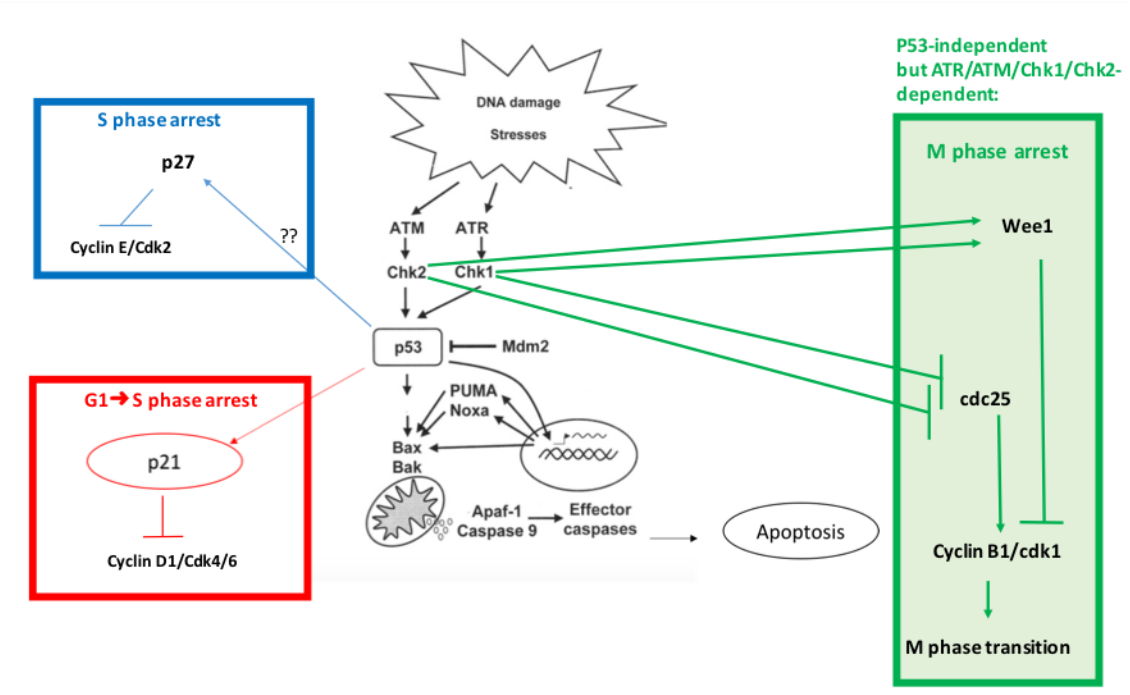

Figure 1-2 : Mechanism of cell cycle arrest and apoptosis during DNA damage.
In response to DNA damage or stress, *atm*/*atr* checkpoint regulators are activated and phosphorylate *tp53* via *chk2*, leading to *tp53* stabilization. Then, *tp53* activates *p21(cdkn1a),* which subsequently induces cell-cycle arrest through the inhibition of *cyclinD1/cdk4/6* (red pathway) or promotes cell death through the activation of transcription of cell death-related genes such as *bax*, *puma* (*bbc3*), and *noxa*. Bcl-2 family proteins, *bak* and *bax*, form high order oligomer on mitochondria outer membrane and alter its membrane permeability, releasing cell death-inducing factors called the Apaf-I-caspase 9 apoptosome. Apoptosome activates effector caspases, leading to apoptosis (black pathway). In addition, *tp53* may activate the transcription of another cell-cycle arrest gene, *p27*. *p27* is a cyclin-dependent kinase-inhibitor and binds *cyclinE/Cdk2* complexes to inhibit cell-cycle progression in S-phase. *mdm2* is an E3-ubiquitin ligase, which degrades *tp53*, and DNA damage/cellular stress inhibits *mdm2* to facilitate *tp53* stabilization (Benchimol 2001, Schuler and Green 2001, Shen and White 2001). DNA damage also imparts *tp53*-independent cell-cycle arrest (green pathway). *chk1/2* activates *wee1*, an inhibitor of M phase cyclin, *cyclinB1/cdk1,* whereas *chk1*/2 inhibits *cdc25*, promoting *cyclinB1/cdk1* and M-phase transition. So, activation of the *atr*/*atm*/*chk1* pathway causes cell-cycle arrest at M phase (Furnari, Rhind et al. 1997, Benchimol 2001, Schuler and Green 2001, Shen and White 2001) (Figure adopted and modified from (Schuler and Green 2001)).

1.1.3 BTG3-associated nuclear protein (Banp)

Btg3-associated nuclear protein (Banp) or scaffold/matrix attachment region binding protein (SMAR1) was identified in 2000 as an alternatively spliced gene product that binds to the matrix-associated region (MAR) of the β-locus in murine T cell receptors (Birot, Duret et al. 2000, Chattopadhyay, Kaul et al. 2000). MARs are closely associated with transcriptional promoters and enhancers in several gene loci as cis-regulatory elements (Scheuermann and Garrard 1999). Chromosomal DNA is thought to be organized topologically through association with periodic loop domains, called MARs, to facilitate DNA replication, transcription, repair, and recombination (Blasquez, Sperry et al. 1989, Hart and Laemmli 1998). The human homolog of Banp is identified as a potential B-Cell Translocation Gene Anti-Proliferation Factor 3 (btg3)-binding partner; hence, it is known as btg3-associated nuclear protein (Banp) (Matsuda, Rouault et al. 2001). Btg3 is a member of the TOB/BTG family, including other members like *btg1*, *btg2*, *tob*, and *tob2*, all of which repress the cell cycle (Matsuda, Rouault et al. 2001). *banp* has 91 orthologs and is conserved across vertebrate species (Birot, Duret et al. 2000). *banp* gene maps to chromosomes 8, 16, and 25 of mice, humans, and zebrafish, respectively. In humans, the gene *banp* is located on chromosome 16q24. The loss of heterozygosity in this region in various tumors made this gene interesting because of its potential tumor suppressor function (Tsuda, Callen et al. 1994, Wang, Gleich et al. 1999). Indeed, *banp* has been characterized as a tumor suppressor in multiple studies (Kaul, Mukherjee et al. 2003). It was predicted to have functions similar to transcription factors due to its BEN domain and similarity in amino acid composition to transcription factors (Birot, Duret et al. 2000). By 2021, It was confirmed as a fundamental and essential transcription factor (Grand, Burger et al. 2021). However, the physiological and developmental role of the Banp remains elusive.

1.1.4 Structure and functional domains of Banp

Human and mouse *banp* genes have 27 and 16 splice variants, respectively; however, the zebrafish *banp* gene has a single splice variant that encodes a 508-amino acid protein containing 13 exons. In mice, *banp* mRNA is expressed in the heart, thymus, spleen, bladder, and muscle, along with ubiquitous expression during embryonic development (Birot, Duret et al. 2000). The protein is localized in the nucleus, exhibiting its matrix-associated region-binding (MARBP) ability (Birot, Duret et al. 2000). Banp is denoted as SMAR1 in most of the studies published. Banp has protein as well as DNA-binding domains (Figure 1-3). Mammalian Banp consists of a C-terminal DNA-binding domain (350-548 aa) that binds MAR sequences near promoters (Kaul-Ghanekar, Jalota et al. 2004). A BEN domain (218-291 aa) acts as a transcription factor (Rampalli, Pavithra et al. 2005). A nuclear localization signal (245-288 aa) and an arginine-serine-rich (RS) domain (288-350 aa) enables protein interactions. Banp also shares a homologous region (330-456 aa) with other matrix-associated region-binding proteins, such as BRIGHT, CUX, and SATB1, at their MAR binding domains (Malonia, Sinha et al. 2011). The mouse ortholog of Banp shows 95 % and 68 % similarity with human and zebrafish proteins, respectively. All three have a conserved BEN domain.

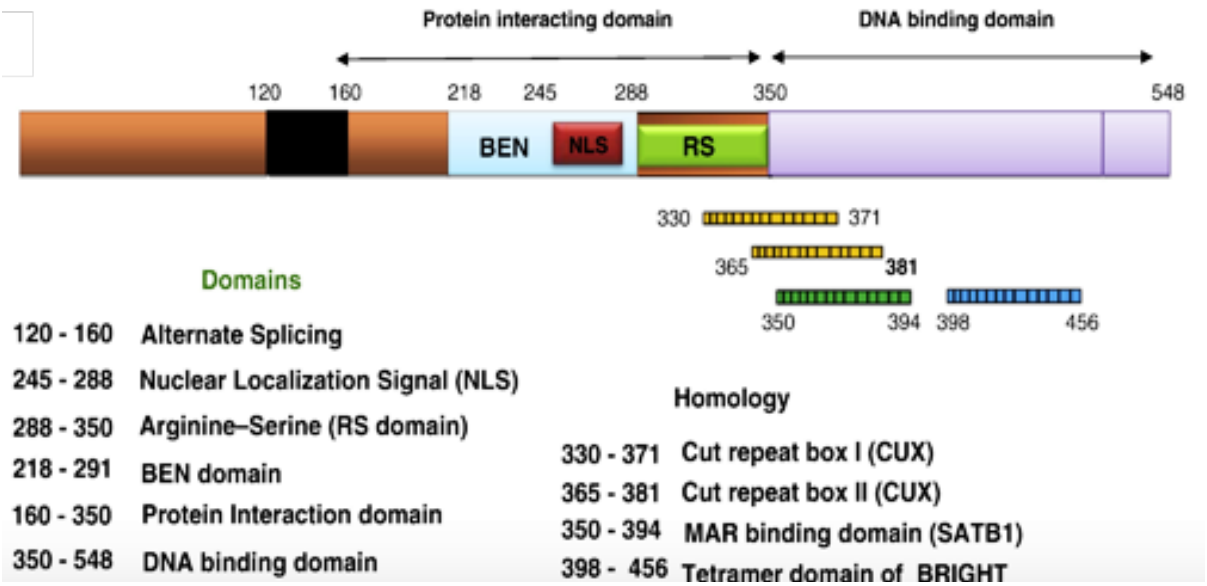

Figure 1-3: Structural and functional domains of Banp (SMAR1)
Figure adapted from (Malonia, Sinha et al. 2011)

1.1.5 *banp* interaction and regulation with the help of *tp53*

Banp has a protein and DNA binding domain that enable interaction with many proteins, including Tp53. Tp53 is considered the "guardian of the genome" (Ahnen 1996) and is involved in a broad range of cellular mechanisms. *tp53* promotes DNA repair, maintains cell-cycle progression, induces apoptosis, and regulates senescence and angiogenesis in a context-dependent manner. While *tp53* remains latent during normal conditions, its activity is very carefully orchestrated by transcriptional, translational, proteasomal, and covalent modifications in response to stress or DNA damage (Oren 1999, Riley, Sontag et al. 2008, Meek 2009). Although the precise mechanism of *tp53* activation is not entirely understood, Banp has been identified as one of the *tp53* regulators (Kaul, Mukherjee et al. 2003). Banp directly interacts with the N-terminal 27 amino acids of *tp53* (Pavithra, Mukherjee et al. 2009) through its arginine-serine rich [RS] domain and stabilizes *tp53* by promoting phosphorylation of *tp53* Ser-15 (Kaul, Mukherjee et al. 2003). Phosphorylation of Ser-347 of Banp RS domain by protein kinase C is essential for activation and nuclear retention of *tp53* (Jalota-Badhwar, Kaul-Ghanekar et al. 2007), which imposes cell-cycle arrest by inducing a cdk inhibitor *p21(cdkn1a)* (Kaul, Mukherjee et al. 2003). Thus, Banp stabilizes *tp53*. On the other hand, Banp inhibits the acetylation of Tp53 by histone acetyltransferase p300 and impairs activation of *tp53* dependent pro-apoptotic genes (Sinha, Malonia et al. 2012). Acetylation of *tp53* is indispensable for the induction of apoptosis. Thus, Banp inhibits *tp53*-mediated apoptosis. Interestingly, *tp53* directly binds to the Banp promoter and increases Banp activity (Singh, Mogare et al. 2007). Treatment with Doxorubicin, a DNA-damaging agent that acts through *tp53* activation, disclosed that Banp was induced upon treatment in cells containing wild-type *tp53* but not mutant *tp53*, suggesting that Banp transcription is dependent on *tp53*. So, Doxorubicin increases *tp53*-mediated transcription of *banp*, stabilizing *tp53* (Singh, Mogare et al. 2007). Thus, *tp53* and *banp* regulate one another in a positive feedback loop, and that this feedback loop is vital to maintaining cellular homeostasis.

1.1.6 Combined regulation of cellular stress response by *banp* and *tp53*

banp, in conjunction with *tp53*, also dictates cell fate upon cellular stress, ranging from cell cycle arrest to apoptosis, depending upon the extent of DNA damage occurred (Pavithra, Mukherjee et al. 2009, Sinha, Malonia et al. 2010, Sinha, Malonia et al. 2012). During genotoxic stress, *tp53* is activated to induce damage response genes, including a cdk inhibitor *p21(cdkn1a),* which facilitates cell-cycle arrest, during which the damage is repaired by cellular repair machinery. Transcriptional activity of damage response genes must be shut off once the damage is repaired, allowing cells to re-enter the cell cycle. Banp participates in damping *tp53* response during post-stress recovery by forming a stable triple complex with Tp53-Mdm2 and deacetylating *tp53* at lysine 373/382 by masking the active phosphorylation site of *tp53*. This dampening of *tp53* activity follows the re-entry of the cells into the cell cycle (Pavithra, Mukherjee et al. 2009).

Another way *banp* determines cell fate is by regulating the promoter activity of pro-apoptotic genes, *bax*, and *puma* (*bbc3*), by binding to an identical MAR element that brings the promoters to close enough form intra-chromosomal loops that exert regulatory effects. Generally, activated *tp53* can induce the expression of *bax* and *puma* (*bbc3*). However, Sinha et al. report that following mild DNA damage, Banp represses *tp53*-mediated transcription of *bax* and *puma* (*bbc3*) genes by promoting histone deacetylase 1 (*hdac1*)-dependent *tp53* deacetylation (Figure 1-4, left), whereas Banp simultaneously induces *p21(cdkn1a)* transcription and facilitate a cell-cycle arrest. In addition, Banp can trans-repress *bax* and *puma* (*bbc3*) transcription in a *tp53*-independent manner (Figure 1-4, left). Thus, Banp generates anti-apoptotic signals favoring cell-cycle arrest to repair the damage. However, following severe DNA damage, Banp is sequestered in Promyelocytic Leukemia (PML) nuclear bodies. PML bodies are small spheres (diameter 0.1–1.0 μm) that increase during severe DNA damage or stress (Sahin, Lallemand-Breitenbach et al. 2014). Once Banp is sequestered in PML bodies, it can no longer recruit Hdac1 to the MAR of *bax* and *puma* (*bbc3*) promoter and to the Tp53 protein to keep it deacetylated (Figure 1-4, right). Thus, Banp inactivation promotes prolonged acetylation and activation of *tp53*, which subsequently induces *bax* and *puma* (*bbc3*) transcription, thereby facilitating apoptosis (Sinha, Malonia et al. 2010). Banp knockdown accumulates acetylated *tp53*, which increases apoptosis at a 15% higher rate than in the case of mild DNA damage. Thus, Banp regulates the balance between cell-cycle arrest and apoptosis in *tp53*-mediated DNA damage response.

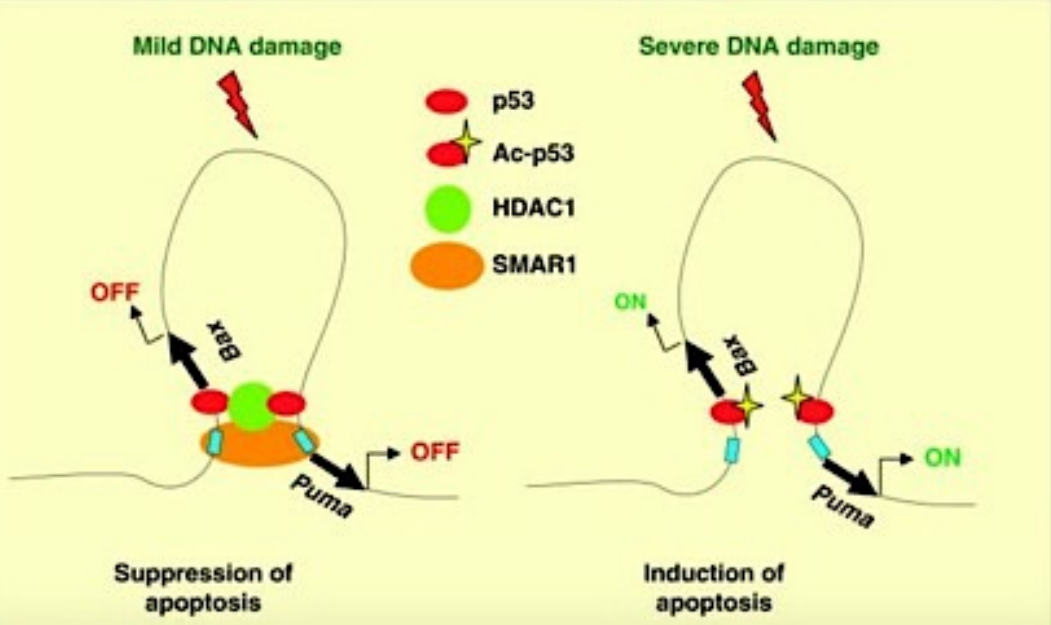

Figure 1-4: *bax*, *puma (bbc3)* transcriptional regulation by Banp.
Left panel, SMAR1/Banp (orange) forms a repressor complex with Hdac1 (green) and Tp53 (red) to bind to this similar MAR region, turning off transcription after minor DNA damage (suppression of apoptosis). Right panel, Banp is no longer linked to the MAR element after severe DNA damage, allowing for Tp53 acetylation and *bax* and *puma* transcription (induction of apoptosis). Figure adapted from Sinha et al. (Sinha, Malonia et al. 2010).

1.1.7 Banp interaction and regulation with the help of Histone deacetylases

Banp, with its simultaneous DNA- and protein-binding ability, acts as an adaptor protein for various regulatory functions. Histone deacetylases (Hdacs) are enzymes that remove acetyl groups from various proteins, including histones. Removing acetyl groups from lysine residues in histones allows chromatin to condense and to repress transcription. Control of Hdac activity is also crucial for modifying the regulatory roles of other proteins. Several studies reported Banp as an adaptor molecule that helps Hdacs to modulate an assortment of genes. Specifically, Banp:

- Represses *cyclinD1*. Recruits the Banp-Hdac1-sin3 repressor complex to the MAR site of the promoter to repress *cyclinD1* (Rampalli, Pavithra et al. 2005).
- Deacetylates Tp53 by forming a Tp53-Mdm2-Banp complex to recruit Hdac1 (Pavithra, Mukherjee et al. 2009).
- Represses *cd40* by recruiting Banp-Hdac1 repressor complex to its promoter (Singh, Sinha et al. 2010).
- Represses long terminal repeat-mediated transcription of human immunodeficiency virus-1 by recruiting Banp-Hdac1-mSin3 repressor complex to reduce virion production (Sreenath, Pavithra et al. 2010).
- Recruits Banp-Hdac1 to the MAR region of gene *slug*. Imparting repression of E-cadherin repressor gene *slug*, thereby restoring E-cadherin that helps to reduce epithelial to mesenchymal transition. (Adhikary, Chakraborty et al. 2014).

These studies suggest the roles of Banp in the recruitment of chromatin modulators to the promoter site for transcriptional regulation.

1.1.8 The *banp*-regulatory mechanism involved in DNA damage response

Apart from regulation via *tp53* as described in sections 1.1.5 and 1.1.6, Banp is a downstream phosphorylation target of *atm* kinase during an ionizing radiation (IR)-induced DNA damage. In this context, Banp deacetylates Ku70, a DNA-damage response protein with the help of Hdac6. Deacetylated Ku70 remains inactive, leading to less efficient repair of DNA damage. Upon encountering a double-stranded break in DNA, Banp is recruited to the double-strand break (DSB) sites, followed by phosphorylation by *atm*. Thus, Banp keeps Ku70 functional at DSB sites in the deacetylated form and parallel sequestration of *bax*. Banp, Ku70, and other repair factors efficiently repair the damage (Chaudhary, Nakka et al. 2014).
Additionally, a high throughput screening for DNA DSB-associated proteins was paired with orthogonal datasets that assessed DNA DSB binding to uncover additional DNA DSB repair factors. In this work, Banp was confirmed to be one of the proteins enriched in the presence of a DSB (Tay 2018). The alterations in global gene expression in normal human fibroblasts in response to IR-induced DNA damage were investigated by Zhou et al. (Zhou, Chou et al. 2006). Their findings show that human diploid fibroblasts respond to IR in a very stereotypical fashion that indicates synchronization principally behind the G1 checkpoint and substantial induction of other markers of G_0 quiescence. According to this study, *banp* belonged to a group that only demonstrated repression after 2 hours. This pattern was anticipated to suppress *e2f1* and its target gene expression. Taken together, the presence of Banp in multiple independent studies of DNA damage responses provides evidence that Banp is required for DNA damage repair, although the exact mechanism remains elusive.

1.1.9 Banp is involved in the regulation of alternative splicing.

Banp contains an RS domain that aids RNA binding and interacts with snRNAs, which are essential components of the splicing machinery (Nakka, Chaudhary et al. 2015). In breast cancer cell lines, Banp has been shown to regulate the splicing of *cd44* variants by deacetylating Sam68 with the help of Hdac6 (Nakka, Chaudhary et al. 2015). Banp modulates FAS ligand alternative splicing in addition to *cd44* variants. Banp controls pyruvate kinase muscle (*pkm)* alternative splicing by deacetylating Ptbp1 with the help of Hdac6. Alternate splicing by Banp inhibits cancer cell metabolism and breast cancer growth by suppressing the oncogenic isoform *pkm2* (Choksi, Parulekar et al. 2021). Banp has multiple global gene targets involved in the control of RNA processing and alternative splicing, according to ChIP-sequencing research in HCT116 cells (Mathai, Mittal et al. 2016). According to the studies mentioned above, Banp has the potential to control alternative splicing of various genes.

1.1.10 *banp* and its regulatory role in cancer

The tumor suppresser function of *banp* has been investigated. First, Kaul et al. reported that mRNA expression levels of one of the splice variants of *banp*, called SMARs, are decreased in most human cancer cell lines. On the other hand, overexpression of SMARs in mouse melanoma cells leads to growth arrest in the G2/M phase. Tumor growth was also delayed upon *in-vivo* injection of SMARs in mice. They also showed physical interaction and co-localization of SMARs with *tp53* (Kaul, Mukherjee et al. 2003). Later, the arginine/serine rich RS domain (residues 160-350) was identified as the minimal domain of Banp indispensable for tumor suppression (Jalota-Badhwar, Kaul-Ghanekar et al. 2007). Another critical target of Banp for cell-cycle regulation is *cyclinD1*. *cyclinD1* regulates G1/S transition typically but is

overexpressed in many transformed cells (Bartkova, Lukas et al. 1995). Chromatin condensation by *hdac1*-mediated deacetylation inhibits gene transcription (Rampalli, Pavithra et al. 2005). When Banp is overexpressed, Banp represses transcription of *cyclinD1* by recruiting the Banp-SIN3a-Hdac1 repressor complex to its promoter. Pavitra et al. provided evidence that an anticancer agent, prostaglandin A2, mediates downregulation of *cyclinD1* and results from the stabilization of Banp mRNA (Pavithra, Rampalli et al. 2007). Furthermore, Banp overexpression in MCF7 breast cancer cell lines increased the sensitivity to radiation through the activation of *tp53*. This increased sensitivity to radiation suggesting its potential use in clinical therapy (Liu, Ma et al. 2014). Studies by Chemmannur et al., where Banp His 5 was delivered *in-vivo* (a minimal domain required for anticancer activity) via carbon nanospheres, showed promise for its therapeutic activity. Significant regression of breast tumors in mice was observed upon His 5 deliveries (Chemmannur, Bhagat et al. 2016). By regulating alternate splicing, Banp can also prevent an oncogenic form of *cd44* (Nakka, Chaudhary et al. 2015).
Banp undergoes anaphase-promoting complex (APC/CCdc20)-dependent proteasomal degradation (Paul, Ghorai et al. 2017). Cell-division cycle protein 20 (Cdc20), a substrate receptor subunit of APC/CCdc20, promotes cancer cell invasion by proteasomal degradation of Banp. This degradation of Banp was confirmed by the inverse relationship between Banp and Cdc20 in breast cancer cell lines (Paul, Ghorai et al. 2017). Banp also regulates β-catenin. β-catenin is upregulated in more than 70% of colorectal cancers. Banp binds to the β-catenin promoter and imparts transcriptional repression with the help of Hdac5. Stabilizing Banp by masking D-box elements, the target sequence that promotes proteasomal degradation with microbial peptides reduces proteasomal degradation of Banp, followed by decreasing β-catenin expression. Similar stabilization of Banp can reduce tumor progression *in-vivo* (Taye, Alam et al. 2018). Stabilizing Banp protein is being proposed as a therapeutic strategy for certain tumor regression. However, under section 1.1.6 we saw that knocking down *banp* can push transformed cells towards cell death. A possible reason for such variable and context dependent function of *banp* in cancer cells is likely due to its aberrant methylation (Grand, Burger et al. 2021).

1.1.11 Role of *banp* in cell cycle regulation and maintaining stem cell fitness

Genome-wide CRISPR screen is a gene-editing system coupling CRISPR cas9 and single guide RNAs libraries that target every gene in the genome. Recently, it has emerged as a powerful tool to identify a repertoire of essential genes in complex cellular signaling networks involved in fundamental processes such as stem cellness, cancer proliferation, and differentiation (Cheung, Cowley et al. 2011, Hart, Chandrashekhar et al. 2015, Wang, Birsoy et al. 2015, Meyers, Bryan et al. 2017, Henriksson, Chen et al. 2019). A Genome-wide CRISPR screen in search of essential genes required for human pluripotent stem cell fitness identified *banp* as one of the most significant core essential genes irrespective of substrate dependencies (Mair, Tomic et al. 2019). This study demonstrates that *banp* is required for the maintenance of human stem cell pluripotency. Instances of *banp* activation promoting cell proliferation have also been validated in a study where pre-adipocyte proliferation showed upregulation of *banp* via CCAAT/enhancer-binding protein beta (Liu and Huang 2010). Using online datasets, in another study, researchers discovered that *banp* expression is positively connected with osteosarcoma patients' overall survival and negatively connected with the expression of stemness markers. Banp overexpression reduces the stemness of osteosarcoma cells, as evidenced by decreased

stemness marker expression, sphere-forming ability, and aldehyde dehydrogenase activity, according to functional studies (Xu, Liu et al. 2021). The findings stated above once again reveal, *banp* can have a context-dependent function according to various perspectives (cell type, tissue, or organism).

1.2 Regulation of cell-cycle progression and neurogenesis in the zebrafish retina

In vertebrate animals, the retinal precursor region is initially induced in the anterior neural plate and evaginate from the lateral wall of the diencephalon to form an optic vesicle after neural keel forms. The dorsal and ventral regions of the optic vesicle are specified into the neural retina and pigment epithelium, respectively. During the morphogenesis from optic vesicle to optic cup, the neural retina becomes positioned in the inside layer of the optic cup, whereas pigmented epithelium covers the neural retina as the outside layer of the optic cup (Harris 1997). In the neural retina, six major classes of neurons; retinal ganglion cells (RGC), three types of interneurons (amacrine cells, bipolar cells, and horizontal cells), two types of photoreceptors (rods and cones), and one type of glial cells (Müller cells) differentiate to form neural circuits responsible for phototransduction and visual processing (Harris 1997) (Figure 1-5). Importantly, in mice, frogs, and chicks, these different retinal cell types are derived from normal retinal progenitor cells, and cell fate decision does not depend on cell lineage. Thus, retinal progenitor cells are believed to be multipotent and can generate all the retinal cell types in response to extrinsic and intrinsic cues across vertebrate species.

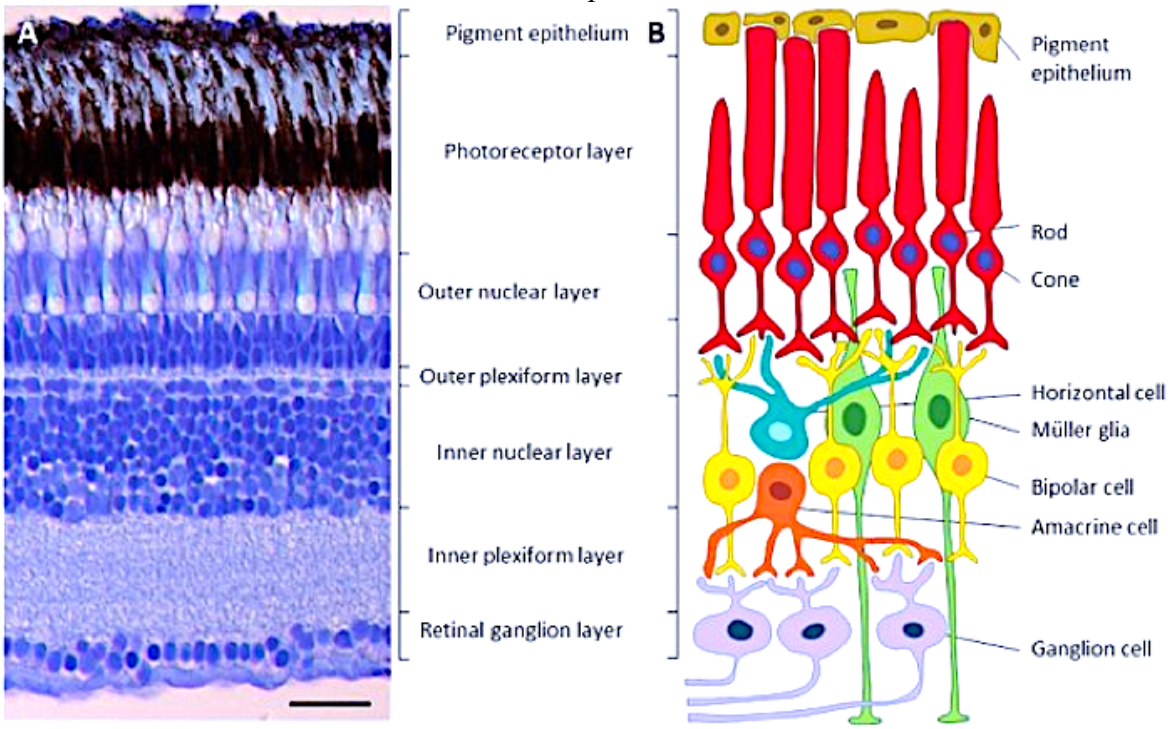

Figure 1-5: Neural circuit of the zebrafish retina.
(A) Toluidine blue-stained section of the adult zebrafish retina. (B) Cartoon showing retinal cell types and neural circuits. Three nuclear layers and two plexiform layers are formed. Figure adapted from (Gramage, Li et al. 2014)

In zebrafish retinas, neurogenesis starts at 25 hpf. Interestingly, the progression of retinal neurogenesis is spatially and temporally regulated. In zebrafish, neurogenesis is initiated at a few cells of the ventro-nasal retina just adjacent to the optic stalk. Then neurogenic area spreads from the ventro-nasal region to the dorsal region of the neural retina and finally reaches the temporal retina (Masai, Stemple et al. 2000). It was reported that fibroblast growth factor (*fgf*) 3/8 is expressed in the optic stalk in zebrafish and that blockade of the Fgf signaling pathway inhibits the initial induction of retinal neurogenesis (Martinez-Morales, Del Bene et al. 2005). Consistently, laser ablation of the optic stalk severely reduces the initial induction of retinal neurogenesis in zebrafish (Masai, Stemple et al. 2000). It was reported that the progression of retinal neurogenesis is delayed in zebrafish hedgehog (Hh) pathway mutants (Neumann and Nuesslein-Volhard 2000). Activation of protein kinase A (*pka*), which is a potent inhibitor of the Hh signaling pathway, does not inhibit the initial induction of retinal neurogenesis in zebrafish but markedly inhibits the progression of retinal neurogenesis from the ventro-nasal retina (Masai, Yamaguchi et al. 2005). Thus, Fgf and Hh signaling pathways cooperatively regulate the induction and progression of retinal neurogenesis in zebrafish (Figure 1-6). In the Xenopus retina, Hh promotes the cell-cycle progression of retinal progenitor cells by decreasing the G1 and G2 phases (Locker, Agathocleous et al. 2006).
Interestingly, cell-cycle length varies at different time points in developing zebrafish retina. Cell-cycle length of retinal progenitor cells is initially long, around 32-49 hours from 6-24 hpf; however, it is abruptly shortened to 8-10 hours after 24 hpf (Harris 1997, Li, Hu et al. 2000), suggesting that cell-cycle progression is also activated after retinal neurogenesis begins. Hh may promote the propagation of retinal neurogenesis by an acceleration of cell-cycle progression in zebrafish.

Previous genetic studies revealed regulatory factors that regulate the balance between cell proliferation and neurogenesis in the zebrafish retina. In zebrafish *hdac1* mutants, retinal progenitor cells fail to exit from the cell cycle but continue to proliferate, suggesting that the switch from cell proliferation to neurogenesis depends on the histone acetylation status of the zebrafish retina. In zebrafish retina, *wnt* and *notch* signaling promote cell proliferation and inhibits neurogenesis, respectively. Hdac1 suppresses *wnt* and *notch* signaling pathways to promote retinal neurogenesis (Yamaguchi, Tonou-Fujimori et al. 2005) (Figure 1-6). Opposite phenotypes were observed in zebrafish dynactin-1 mutants. In *dynactin-1* mutant retinas, premature neurogenesis occurs, resulting in increased early born-neurons such as RGCs and a decrease of late born-neurons such as bipolar cells and Müller glia. Dynactin-1 is required for interkinetic nuclear migration (INM) of retinal progenitor cells in zebrafish. In the developing retina, mitosis occurs typically at the apical region of the neural retina; however, mitotic cells fail to reach the apical region but are positioned more basally in *dynactin-1* mutants (Del Bene, Wehman et al. 2008). Since Notch activity forms a high-low gradient along the apicobasal axis in the zebrafish retina, Notch activity is downregulated in *dynactin-1* mutant mitotic cells, leading to premature neurogenesis. This study is consistent with the time-lapse observation of zebrafish retinal INM, indicating that retinal cells undergoing more basal INM tend to enter neurogenic cell division, whereas retinal cells undergoing more apical INM tend to enter proliferative cell division (Baye and Link 2007). These data suggest that nuclear migration dynamics of retinal cells influence neurogenic rate through the Notch signaling pathway.

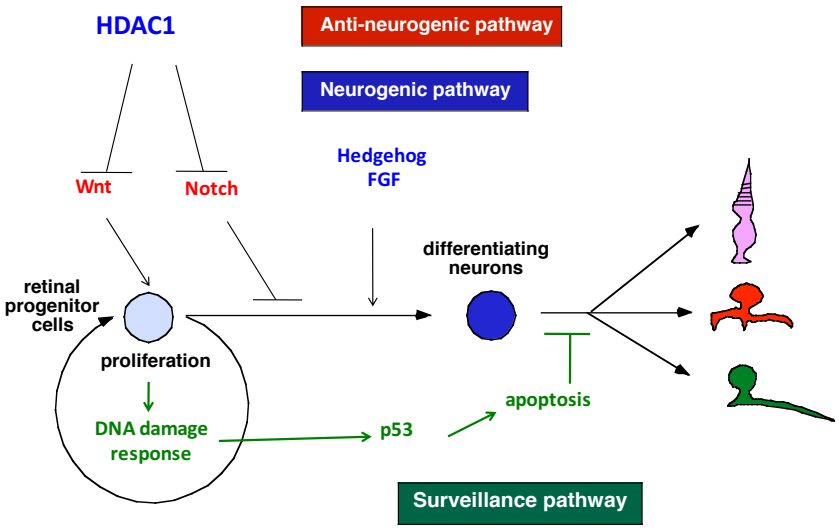

Figure 1-6: Mechanism regulating retinal neurogenesis and surveillance pathway
In developing zebrafish retina, multipotent retinal progenitor cells undergo proliferation. The progenitor cells undergo differentiation under the influence of Fgf or hedgehog signals, giving rise to different retinal neurons (Figure 3.2). However, Wnt and Notch inhibit neurogenesis as anti-neurogenic signals. On the other hand, Hdac1 promotes neurogenesis by inhibiting anti-neurogenic pathways, Wnt and Notch. In zebrafish, cell-cycle progression is enhanced after retinal neurogenesis starts. This cell cycle activation may be essential to keep a pool of retinal progenitor cells, which generate the late-born neurons. However, such enhanced proliferation likely increases DNA replication errors. *tp53* dependent DNA damage response repairs DNA damages and eliminates cells with irreparable damage. This surveillance mechanism functions like quality control for retinal neurogenesis.

1.2.1 *tp53*-dependent apoptosis links to retinal neurogenesis in zebrafish

Masai lab previously performed large-scale mutagenesis using zebrafish and isolated more than 700 zebrafish mutants that show retinal development defects. Zebrafish mutants, namely *rw255*, *rw329*, and *rw564*, show severe apoptosis in the developing retina. Preliminary analyses indicate that retinal apoptosis in these four mutants depends on *tp53*, indicating that *tp53*-dependent DNA damage response is abnormally activated in these mutant retinas. Masai lab cloned the *rw255* mutant gene and found that it encodes a small subunit of DNA primase (*prim1*). *prim1* is essential for DNA replication along the lagging strand of the DNA replication fork. It was reported that dysfunction of Prim1 or uncoupled coordination of DNA replication regulatory factors including Prim1, DNA polymerase α and δ, and Mcm helicases activates a DNA replication checkpoint factor, *atr*. So, it is likely that DNA replication stress activates *tp53*-mediated apoptosis in *prim1* mutants. Consistently, retinal apoptosis in *prim1* mutants depends on not only *tp53* but also *atm* and *chk2*, suggesting that *atr/atm-chk2-tp53* pathway actively monitors DNA damages during retinal neurogenesis in zebrafish. Thus, the *atr/atm-chk2-tp53* pathway functions as a safeguard to ensure the integrity of retinal cell proliferation and

neurogenesis (Figure 1-6). Zebrafish retinas provide a good model for studying the *tp53*-mediated signaling network for DNA damage response.

1.2.2 Role of DNA damage response factors in zebrafish retinal development

DNA damage response is essential to maintain genomic integrity. DNA lesions, which occur as a result of DNA replication, cellular metabolism, and environmental stress, continually challenge the integrity of the genome (Thompson and Schild 2002). Significantly enhanced cell proliferation increases the rate of DNA replication errors and subsequently induced double-strand DNA breaks, so DNA damage repair is vital to ensure the integrity of development and eliminate precocious cancer cells (Murga, Bunting et al. 2009). The retina is one of the rapidly proliferating tissues in embryos. Consistently, oxidative DNA damage repair is usually observed in zebrafish developing retinas, and its peak is at 3 dpf (Biehlmaier, Neuhauss et al. 2001, Sasagawa, Nishimura et al. 2016). Furthermore, exposure to DNA damage agents induces excessive apoptosis in developing zebrafish retina (Sasagawa, Nishimura et al. 2016). There are reports that deficiencies of DNA damage-repair factors specifically induce apoptosis in developing mouse retina, but not in other tissues (Rodrigues, Grigaravicius et al. 2013). Similarly, zebrafish embryos in which DNA damage-response genes like DNA damage-binding protein 1 (Ddb1) (Hu, Holzschuh et al. 2015), Fanconi anemia group D2 (Fancd2) (Liu, Howlett et al. 2003), and Ku80 (Xrcc80) (Bladen, Lam et al. 2005) are compromised show increased levels of apoptosis. It is primarily observed in the highly proliferating retina and brain. These reports suggest that defects in DNA-damage response can be reflected in developing the retina.

Zebrafish retina orchestrates cell-cycle length, differentiation, and apoptosis to attain the correct cell number and volume in the retina and achieve its functional multilayered structure (Figure 1-5), making the zebrafish retina a good model for studying these processes as well as genes involved in these processes (Siefert, Clowdus et al. 2015). Furthermore, Banp is also involved in DNA-damage response, discussed above (review of literature page number; 6, 7, 9). Banp may thus help maintain genomic integrity in cells, and its physiological and cellular significance can be unraveled using the zebrafish *banp* mutant retina as a model system.

1.3 Objectives

Considering the potential role of Banp in regulating cell-cycle and genomic integrity, I hypothesize that Banp may regulate the balance between cell-cycle progression and apoptosis, potentially by maintaining genomic integrity in developing zebrafish. As the retina is one of the highly proliferating tissues in developing zebrafish, the rate of intrinsic DNA damage is expected to be higher than other tissues. The absence or reduction of DNA damage response may facilitate chronic DNA damage accumulation, leading to cell-cycle arrest and apoptosis. Utilizing the retina of zebrafish *banp*^{rw337} mutant, I shall investigate the cellular and molecular roles of Banp under physiological conditions.

The objectives of my research are:
Objective 1: Understand phenotype of *banp* knock out zebrafish (Chapter 2)
Objective 2: Identify cellular process and molecular pathways regulated by *banp* in zebrafish (Chapter 3)
Objective 3: Validate potential regulatory targets of *banp* in zebrafish (Chapter 4)

This research will advance our understanding of Banp's cellular and molecular mechanisms in physiologic conditions, which will be a step forward from its *in vitro* functions.

CHAPTER 2

Functions of Banp in developing zebrafish

2.1 Motivation

Zebrafish is an excellent vertebrate animal model to study development and diseases. They have ex-vivo fertilization and embryogenesis in contrast to mice, where it is in-utero. When fertilization occurs in-utero, it is difficult to evaluate the physiological functions and early developmental implications of embryonic lethal genes. In this situation, ex-vivo fertilization and optically transparent embryos enable zebrafish to be a better model for studying the physiological and developmental effects of embryonic lethal genes. Additionally, zebrafish is well characterized with a 1.5 Gbp genome and can be easily grown and maintained in the lab. Around 80 percent of human disease-causing genes are present in zebrafish. They also possess most of the organ systems compared to humans. Due to the advancement of CRISPR/Cas9 gene-editing tools, targeting the specific gene in zebrafish has become an easy tool to accomplish various aspects of research (Lieschke and Currie 2007, Chavez, Aedo et al. 2016).
To investigate the physiological and developmental functions of gene *banp*, I am utilizing zebrafish as a model system. Since the earlier attempts to genetically knockout Banp were reportedly embryonic lethal (Chemmannur, Badhwar et al. 2015) or unsuccessful (Grand, Burger et al. 2021), I shall use whole-body *banp* knockout zebrafish, *rw337* to unravel its fundamental physiological functions.

2.2 Materials methods

2.2.1 Reagents used

Embryo lysis buffer (40 mL)

Reagent	Volume
10X PCR buffer containing 15mM MgCl2	4 mL
NP40(0.3% in total volume)	120 uL
Tween 20 (0.3% in total volume)	120 uL
Make up volume to 40 mL using MilliQ H20	

2.2.2 Zebrafish maintenance

Zebrafish (*Danio rerio*) were maintained using standard procedures (Westerfield 1993). RIKEN Wako (RW) was used as a wild type strain for mutagenesis where *banp*^{rw337} *mutation* was generated. Mapping and mutant studies were carried out on WIK and Okinawa wild type (oki) respectively. *banp*^{rw337}mutants showed mendelian ratio and similar phenotypes in all three genetic backgrounds. Banp mutant alleles banprw337 and banpsa12976 were used in my study. banpsa12976 was obtained from Zebrafish International Resource Center (ZIRC, Eugene, OR, USA). Homozygous mutants (banp-/-) will be referred to as "mutants". Heterozygous

(banp+/-) siblings do not have phenotypic defects and behave similarly to wild type. The wild type (banp+/+) and heterozygous (banp+/-) siblings together are referred to as "wild type". All comparative experiments are carried out with mutants versus wild type. Zebrafish transgenic line Tg[EF1α:mCherry-CAAX]oki049 (Mochizuki, Luo et al. 2017) were used to visualize plasma membranes. Tg[ath5:EGFP] (Masai, Yamaguchi et al. 2005) was used to visualize retinal differentiation.

2.2.3 Mutagenesis, mapping, and cloning of *banp^{rw337}*

Mutagenesis, mapping, and cloning were performed as previously described by Masai lab (Masai, Lele et al. 2003). The polymorphic markers, 070702B and zC93F2D, shown below, were designed and used for restricting the genomic region covering the *banp^{rw337}* mutation.
070702B forward: 5'-ACTTCTTATCAGGGCTGTGC-3'
070702B reverse: 5'-TCAGTCAAGAGCAGTGAGAG-3'
zC93F2D forward: 5'-TGGGATCTCTTTAAGTGAGTGAG-3'
zC93F2D reverse: 5'-TCCAACTATGTGGGTCAAACC-3'

2.2.4 Plastic sectioning and toluidine blue staining

Embryos at the age of interest were dechorionated and fixed with 4% PFA at 4^{o}C overnight. Followed by washes in PBS (3 times x 5 minutes) at RT. PBS was serially replaced with 100% ethanol as follows.

Percentage Ethanol	Time in minutes
30%	2
50%	2
70%	2
100% X two times	2

Then embryos were transferred to 100% Ethanol/JB4 solution (1:1) for 3 hours at RT and then to JB4 solution overnight at 4^{o}C. Next, embryos were embedded in a rectangular silicone mold using a JB4 (A+B) solution. In the mold, embryos were adjusted to the required orientation. The mold was covered with transparent cellophane paper to cut the air supply. When the solution has solidified, the sample was trimmed and mounted on a wooden block. The mounted sample was then cut into 5-7 µm thin sections using a microtome. Each section was then arranged on top of distilled water domes on a slide and dried on a hot plate. After drying, the slide was immersed in 0.1% toluidine solution for one dip. Slides were washed with distilled water until excessive toluidine blue dye is removed from tissues. Slides were then dried on a hot plate and mounted with inclusion reagent.

2.2.5 Genotyping *banp^{rw337}*

banp^{rw337} mutants were difficult to phenotypically distinguish from wild type until 4 dpf. Identification of mutants at earlier time points is performed using PCR amplification of genomic region using specific primers that enabled restriction digestion of only mutated sequence using MboII. Primers used are given below.
Forward: CGATGTTGATATCCATCAGTCAGGCGATC
Reverse primer: GGTGCTGGTGTATAAATCACATGACCTATGGTCCTCTT

2.2.5.1 Genomic DNA isolation

Tissue samples were collected and transferred to a 50 µl lysis buffer. In the case of embryos, the required developmental stages were dechorionated, and embryo tails were cut and transferred to 50 µl lysis buffer. When genotyping adult fishes to identify potential ID pairs, a fin clip was performed and transferred to a 50 µl lysis buffer. If tissue was fixed overnight in 4% PFA, the next day, the embryo tails were cut and transferred to 1x PBS, followed by 5-minute PBS wash X 3 times before transferring to lysis buffer. After immersing the tissue in 50 µl of lysis buffer, it is incubated at 98^{o}C for 10 minutes and 4^{o}C for 2 minutes. Then 5 µl Proteinase K (10mg/mL) is added, followed by incubation at 37^{o}C overnight. The next day, the sample is quenched using a thermocycler 98^{o}C-10 min, 4^{o}C-5 minute to inactivate Proteinase K. Next, Centrifuge samples at 4000 rpm for 15 min at 4^{o}C. Collect 20 mL of supernatant for further PCR amplification or store this genomic DNA at -20^{o}C for future use.
PCR for genotyping: Prepare the PCR reaction mix and run the PCR as follows

PCR Reagents	Volume in µL
Master mix	19
Forward primer (100mMol)	0.04
Reverse primer (100mMol)	0.04
AmpliTaq Gold™ DNA Polymerase	0.015
Genomic DNA (template)	2

PCR cycle conditions			
Initial Denaturation	96 ^{o}C	6 minute	
Denaturation	95 ^{o}C	30 seconds	
Annealing	55 ^{o}C	30 seconds	45 cycle
Extension	72 ^{o}C	30 seconds	
Final Extension	72 ^{o}C	7 minutes	
	15 ^{o}C	3 minutes	
	4 ^{o}C	hold	

Following the PCR, check for PCR product amplification by resolving 5µL PCR product on a 4 percent agarose gel for 80 minutes (150Volts). Product size above 200 bp should be observed if amplified. Upon correct product amplification, proceed to MboII enzyme digestion as follows.

Reagents	Volume in µL
PCR product	10-15
MboII enzyme	0.1
10x (L) buffer	2
MilliQ H20	3

5 µL of digested PCR product is resolved on a 4 percent agarose gel for 80 minutes (150Volts). This setting will resolve wild type, mutant, and heterozygous as 239, 200, (239 and 200) bp. This PCR method of genotyping was used to distinguish wild type mutant or heterozygote

embryos whenever the embryos were phenotypically indistinguishable (e.g., morpholino rescue experiments, early developmental stages).

2.2.6 Genotyping *banp*^{sa12976}

Genotyping of this fish line *banp*^{sa12976} was performed to confirm the mutation in the gene *banp*. We sequenced the genomic region of potential mutation to evaluate mutation. The sequencing protocol was performed as follows. Primers used;
Forward: TGTTGATATCCATCAGTCAG; Reverse: GGTGTATAAATCACATGACC.
Fins of adult fishes were clipped, and genomic DNA was isolated as mentioned in section 2.2.5.1. and performed PCR as follows.

PCR Reagents	Volume in µL
Master mix	13.3
Forward primer (10mMol)	0.3
Reverse primer (10mMol)	0.3
AmpliTaq Gold™ DNA Polymerase	0.15
Genomic DNA (template)	1

PCR cycle conditions			
Initial Denaturation	96 °C	10 minute	
Denaturation	96 °C	30 seconds	
Annealing	55 °C	50 seconds	45 cycle
Extension	72 °C	45 seconds	
Final Extension	72 °C	10 minutes	
	15 °C	3 minutes	
	4 °C	hold	

After confirming product amplification by gel electrophoresis (product length 230 bp), the PCR product was purified using a purification column (QIAquick PCR Purification Kit) following the manufacturer's protocol. Then the eluted product was used to set up sequencing PCR as follows.

PCR Reagents	Volume in µL
BigDye™ Terminator v1.1 (Applied Biosystems)	0.2
5x sequencing buffer	1.9
Forward primer (1.6 µMol)	2
MilliQ H20	4.9
Purified PCR product	1

PCR cycle conditions			
Initial Denaturation	94 oC	1 minute	
Denaturation	95 oC	10 seconds	
Annealing		5 seconds	40 cycle
Extension		2 minutes	

	50 oC 60 oC	
	4 oC	hold

After sequencing PCR, the product was cleaned up using clean seq (A29151) following manufacturers protocol and sequencing in a capillary sequencer (Applied Biosystems, 3730xl). After sequencing, the expected mutation site was evaluated and identified heterozygous fishes for further crossing to generate homozygous mutant embryos.

2.2.7 Acridine orange staining

Larvae at 2 dpf were incubated at 28^{o}C in 5mg/mL acridine orange (AO) in E3 medium (5mM NaCl, 0.17mM KCl, 0.33mM $CaCl_2$, 0.33mM $MgSO_4$) for thirty minutes, protected from light. To visualize dead cell accumulation at earlier time points, embryos were rinsed in E3 medium and examined with an epifluorescence microscope (Zeiss). This method was used to identify live mutant embryos at 2 dpf.

2.2.8 qRT-PCR

RNA isolation and cDNA synthesis were done as described in Section 3.2.3 (Chapter 3, Materials and Methods). Primers used for real-time PCR are listed below.
banp Forward: GATGGGCAAGAACCAGTCAA
banp Reverse: GGGAACAACACAGCGTACTT

2.2.9 *In-situ* hybridization

At the indicated developmental stages, whole-mount *in-situ* hybridization was performed on embryos. For whole-mount in situ hybridization, the steps were performed as previously described (Xu, Holder et al. 1994). To make in situ probes, gene *banp* was PCR amplified and sub-cloned into the pBluescript II SK (+) vector (Stratagene/Agilent Technologies). Probe incorporated plasmids were digested with restriction enzyme EcoR1 (Takara) to make DNA templates. Digoxigenin-labeled *banp* RNA probes were generated by *in vitro* transcription using the DIG RNA Labeling Kit (11277073910 Roche). The generated RNA probes were column purified using Micro Bio-Spin® Chromatography Columns (Biorad). *In situ* hybridization signals were detected using anti-DIG alkaline phosphatase (AP)-conjugated antibody (Roche) with an AP substrate BM-Purple (11442074001, Roche) for whole-mount embryos. The embryos were imaged using SteREO Discovery.V12 (ZEISS) microscope.

2.2.10 mRNA Rescue experiment

To induce the expression of Banp protein for protein localization studies and rescue experiments, zebrafish-Banp *(z*Banp*)* with EGFP reporter was generated. The Coding region of *z*Banp was amplified and cloned into a PCSII vector with an EGFP reporter at its C-terminal (banp(wt)-EGFP) or N-terminal (EGFP-banp(wt)) (Figure 2-7 A). Similarly, the *banp*^{rw337} mutant sequence was also cloned to generate N-terminal EGFP reporter tagged construct EGFP-banp(rw337)mutant construct (Figure 2-7 A). Next, linearized the plasmids using Not1.

Linearized plasmids were used in a standard *in vitro* transcription reaction using SP6 polymerase (mMESSAGE mMACHINE™ SP6 Transcription Kit, Invitrogen). For the zebrafish Banp protein localization studies, mRNA injections were performed at the single-cell stage of oki wild type embryos using the banp(wt)-EGFP construct. Similarly, mRNA injection onto single-cell embryos obtained from crossing *banp*^{rw337} heterozygous fishes was used in banp(wt)-EGFP rescue experiments. banp(wt)-EGFP injected embryos were stained with acridine orange at 48 hpf to validate cell death. Further, at 54 hpf, acridine orange negative embryos were genotyped using PCR to identify mutants. Plastic sections were obtained to evaluate the phenotype of *banp*^{rw337} mutant embryos injected with banp(wt)-EGFP and EGFP-banp(rw337)mutant. The concentration of mRNA used for injection is 50 ng.

2.2.11 Morpholino injection

To eliminate *banp* protein expression, ATG morpholino (MO) was used. Embryos at the one-cell stage were used for injections. *banp*-MO was standardized for a concentration that showed a similar phenotype to the *banp*^{rw337} genetic mutant. 1mMol *banp*-MO (5'-CCACTAAATCTTGCTCTGACATCAT-3') was used for injections compared with 5 mismatch *banp*-MO (banp 5misMO) (5'-CCtCaAAATgTTcCTCTcACATCAT-3') as control.

2.2.12 Histology

Plastic sectioning, immunostaining of cryosections, paraffin sectioning, and BrdU incorporation were performed as described previously (Imai, Yoshizawa et al. 2010), except that we injected BrdU solution into the yolk of embryos at 48 hpf instead of soaking embryos in 10mM BrdU solution. Anti- pH3 antibody (Cell signalling technology, 6G3, 9706; Sigma-Aldrich, 06-570), anti-Pax6 antibody (Covance; PRB-278P), zpr1 antibody (ZIRC, Eugene, Oregon), anti-Prox1 antibody (GeneTex, GTX128354), anti-glutamine synthetase (GS) (Millipore, MAB302), anti-BrdU antibody (abcam, Ab6326), anti-PCNA (Sigma-Aldrich, P8825) were used at 1:500, 1:500, 1:100, 1:500, 1:100, 1:200, 1:200 dilutions, respectively. Nuclear staining was performed using SYTOX Green (Molecular Probes). Filamentous actin (F-actin) was stained using 0.1 mM rhodamine-conjugated phalloidin (Molecular Probes). Terminal deoxynucleotide transferase-mediated dUTP nick-end labeling (TUNEL) was performed using the In Situ Cell Death Detection Kit (Roche). Images were scanned using an LSM710 confocal laser scanning microscope (Zeiss). Number of fluorescent-positive cells and percentage of fluorescence-positive area relative to the region of interest was calculated using original scanning images with IMARIS (Bitplane) and Zen (Zeiss) or Image-J (NIH) software, respectively.

2.2.13 Whole-mount immunostaining for caspase 3 and HuC/D labeling

The protocol for whole-mount caspase 3 labeling was adapted and modified from Sorrells et al. (Sorrells, Toruno et al. 2013). Embryos were genotyped using acridine orange (AO) and fixed overnight in 4% paraformaldehyde (in PBS) at 4°C. The next day, embryos were washed three times in 1X PBS and permeabilized with 100% methanol for 2 hours at −20°C. Then the embryos were washed twice with PDT [1× PBST (0.1% Tween 20 in PBS 1×), 0.3% Triton, and 1% DMSO] for 20 minutes at RT. They were then incubated in blocking solution (10% Goat serum in PBST) for 1 hour at room temperature before being transferred to 1% blocking solution diluted with primary antibody for 2 days at 4°C. Primary antibodies used anti-active caspase3

(1:200) (BD Pharmingen, Clone C92-605), anti-HuC/D (1:200) (Thermo Fisher, A-21271). Then they were washed with PDT solution and then incubated with fluorescent conjugated secondary antibodies in 1% blocking solution. Embryos were incubated in the dark with secondary antibodies for 2 days at 4°C. Next, all samples were washed in PDT (X3 times) followed by glycerol storage at 4°C until imaging. The samples were observed with a confocal microscope LSM 710 (Zeiss) followed by image analysis using zen software (Zeiss).

2.2.14 BrdU labeling

2 days after fertilization, tricaine was used to anesthetize dechorionated embryos. Next, to detect mutants, embryos were genotyped using AO staining (section 2.2.7). Then embryos were injected with 10 mM BrdU (10% Dimethyl sulfoxide) onto its yolk. Change embryos to E3 medium and incubate for 30 minutes at 28°C. Embryos were further fixed using 4% PFA overnight, after the 30-minute BrdU chase. Cryo-sections of fixed embryos were performed as described in section (2.2.12), followed by immunofluorescence. Cryosections were incubated in 2N HCl for 1 hour before antibody labeling during immunofluorescence. The labeled DNA is denatured in this step, exposing the BrdU epitope.

2.2.15 RNA sequencing

RNA was isolated using Direct-zol RNA Miniprep Kit from banprw337 mutant and sibling embryos at 4 dpf. It is followed by library preparation for sequencing using NEBNext® Ultra™ II Directional RNA Library Prep Kit for Illumina® according to the manufacturer's instruction. Paired-end sequencing was performed using NovaSeq6000 SP. The quality of sequenced reads was evaluated with FastQC (Andrews 2010) and adaptor trimming and quality filtering were done with fastp (Chen, Zhou et al. 2018). Cleaned reads were then mapped to the zebrafish reference genome (GRCz11) using hisat2.1.0 (Kim, Paggi et al. 2019) and mapped reads were counted with FeatureCounts from the Subread package (Liao, Smyth et al. 2014) using annotation from Ensembl (Danio_rerio.GRCz11.95.gtf). Differentially expressed gene (DEG) analysis was performed using the EdgeR package (Robinson and Oshlack 2010). Genes with false discovery rates (FDR) < 0.01 were considered significant DEGs. The EnhancedVolcano package (Blighe, Rana et al. 2018) was used to create a volcano plot with Log2FoldChange (wild type – mutant) values and FDR calculated with EdgeR.

2.2.16 Mass spectrometry sample preparation, In-gel digestion

Extracted protein samples, 10 µl volume, were separated in an LDS-PAGE Bis-Tris Gel (4-12%) using MOPS buffer and stained with Colloidal Coomassie Blue Staining Kit (Invitrogen LC6025). Gel bands were excised and labeled according to molecular weight, in decreasing order.

Each fraction was processed for in-gel digestion. Briefly, fractions were reduced at 56ºC with 10mM dithiothreitol in 50 mM ammonium bicarbonate for 10 minutes and then alkylated with 55mM iodoacetamide in 50mM ammonium bicarbonate for 20 minutes in darkness. Last, a wash with a 50 mM ammonium bicarbonate in 50% acetonitrile, followed by pure acetonitrile to completely dry. After each fraction was digested with trypsin overnight at 37ºC, peptides were extracted from the gel using 5% formic acid and 50% acetonitrile in water for 45 minutes. After extraction, peptides were concentrated by speed vacuum concentrator (Genevac EZ-2 Elite) and then re-suspended with 30 µl of 0.1% formic acid in water for LC/MS injection.

2.2.16.1 LC/MS analysis

All samples were analyzed using a Thermo Scientific Q-Exactive Plus Orbitrap hybrid mass spectrometer (Thermo Fisher Scientific, Waltham, MA, USA), which was equipped with an HPLC (Dionex Ultimate 3000 nanoRSLC), an autosampler (HTC PAL, CTC Analytics), and a nanoelectrospray ion source. Each sample, 5µl volume, was separated on a Zorbax 300SB C18 column (0.3 × 150 mm; Agilent, Agilent Technologies, Waldbronn, Germany) at 40 °C. A one-hour gradient was employed (1%B to 32%B in 45 min, 32%B to 45%B in 15 min, with a final wash at 75%B for 5 min and re-equilibration at 1%B for 10 min.). A flow rate of 3.5 µL/min was used for peptide separation. The heated capillary temperature was 300 °C, and 1.9 kV spray voltage was applied to all samples. Mass spectrometer settings were, full MS scan range 350 to 1500 m/z, with a mass resolution of 70,000,30 µs scan time, and AGC set to 1 × e6 ions and fragmentation MS2 of the 20 most intense ions.

2.2.16.2 Protein identification

Protein identification was performed using Proteome Discoverer software v2.2, combining results from Sequest HT and Mascot. Uniprot Danio rerio (zebrafish) (Brachydanio rerio) reference proteome (UP000000437), and the common Repository of Adventitious Proteins (cRAP; http://www.thegpm.org/crap/), was used for identification. Search parameters for both algorithms were; trypsin enzyme, a maximum of two missed cleavages, with precursor and fragment mass tolerance set to 20 ppm and 0.02 Da, respectively. Carboxyamidomethylation of cysteine was set as a fixed modification, while methionine oxidation, asparagine, and glutamine deamidation, and N-terminal acetylation were set as variable modifications. The results were filtered using a False Discovery Rate of <1% as a cutoff threshold, determined by the Percolator algorithm in Proteome Discoverer software. The differentially regulated proteins more than 1.5-fold consistently in all three biological replicas are considered differentially regulated in mutants and further used for GO analysis.

2.2.17 Statistics

The significance of differences between groups (wild type vs mutant) was tested using GraphPad Prism (GraphPad Software Version 9.1.2). The statistics used for comparison are noted in the figure legends. The data are presented as a mean ± SD. A statistically significant p-value of 0.05 was used. The number of biological replicates used per experiment is represented on each graph and in figure legends. Experiments were repeated until obtaining ≥ 3 biological replicates.

2.3 Results:

2.3.1 Phenotype of *rw337* mutant zebrafish

rw337 is a recessive lethal mutation isolated by a large-scale N-ethyl-N-nitrosourea (ENU)-induced mutagenesis performed at RIKEN. *rw337* heterozygous embryos result in no phenotype. However, *rw337* homozygous mutants show comparatively smaller eyes from 4 dpf (Figure 2-1), followed by curl-down body shape and embryonic death by 7-8 dpf. Other phenotypes of development appear normal, including touch responses, heart formation, and pigmentation. However, the swim bladder is reduced in size. Because *rw337* mutant eyes were smaller, the tissular phenotype of retinas was evaluated at 4 dpf. Plastic sections with toluidine blue staining of retinal tissues were performed. *rw337* mutants had abnormally aggregated cells with pyknotic nuclei representing dying cells (Figure 2-2 C), whereas wild type embryos had their

characteristic multi-layered neural retina (Figure 2-2 A). These pyknotic cells suggested that cellular level defects in the mutant retina were likely to accumulate dead cells. The mutant retina also revealed that neuronal cells in the outer nuclear layer (ONL) are severely defected (Figure 2-2 B).

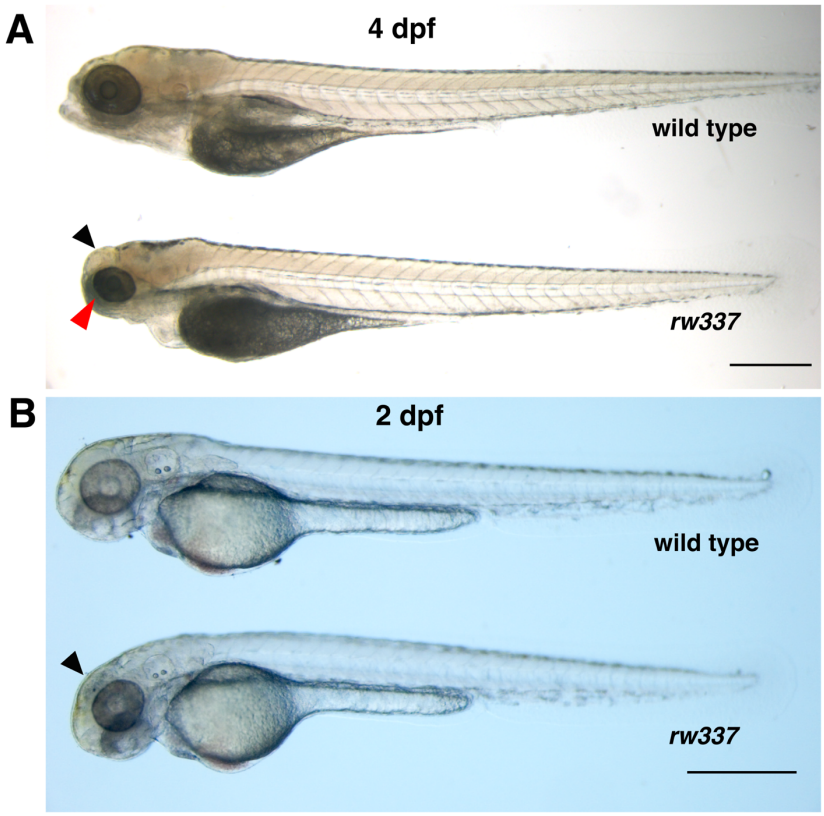

Figure 2-1: *rw337* mutant phenotype
Whole-body phenotype of wild type and *rw337* mutant embryos at (A) 4 dpf (B) 2 dpf . *rw337* mutant embryos show smaller eyes compared to wild type at 4 dpf (red arrow). The black arrow shows cloudy tectum in *rw337* mutant embryos representing cell death. Scale bar = 100 µm.

2.3.2 *rw337* mutants encode mutation on gene *banp*

rw337 mutation was mapped to the gene *banp* on chromosome 25 (Figure 2-3 A). The nucleotide T at the exon 4 and intron 4/5 junction is mutated to G, which results in an alteration at the donor splice site of exon 4 from GT to GG. This mutation causes a splicing error in exon 4, resulting in the insertion of 52 nucleotides from intron 4/5 along with an extra stop codon in *rw337* mutant exon 4 (Figure 2-3 B). qRT-PCR analysis to detect *banp* mRNA using primer spanning exon 4-exon 5 junction showed a significant reduction of *banp* mRNA in $banp^{rw337}$ mutant embryos (Figure 2-3 D). This exon 4 specific qRT-PCR confirmed the defective splicing in *banp* mRNA in $banp^{rw337}$ mutants. The newly introduced premature stop codon in mutant mRNA is predicted to impair functional protein production (Figure 2-3 C), resulting in loss of function of Banp and phenotypic defects in $banp^{rw337}$ mutant embryos.

2.3.3 *banp*^{sa12976} mutant embryos show phenotype similar to *banp*^{rw337} mutants

In order to confirm the loss of function of gene *banp* and its observed retinal phenotypes in *banp*^{rw337} mutants, we examined another *banp* mutant allele, *sa12976*, provided by Zebrafish International Resource Center, ZIRC (Oregon University, USA). This mutant allele also carries a mutation in exon 4 (Figure 2-4 A). *banp*^{sa12976} has a point mutation in which a **C** is mutated to **T**, leading to a premature stop codon (Figure 2-4 B). After acquiring the fish line, heterozygous mutant male and female pairs are identified via genotyping and intercrossed to collect homozygous mutant embryos. Homozygous *banp*^{sa12976} mutants show morphological defects very similar to *banp*^{rw337} mutants (Figure 2-5 B). They show a smaller eye phenotype and accumulation of pyknotic cells in the retinas at 4 dpf (Figure 2-5 F). Additionally, heterozygous *sa12976* (*banp*$^{sa12976+/-}$) and *rw337* (*banp*$^{rw337+/-}$) were intercrossed to generate a trans-heterozygous *banp*$^{sa12976/rw337}$ mutant. This heteroallelic combination of *banp* mutants exhibits the same phenotype and retinal defect as the *banp* mutant lines (Figure 2-5 C,G). These results confirm that the retinal phenotype in *banp*^{rw337} mutants results from loss of function of Banp. *banp*^{rw337} line is used for further study because the mutation is found to be stable over multiple generations and has exhibited mendelian inheritance in various genetic backgrounds.

2.3.4 *banp* morpholino knock down in zebrafish phenocopied *banp*^{rw337} mutants

Morpholino (MO) is an efficient tool to knock down specific genes. ATG morpholinos inhibit protein translation and thus function by targeting the ATG start site of mRNA. A *banp* specific ATG MO was generated to target and knock down functions of Banp protein. To assess the phenotype of embryos, *banp* ATG MO was injected at the single-cell stage. A control morpholino with 5 mismatch sequences in *banp* ATG MO was used to evaluate off-target effects of morpholino injection. The phenotype of *banp* morphant embryos was compared to *banp*^{rw337} mutants to evaluate the efficiency and concentration of banp-MO. 1mMol MO injections showed a phenotype very similar to *banp*^{rw337} mutants (Figure 2-5 D, H). *banp* morphants exhibited phenotypic and retinal defects similar to *banp*^{rw337} mutants (Figure 2-5H). This morpholino-based inhibition of Banp protein in zebrafish confirms that the retinal defects observed in *banp*^{rw337} mutants are due to the loss of function of Banp protein.

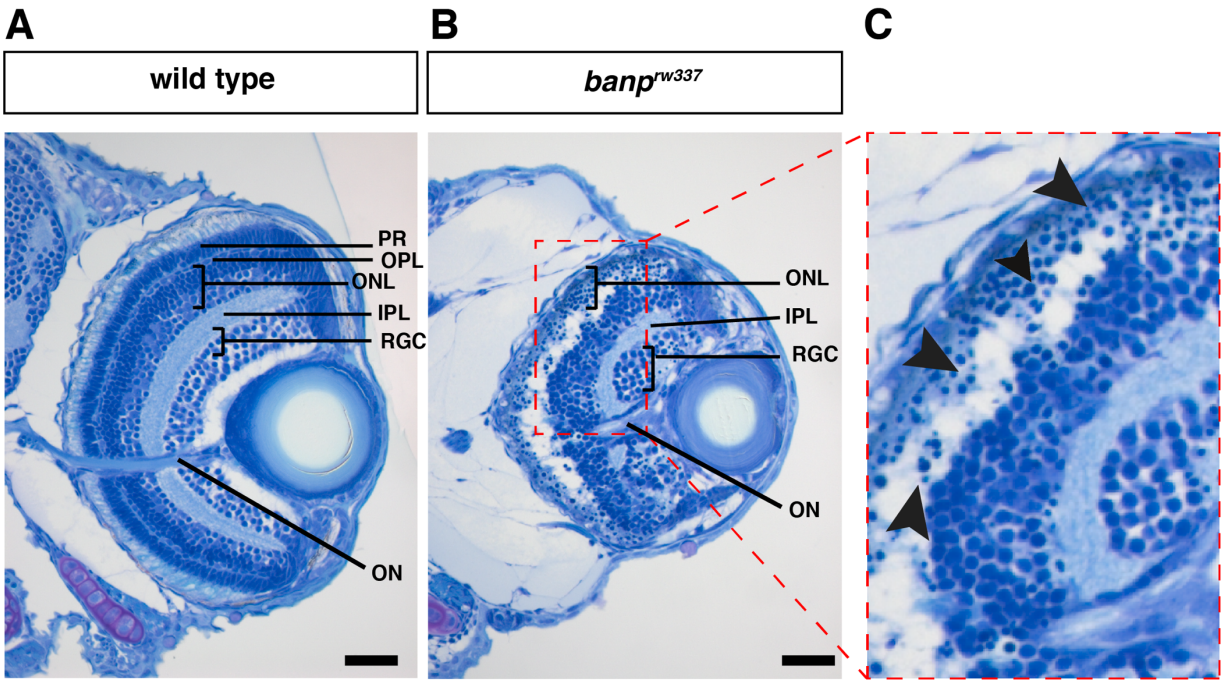

Figure 2-2: Retinal defects in *banp*^{rw337} mutants at 4dpf
A) A wild type zebrafish retina representing its intact neuronal layers. B) *banp*^{rw337} mutant retina showing a defect in neuronal layers. OPL shows severe damage. C) magnified *banp*^{rw337} mutant retina showing accumulated pyknotic cells (black arrowhead). PR-photoreceptor, OPL-outer plexiform layer, IPL- inner plexiform layer, ONL-outer nuclear layer, RGC-retinal ganglion cells, ON-optic nerve. Scale bar =20 µm.

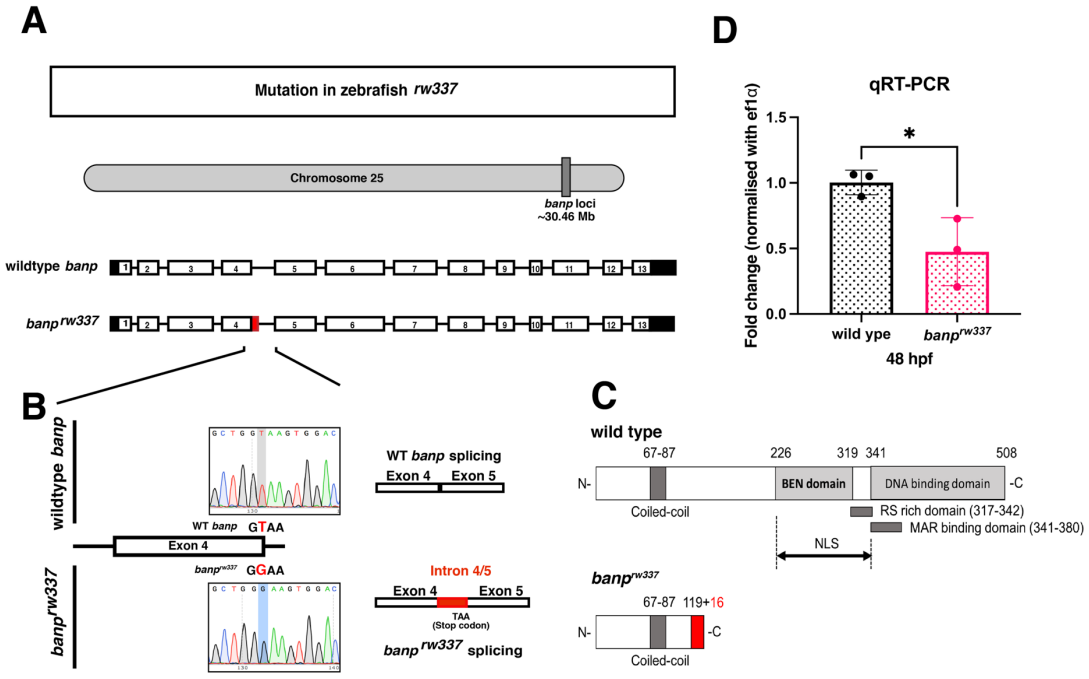

Figure 2-3: Mutation map of *banp*^{rw33} mutant fish line
A) In *banp*^{rw337,} the mutation is mapped to the gene *banp* on chromosome 25. Wild type *banp* mRNA contains 13 exons, whereas *banp*^{rw337} mutants have an additional intronic region at exon 4 (red region at exon 4).

B) In *banp*^{rw337} mutants, T at the exon-intron junction of exon 4 is converted to G (bottom panel), which results in a mutation at the donor splice site of exon 4 from GT to GG. This mutation compromises the splicing at exon 4, causing the insertion of 52 nucleotides from intron 4 (red region) with an additional stop codon (TAA) at exon 4.
C) Structural domains of wild type Banp protein (top). Predicted protein in *banp*^{rw337} mutants (bottom).
D) qRT-PCR evaluation showing *banp* mRNA expression at 48 hpf. Mann Whitney test. [n=3 $p < 0.05$ (*)].

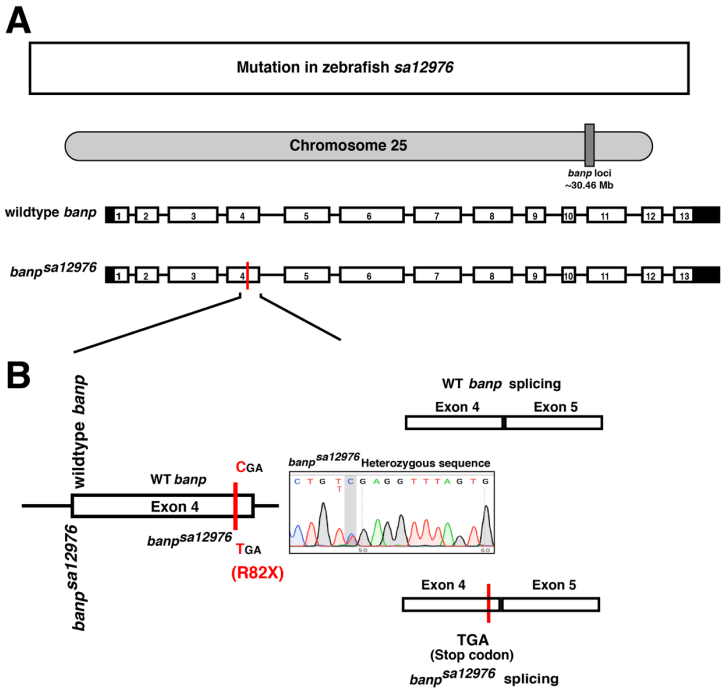

Figure 2-4: Mutation map of *banp* ^{sa12976} mutant fish line
A) Map of *banp*^{sa12976} mutation. Wild type *banp* mRNA contains 13 exons. *banp*^{sa12976} mutant fishes have a mutation on exon 4.
B) In *banp* ^{sa12976} mutants a C is converted to T. This mutation introduces an additional stop codon (TGA) at exon 4 (bottom panel). This premature stop codon at exon 4 in *banp* ^{sa12976} mutant embryo is predicted to form a truncated protein compromising the function of Banp.

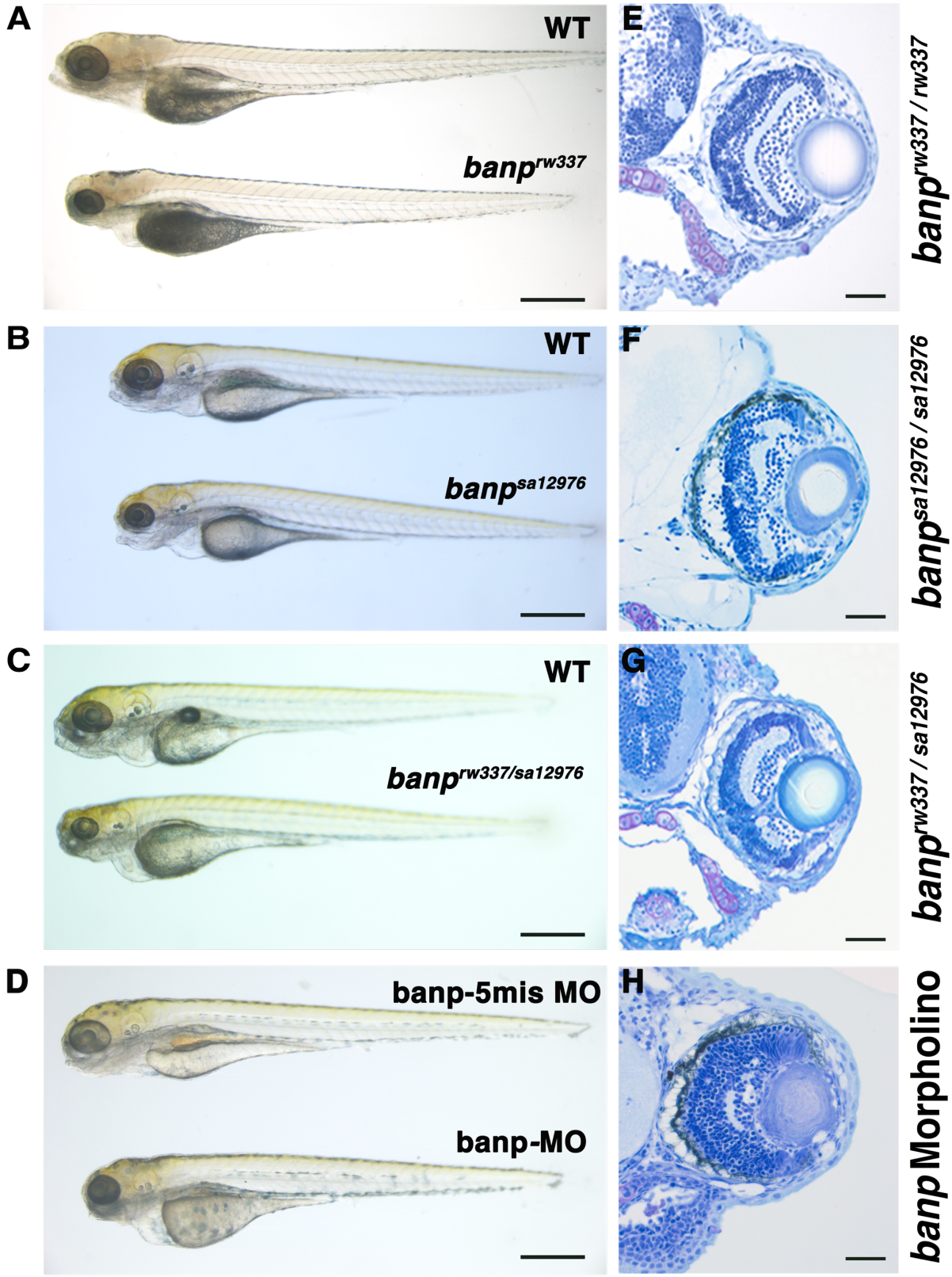

Figure 2-5: Phenotype of *banp* knock out zebrafish at 4dpf
The whole-body phenotype of wild type (WT) or banp-5mis control embryos compared to respective mutants or *banp* morphants at 4 dpf. A) $banp^{rw337}$ ID pair intercross B) $banp^{sa12976}$ ID pair intercross C)

Crosses between heterozygous parent line *rw337* and *sa12976* generating transheterozygous *banp* mutant D) wild type oki embryos injected with banp-5mis and banp morpholino knockout. All mutant and morphant embryos show smaller eyes than WT or banp-5mis control embryos. Scale bar =100 µm. (E-H) Toluidine blue stained retinas of mutants with respective genotype and *banp* morphant. All retinas showed a similar phenotype with an accumulation of pyknotic cells and defected OPL compared to a wild type retina in Figure 2-2 A. Scale bar =20 µm.

2.3.5 Banp protein localization into the nucleus is conserved in zebrafish

We have seen that Banp can perform a variety of critical regulatory functions (Literature review-Chapter 1). However, none has been reported in zebrafish to date. Therefore, first, in order to evaluate the localization of zebrafish Banp protein (zBanp), a banp(wt)-EGFP construct was generated. This C-terminal EGFP reporter tagged banp construct was initially injected to *banp*^{rw337} embryos to evaluate whether banp(wt)-EGFP mRNA could rescue mutant phenotype. Following injection, 54 hpf *banp*^{rw337}embryos were stained with AO and found to be AO negative. Further genotyped using PCR to identify the mutants. banp(wt)-EGFP injection revealed that overexpressing zBanp indeed rescued the cell death in the mutant retina at 54 hpf (Figure 2-6 G, H). However, banp(rw337) mutant-EGFP did not (Figure 2-6 K, L). This cell death rescue study upon zBanp over expression demonstrates that a lack of function of Banp causes the cell death phenotype and that the banp(wt)-EGFP construct mimics functional Banp in zebrafish. Hence, banp(wt)-EGFP was further used for protein localization studies.
Interestingly, both N-terminal and C-terminal EGFP incorporation to zBanp showed nuclear localization (Figure 2-7 A). Furthermore, at the one-cell stage, we co-injected mRNA encoding banp(wt)-EGFP and *banp*-MO and discovered that banp-MO inhibited the expression of banp(wt)-EGFP while the control-MO did not (Figure 2-7 B, C). This specific inhibition of EGFP expression of banp(wt)-EGFP constructs confirms the specificity of banp-MO once more.

banp(wt)-EGFP localization is visualized at 24 hpf. banp(wt)-EGFP localizes to the nucleus (Figure 2-7 A and Figure 2-8 A). It is consistent with what has been observed in mammals (Singh, Sinha et al. 2009, Chemmannur, Badhwar et al. 2015). This study suggests that Banp protein localization in the nucleus is conserved in zebrafish. During live-cell division, the localization dynamics of the zBanp protein are studied. Throughout division, the majority of the time, Banp expression is in the nucleus (Figure 2-8 A). However, right before cytokinesis, the expression is diminished (Figure 2-8 B). This reduced expression occurs likely during the late mitotic phase of the cell cycle (Figure 2-8 B). Nuclear expression reappears shortly after cytokinesis. This expression dynamics during cell division leads us to speculate on the possible role of Banp during cell division.
PRALINE protein conservation analysis revealed that the region 210 to 350 (Figure 2-9) corresponding to the BEN domain is conserved across zebrafish, mice, and humans. Proteins with the BEN domain show DNA binding properties, protein binding properties, transcription factor activity, and adaptors to recruit chromatin-modifying complexes (Abhiman, Iyer et al. 2008, Malonia, Sinha et al. 2011, Nakayama, Sakashita et al. 2020). Several examples confirming the BEN domain's characteristics in Banp have been reported (Malonia, Sinha et al. 2011, Chemmannur, Bhagat et al. 2016, Mathai, Mittal et al. 2016, Bhagat, Jadhav et al. 2018). These evidence of conserved nuclear localization and BEN domain relates to the possibility of conserved transcription regulation or nuclear functions by Banp in vertebrates.

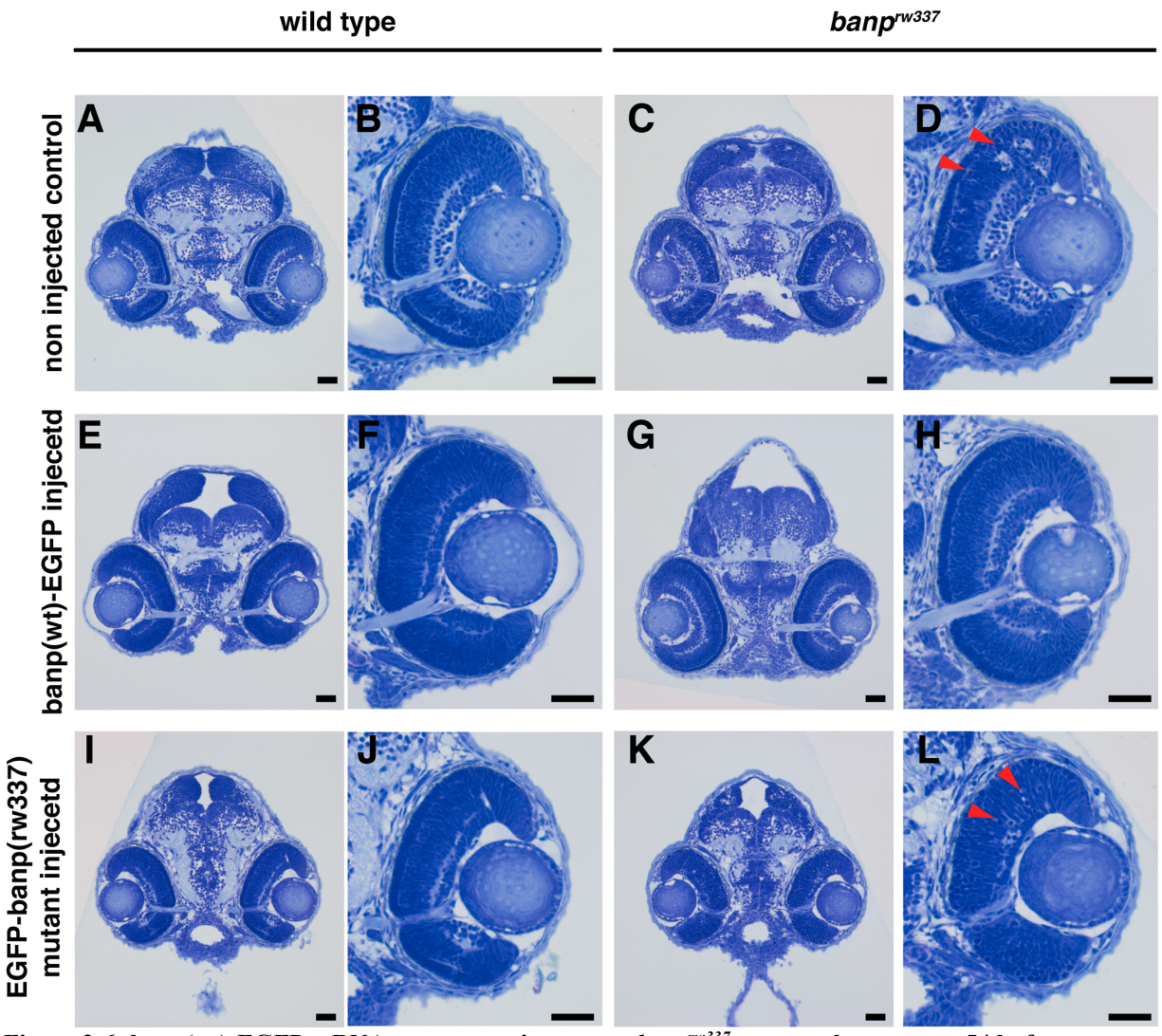

Figure 2-6: banp(wt)-EGFP mRNA overexpression rescue *banp*^{rw337} mutant phenotype at 54 hpf

Tissue morphology at 54 hpf A) wild type embryo head B) wild type retina C) *banp*^{rw337} mutant embryo head D) *banp*^{rw337} mutant retina. C-D shows pyknotic cells indicating cell death.

banp(wt)-EGFP mRNA overexpressed embryos E) wild type embryo head F) wild type retina G) mutant embryo head H) mutant retina. G-H shows rescue of cell death in *banp*^{rw337} mutant with morphology comparable to wild type. EGFP-banp(rw337) mutant mRNA overexpressed embryos I) wild type embryo head J) wild type retina. K) mutant embryo head L) mutant retina. K-L shows pyknotic cells indicating cell death.

Red arrow indicates pyknotic cells. Scale bar =20 µm.

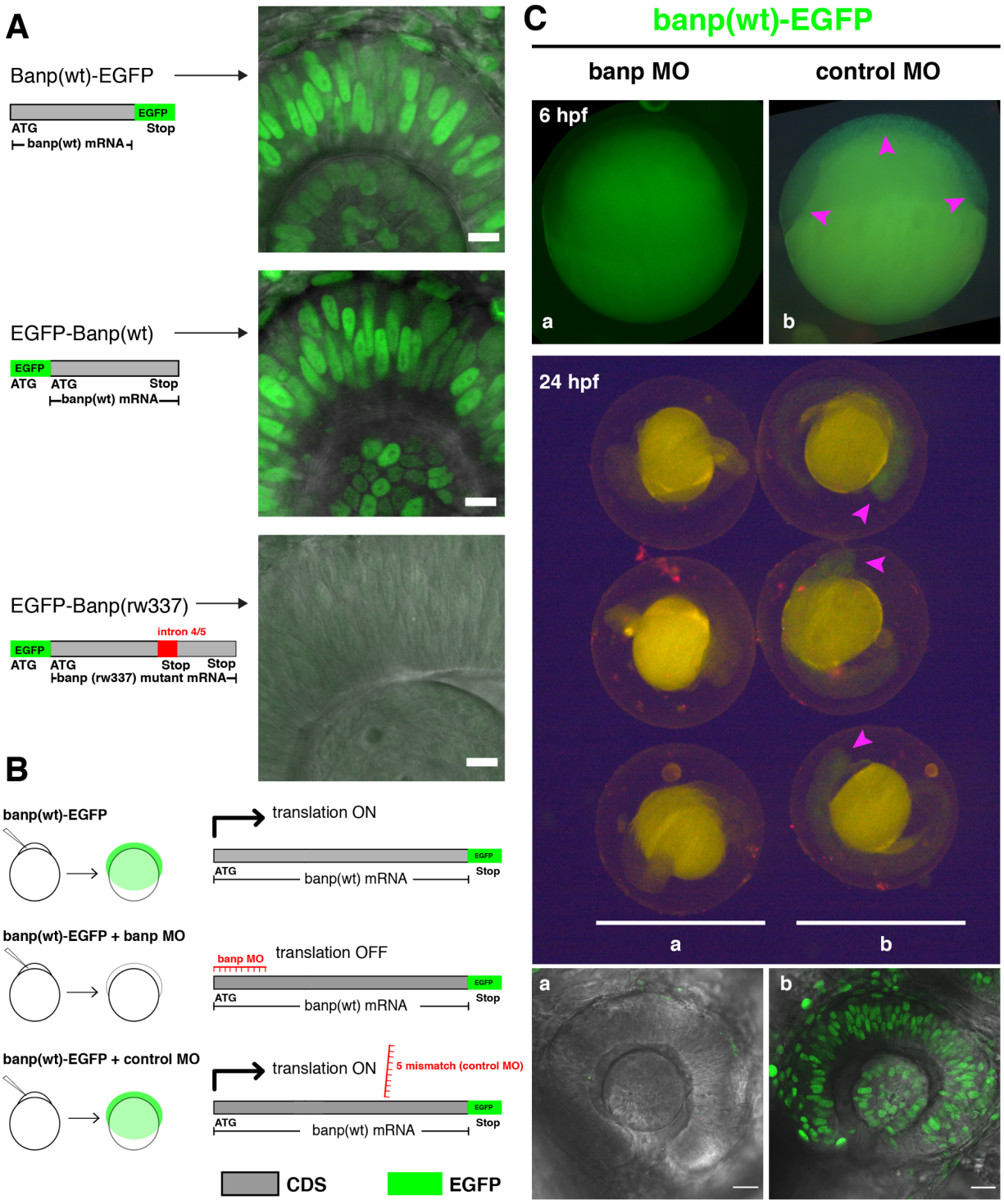

Figure 2-7: *banp* ATG morpholino inhibits the expression of Banp protein.
(A) Expression of banp(wt)-EGFF, EGFP-banp(wt) and EGFP-banp(rw337) mRNA in zebrafish retina at 1dpf. Wild type *banp* mRNA expression shows nuclear localization of Banp irrespective of the location of the EGFP reporter. Wild-type Banp is localized in the nucleus, indicating that nuclear localization is conserved in zebrafish Banp. EGFP-banp(rw337)mutant mRNA over expression show no EGFP expression, suggesting that the non-sense mutation decay mechanism probably degrades EGFP-Banp(rw337). (Scale bar: 10 μm)

(B) Experiment design to check the specificity of banp-MO and control-MO (banp-5mis MO).
(C) (a) Embryos co-injected with banp-MO and banp(wt)-EGFP mRNA. banp-MO effectively inhibits the translation of Banp(wt)-EGFP protein in zebrafish embryos injected with RNA encoding Banp(wt)-EGFP. (b) banp(wt)-EGFP mRNA con injected with control morpholino (banp-5mis MO). banp-5mis MO did not inhibit the translation of Banp(wt)-EGFP protein (red arrow). Bottom most panel show expression in retina at 24 hpf. Scale bars: 20μm. Taken together suggesting that banp-MO specifically inhibits Banp protein translation.

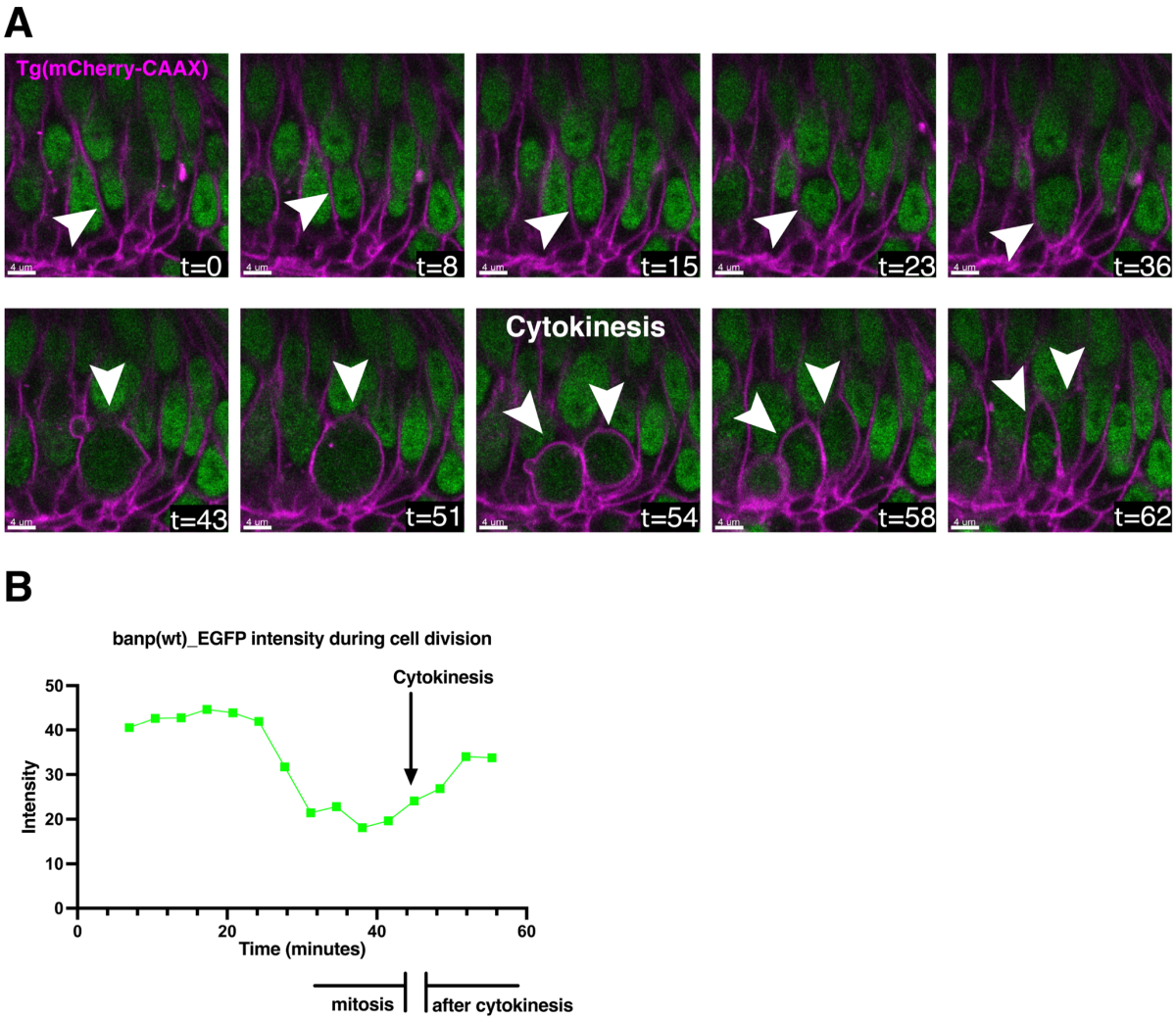

Figure 2-8: Banp(wt)-EGFP is localized in the nucleus during the interphase.
(A) Time-lapse confocal scanning of mitosis of *Tg[EF1α:mCherry-CAAX]* transgenic wild type retinal cells expressing Banp(wt)-EGFP. EGFP fluorescence is indicated in green, whereas mCherry-CAAX fluorescence labels plasma membrane and is indicated in magenta. White arrowheads indicate time-lapse change of a retinal progenitor cell undergoing mitosis. Banp(wt)-EGFP is localized in the nucleus in the interphase, whereas it spreads into the whole cell region during mitosis. Scale bars =4 μm. (B) Histogram of intensity of Banp(wt)-EGFP during cell division shown in (A). Signals decline from mitosis to cytokinesis.

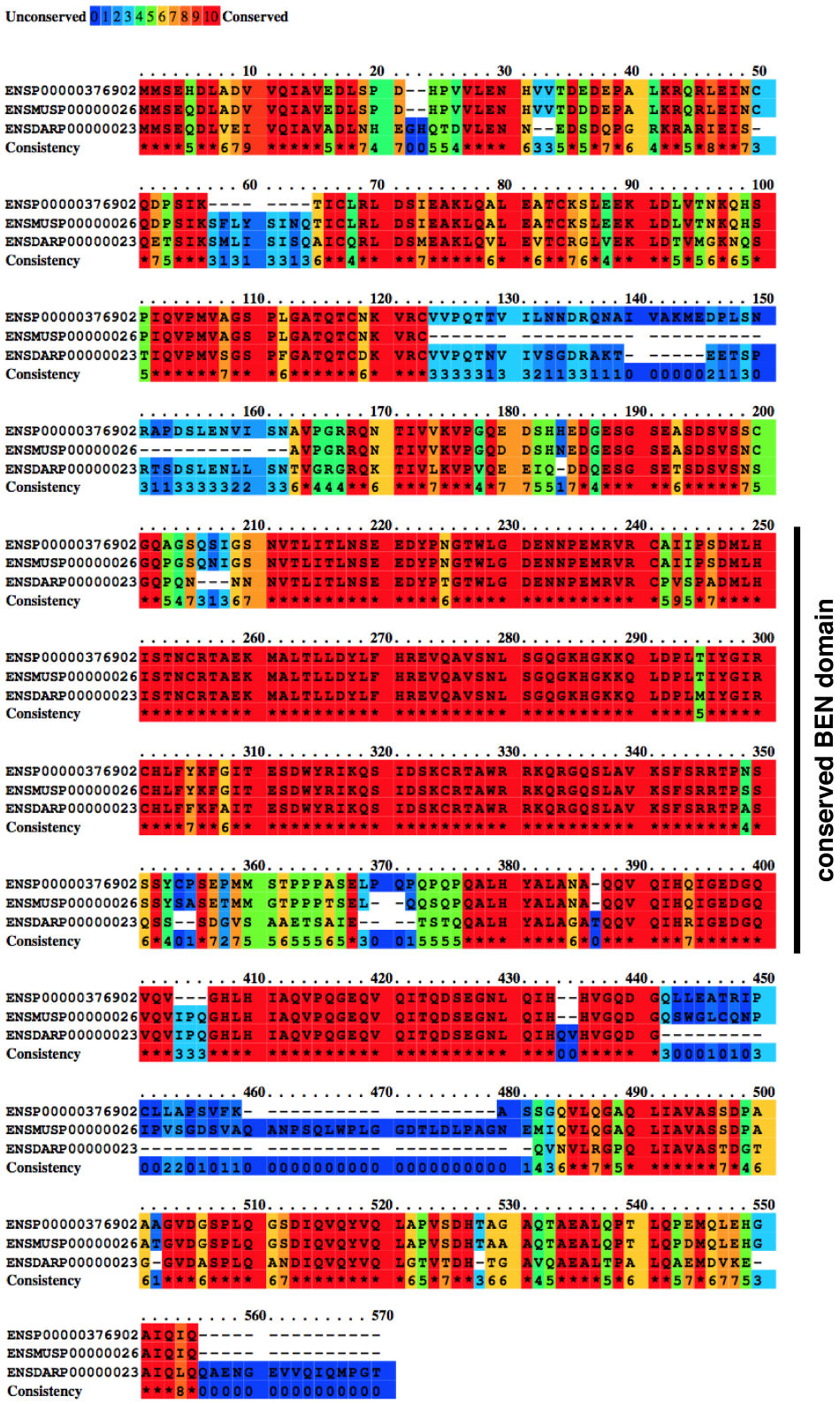

Figure 2-9: Evaluation of Banp protein conservation across humans, mice, and zebrafish. Analysis of protein conservation using PRALINE.

Results color-coded for amino acid conservation. The conservation scoring is performed by PRALINE. The scoring scheme works from 0 for the leased conserved alignment position up to 10 for the most conserved alignment position.

2.3.6 Spatial and temporal expression of *banp* mRNA during zebrafish development

So far, only one transcript variant of *banp* has been identified in the zebrafish genomic database. It suggests that *banp*^{rw337} mutation can cause loss of function of *Banp* without compensation by its duplicates. Indeed *banp* whole-body knockout causes embryonic lethality in zebrafish, similar to what has been reported in mice (Chemmannur, Badhwar et al. 2015). This embryonic lethality suggests that the banp may play an essential role in vertebrate development. We examined the spatiotemporal expression of *banp* mRNA in developing zebrafish embryos to understand the potential developmental function. We developed *banp* in-situ hybridization probes to study mRNA expression patterns during development. Our whole mount in-situ hybridization (WISH) study revealed that *banp* has ubiquitous maternal (Figure 2-10 A, 4 cell stage) and zygotic (Figure 2-10 A, 5 somite) expression in embryos emphasizing its importance during early vertebrate development. *banp* mRNA expression is ubiquitous from the single cell to 30 hpf (Figure 2-10 A), but by 48 hpf, it is restricted to the central nervous system (CNS). We observed specific expressions of *banp* in the brain at 48 and 72 hpf (Figure 2-10 A), indicating that *banp* expression is related to neuronal development. *banp* mRNA was ubiquitously expressed in the neural retina at 21 somite, 23 hpf and 30 hpf, suggesting that retinal progenitor cells express *banp* mRNA (Figure 2-10 A, R). Transverse sections of embryo at 24 hpf show ubiquitous expression in retina and at 48 hpf it show an expression at CMZ confirming that retinal progenitor cells express *banp* mRNA (Figure 2-10 B, CMZ). It is worth mentioning that towards 5 dpf, *banp* expression gets restricted to lateral lines (LL), which are sensory organs known to have a stem cell nature (Lush, Diaz et al. 2019). It will be interesting to study the function of *banp* in lateral lines in the future. My research uses the zebrafish neural retina as a model to investigate the developmental function of gene banp under physiological conditions.
The *banp* mutations are predicted to make nonfunctional Banp protein. I thought to visualize *banp* mRNA in mutant embryos. WISH with the *banp* mRNA probe showed that the levels of *banp* mRNA were significantly lower in *banp*^{rw337} mutants (Figure 2-11), implying nonsense-mediated decay of mutant *banp* mRNAs.

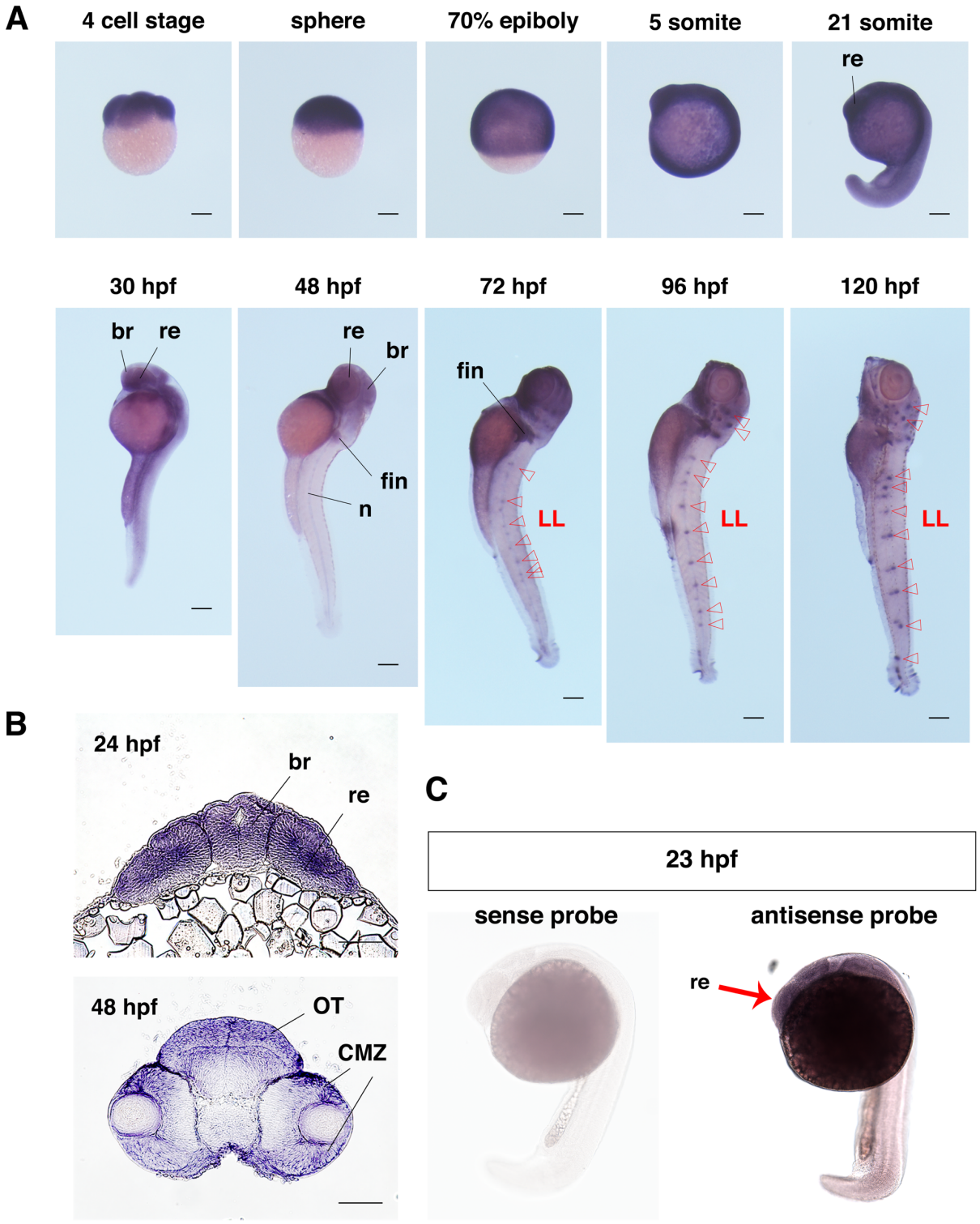

Figure 2-10: Spatial and temporal expression pattern of zebrafish *banp* mRNA transcript:
(A) Whole-mount in situ hybridization of zebrafish banp mRNA probe. *banp* mRNA is expressed in the 4-cell stage, suggesting maternal expression. *banp* mRNA is ubiquitously expressed during development from the sphere stage until the 21-somite stage. mRNA expression is restricted in the brain including the retina at 30 hpf. At 48 hpf, mRNA is prominently expressed in the brain, fins, and notochord. At 72 hpf

and later, mRNA expression appears in neuromasts of the lateral lines (red open arrowheads). br, brain; re, retina; LL, neuromasts of the lateral line; n, notochord. Scale bars: 200 μm.
(B) Frontal sections of zebrafish head labeled with *banp* RNA probe at 24 hpf and 48 hpf. *banp* mRNA is expressed in the entire neural retina at 24 hpf and in the CMZ at 48 hpf, suggesting the expression of *banp* mRNA in retinal progenitor cells. OT, optic tectum; CMZ, ciliary marginal zone. Scale bars: 50 μm
(C) Whole-mount RNA in-situ hybridization using sense and antisense *banp* probe at 23 hpf. re, retina.

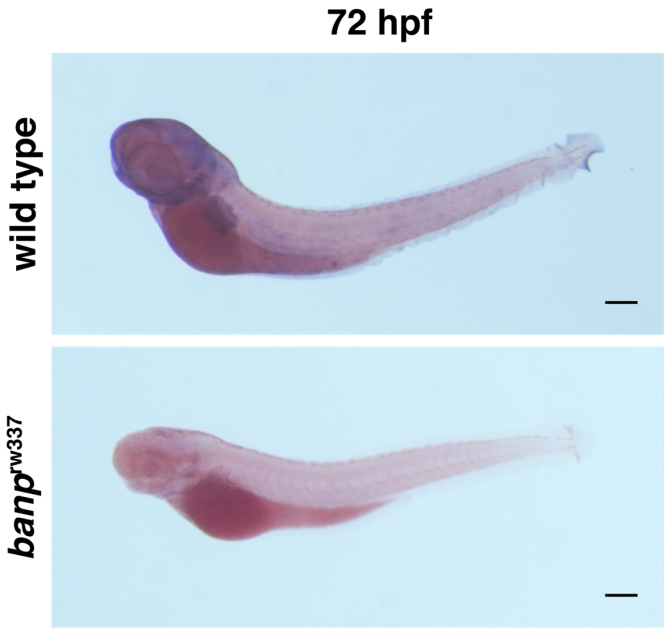

Figure 2-11: *banp* whole mount in-situ hybridization on *banp*^{rw337}
Whole mount *In-situ* hybridization showing the mRNA expression of gene *banp*. *banp* mutant embryos show reduced mRNA expression in comparison to wild type. Scale bar = 200 μm

2.3.7 Cellular defects in *banp*^{rw337} mutants at 4 dpf

The mutant retina lacks the outer plexiform layer and a fully developed photoreceptor layer. However, isolated photoreceptor cells were observed (Figure 2-5 E). At 4dpf, a wild type zebrafish retina consists of five types of differentiated neurons and muller glia arranged in a stereotypic layered structure. Hence, to understand the state of cellular differentiation in mutant retina, I analyzed whether all cell fates are achieved in *banp*^{rw337} mutants. For specific retinal cell types, cell-specific markers were used to confirm cellular differentiation and laminar positioning of cells at 4dpf. Immunolabeling using ath5:EGFP (RGCs), Pax6 (RGCs and amacrine cells), Prox1 (bipolar cells and horizontal cells), glutamine synthetase (Müller cells), and zpr1 (green/red cone photoreceptors) and phalloidin (filamentous actin) revealed that most retinal cell-types differentiate by 4 dpf in *banp*^{rw337} mutants (Figure 2-12), except photoreceptor cells, which were significantly reduced at 4 dpf (Figure 2-12 H). Immunolabeling also revealed a decrease in the overall number of neurons. Mild disruption of retinal lamination and loss of the outer plexiform layer was observed as visualized from phalloidin labeling (Figure 2-12 M, N). Overall, immunolabeling in the retina revealed that *banp*^{rw337}mutants show the possibility of neuronal degeneration, yet laminar patterning and cell type determination are not eliminated at 4dpf.

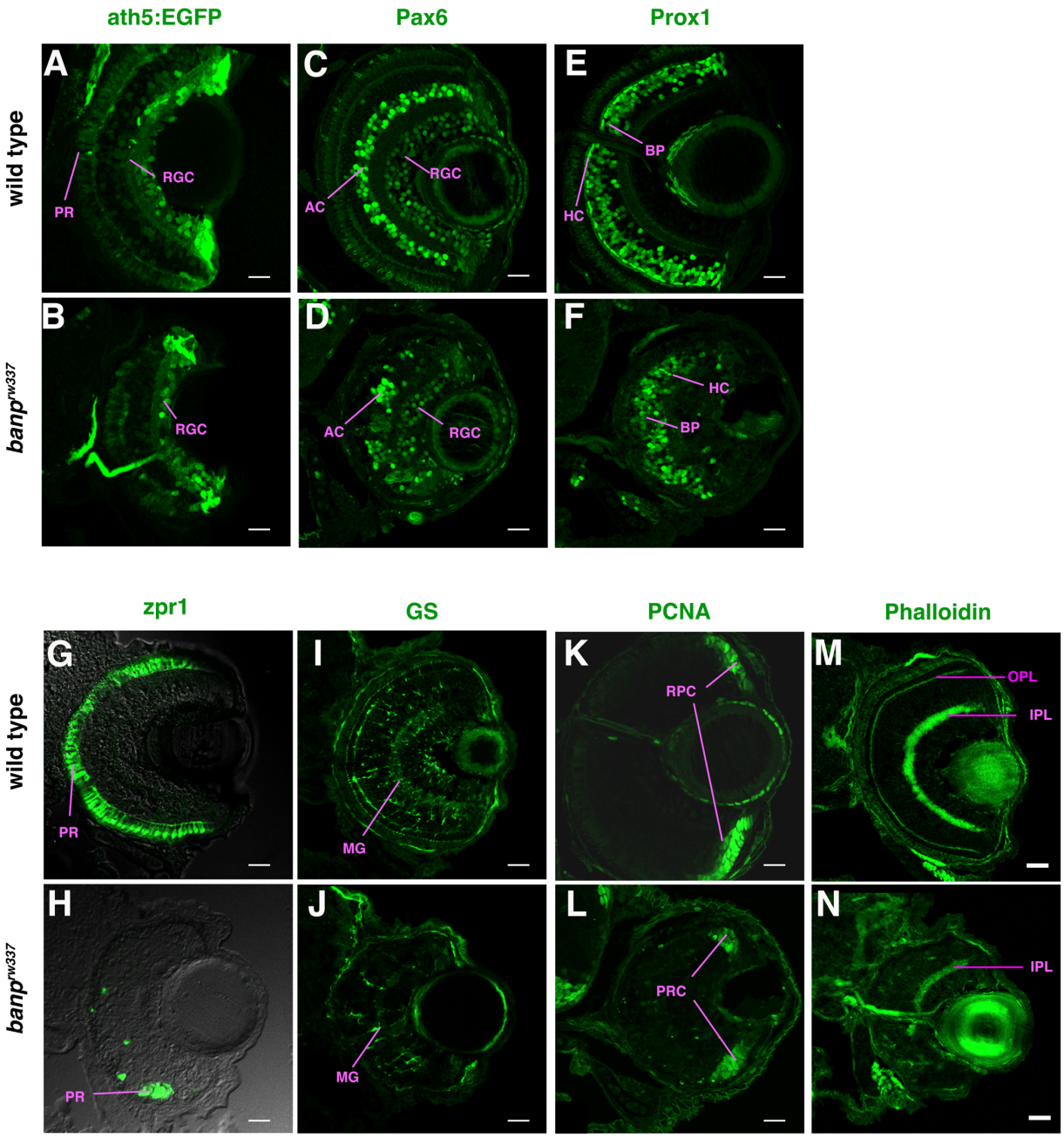

Figure 2-12: *banp*^{rw337} mutants show differentiation of retinal neurons at 4 dpf.
(A, B) ath5:EGFP expression in wild type (A) and *rw337* mutant (B) retinas at 4 dpf. ath5:EGFP is strongly expressed in RGCs and weakly expressed in amacrine cells and photoreceptor precursors. In *rw337* mutants, ath5:EGFP expression in RGCs, amacrine cells and photoreceptor precursors is detected.
(C, D) Wild type (C) and *rw337* mutant (D) retinas labeled with anti-Pax6 antibody at 4 dpf. Pax6 is strongly expressed in amacrine cells and weakly expressed in RGCs. In *rw337* mutants, amacrine cells seem to be decreased in number.
(E, F) Wild type (E) and *rw337* mutant (F) retinas labeled with anti-Prox1 antibody at 4 dpf. Prox1is expressed in bipolar cells and horizontal cells. In *rw337* mutants, both bipolar-like round nuclei and horizontal-like flat nuclei are observed, but horizontal-like cells are very few.

(G, H) Wild type (G) and *rw337* mutant (H) retinas labeled with zpr1 antibody at 4 dpf. zpr1 antibody labels double-cone-type photoreceptors in zebrafish. In *rw337* mutants, only a small cluster of zpr1-positive cells is observed in the ventro-nasal retina, suggesting that a majority of photoreceptors fail to differentiate in *rw337* mutants.
(I, J) Wild type (I) and *rw337* mutant (J) retinas labeled with anti-GS antibody at 4 dpf. Anti-GS antibody labels Müller cells. In *rw337* mutants, Müller cells are decreased in number.
(K, L) Wild type (K) and *rw337* mutant (L) retinas labeled with anti-PCNA antibody at 4 dpf. Anti-PCNA antibody labels retinal progenitor cells in the CMZ at 4 dpf. In *rw337* mutants, retinal progenitor cells are maintained in the CMZ.
(M, N) Phalloidin labeling of wild type (M) and *rw337* mutant (N) retinas. Phalloidin visualizes retinal synaptic layers, the IPL and OPL. In *rw337* mutants, the IPL is detected, but not fully formed on the ventral side. Furthermore, there is no OPL, which is consistent with the lack of photoreceptors in *rw337* mutants. Scale bars: 20μm.
RGC, retinal ganglion cell, AC, amacrine cell; BP, bipolar cell; HC, horizontal cell; PR, photoreceptor; MG, Müller cell; RPC, retinal progenitor cell; OPL, outer plexiform layer; IPL, inner plexiform layer.

2.3.8 Molecular defects in *banp*^{rw337} mutants at 4 dpf

We have seen that the process of differentiation and maturation of neurons is not eliminated in *banp*^{rw337} mutant retinas (Figure 2-12 A-N). Because *banp* has received little attention for its physiological function, the information to define our observed cellular phenotype was limited. Hence, to have a further insight towards the molecular basis of cellular phenotype in *banp*^{rw337} *mutants,* I sought to identify differentially expressed mRNA and protein at 4 dpf in mutants. First, we performed RNA-sequencing on three independent pools of embryo heads at 4 dpf from wild type and mutant samples. Per sample, illumina sequencing generated more than 150 million paired end reads from cDNA libraries. Reads were then mapped as protein-coding genes. Among detected protein-coding genes, 241 were upregulated, and 568 were downregulated (Figure 2-13 C). Our gene ontology analysis revealed that, among upregulated genes, the highest number of genes are enriched in the process of apoptosis and cell cycle regulation (Figure 2-14 A-C).
The top few upregulated targets are *tp53*, *caspase8*, *ccng1*, and *smc1*. These genes have previously been linked to cell cycle arrest and apoptosis in response to DNA damage (Yu and Zhang 2005, Fischer 2017). Upregulation of *caspase8* is likely attributed to cell death and agrees with our *in vivo* phenotype of observed cell death in mutants (Figure 2-2 C). Furthermore, our gene ontology pathway analysis study suggests the possibility of cell cycle arrest in mutants (Figure 2-14 B). Similarly, mass spectrometric protein profiling was performed to detect differentially expressed proteins in mutants at 4 dpf (Table 2-1). Differentially expressed protein targets globally agreed to molecular pathways that were suggested by RNA sequencing data. For example, mRNAs and proteins involved in the process of phototransduction were consistently downregulated (Figure 2-15 C). Our gene ontology pathway analysis from RNA sequencing and protein profiling predicted the downregulation of the photo-transduction pathway. Interestingly, our findings from the histology study corroborate this, revealing that the retina has fewer photoreceptor cells (Figure 2-12 G, H). Overall, this demonstrates that our bulk RNA and protein profiling study can predict the molecular components that cause cellular abnormalities in *banp*^{rw337} mutants.

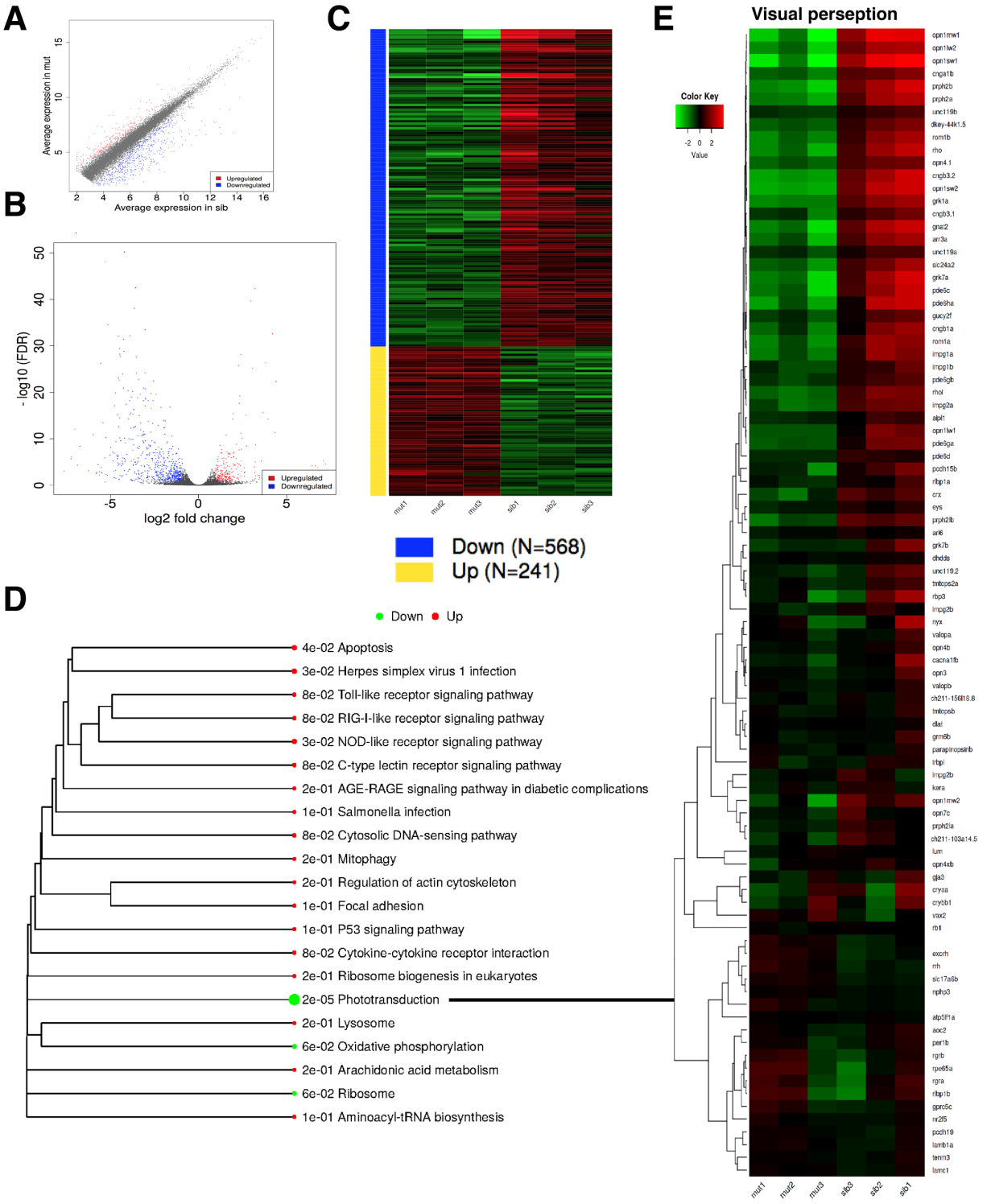

Figure 2-13: Differential expression of mRNA from bulk RNA sequencing at 4 dpf

A) Comparison of average mRNA expression between wild type and *banp*^{rw337} mutants B) Volcano plot obtained from DESeq2 analysis of the wild type and mutant embryos. C) A heat map indicating genes that are differentially expressed more than 2 fold. D) Gene ontology enrichment analysis indicating the biological processes that are differentially regulated in mutants. E) A heat map of genes regulating visual perception and its differential expression in mutants is provided on the right side.

A **Enriched pathways in differentially expressed genes at 4 dpf**

Direction	adj.Pval	nGenes	Pathways
Down regulated	1.3e-25	21	Phototransduction
	3.7e-06	15	Purine metabolism
Up regulated	3.3e-07	9	P53 signaling pathway
	1.6e-05	10	Herpes simplex virus 1 infection
	3.7e-04	8	Apoptosis
	3.7e-04	7	C-type lectin receptor signaling pathway
	4.8e-03	6	Cell cycle
	9.7e-03	6	FoxO signaling pathway

B

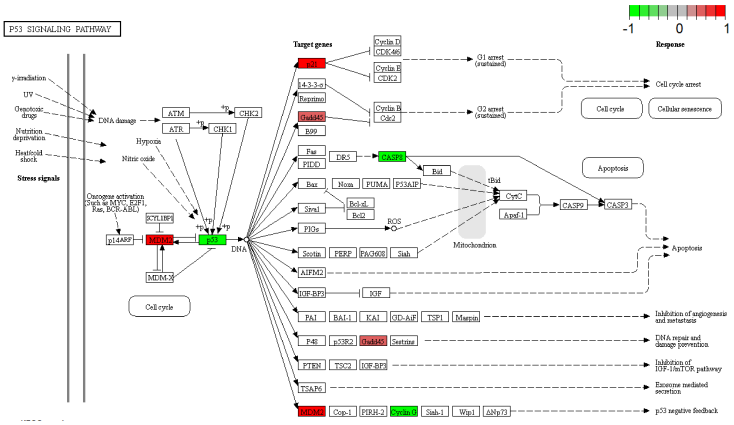

C

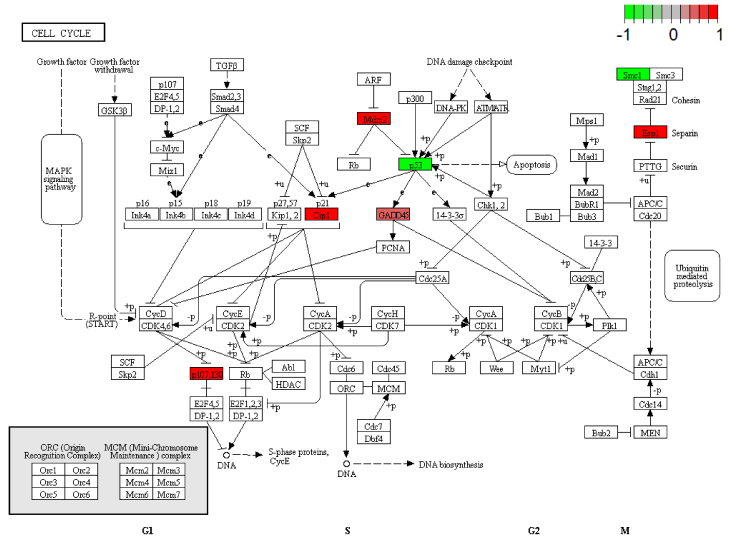

Figure 2-14: Enriched pathways from RNA sequencing at 4 dpf

A) KEGG Gene ontology enrichment analysis indicating top differentially regulated pathways in *banp*^{rw337}mutants. B) tp53 signaling C) Cell cycle. Green represents upregulated, and red represents downregulated genes in mutants.

Upregulated		Downregulated	
Uniprot ID	Protein	Uniprot ID	Protein
A5JEM4	Nuclear distribution protein nudE-like 1-A	Q90WX5	Cone transducin alpha subunit
Q6DGS0	Adaptor-related protein complex 3, sigma 2 subunit	Q9W6A5	OS=Danio rerio GN=opn1mw1 PE=1 SV=2
Q803Q2	Nuclear distribution protein nudE-like 1-B	A0A0R4ID52	Arrestin 3b, retinal (X-arrestin) (Fragment)
Q1LVM0	N-ethylmaleimide-sensitive factor attachment protein, beta b	A0A0R4IPJ0	Guanylate kinase 1b
A0A0R4IQD1	Nuclear distribution protein nudE-like 1-A	A0A0R4IFN4	Guanylate kinase 1b
Q7SXI6	Nuclear distribution protein nudE-like 1-A	B8JJJ6	Guanylate kinase 1b
F1R1G7	Si:dkey-9l20.3	B8JJJ5	Guanylate kinase 1b
A0A140LFT8	Si:dkey-9l20.3 (Fragment)	Q6DH07	Arrestin 3, retinal (X-arrestin), like
A0A0R4IQH9	Heat shock protein 12A	Q6PBM9	Arrestin 3, retinal (X-arrestin)
E9QIJ3	Adaptor-related protein complex 3, sigma 2 subunit	A0A0R4IMS8	Arrestin 3b, retinal (X-arrestin)
F1R1N9	CD2-associated protein	Q08BC3	Si:ch211-133n4.4
E9QD83	Peptidyl arginine deiminase, type II (Fragment)	F1QX07	Interphotoreceptor retinoid-binding protein
B0UYD7	Glutaminyl-tRNA synthetase (Fragment)	F1Q9N9	Interphotoreceptor retinoid-binding protein
A0A0R4IH14	Testis-derived transcript (3 LIM domains)	Q6PC38	Recoverin
F1QNJ3	Testis-derived transcript (3 LIM domains)	A0A0R4ILW6	N-myc downstream-regulated 1a
A5JEM4	Nuclear distribution protein nudE-like 1-A	Q90WX5	Cone transducin alpha subunit

Table 2-1: Top 15 differentially expressed proteins in *banp*^{rw337} mutants.

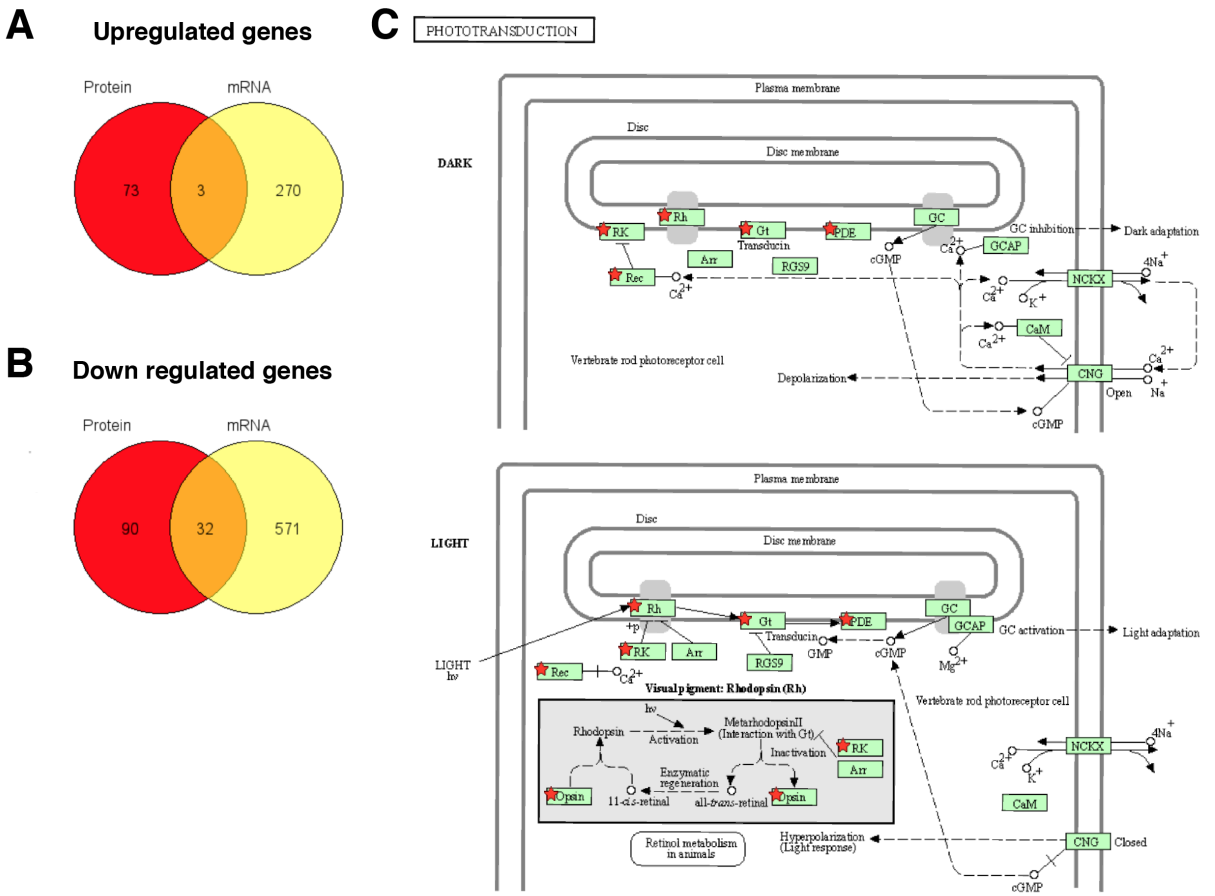

Figure 2-15: Differential expression of proteins from mass spectrometric protein profiling at 4 dpf
A) Venn diagram showing the number of upregulated mRNA and proteins in mutants. B) Venn diagram showing the number of downregulated mRNA and proteins in mutants. C) Genes involved in phototransduction pathway. The pathway was generated using DAVID v6.8; red star indicates downregulated **proteins** in *banp*^{rw337} mutants.

2.3.9 Early-onset of cellular defects in *banp*^{rw337} mutants

Our omics study to identify potential differential regulated molecular pathways primarily suggested evidence of cell death and cell cycle defect. Plastic sections of mutant retina showed cellular defects from 2 dpf (Figure 2-1). In order to confirm the presence of dead cells, we performed TUNEL staining, which enables us to identify and visualize dead cells. Our TUNEL labeling in the retina over the course of development from 24 to 101 hpf revealed that cell death indeed occurs in the mutant retina and starts from 53 dpf in mutants compared to wild type (Figure 2-17 A, C). Furthermore, our gene ontology study suggested the possibility of cell cycle arrest. To validate our *in-silico* prediction, we further evaluated the possibility of an *in-vivo* cell cycle defect. Performed immunofluorescence labeling of retinal tissue with phospho-histone (serine-10) H3 antibody (pH3). pH3 labeling enables us to detect cells that are at the mitotic phase of the cell cycle. The results showed a significant increase in the number of mitotic cells from 53 dpf (Figure 2-17 B, D). The accumulation of mitotic cells was highest in *banp*^{rw337} mutant at 53 hpf compared with later stages (Figure 2-17 B). We speculate that this could be because of higher cell division events in the zebrafish retina during 1 to 2 dpf (Weber, Ramos

et al. 2014). At later developmental stages, the cell division is mainly restricted to the ciliary marginal zone (CMZ) by 3 dpf.

Furthermore, we performed BrdU labeling to evaluate the rate of proliferation in the retina at 48 hpf. *banp*^{rw337} mutants did not show a significant change in the percentage of BrdU positive cells in the retina compared to wild type (Figure 2-18 A, C). The *Tg[ath5:EGPF]* transgenic fish line, which labels post-mitotic neurons, was used to test retinal neurogenesis at 48 hpf and found that neurogenesis was reduced in *banp*^{rw337} mutants (Figure 2-18 B, C). The loss of ath5:EGFP+ cells is noticeable on the apical side of the retina. The ath5:EGFP+ cells positioned towards the apical side are most likely differentiating neurons according to their position. Overall, at 48 hpf in *banp*^{rw337}mutant retinas, the proliferation rate is comparable to the wild type with reduced neurogenesis.

Next, we labeled wild type and *banp*^{rw337} mutant retinas with anti-activated caspase 3 and anti-pH3 antibodies at 48 hpf (Figure 2-18 D, E). Caspase 3 is a pro-apoptotic marker, and it labels cells that are undergoing early stages of apoptosis. Both activated caspase3+ cells and pH3+ cells increased in number in *banp*^{rw337} mutants (Figure 2-18 F). Furthermore, activated caspase3+ cells were mostly located in the intermediate zone of the neural retina along the apico-basal axis, whereas pH3+ cells were localized in the apical surface of the neural retina (Figure 2-18 G), suggesting that apoptosis occurs mostly in retinal progenitor cells undergoing G1 or S phase, or differentiating neurons.

Next, we conducted double labeling of wild type and *banp*^{rw337} mutant retinas with anti-activated caspase 3 and ath5:EGFP at 48 hpf to examined whether apoptosis occurs in early differentiating retinal neurons (Figure 2-18 H). The percentage of ath5:EGFP- and caspase 3-double-positive cells to the total number of caspase 3+ cells was 9.44±13.1% in *banp* mutants at 48 hpf and higher than that of wild-type siblings (0.00±0.00%), although the difference was not significant (Figure 2-18 I).

Next, we examined whether apoptosis occurs in mature retinal neurons. HuC/D is expressed in maturing neurons (Park, Hong et al. 2000) (Choy, Cheng et al. 2010, Schultz-Rogers, Almeida et al. 2018). We performed whole-mount immunofluorescent labeling of embryos at 48 hpf with caspase3 and HuC/D antibodies. At 48 hpf in the zebrafish retina, HuC/D is expected to label RGCs. As a result, co-labeling is expected to reveal information about the apoptotic nature of differentiated cells. Our immunofluorescent labeling revealed that HuC/D and caspase 3 signals were not spatially overlapping in the mutant retina (Figure 2-18 J, K). The fraction of activated caspase 3 and HuC/D double positive cells in the total activated caspase 3-positive cells were almost zero in both wild type and *banp*^{rw337} mutants (Figure 2-18 K). These data suggest that apoptosis is not initiated in the maturating retinal neuron in *banp* mutants.

At 48 hpf, HuC/D negative cells are proliferating/differentiating progenitor cells (Del Bene, Wehman et al. 2008). The association of caspase 3 signals with HuC/D negative cells suggests that apoptosis is associated with RPCs in *banp*^{rw337} mutants. Additionally, the association of cell death only with ath5:EGFP positive cells but not with HuC/D implies that some differentiating progenitor cells are likely undergoing apoptosis (Figure 2-18 L). In summary, the cellular abnormality in the retina arises as early as 48 hpf, although embryos appear phenotypically similar to wild type (Figure 2-16 and Figure 2-17) and cell death is associated with retinal progenitor cells (RPCs) at 48 hpf (Figure 2-19). Since mitotic arrest was transiently observed at 53 hpf but apoptosis continues in the central retina of *banp*^{rw337} mutants after 53 hpf, it is likely that apoptosis occurs following mitotic arrest (Figure 2-19).

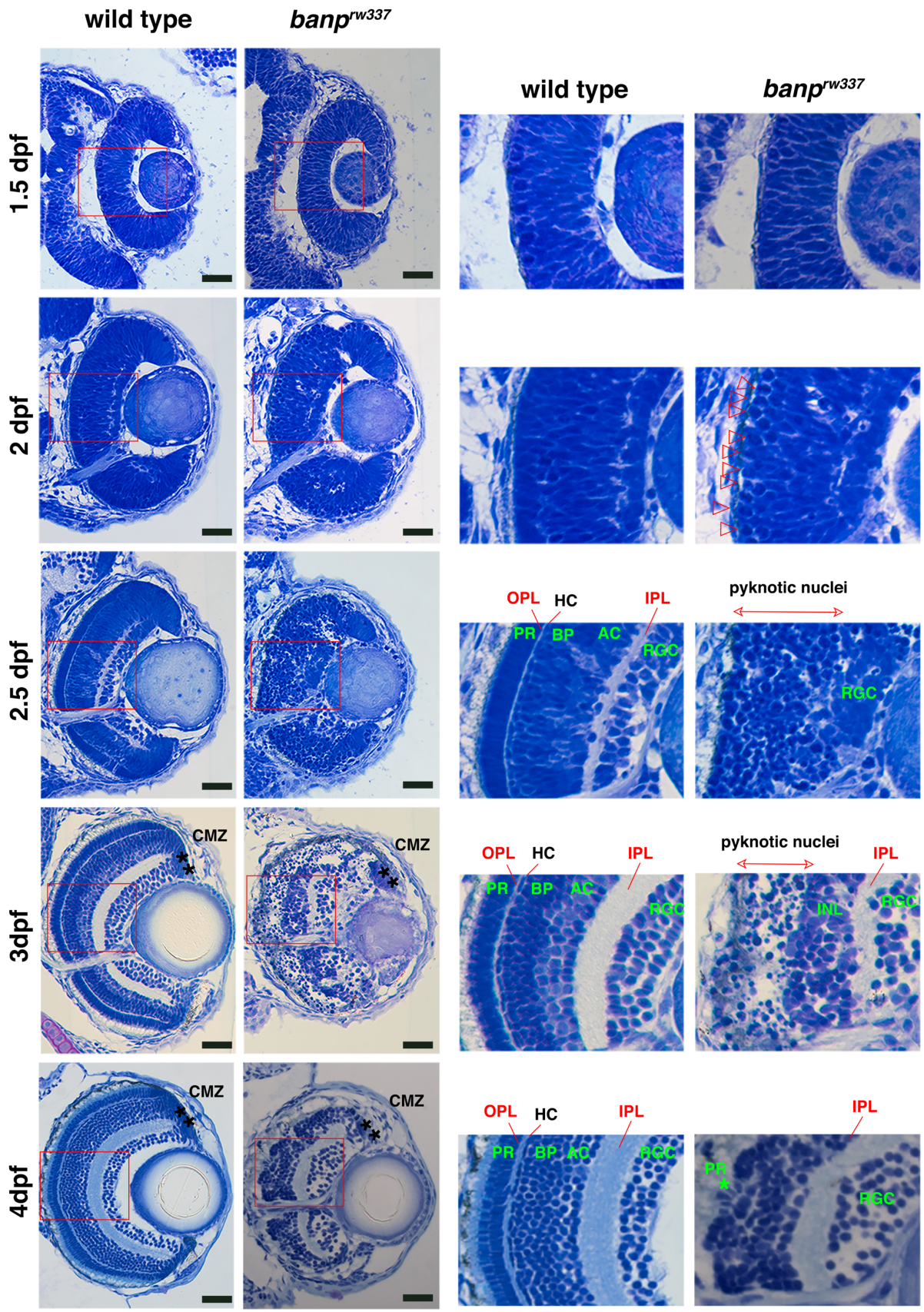
wild type
banprw337
wild type
banprw337
1.5 dpf
2 dpf
2.5 dpf
3dpf
4dpf
CMZ
CMZ
CMZ
CMZ
OPL
HC
IPL
PR
BP
AC
RGC
pyknotic nuclei
RGC
OPL
HC
IPL
PR
BP
AC
RGC
pyknotic nuclei
IPL
INL
RGC
OPL
HC
IPL
PR
BP
AC
RGC
IPL
PR
RGC

Figure 2-16: Cellular defect in *banp*^{rw337} mutant neural retina
Plastic sections of wild type and *banp*^{rw337} mutant retinas during development. Higher magnification images of red squares in the left columns are shown in the right panel. Retinal neuroepithelium is normal in *banp*^{rw337} mutants at 1.5 dpf. However, many round-shaped cells reminiscent of mitotic cells accumulate in the apical region of *banp*^{rw337} mutant retinas at 2 dpf, suggesting the mitotic arrest of retinal progenitor cells. In wild type retinas, three nuclear layers and two plexiform layers are formed at 2.5 dpf. However, only RGCs appear near the lens, and the outer region was occupied by pyknotic nuclei indicating dead cells in *banp*^{rw337} mutant retinas at 2.5 dpf. At 3 dpf, INL is formed, but pyknotic nuclei still occupy the outer region in *banp*^{rw337} mutant retinas. At 4 dpf, pyknotic nuclei are reduced. However, the PR layer disappeared, and a small number of photoreceptor-like columnar cells are observed in putative INL in *banp*^{rw337} mutant retinas (asterisks).
RGC, retinal ganglion cell; AC, amacrine cell, BP, bipolar cell; HC, horizontal cell; PR, photoreceptor; OPL, outer plexiform layer; IPL, inner plexiform layer; ONL, outer nuclear layer; CMZ, ciliary marginal zone.

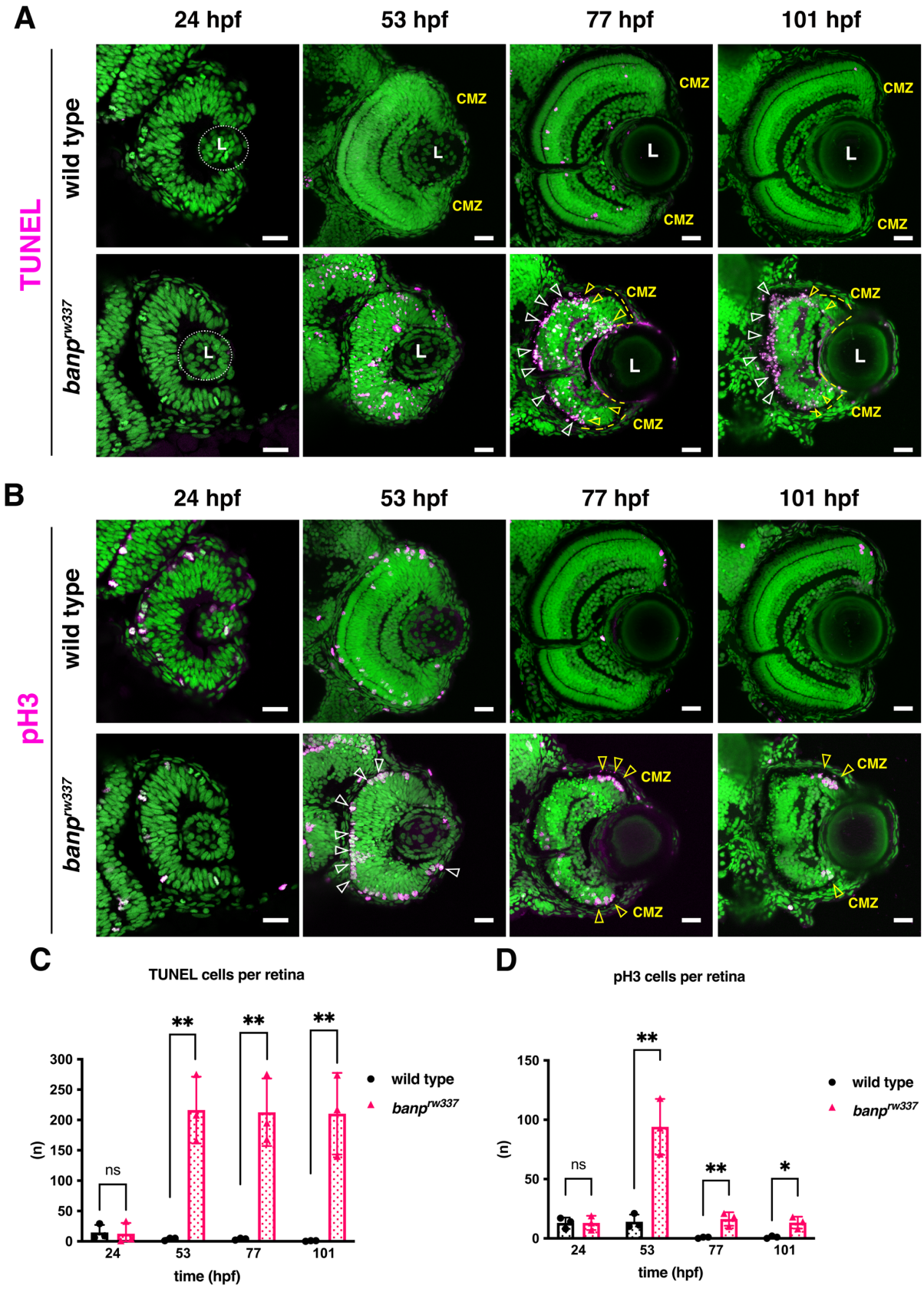
A
24 hpf
53 hpf
77 hpf
101 hpf
TUNEL
wild type
banprw337
L
CMZ
B
pH3
C
TUNEL cells per retina
(n)
time (hpf)
ns
wild type
banprw337
D
pH3 cells per retina

Figure 2-17: Validation of cell death and cell cycle arrest in *banp*^{rw337} mutants.
A) Elevated cell death in *banp*^{rw337} mutant retinas throughout embryonic development. TUNEL labeling showed an increased number of apoptotic cells in retinas of *banp*^{rw337} mutants (right panels) compared to wild type (left panels) from 53 to 101 hpf. However, there is no significant difference in the number of apoptotic cells between wild type and *banp* mutants at 24 hpf. Scale bar =20 μm. B) Quantitation of the number of TUNEL positive cells per retina: Quantitative analysis for TUNEL positive dying cells indicates a significant increase of apoptosis in mutants from 53 hpf. Multiple unpaired t-test. [n=3 $p < 0.05$ (*), $p < 0.01$ (**), $p < 0.001$ (***), NS (not significant)].
C) *banp*^{rw337} mutant retina shows an increased number of cells at the M-phase. Immunofluorescence labeling for pH3 antibody marks the early Mitotic phase of the cell cycle, revealed that the number of cells undergoing M-phase is higher in mutant retinas (right panel) than wild type (left panel) from 53 hpf. However, there is no significant difference in the number of mitotic cells between mutants and wild type at 24 hpf. Scale bar =20 μm. D) Quantitation of the number of pH3 positive cells per retina: Quantitative analysis of the same result shown in (D) indicates a significant increase of pH3 cells after 53 hpf. Multiple unpaired t-test. [n=3 $p < 0.05$ (*), $p < 0.01$ (**), $p < 0.001$ (***), NS (not significant)].

.

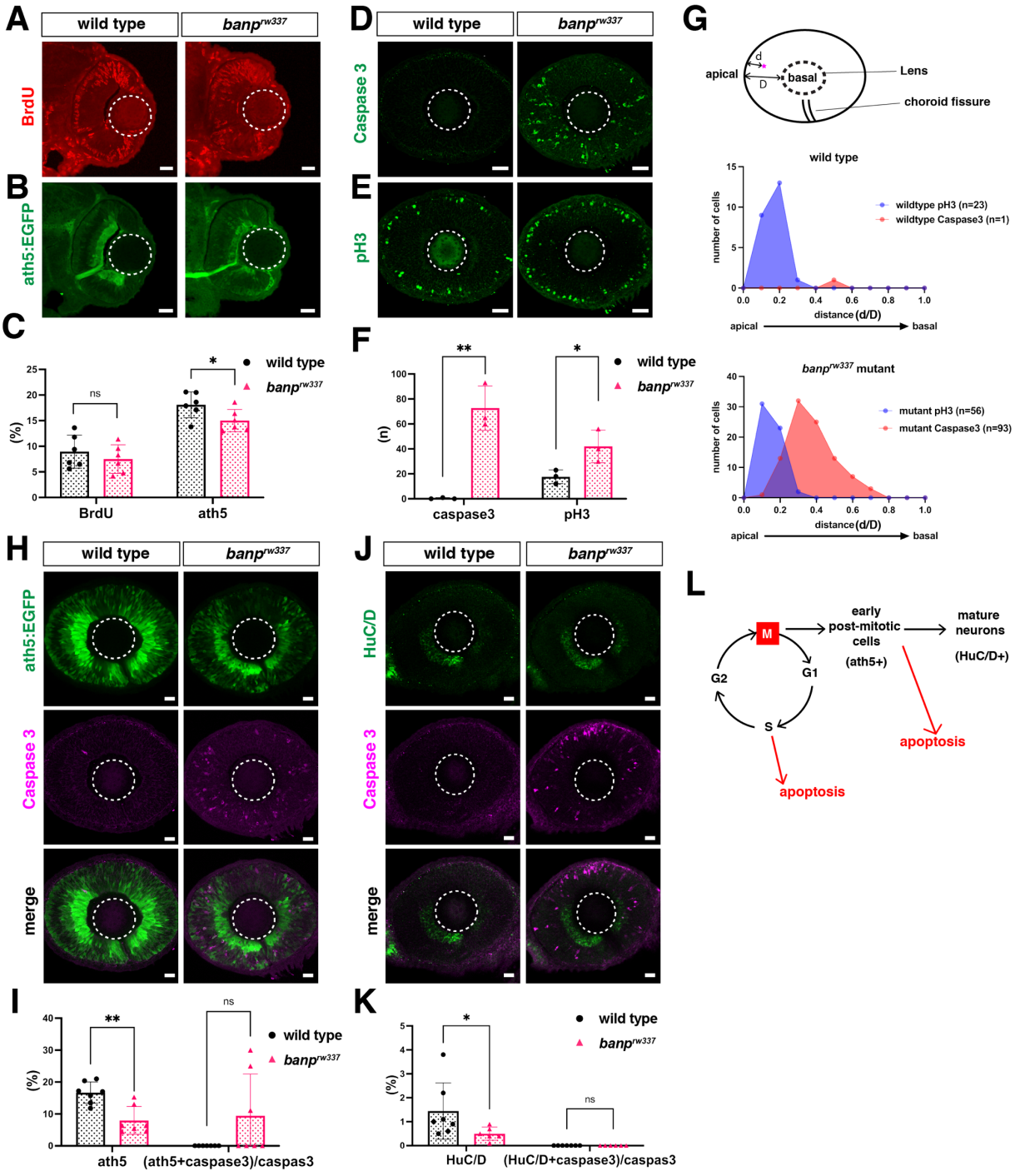

Figure 2-18: RPCs undergo cell death in *banp*^{rw337} mutant retinas when compared to wild type at 48 hpf
(A) BrdU labeling of wild type and *banp*^{rw337} mutant retinas at 48 hpf.
(B) ath5:EGFP expression of wild type and *banp*^{rw337} mutant retinas at 48 hpf.
(C) Percentage of BrdU-positive area or ath5:EGFP-positive area relative to the total retinal area. There is no significant difference in BrdU-positive area between wild type and *banp*^{rw337} mutant retinas. Unpaired t-test (two-tailed) [n= in graph, $p < 0.05$ (*),NS (not significant)].
(D) Labeling of wild type and *banp*^{rw337} mutant retinas with anti-caspase 3 antibody at 48 hpf.
(E) Labeling of wild type and *banp*^{rw337} mutant retinas with the anti-pH3 antibody at 48 hpf.

(F) Number of caspase 3-positive or pH3-positive cells per section of retina. Number of caspase 3-positive cells and pH3-positive cells is significantly higher in *banp*^{rw337} mutants than in wild-type siblings. Unpaired t-test (two tailed) [n= 3, $p < 0.05$ (*), $p < 0.01$ (**)].
(G) Location of caspase 3-positive or pH3-positive cells in the apico-basal axis of the retina. *banp*^{rw337} mutant retina shows a spatial separation of caspase3-positive cells from pH3-positive cells.
(H) Double labeling of wild type and *banp*^{rw337} mutant retinas with ath5:EGFP transgene and anti-caspase 3 antibodies.
(I) Percentage of ath5:EGFP-positive area relative to the total retinal area (left) and percentage of ath5:EGFP- and caspase 3-double positive cells relative to the total number of caspase 3-positive cells (right).
(J) Double labeling of wild type and *banp*^{rw337} mutant retinas with anti-HuC/D antibody and anti-caspase 3 antibodies.
(K) Percentage of HuC/D-positive area relative to the total retinal area (left) and percentage of HuC/D- and caspase 3-double positive cells relative to the total number of caspase 3-positive cells (right).
(L) A possible model on how apoptosis is induced during retinal progenitor cell proliferation and retinal neurogenesis in *banp*^{rw337} mutants. Apoptosis is induced in retinal progenitors and newly differentiating neurons in *banp*^{rw337} mutants. Scale bar: 20μm

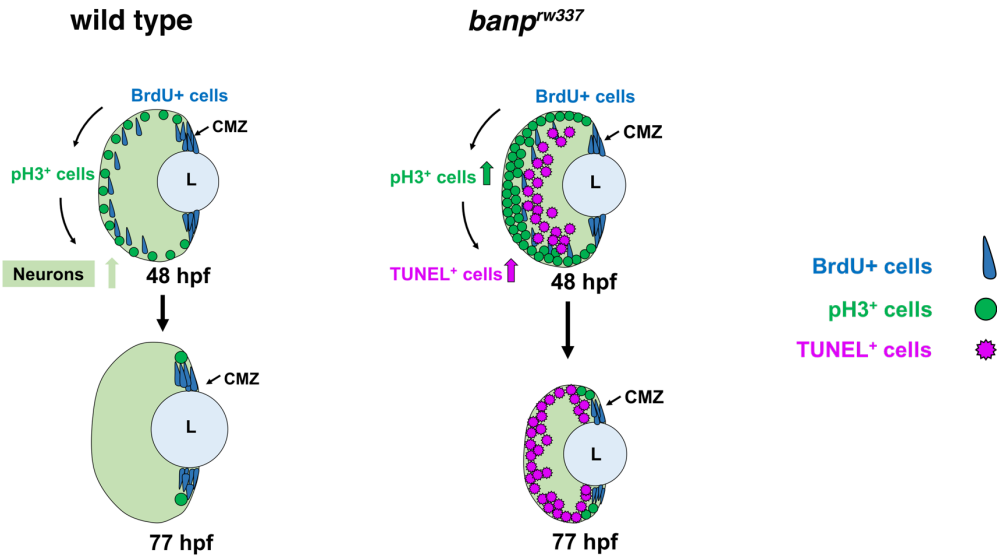

Figure 2-19: A schematic of neuronal differentiation in the wild type and *banp*^{rw337} mutant retina is depicted.
Schematic diagram of wild-type retinas from 48 to 77 hpf. Neuronal differentiation proceeds from the central to the peripheral retina. At 48 hpf, the proliferating area is gradually restricted in the CMZ; however, there are still retinal progenitor cells that proliferate in the central retina. Daughter cells start to exit from the cell cycle to produce differentiated neurons (light green color). At 77 hpf, most progenitor cells exit from the cell cycle, except at the CMZ. BrdU-labeled cells and pH3-positive cells are indicated in blue and green, respectively.
Schematic diagram of *banp*^{rw337} mutant retinas from 48 to 77 hpf. At 48 hpf, mitotic cells are significantly accumulated at the apical surface of the neural retina and apoptosis starts in the intermediate region of the central retina. At 77 hpf, the apoptotic area is more restricted to the apical region of the retina and at the interface between the central retina and the CMZ. Mitotic cells accumulate in the apical region of the CMZ at 77 hpf. TUNEL-positive cells are indicated in magenta.

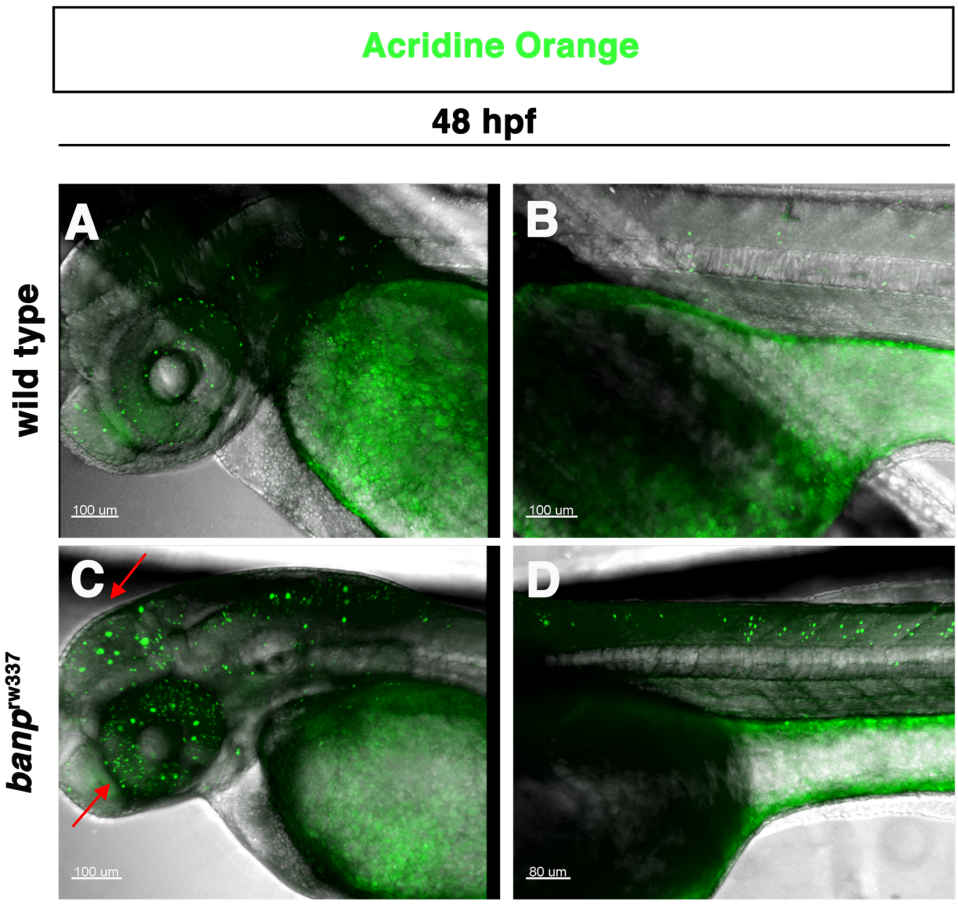

Figure 2-20: Acridine orange staining show increased cell death *banp*^{rw337} mutants at 48 hpf
AO staining of live embryos at 48 hpf. (A-B) wild type embryo (C) Reveals elevated cell death in mutant brain and retina (red arrowheads) (D) AO positive cells in the spinal cord of mutant embryo.

2.4 Discussion

A chemical ENU mutagenesis screen in zebrafish conducted at RIKEN revealed a new *rw337* mutant allele. Masai lab mapped *rw337* mutation to the gene *banp*. Furthermore, I evaluated *rw337* mutants and observed that the *rw337* mutation disrupts the normal splicing of exon 4 to exon 5, likely resulting in a truncated Banp protein lacking the conserved BEN domain (Figure 2-3 C). *rw337* is a recessive lethal mutation. Hence, we used *banp*^{rw337} mutants to investigate the developmental function of Banp in a physiological condition. On the first and second-day post-fertilization, *banp*^{rw337} mutant embryos morphologically resembled wild type. However, a phenotype with smaller eyes can be identified at 4 dpf. (Figure 2-1).

We studied *banp* mRNA expression throughout the embryonic and early larval stages of zebrafish to better understand its function. *banp* mRNA was maternally expressed according to our whole mount in situ hybridization (Figure 2-10, A 4 cell stage). As a result, maternally produced Banp protein may compensate for the loss of function of Banp in the *banp*^{rw337} mutants during early development and potentially repair developmental abnormalities during cleavage, gastrulation, and somitogenesis. Zygotic *banp* mRNA expression was ubiquitous (Figure 2-10, A 5 somite). Later, it became progressively restricted to the CNS towards 2 dpf. This distribution of *banp* mRNA in CNS suggested that the *banp* might play a role in CNS development. Interestingly, *banp*^{rw337} mutants showed cell death in the CNS at 2dpf (Figure 2-20 C, D). This cell death in the CNS due to loss of function of the Banp demonstrates that *banp* is required for cell survival in the developing CNS.

We further investigated the cellular and molecular defects in *banp*^{rw337} mutant embryos to get insights into the function of Banp. There were no cellular and phenotypic defects in the heterozygous *banp*^{rw337} zebrafish. However, at 4 dpf, the *banp*^{rw337} mutant embryos have displayed morphological defects such as microphthalmia and an undeveloped swim bladder (Figure 2-1). Furthermore, histological analysis was performed on retinal sections of wild type and *banp*^{rw337} mutant zebrafish since the eye is most obviously impaired. The mutants displayed a deficiency in retinal lamination, particularly OPL, and increased cell death by 48 hpf, in contrast to the distinct retinal layers in wild type (Figure 2-17 and Figure 2-16). These abnormalities exacerbated with time, and the embryos died around 6-7 days after fertilization. Additionally, in *banp*^{rw33} mutant retinas, all neuronal populations were differentiated and maintained until 4 dpf (Figure 2-12). The presence of all neuronal cell types reveals that differentiation is not eliminated.

Furthermore, caspase 3 and TUNEL labeling confirmed cell death in mutants at 48 hpf (Figure 2-17 A and Figure 2-18 D, F). Importantly, introducing wild type *banp* mRNAs rescued cell death at 54 hpf in *banp*^{rw337} mutant retinas demonstrating that cell death was caused by loss of function of Banp (Figure 2-6 G, H). Aside from cell death, our histology (Figure 2-17 B) and omic (Figure 2-14) analyses revealed that *banp* mutants have a cell cycle defect. Since 48 hpf, mutants showed a significant increase in pH3 positive mitotic cells confirming mitotic arrest.

The zebrafish neural retina at 48 hpf comprises differentiated neurons, RGCs, and retinal progenitor cells (RPCs). At 48 hpf RPCs are either proliferating or differentiating. Our caspase3 labeling revealed that at 48 hpf, apoptotic signals are accumulated in HuC/D negative cells (Figure 2-18 J, K) and at the intermediate zone of apico-basal axis of retina (Figure 2-18 G). This specific accumulation of apoptotic signals shows that the cellular defect and accumulation of apoptotic signals occurs primarily in RPCs. *banp*^{rw337} mutants display a reduction in differentiation at 48 hpf, according to our HuC/D (Figure 2-18 K) and ath5:EGFP (Figure 2-18

C, I) labeling for neuronal cells. Activation of apoptosis in differentiating neurons likely accounts for this reduction in neuronal cells at 48 hpf (Figure 2-18 L).
Next, we used BrdU to determine the rate of cell proliferation and discovered that the mutant retina show proliferation rate comparable to wild type (Figure 2-18 A, C). The intact proliferation rate indicates that the pH3 positive cells have accumulated likely due to cell cycle arrest during the mitotic phase. Additionally, pH3 cells accumulate in the apical side of retinas at 48 hpf, where RPCs are predominant (Figure 2-17 B, white open arrow). It can also be seen at the interface between the CMZ and the neural retina at 3 and 4 dpf, where RPCs are undergoing differentiation (Figure 2-17 B, yellow open arrow). This spatial association of pH3 shows that mitotic arrest and subsequent cell death are strongly linked to RPC differentiation in mutants. Overall, our results suggest that the absence of *banp* triggers a cellular dysfunction primarily in RPCs, resulting in cell cycle arrest and subsequent cell death (Figure 2-19).

CHAPTER 3

Interacting networks of Banp in zebrafish

3.1 Motivation

Mammalian Banp is reported to have a characteristic BEN domain. Zebrafish Banp (zBanp) also has its BEN domain conserved (Section 2.3.5, Figure 2-9). Proteins with the BEN domain show DNA binding properties, protein binding properties, transcription factor activity, and adaptor functions to recruit chromatin-modifying complexes (Abhiman, Iyer et al. 2008, Malonia, Sinha et al. 2011, Nakayama, Sakashita et al. 2020, Grand, Burger et al. 2021). Several examples confirming characteristics of the BEN domain in Banp are reviewed in previous section (Literature review-chapter 1). Among these, the ability of Banp to act as a transcription factor is very significant (Grand, Burger et al. 2021). We know that transcription factors play a critical role in regulating transcription and, consequently, cell fate. However, evidence of transcription regulation by zBanp is not known. Additionally, we have confirmed that nuclear localization is conserved in zBanp (Section 2.3.5). If zBanp has specific gene targets that operate as a transcription factor/regulator, the *banp*^{rw337} mutant is an ideal system for discovering Banp specific gene targets during development and under physiological conditions. In this chapter, I have combined my efforts to discover potential transcription targets of zBanp.

ATAC-seq (Assay for Transposase-Accessible Chromatin using sequencing) is used to identify chromatin accessibility across the genome. ATAC-seq provides us with information regarding nucleosome placement, open or closed chromatin, and transcription factor accessibility. RNA-sequencing can provide us with information regarding the differential expression of mRNA transcripts at a given experimental condition. The differential expression of mRNA transcripts can be due to differential transcription or differential mRNA degradation/stabilization. Gene targets experiencing transcriptional regulation cannot be distinguished from targets undergoing differential mRNA degradation/stabilization by RNA sequencing alone. In such cases, ATAC-sequencing combined with RNA-sequencing allows us to distinguish between transcriptionally active/repressed gene targets and differentially stabilized gene targets. I have combined my data from ATAC and RNA sequencing using *banp*^{rw337} mutant in this chapter. This method was expected to reveal molecular components dysregulated in the *banp*^{rw337} mutant at 48 hpf, presumably shedding insights on regulatiory networks involving *banp*.

3.2 Materials methods

3.2.1 ATAC sequencing

48 hpf embryos were used for ATAC sequencing. We used Kaestner Lab ATAC seq protocol (Ackermann and Kaestner 2019) until library preparation followed by sequencing using NovaSeq6000 SP. We generated reads for three independent *banp*^{rw337} mutant as well as three independent *banp*^{rw337} wildtype samples. Each sample contained a pool of 3 embryo heads. Quality check of reads was performed using FastQC. Reads from each sample were adaptor trimmed and aligned using fastp and Bowtie2 to zebrafish reference genome (GRCz11)(Langmead and Salzberg 2012) respectively. For quality control, aligned reads were

filtered for low quality reads, non-unique alignments and PCR duplicates using samtools (Li, Handsaker et al. 2009, Yan, Powell et al. 2020). Further the alignment files were peak called using Genrich along with removal of mitochondrial reads (Gaspar 2019). Differentially enriched peaks between wildtype and mutant were identified using DiffBind R package (Stark and Brown 2021). The obtained differential peaks were annotated using annotatePeaks tool of HOMER software (Heinz, Benner et al. 2010). findMotifsGenome tool of HOMER is used to presume the enriched motifs in the differential peaks. To compare the coverage tracks across the gene of interest between *banp*^{rw337} mutant and wildtype in RNA-seq and ATAC-seq data, the distribution of mapped reads in each replicates were averaged and plotted by SparK (Kurtenbach and Harbour 2019).

3.2.2 RNA sequencing

Embryo heads were homogenized using Polytron 1200E homogenizer (KINEMATICA) using TRIzol reagent (Invitrogen). RNA was isolated using Direct-zol RNA Miniprep Kit (ZYMO RESEARCH) from three replicates of *banp*^{rw337} mutant and wildtype embryos at 48 hpf. Each sample contained seven embryo heads, and head dissection was performed as described in Figure 3-1 A. RNA isolation was followed by library preparation for sequencing using NEBNext® Ultra™ II Directional RNA Library Prep Kit for Illumina® according to the manufacturer's instruction. 151-bases paired-end sequencing was performed using NovaSeq6000 SP. The quality of Sequenced reads was evaluated by FastQC (Andrews 2010). Adaptor trimming, quality filtering was done by fastp (Chen, Zhou et al. 2018). The cleaned reads were then mapped to the zebrafish reference genome (GRCz11) using hisat2.1.0 (Kim, Paggi et al. 2019), and mapped reads were counted with FeatureCounts from the Subread package (Liao, Smyth et al. 2014) using annotation from Ensembl (Danio_rerio.GRCz11.95.gtf). Differentially expressed gene (DEG) analysis was performed using the EdgeR package (Robinson and Oshlack 2010). The genes with a false discovery rate (FDR) < 0.01 were considered as significant DEGs. Enhanced Volcano package (Blighe, Rana et al. 2018) was used to create a volcano plot with Log_2FoldChange (wildtype – mutant) values and FDR calculated by EdgeR. The difference in alternative splicing between mutant and wildtype was tested using the DEXseq package (Anders, Reyes et al. 2012). Adjusted *p*-value < 0.01 was considered as significant.

3.2.3 qRT-PCR

To validate the mRNA expression from embryos, qRT-PCR analysis was performed. For qRT-PCR analysis, initially RNA was extracted from embryo heads from which cDNA was synthesized. Then the qRT-PCR reaction was set up using this synthesized cDNA. The detailed protocol is as follows.

3.2.3.1 RNA extraction

Embryos heads at 2 dpf were dissected and transferred to 50 µl Sepasol RNA I Super (Nacalai, Japan). RNA was extracted immediately, or heads were stored at –80ºC. Further for RNA extraction heads were homogenized using a mechanical homogenizer (Biomaster II-EOG sterilized). 20 µl CHCl3 was added to samples homogenized in Sepasol and mixed vigorously, followed by incubation at RT for 10 min. Samples were then centrifuged at 40ºC for 15000g for 20 min. The aqueous phase was then transferred to 1.5ml eppendorf, and 100 µl of isopropanol was added. This solution was incubated at RT for 10 min and centrifuged at 4ºC for 15000g for

15 minutes. The supernatant was discarded, and the pellet was washed twice with fresh 75% EtOH at 8000g for 5 minutes at 4ºC. EtOH was removed completely, and the pellet was air-dried for 5 min. The pellet was re-suspended in 10-15 µl nuclease-free water, and RNA concentration was measured using NanoDrop. RNA was used for cDNA synthesis or stored at – 80ºC.

3.2.3.2 cDNA synthesis

cDNA was synthesized using Toyobo cDNA kit, total RNA (500 ng) was reverse transcribed by following steps:

RNA (500 ng)	x µl
4xDN	2 µl
Incubate at 37ºC for 5 minutes	
Water (RNA grade)	(8-x) µl
5x RT MM II	2 µl

Temperature	Time
37ºC	15 minutes
50 ºC	5 minutes
98 ºC	5 minutes
4 ºC	∞

Once cDNA was synthesized from reverse-transcribed RNA, the expression profile of required genes was evaluated using the specified primers listed below using Luna® Universal qPCR Master Mix (NEB) according to the manufacturer's instructions. Quantitative RT-PCR was performed using StepOnePlus (Applied Biosystems). The relative expression was calculated using ΔΔCt method with the reference gene ef1α. Primers used in qRT-PCR analysis; mdm2 (Wilkins, Lorent et al. 2013), p21 (Stiff, Tena et al. 2016), FL tp53 and Δ113 tp53 (Chen, Semenova et al. 2016), ef1α (McCurley and Callard 2008).

Gene	RT PCR-Forward primer	RT PCR-Reverse primer
mdm2	caggaggaggagaagcagtg	agggaaaagctgtccgactt
P21	aagcgcaaacagaccaacat	gcagctcaattacgataaaga
FL *tp53*	tggagaggaggtcggcaaaatcaa	gactgcgggaacctgagcctaaat
Δ*113 p53*	atatcctggcgaacatttggaggg	cctcctggtcttgtaatgtcac
puma(bbc3)	ctgaggaggaccccacact	tctccagttctgccagtgc
ccng1	ccctggagattgaggatcag	cacacaaaccaggtctccaa
ef1-α	cttctcaggctgactgtgc	ccgctagcattaccctcc

3.2.4 Western blot

Embryos heads were cut out in ice-cold E3 medium and homogenized in sample buffer (125mMol NaCl, 50mMol Tris HCl p^H 7.4, 0.5mMol EDTA, 1% TritonX100, 1X Protease inhibitor). Appropriate volumes of samples were diluted in sample buffer to provide equal

protein amounts and used for SDS-PAGE (BIO-RAD, Mini-PROTEAN TGX Gels). Western blot analysis was performed to 3 samples for wild-type and *banp*^{rw337} mutants, respectively, according to standard protocols using anti-tp53 antibody (GeneTex, GTX128135) at a 1:1000 dilution. β-actin protein level was evaluated by western blot analysis of rehybridized membranes (Restore™ PLUS Western Blot Stripping Buffer, Thermo Scientific) with anti-β-actin antibody (Sigma, A5441) at a 1:5000 dilution, and used to normalize tp53 protein level for each sample. For secondary antibodies, horseradish peroxidase-conjugated anti-rabbit or anti-mouse IgG antibodies (Amersham, NA931 and NA934) were used. Enzyme activity was detected using Immunostar® LD (Wako) and luminescence was imaged and quantified using iBright 1500 (Thermo Fisher Scientific).

3.2.5 *tp53* morpholino injection

To investigate the role of *tp53* in the *banp*^{rw337} mutant phenotype, *tp53* was knocked down using a previously described morpholino (Langheinrich, Hennen et al. 2002). *banp*^{rw337} heterozygous fishes were intercrossed to obtain potential *banp*^{rw337} mutant embryos. According to Mendelian genetics, one-fourth of the obtained embryos will be *banp*^{rw337} mutants. tp53-MO was injected onto *banp*^{rw337} embryos at the one-cell stage. Generally, at 48 hpf, AO staining reveal *banp*^{rw337} mutants (0.25%) with a visible accumulation of dead cells in the CNS (Figure 2-20). When tp53-MO was injected into *banp*^{rw337} embryos, none showed cell death accumulation at 48 hpf when stained with AO. tp53-MO injected embryos were genotyped as mentioned in section 2.2.5 to confirm their genotype. After identifying the *banp*^{rw337} mutant genotype, those embryos were used for immunofluorescence staining. To knock down Δ113tp53, morpholino antisense oligos for Δ113tp53 (Δ113tp53 MO; also referred to as MO6-tp53 in zebrafish database ZFIN) (5'-GCAAGTTTTTGCCAGCTGACAGAAG-3') was used (Chen, Ng et al. 2009).

3.2.6 Data availability

Raw RNA-seq and ATAC-seq datasets of *banp*^{rw337} mutant and wildtype sibling are available at DDBJ Sequence Read Archive (DRA012572).

3.3 Results

3.3.1 RNA sequencing revealed candidate genes responsible for the phenotypic defect in *banp*^{rw337} mutants

In chapter 2, we have seen that even though a phenotypic defect is observed at 4 dpf, the cellular defects occurred from 48 hpf in *banp*^{rw337} mutant embryos. Hence, this earlier time point needed to be studied to understand the primary molecular defects that occurred due to the loss of function of the *banp.* First, we performed a bulk RNA sequencing of *banp*^{rw337} mutant embryos and wildtype at 48 hpf. Three independent pools of embryo heads (n=7 each) at 48 hpf from wildtype and mutant samples were used for sequencing Figure 3-1 A. Sequencing and mapping of reads were performed as described (3.2.2). Illumina sequencing generated more than 50 million paired-end reads from cDNA libraries. 27,771 protein-coding genes were detected. Among detected protein-coding genes, 258 were upregulated, and 81 were downregulated (Figure 3-1 B). Our gene ontology analysis revealed that, among the top 15 upregulated genes, most genes are enriched in *tp53* dependent cell cycle regulation (Figure 3-1 C, *). qRT-PCR validation of *tp53* target genes targets genes *p21(cdkn1a), puma(bbc3)*, *ccng1*, *mdm2* confirmed *tp53* pathway is indeed activated in mutants (Figure 3-2).

In addition to the *tp53* pathway, our gene ontology analysis revealed that one of the primary pathways deregulated in mutants is mitotic cell cycle regulation (Figure 3-3, black arrow). Multiple genes involved in mitotic cell cycle regulation are deregulated in mutants (Figure 3-4). This result was consistent with our immunofluorescent labeling study, showing an increased number of pH3 positive mitotic cells in *banp*^{rw337} mutants at 2 dpf (Figure 2-17). Thus, RNA sequencing revealed several differential expressed genes, potentially causing the accumulation of mitotic cells in *banp*^{rw337} mutants (Figure 3-4). Furthermore, genes such as *caspase8*, *bbc3* involved in cell death were also upregulated in mutants confirming an activated cell death pathway.

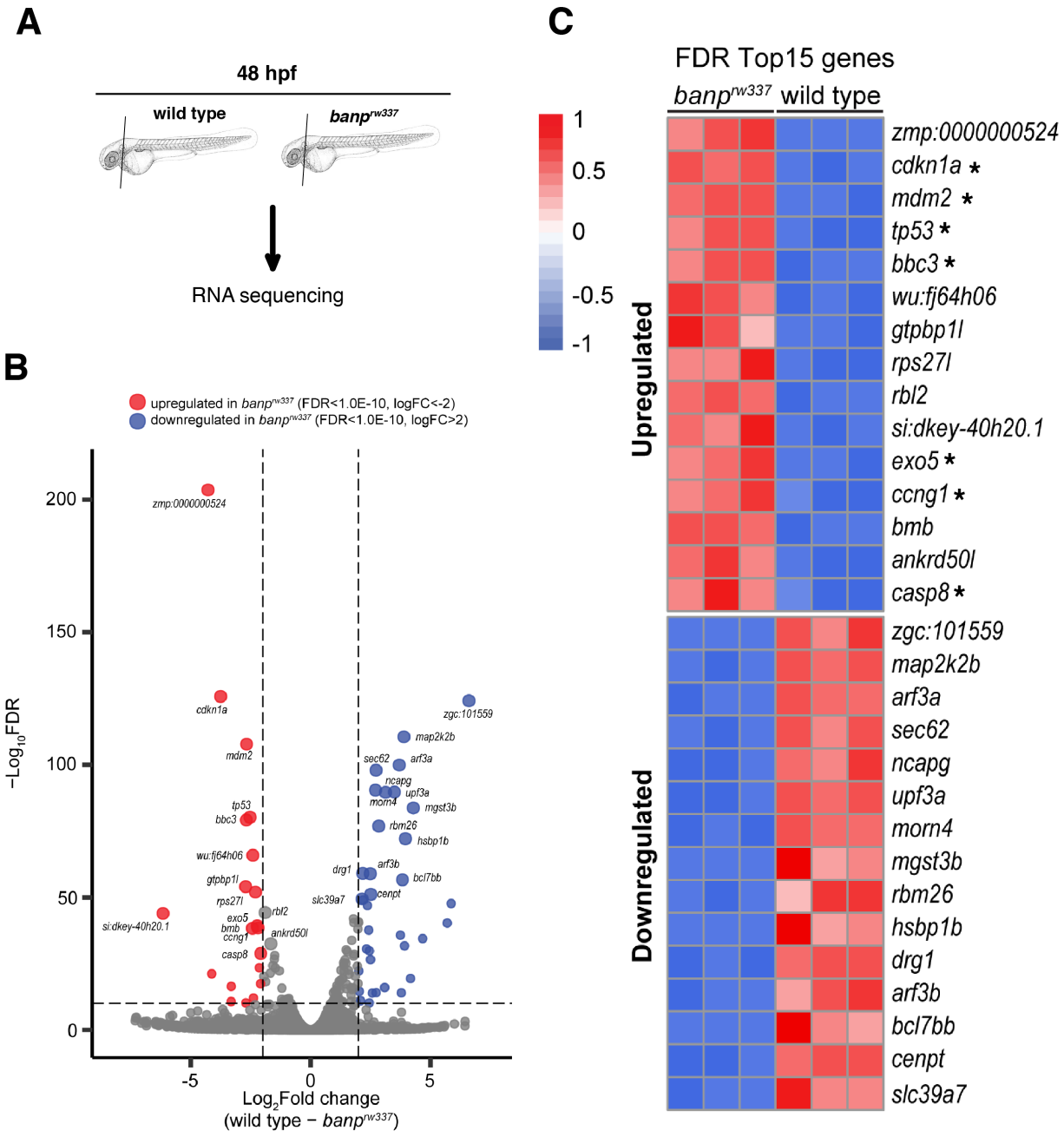

Figure 3-1: RNA sequencing at 48 hpf

(A) Schematic showing tissue preparation for mRNA sequencing experiment from zebrafish embryos.

(B) Volcano plot obtained from EdgeR analysis of the wild type and *banp*^{rw337} mutant embryos. Red dots and blue dots represent genes that differentially express more than 2-fold. Red dots represent upregulated genes, and blue dots represent downregulated genes in *banp*^{rw337}mutants.

(C) Heat map of top 15 differential gene expression profile for wild type and *banp*^{rw337} mutants. * Represent genes involved in the *tp53* pathway.

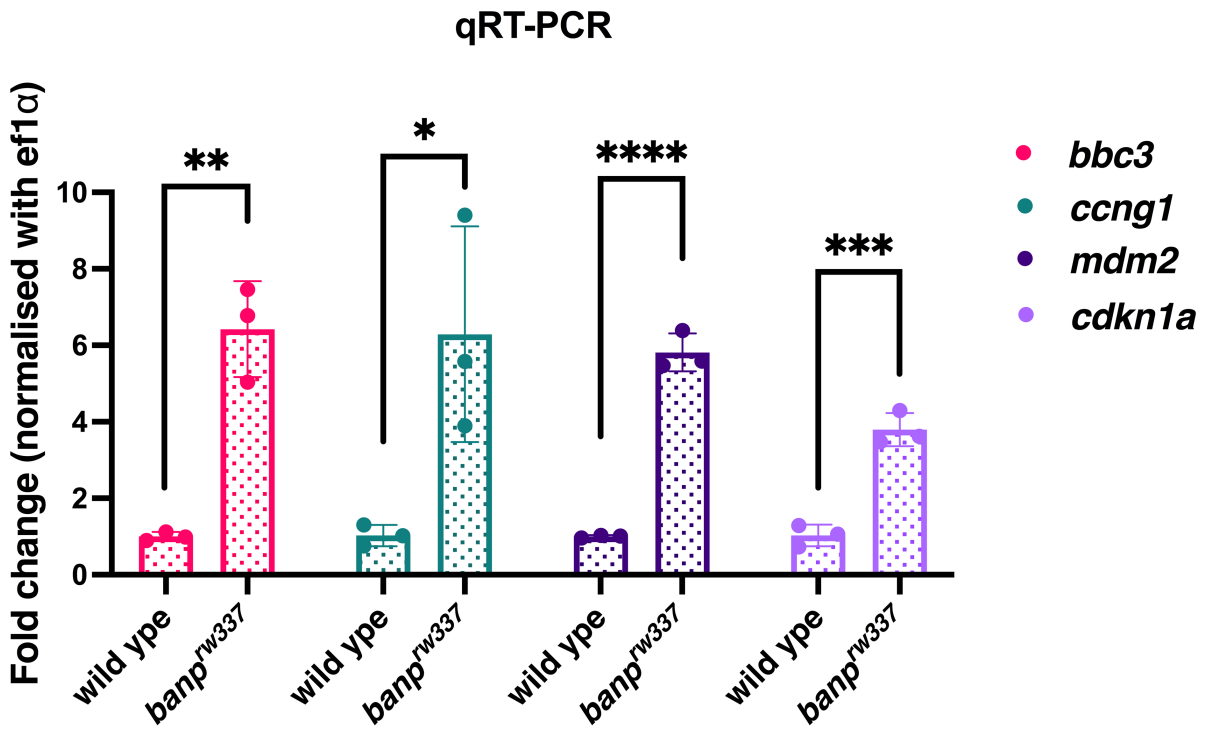

Figure 3-2: qRT-PCR validation of *tp53* target genes at 48 hpf
Relative mRNA expression levels of upregulated targets in *banp*^{rw337} mutant embryos. Unpaired t-test (two tailed) [n=3 $p < 0.05$ (*), $p < 0.01$ (**), $p < 0.001$ (***), $p < 0.0001$ (****)].

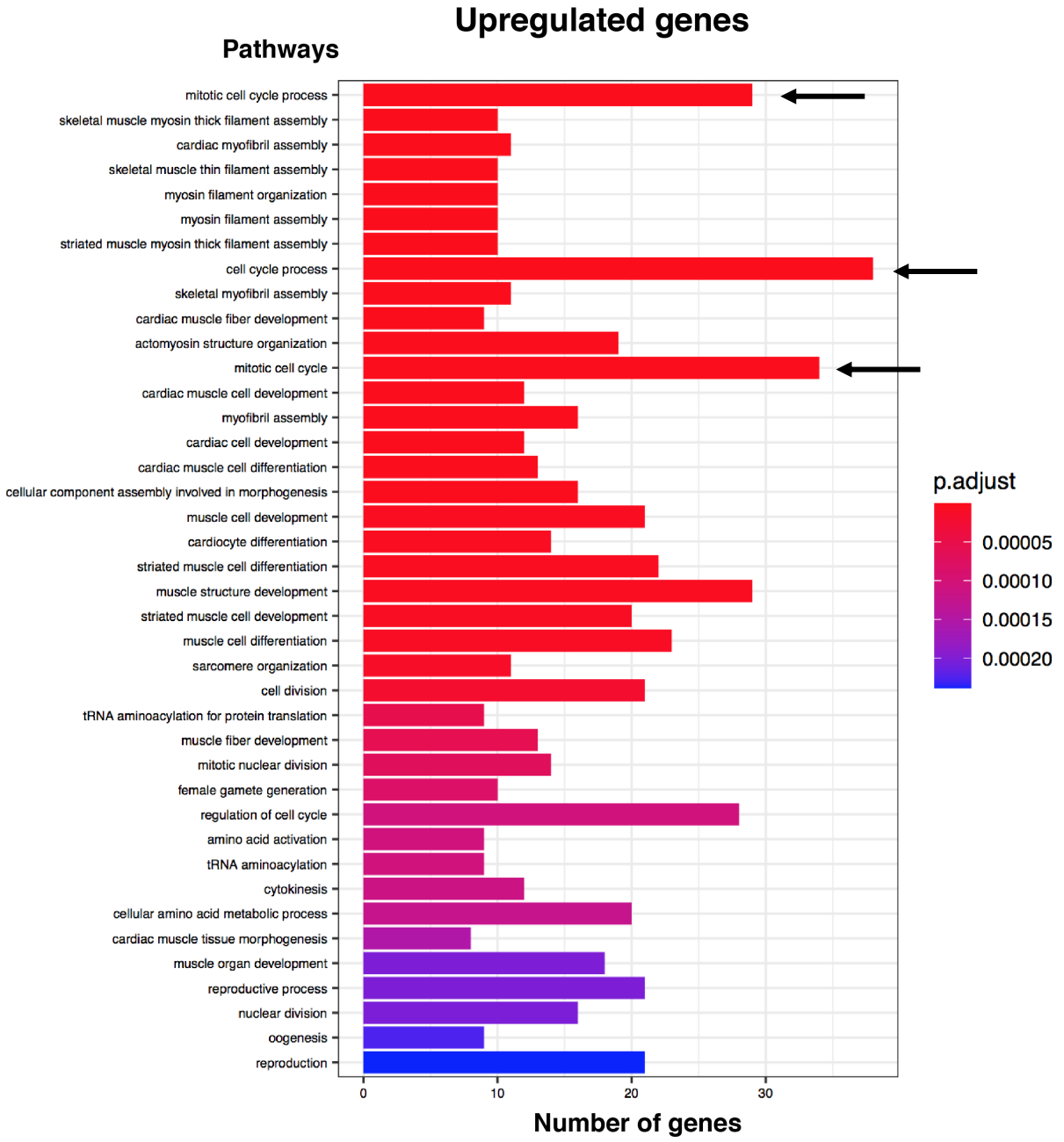

Figure 3-3: Gene ontology enrichment analysis of differentially expressed mRNA at 48 hpf
Gene ontology enrichment analysis of biological processes regulated by upregulated genes. The primarily differentially regulated biological process in the *banp*^{rw337} mutant is the mitotic cell cycle (black arrow).

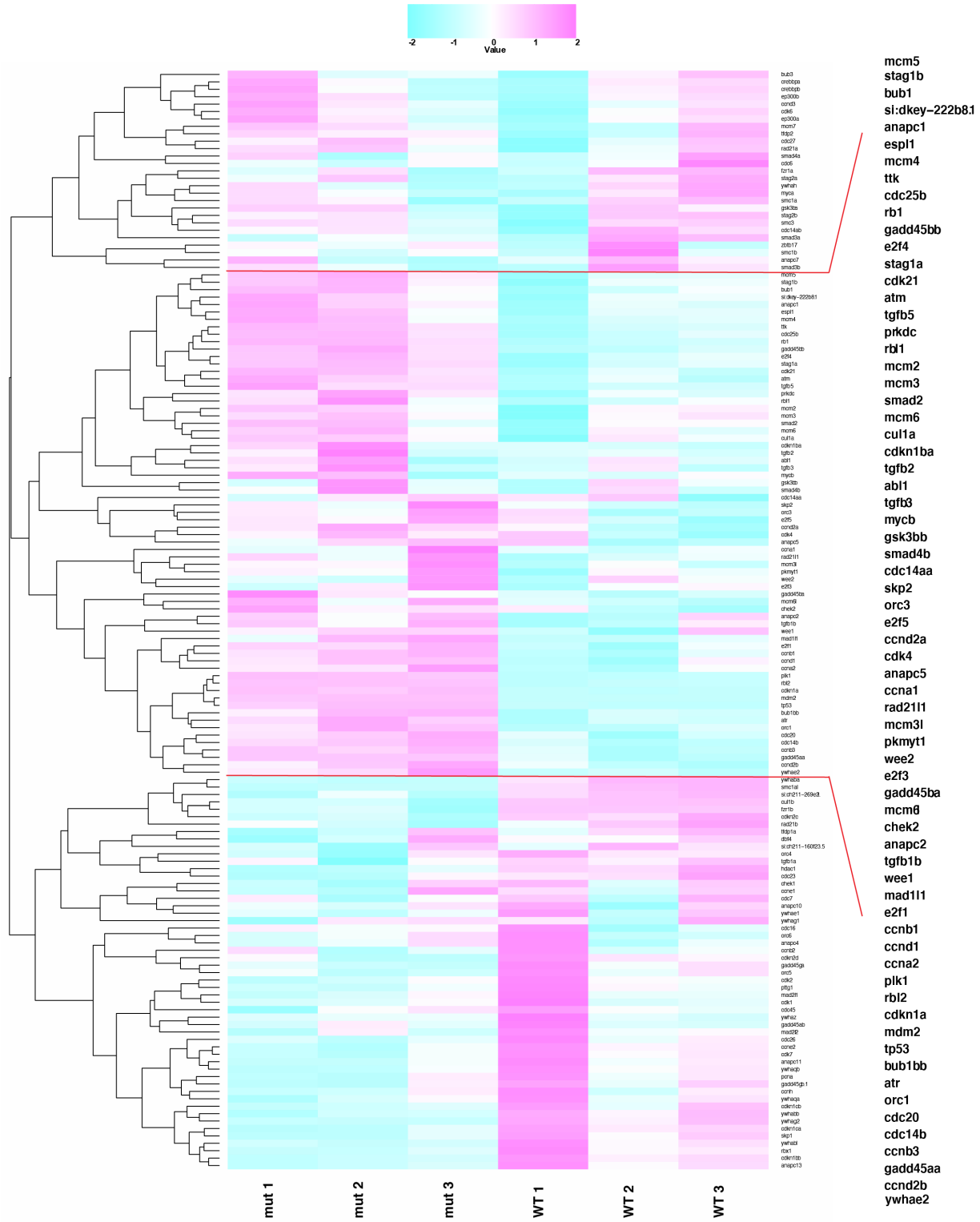

Figure 3-4: Heat map showing differential expression of genes involved in the regulation of the cell cycle
Heat maps represent differentially expressed genes involved in the process of cell cycle regulation. *banp*^{rw337} mutant embryos show a clear differential expression of multiple genes involved in cell cycle regulation. Genes upregulated in *banp*^{rw337} mutants are highlighted in an enlarged font.

3.3.2 ATAC sequencing revealed conserved Banp motif in zebrafish

The first analysis that we performed on ATAC-sequencing data was to identify the differentially regulated peaks in mutants. Mutant-specific genomic regions/peaks were used to annotate the corresponding genes or coding regions. It includes peaks that are specifically open/upregulated and peaks that are closed/downregulated in *banp*^{rw337}mutants. The distribution of differentially regulated peaks across the genome is depicted in Figure 3-5 A, B. This distribution demonstrates that promoter regions account for 26.02 percent of upregulated peaks (Figure 3-5 C). In mutants, the genes corresponding to these peaks are likely to be activated by transcription. Similarly, Figure 3-5 A depicts the distribution of downregulated peaks in mutants. In mutants, 20.08 percent of total downregulated peaks are in the promoter region, indicating that those genes are likely undergoing transcription suppression. Figure 3-5 B and D shows an example of a few genes that may be undergoing transcription regulation at their promoter region.

In addition, we performed motif enrichment analysis using Homer (homer v4.11.1), which evaluates given sets of sequences and looks for regulatory components (motifs) overrepresented compared to the reference genome. Table 3-1 represents the list of enriched motifs in the open chromatin region in the *banp*^{rw337} mutants. Motif 10 represents the Tp53 binding motif. This suggests that the activity of Tp53 binding is more active in open chromatin regions in the *banp*^{rw337} mutants. A list of potential Tp53 target genes upregulated in *banp*^{rw337} mutants, along with their predicted Tp53 binding motifs, are listed in Table 3-2. The enrichment of the Tp53 binding motif and activation of Tp53 target genes once again suggests that *tp53* and its downstream targets are active in *banp*^{rw337} mutants.

Table 3-3 represents enriched motifs in the closed chromatin region in the *banp*^{rw337} mutants. We discovered TCTCGCGAGA (also known as Banp motif/CGCG-element-containing motif) as the most enriched motif in the closed chromatin region of *banp*^{rw337} mutants. I.e., loss of function of Banp caused reduced access to TCTCGCGAGA motif in zebrafish. Many human promoters, including those that control housekeeping genes, do not have a TATA box. A tandem TCTCGCGAGA motif was discovered to be a frequent DNA regulatory element in human TATA-less promoters. A significant number of promoters of cell cycle genes, including cyclins and transcription regulators, chromatin structure modulators, translation initiation, and ribosomal protein genes, have this CGCG-element-containing motif. This motif is found in approximately 5% of human gene promoters (Wyrwicz, Gaj et al. 2007). Later, it was discovered that these CGCG element containing motifs are evolutionarily conserved in vertebrates, and it can activate gene expression via RNA Pol II (Mahpour, Scruggs et al. 2018). Through this hitherto orphan CGCG element containing motif, a recent study established Banp as a transcription factor, demonstrating that Banp is required for the activity of numerous essential genes and adequate and autonomous for substantial gene activation in chromatin (Grand, Burger et al. 2021). Grand et al. (2021) discovered that Banp is the only binding factor to this TCTCGCGAGA motif (Banp motif). They propose a model in which methylation-sensitive transcription factors like Banp, which are capable of chromatin opening, are required to activate the Banp motif in promoters. Taken together, our current finding revealing the conserved Banp motif in zebrafish makes zebrafish the most suitable model to evaluate the physiological and developmental function of Banp.

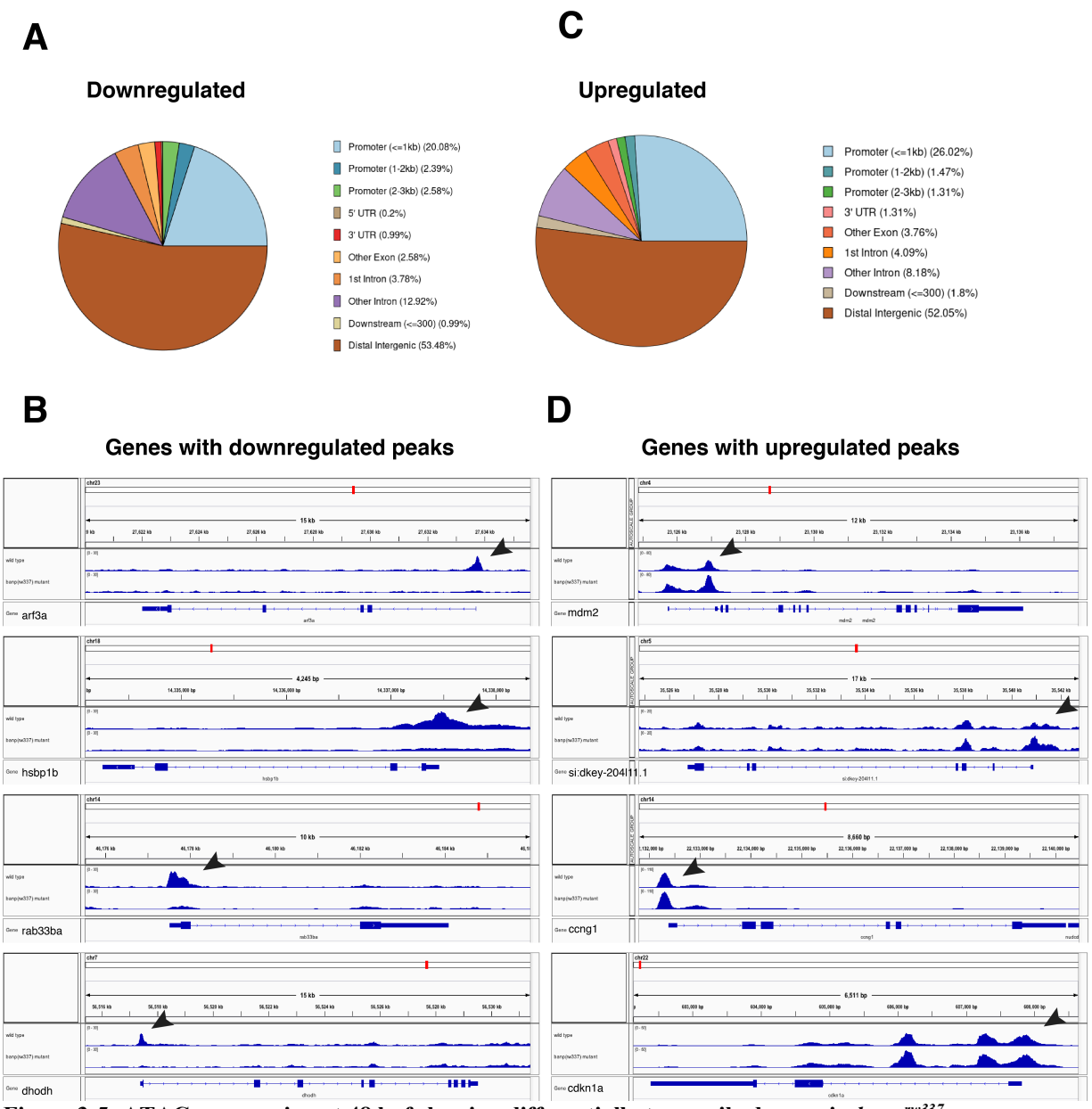

Figure 3-5: ATAC- sequencing at 48 hpf showing differentially transcribed genes in *banp*^{rw337}
(A) Distribution of downregulated peaks across the genome in *banp*^{rw337} mutants. (B) Genes showing reduced transcription in mutants visualized using the Integrative Genomics Viewer. A peak at TSS represents active transcription. (C) Distribution of upregulated peaks across the genome in *banp*^{rw337} mutants. (D) Genes showing higher transcription in mutants. Black arrowheads show a differential regulated peak.

Rank	Motif	Name	P-value	log P-pvalue	q-value (Benjamini)	# Target Sequences with Motif	% of Targets Sequences with Motif
1		Hoxb4(Homeobox)/ES-Hoxb4-ChIP-Seq(GSE34014)/Homer	1e-17	-4.039e+01	0.0000	35.0	6.97%
2		HOXA1(Homeobox)/mES-Hoxa1-ChIP-Seq(SRP084292)/Homer	1e-17	-3.975e+01	0.0000	44.0	8.76%
3		HOXA2(Homeobox)/mES-Hoxa2-ChIP-Seq(Donaldson_et_al.)/Homer	1e-16	-3.684e+01	0.0000	27.0	5.38%
4		LIN-39(Homeobox)/cElegans.L3-LIN39-ChIP-Seq(modEncode)/Homer	1e-13	-3.186e+01	0.0000	83.0	16.53%
5		Pdx1(Homeobox)/Islet-Pdx1-ChIP-Seq(SRA008281)/Homer	1e-11	-2.732e+01	0.0000	76.0	15.14%
6		PBX2(Homeobox)/K562-PBX2-ChIP-Seq(Encode)/Homer	1e-11	-2.540e+01	0.0000	69.0	13.75%
7		Hoxc9(Homeobox)/Ainv15-Hoxc9-ChIP-Seq(GSE21812)/Homer	1e-7	-1.837e+01	0.0000	39.0	7.77%
8		p73(p53)/Trachea-p73-ChIP-Seq(PRJNA310161)/Homer	1e-6	-1.534e+01	0.0000	9.0	1.79%
9		HOXA9(Homeobox)/HSC-Hoxa9-ChIP-Seq(GSE33509)/Homer	1e-6	-1.526e+01	0.0000	47.0	9.36%
10		p53(p53)/Saos-p53-ChIP-Seq(GSE15780)/Homer	1e-5	-1.312e+01	0.0002	11.0	2.19%

Table 3-1: Table showing top 10 motifs enriched in open chromatin in the *banp*^{rw337} mutants.

Offset	Sequence (*tp53* binding motif)	Strand	MotifScore	Ensembl ID	Gene Name
-103	GACTTGCCCGGGCTTGCATC	+	11.4	ENSDARG00000086374	isg15
-86	GAGACTTGCCCGGGCTTGCA	-	11.2	ENSDARG00000086374	isg15
-78	ATCATGTCTGGGCATGTCTT	+	13.2	ENSDARG00000100513	rps27l
-61	GGATCATGTCTGGGCATGTC	-	13.4	ENSDARG00000100513	rps27l
-91	AGCAAGTACCAACATGCCCA	+	10.1	ENSDARG00000037804	phlda3
-74	GGAGCAAGTACCAACATGCC	-	10.1	ENSDARG00000037804	phlda3
-245	TAAACTTGTCTGAACATCAC	-	8.8	ENSDARG00000043196	rnasel2
-237	AAGTTGTTCGGGCATGTCTC	+	10.0	ENSDARG00000042727	exo5
-220	GGAAGTTGTTCGGGCATGTC	-	9.6	ENSDARG00000042727	exo5
-117	AGCATGTCAGGGCTTGTTAT	+	11.3	ENSDARG00000069282	bbc3
-100	TGAGCATGTCAGGGCTTGTT	-	12.1	ENSDARG00000069282	bbc3

Table 3-2: Upregulated genes in *banp*^{rw337} mutants with *tp53* binding motif (p53(p53)/Saos-p53-ChIP-Seq (GSE15780)/Homer).

Rank	Motif	Name	P-value	log P-pvalue	q-value (Benjamini)	# Target Sequences with Motif	% of Targets Sequences with Motif
1		GFX(?)/Promoter/Homer	1e-24	-5.720e+01	0.0000	20.0	3.27%
2		ZBTB33(Zf)/GM12878-ZBTB33-ChIP-Seq(GSE32465)/Homer	1e-20	-4.674e+01	0.0000	29.0	4.75%
3		bcd(Homeobox)/Embryo-Bcd-ChIP-Seq(GSE86966)/Homer	1e-15	-3.482e+01	0.0000	87.0	14.24%
4		Otx2(Homeobox)/EpiLC-Otx2-ChIP-Seq(GSE56098)/Homer	1e-13	-3.095e+01	0.0000	65.0	10.64%
5		GSC(Homeobox)/FrogEmbryos-GSC-ChIP-Seq(DRA000576)/Homer	1e-9	-2.204e+01	0.0000	82.0	13.42%
6		Zfp281(Zf)/ES-Zfp281-ChIP-Seq(GSE81042)/Homer	1e-8	-1.861e+01	0.0000	14.0	2.29%
7		CRX(Homeobox)/Retina-Crx-ChIP-Seq(GSE20012)/Homer	1e-7	-1.711e+01	0.0000	127.0	20.79%
8		YY1(Zf)/Promoter/Homer	1e-5	-1.275e+01	0.0004	12.0	1.96%
9		Pitx1(Homeobox)/Chicken-Pitx1-ChIP-Seq(GSE38910)/Homer	1e-5	-1.197e+01	0.0007	185.0	30.28%
10		NFY(CCAAT)/Promoter/Homer	1e-4	-1.030e+01	0.0034	60.0	9.82%

Table 3-3: Table showing top 10 motifs enriched in closed chromatin in the *banp*^{rw337} mutants
Banp motif (TCTCGCGAGA) is revealed with rank 1. Banp motif was not identified until 2021. Hence Homer shows ambiguous annotation.

3.3.3 Identifying most probable gene targets responsible for the *banp*^{rw337} mutant phenotype

RNA sequencing and ATAC sequencing both revealed gene targets that are modulated differently in *banp*^{rw337} mutants. The next step was to identify the most likely candidate genes differentially regulated in mutants to uncover the molecular basis of the cellular defects in the *banp*^{rw337} mutant. We did this by combining ATAC and RNA sequencing datasets to select consistent differentially regulated targets in both. This selection was made to limit the target genes to those with the highest potential to be validated further. To begin, I chose genes that are differentially regulated in RNA and ATAC sequencing. 12 genes were upregulated, and 45 genes were downregulated (Table 3-4). Selecting differentially spliced genes from them limited the pool even more (Figure 3-6 A, B, green). *tp53*, *mdm2*, *cdkn1a*, and *rbl2(p130)* were the four upregulated genes. Similarly, eleven genes such as *hsbp1b*, *arf3a*, *rab33ba*, *rpl12, puraa, sec62, rpp14, cenpt, upf32, slc39a7* and *map2k2b* downregulated.

We chose *tp53* as our primary candidate for validation among the differentially regulated targets for the following reasons. First, we found that *tp53* is one of the most upregulated transcripts. In addition, the downstream targets of the *tp53* response network were also found to be expressed differentially in the *banp*^{rw337} mutants. Second, analysis of ATAC peaks within the *tp53* genomic area revealed that *tp53* is one of the few transcriptionally active and alternative spliced targets in mutants. Third, earlier results from mammalian systems show that *tp53* and *banp* interact in various ways (Jalota-Badhwar, Kaul-Ghanekar et al. 2007, Singh, Mogare et al. 2007, Sinha, Malonia et al. 2010, Singh, Raina et al. 2012, Sinha, Malonia et al. 2012,

Chakraborty, Adhikary et al. 2014, Liu, Ma et al. 2014). Based on these findings and the phenotype of the *banp*^{rw337} mutants, *tp53* was deemed one of the most plausible candidates responsible for molecular abnormalities in the mutant.

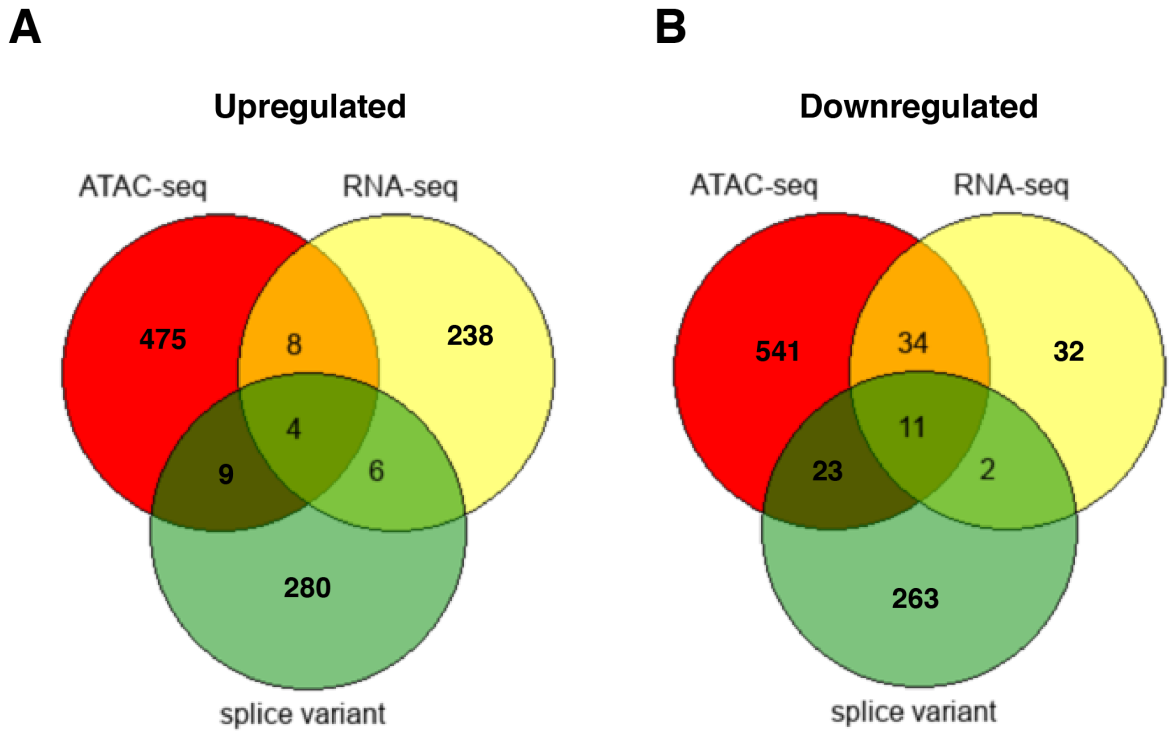

Figure 3-6: Combining RNA sequencing and ATAC-sequencing
(A) Venn diagram showing the number of genes that upregulated its mRNA (yellow), open chromatin region (red), and alternately spliced (green).
(B) Venn diagram showing the number of genes that downregulated its mRNA (yellow), closed chromatin region (red) and alternately spliced (green).

Upregulated (12 genes)		Downregulated (45 genes)	
Ensembl ID	Gene name	Ensembl ID	Gene name
ENSDARG00000007077	ankrd50l	ENSDARG00000040396	bcl7bb
ENSDARG00000033443	mdm2	ENSDARG00000041921	hsbp1b
ENSDARG00000035559	*tp53*	ENSDARG00000044899	tmem183a
ENSDARG00000037804	phlda3	ENSDARG00000051889	dhodh
ENSDARG00000045636	rbl2	ENSDARG00000052290	rab33ba
ENSDARG00000054374	alg13	ENSDARG00000067591	puraa
ENSDARG00000069282	bbc3	ENSDARG00000067795	ifngr2
ENSDARG00000071877	dhrs7cb	ENSDARG00000068918	map2k2b
ENSDARG00000076554	cdkn1a	ENSDARG00000069297	upf3a
ENSDARG00000076667	ccng1	ENSDARG00000069742	cul5a
ENSDARG00000100513	rps27l	ENSDARG00000069808	ostm1
ENSDARG00000104205	cfhl3	ENSDARG00000070109	ncapg
Downregulated (45 genes)		ENSDARG00000070539	arf3a
ENSDARG00000003257	zgc:101559	ENSDARG00000074255	micu3b
ENSDARG00000004260	cul5b	ENSDARG00000075881	SERF2
ENSDARG00000006691	rpl12	ENSDARG00000077306	cutc
ENSDARG00000008592	mtmr8	ENSDARG00000077749	usp54b
ENSDARG00000010941	pomgnt2	ENSDARG00000078166	si:dkey-78p8.1
ENSDARG00000011152	rpp14	ENSDARG00000078599	micu3a
ENSDARG00000012776	smarca1	ENSDARG00000088764	lyplal1
ENSDARG00000014218	mecp2	ENSDARG00000091271	cenpt
ENSDARG00000019951	sec62	ENSDARG00000092934	si:dkey-32e6.3
ENSDARG00000020241	icmt	ENSDARG00000101115	med30
ENSDARG00000023958	rnf181	ENSDARG00000101271	si:ch211-227n13.3
ENSDARG00000028721	mapk14b	ENSDARG00000101631	etfa
ENSDARG00000028786	chst12a	ENSDARG00000103831	ankrd13c
ENSDARG00000033364	mgst3b	ENSDARG00000103996	spdl1
ENSDARG00000039062	morn4	ENSDARG00000104130	rbm26
ENSDARG00000039345	drg1	ENSDARG00000104451	slc39a7

Table 3-4: Table showing genes that are differentially regulated in both ATAC and RNA sequencing.

3.3.4 *tp53* expression in *banp*^{rw337} at 48 hpf

Our western blot analysis of the Tp53 protein revealed that the full-length Tp53 (FL Tp53) protein was significantly more stable in mutants (Figure 3-7 A). Although *tp53* mRNA was increased in our RNA sequencing, our qRT-PCR validation of FL *tp53* showed no significant difference in mutants compared to wild type (Figure 3-7 C). Furthermore, using ATAC-sequencing to compare chromatin accessibility near *tp53*, we discovered that mutants had a particular open chromatin area in intron 4 of *tp53* that is not present in wildtypes (Figure 3-7 B). Therefore, in *banp*^{rw337} mutants, the internal promoter at intron 4 (Chen, Ruan et al. 2005, Chen, Ng et al. 2009) is selectively open (Figure 3-7 B, red box), implying differential transcription of

Δ*113tp53*. Interestingly, a transcript variant of *tp53* known as Δ*113tp53* is transcriptionally active in mutants (Figure 3-7 B, RNA-seq). Using specific primers, qRT-PCR confirmation of differential expression of FL *tp53* and Δ*113tp53* demonstrated that mutants only overexpress Δ*113tp53* (Figure 3-7 C). Differential expression of Δ*113tp53* is thought to enhance cell cycle arrest by imparting anti-apoptotic action. This differential expression is to cope with physiological or environmental stress. It is one of the components that influence how cells respond to stress or DNA damage (Chen, Ng et al. 2009, Chen and Peng 2009, Manfredi 2009, McElderry, Carrington et al. 2019, Joruiz, Beck et al. 2020, Ye, Zhao et al. 2020). In zebrafish, upregulation of Δ*113tp53* indicates DNA double-strand breaks (DSBs) (Gong, Gong et al. 2015). Overall, our findings imply that *banp*^{rw337} mutants show specific transcription of Δ*113tp53*, likely contributing to the cellular abnormalities.

3.3.5 *mdm2* expression in *banp*^{rw337} at 48 hpf

In addition to *tp53*, *mdm2* showed upregulation as well potential alternate splicing in *banp*^{rw337} mutants. A qRT-PCR validation confirmed overexpression of *mdm2* transcript in *banp*^{rw337} mutants (Figure 3-1). We evaluated the transcription regulation at *mdm2,* combining our ATAC and RNA sequencing data. Interestingly, *banp*^{rw337} mutant embryos have enhanced expression of an exon inside intron 1 (Figure 3-8, red box). Additionally, ATAC sequencing data showed a specific higher peak at intron 1 of the *banp*^{rw337} mutant. *mdm2* is a known downstream target of *tp53* (Barak, Juven et al. 1993). The upregulation of *mdm2* is likely due to upregulation *tp53* although activation of *mdm2* may contribute to the cellular phenotype of *banp*^{rw337} mutants.

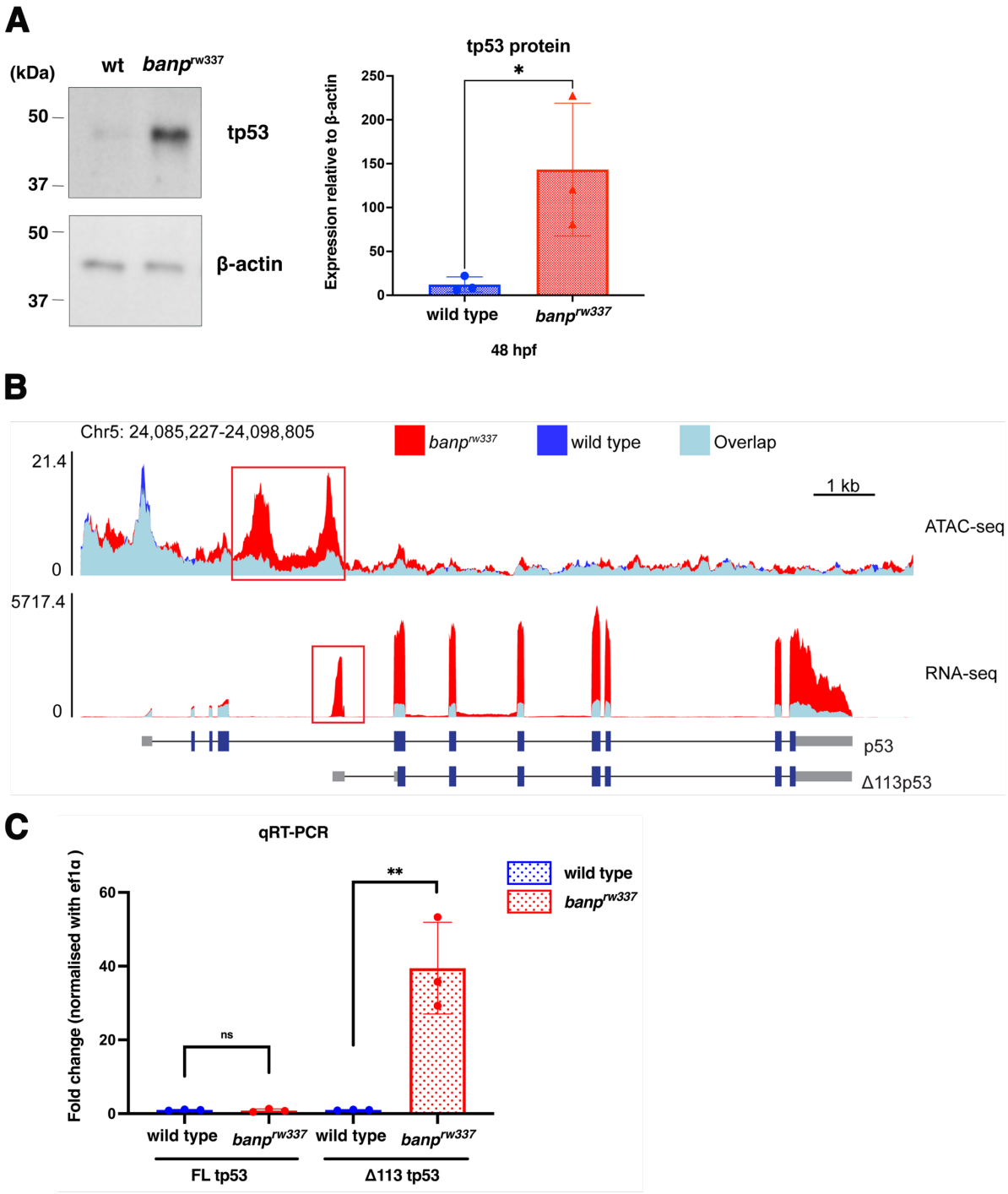

Figure 3-7: differential regulation of *tp53* in *banp*^{rw337} mutants at 48 hpf

(A) Western blot protein expression analysis at 2 dpf. *banp*^{rw337} mutants show increased expression of Tp53 protein. Bar graph represents protein expression normalized with β-actin. Unpaired t-test (two-tailed) [n=3, $p < 0.05$ (*)].

(B) ATAC sequencing data showing chromatin region of *tp53* transcript. We can see two specific open chromatin peaks (red box) at intron 4 of the *tp53* transcript. The first peak corresponds to the promoter region of *Δ113tp53* variant of *tp53*, and the second peak corresponds to exon 1 of *Δ113tp53*. This differential ATAC peak confirms the specific transcription of *Δ113tp53* in *banp*^{rw337} mutants.

(C) qRT-PCR based validation of FL *tp53* and Δ*113tp53* expression at 48 hpf. qRT-PCR showing overexpression of Δ*113tp53* in *banp*^{rw337} mutants in comparison to wildtype. However, the mRNA expression of FL *tp53* is not significantly different in mutants. Unpaired t-test (two-tailed) [n=3, $p < 0.01$ (**), NS (not significant)].

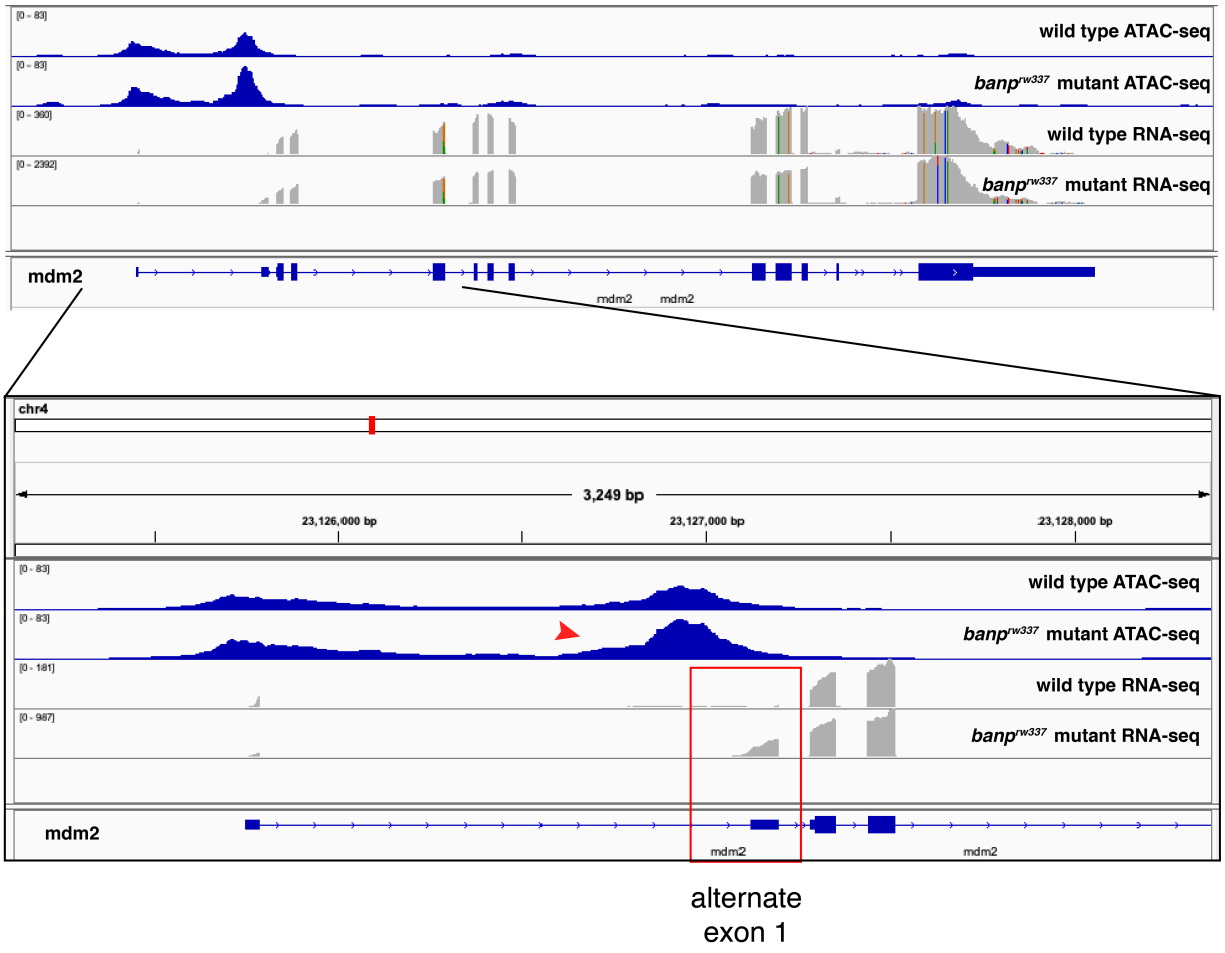

Figure 3-8: Differential expression of *mdm2* in *banp*^{rw337} mutants at 48 hpf
The ATAC-seq and RNA-seq data of *mdm2* were visualized using the Integrative Genomics Viewer. Reads aligning to chromosome 4 at *mdm2*. In *banp*^{rw337} mutant embryos, the *mdm2* transcript shows enhanced expression of alternative exon 1 (red box). The number of ATAC seq peaks mapping to intron 1 in *banp*^{rw337} mutant embryos (red arrow) is also high compared to wildtype.

3.3.6 *tp53* knockdown rescue cell death in *banp*^{rw337} mutants at 48 hpf

Depleting *tp53* will allow us to determine the contribution of *tp53* to cellular defects in mutants, as we have seen upregulation of the Tp53 protein and its downstream targets (section 3.3.4). Knocking down *tp53* using morpholino is known to show effective depletion of *tp53* along with no developmental defects (Langheinrich, Hennen et al. 2002). Hence, we used tp53-MO to knock down FL *tp53* to evaluate cell death. Additionally, we found many downstream targets of *tp53*, such as *cdkn1a*, *mdm2*, and Δ*113tp53* were downregulated in *banp* morphant embryos

at 3dpf when *tp53* was knocked down using MO (Figure 3-9). This *tp53-banp* double knockdown study demonstrates that the activation of *cdkn1a*, *mdm2*, and Δ*113tp53* in *banp* morphant embryos was indeed dependent on *tp53*.

Next, knocking down Tp53 eliminates cell death in *banp*^{rw337} mutant retinas at 48 hpf, implying that activation of *tp53* contributes to cell death in *banp*^{rw337} mutants (Figure 3-10, 48 hpf). However, cell death reappears in tp53-MO injected *banp*^{rw337}mutants by 72 hpf (Figure 3-10, 72 hpf). Although this cell death activation at 72 hpf is not statistically significant in the *banp*^{rw337} mutants, it shows that *banp*^{rw337} mutants may have *tp53*-independent abnormalities (Figure 3-10 C). Furthermore, knocking down Δ*113tp53* alone did not prevent cell death in *banp*^{rw337} mutant retinas at 48 and 72 hpf (Figure 3-10, Δ113tp53-MO). The possibility of bypass mechanisms and regulation independent of *tp53* contributing to cellular defects in the *banp*^{rw337} mutant cannot be ruled out (Nakka and Chattopadhyay 2010, Malonia, Sinha et al. 2011, Chaudhary, Nakka et al. 2014, Malonia, Yadav et al. 2014). Overall, in the *banp*^{rw337} mutants, partial cell death rescue by tp53-MO and selective activation of Δ*113tp53* suggest a cellular dysfunction upstream or parallel to *tp53* and the likelihood of DNA damage accumulation, respectively.

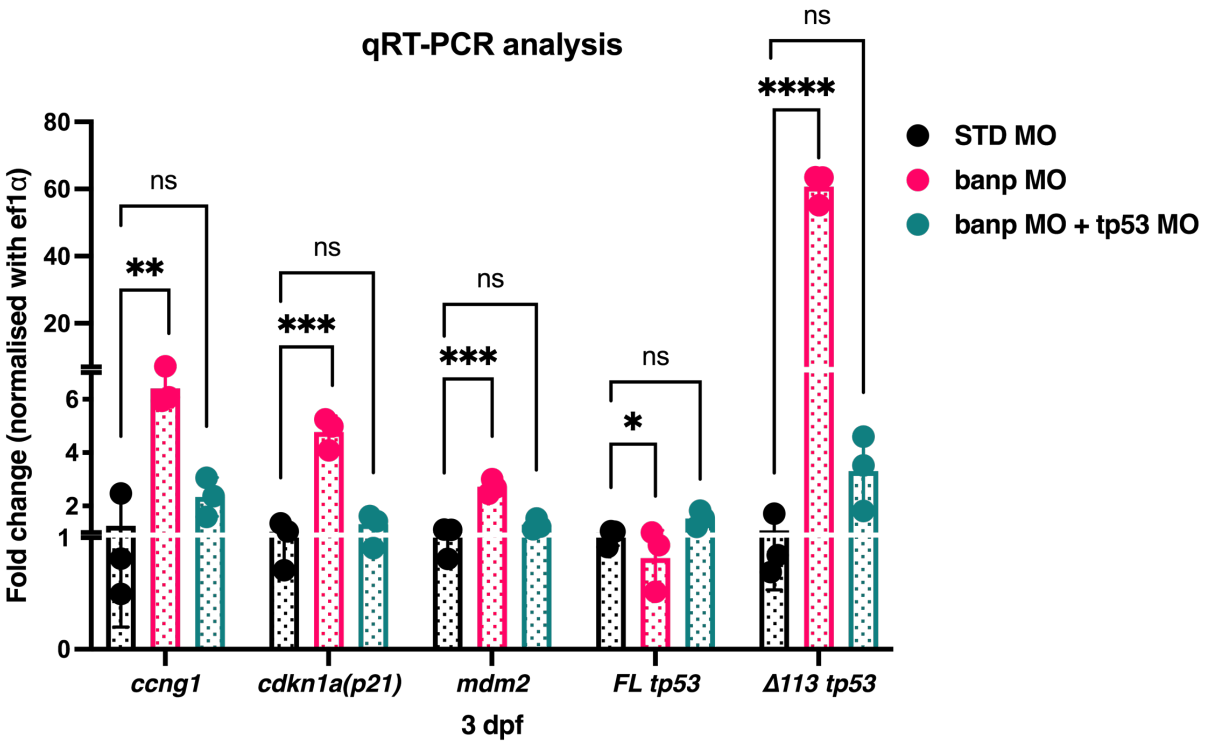

Figure 3-9: *tp53* knockdown reduce expression of its downstream targets in *banp* morphants
qRT-PCR based validation of *tp53* target genes. banp-MO injection shows significant high expression of *tp53* target genes *ccng1*, *cdkn1a*, *mdm2*, Δ*113tp53*. Co-knockdown of *tp53* and *banp* has reduced overexpression of *tp53* targets genes, suggesting that overexpression of *ccng1*, *cdkn1a*, *mdm2* and Δ*113tp53* is likely dependent on Tp53 in *banp* morphants. Unpaired t-test (two tailed) [n=3, $p < 0.05$ (*), $p < 0.01$ (**), $p < 0.001$ (***), $p < 0.0001$ (****), NS (not significant)]

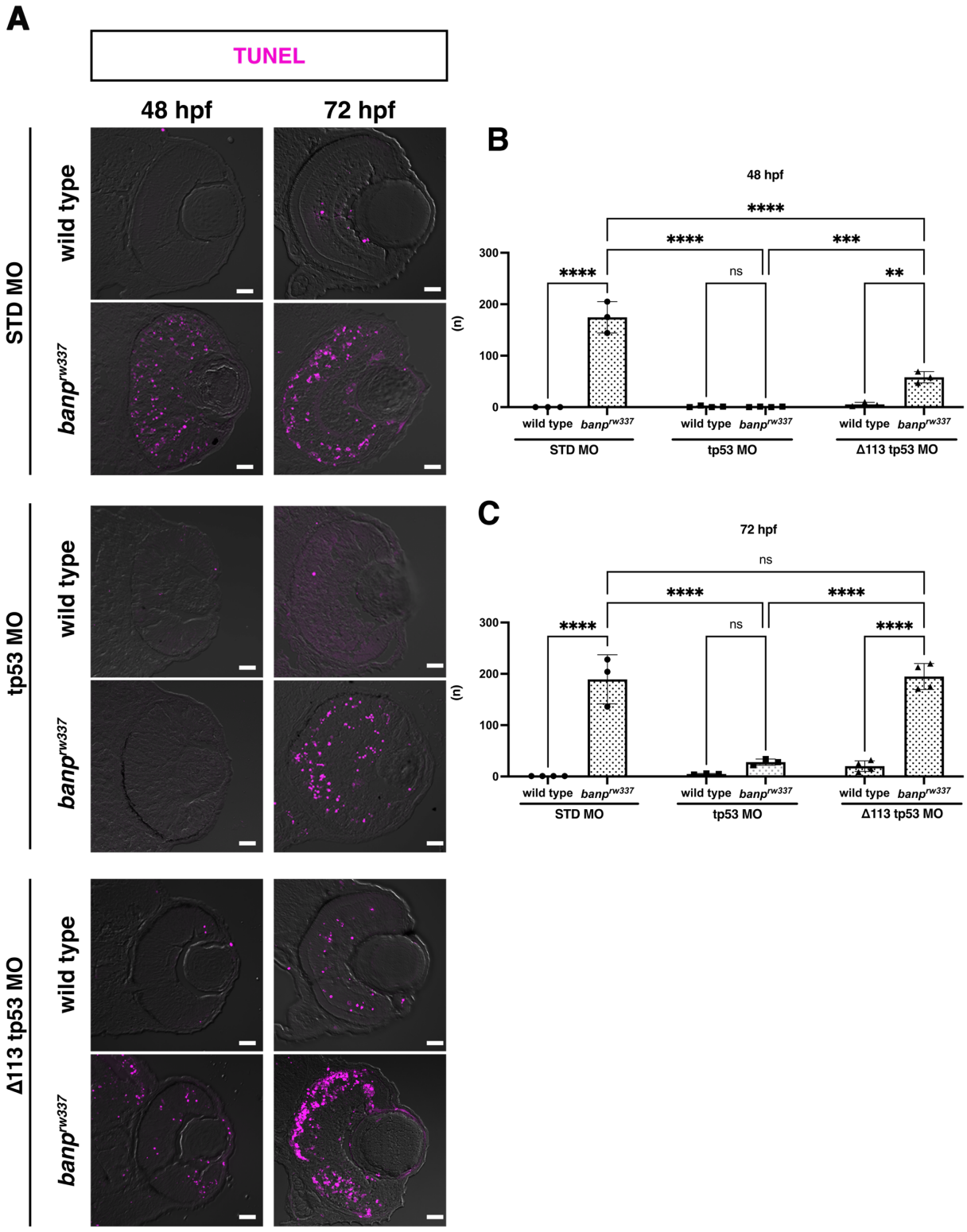

Figure 3-10: *tp53* knockdown partially rescue cell death in *banp*^{rw337} mutants
(A) TUNEL staining of 48 and 72 hpf embryos to detect cell death. Cell death on retinal sections upon knocking down *tp53*, *Δ113tp53* is shown in comparison to STD-MO injection. Scale bar = 20μm (B-C) bar graphs show the number of TUNEL positive cells per retinal section upon knocking down *tp53*, *Δ113tp53*.

(B) At 48 hpf, tp*53* knocked down completely rescue cell death in *banp*^{rw337} mutant embryos compared to wildtype. However, the ∆113tp53-MO injection did not. (C) At 72 hpf, *tp53* and ∆*113tp53* knockdown partially rescue cell death in *banp*^{rw337} mutants. (2way ANOVA with Tukey's multiple comparisons test).

3.4 Discussion

We used RNA-sequencing together with ATAC-sequencing to examine the transcriptome-wide consequences of *banp* deficiency in 48 hpf zebrafish embryos to obtain insight into the molecular function of *banp* in specific biological processes. At molecular level, *banp*^{rw337} mutant embryos had lower expression of exons 1 to 4 of the *tp53* transcript, which corresponds to the full-length *tp53* isoform, and higher expression of an alternate exon within intron 4 correlates to the 5′ untranslated region (UTR) of an alternate isoform ∆*113p53* (Figure 3-7 B). The zebrafish isoform ∆*113p53* is orthologous to the human isoform ∆133p53, thoroughly studied (Joruiz and Bourdon 2016). This variant functions as a *tp53*-response gene. It lacks the first 113 amino acids (133 in humans) from the N-terminal region of the protein, which includes the trans-activation, *mdm2*-binding, and part of the DNA-binding domains (Joruiz and Bourdon 2016).

Furthermore, the *banp*^{rw337} mutant embryos had higher expression of an exon within intron 1(alternate exon 1) of *mdm2,* indicating that *mdm2* transcript variants were expressed differently. An alternate promoter, P2, transcribes this alternate exon 1 (Manfredi 2010, Nag, Qin et al. 2013, McElderry, Carrington et al. 2019). The 5′ UTR transcribed from the distal promoter P2 corresponds to the alternative exon 1 utilized in *banp*^{rw337} mutant embryos. Activated *tp53* is known to trigger this promoter P2 (Manfredi 2010, Nag, Qin et al. 2013). Although the use of the distal promoter P2 does not modify the translation start site or protein sequence of *mdm2*, it has been established that the use of such different 5′ UTRs modulates *mdm2* production in response to activated *tp53* (Manfredi 2010). Additionally, our ATAC sequencing results reveal a specific open region in intron 1 of *mdm2,* indicating the use of a different promoter (Figure 3-8, red arrow). Furthermore, knocking down FL *tp53* indeed downregulates *mdm2* in *banp* morphant embryos (Figure 3-9). As a result, our findings imply that elevated *tp53* levels in *banp*^{rw337} mutant embryos resulted in *mdm2* overexpression via the *tp53*-dependent promoter P2.

In the absence of *banp*, our results suggest that *tp53* expression rises, triggering the alternate distal promoters of *mdm2* and *tp53*, resulting in isoforms, *mdm2* via P2 and ∆*113p53*. The *mdm2* protein acts as a *tp53* inhibitor. It reduces the transcriptional activity of FL *tp53*, promotes its nuclear export, degradation after binding to FL *tp53*. *mdm2* overexpression in tumors suppresses *tp53*, allowing uncontrolled cell proliferation to prevail. ∆*113p53* is an N-terminally shortened version of *tp53* that lacks the *mdm2*-interacting motif and transactivation domain and a portion of the DNA-binding domain (Chen and Peng 2009, Zhao, Ye et al. 2021). So, the differential expression of ∆*113p53* likely disruptions the negative feedback loop between *mdm2* and *tp53*. This differential expression of *tp53* transcript variants changes the expression of *tp53* target genes involved in diverse cell fate decisions (Gong, Gong et al. 2015). Among the dramatically elevated genes in *banp*^{rw337} mutant embryos were *ccng1*, *caspase8* and *bbc3*. These are *tp53* target genes involved in apoptosis. Increased apoptosis was seen in the mutant embryos, as expected. However, the failure of *tp53*, ∆*113tp53* knockdown to completely rescue apoptosis implies that *tp53* activation is not the sole source of the apoptotic phenotype in *banp*^{rw337} mutant embryos (Figure 3-10).

If not *tp53,* the primary cause of cellular defect could be upstream or independent of *tp53*. Considering other molecular evidence in *banp*^{rw337} mutant embryos, specific activation of *exo5* and Δ*113tp53* is notable. These molecular factors have previously been reported to be responsible for DNA damage response (Chen and Peng 2009, Gong, Gong et al. 2015, Khan, Stephen et al. 2019, Ali, Zhang et al. 2020, Joruiz, Beck et al. 2020). Following genotoxic stress, Δ*113p53* causes upregulation of DNA repair genes such as *rad51*, *lig4*, and *rad52* and activation of DNA repair pathways, similar to its human counterpart Δ*133p53*. Δ*113p53* interacts with full-length *tp53* to re-orient its activity towards DNA repair by differentially modulating the expression of its target genes in order to favor DNA DSB repair and cell fate determination upon stress or DNA damage (Chen and Peng 2009, Gong, Gong et al. 2015, Joruiz, Beck et al. 2020). Δ*113p53* has been shown to support zebrafish heart regeneration in a recent study. It accumulates in cardiomyocytes at the injury site, facilitating their proliferation and redox homeostasis, thus myocardial regeneration (Ye, Zhao et al. 2020). A *def* gene mutation upregulates Δ*113p53* expression in zebrafish, resulting in digestive organ development problems (Tao, Shi et al. 2013). A similar mechanism has been identified for *dhx15* mutation, a splicing factor that causes morphological defects and embryo lethality by upregulating Δ*113p53* expression (McElderry, Carrington et al. 2019). Based on this evidence, we presume DNA damage may also occur in the *banp*^{rw337} mutants that cause cellular impairments. I shall investigate this aspect in the following chapter.

It is an intriguing correlation, where investigations utilizing zebrafish and cell lines have identified overexpression of *tp53* as a similar mode of action in response to loss of function of components involved in the surveillance machinery of cell cycle (Bladen, Navarre et al. 2007, Yamaguchi, Fujimori-Tonou et al. 2008, Rodriguez-Mari and Postlethwait 2011, Danilova, Bibikova et al. 2014, Hu, Holzschuh et al. 2015, McElderry, Carrington et al. 2019, Li, Liu et al. 2021). Furthermore, studies compiling *tp53* overexpression in various zebrafish mutants concluded that it is a universal response to the loss of essential genes involved in various biological processes, including DNA damage response (Danilova, Kumagai et al. 2010). When a further study uses RNA-sequencing-based global approaches to analyze knockdown and knockout of cell cycle surveillance genes in cell lines and model species, we may uncover similar regulation of the *mdm2-tp53* pathway as a general mechanism.

In summary, our efforts to identify molecular factors responsible for cellular defects in *banp*^{rw337} mutants revealed *tp53* as the most probable candidate, however knocking down FL *tp53* partially rescued cell death (Figure 3-10 A, 48 hpf). This partial rescue opened possibilities for *tp53* independent molecular (upstream or parallel) defects due to loss of function of Banp. In addition, we confirmed that the Banp motif is conserved in zebrafish.

CHAPTER 4

Transcription targets of Banp in zebrafish

4.1 Motivation

4.1.1 Mitotic chromatin segregation

The goal of mitosis in a somatic cell is to segregate replicated chromosomes into daughter cells without errors. This process of chromosome segregation is achieved by a complex interaction of multiple regulatory factors, which is not yet completely understood. According to our current understanding of eukaryotes, the chromosome cycle initiates with the replication of condensed chromosomes in the S-phase (**Figure 4-1**). Chromosomes in post replicative cells are made up of duplicated sister chromosomes. Further, in the following mitotic phase, the condensed chromosome continues with chromosomal separation and finishes with chromosome translocation into two daughter cells with the help of microtubule structures called spindle apparatus. This segregation is accomplished by a sequence of tightly regulated events consisting of many regulatory factors. Protein complexes such as cohesin assemble on duplicated sister chromatids to link them together since the S-phase of the cell cycle. While proceeding to the mitotic phase of the cell cycle, a specialized protein structure called kinetochore assembles at the centromeric region of sister chromatids (Santaguida and Musacchio 2009). At mitotic metaphase, two sister chromatids are oriented at metaphase plate back-to-back. In mitotic anaphase, sister chromatids are separated towards the spindle poles with the help of the mitotic spindle apparatus. An accurate attachment of spindle apparatus onto chromatids is ensured by spindle assembly checkpoint (SAC). SAC delays the process of anaphase onset until all chromosomes achieve correct alignment at the metaphase plate (Musacchio and Salmon 2007). E3 ubiquitin ligase Anaphase Promoting Complex/Cyclosome (APC/C) is one key regulator that senses SAC to regulate the onset of anaphase (Kops, Snel et al. 2020) (**Figure 4-2**).

Cohesin and condensins are multi-subunit protein complexes located on chromosomes and are highly conserved in eukaryotes (Skibbens 2019). Condensin reorganizes chromosomes into their very compact mitotic structure, whereas cohesin glues replicated sister chromatids together until they separate at anaphase (Skibbens 2019). Cohesin is removed from sister chromatids when separase is activated. The separase inhibitor securin is degraded by APC/CCdc20 activation, resulting in cohesin cleavage required for chromatid segregation in mitosis. The SAC detects kinetochores with unoccupied microtubule-binding sites and, if this is the case, inhibits the anaphase-promoting complex/cyclosome (APC/C) and its activator, Cdc20, delaying the metaphase-to-anaphase transition (Yanagida 2005). This SAC allows for the reliable segregation of paired sister chromatids into two daughter cells. An abnormal number of chromosomes are produced when the genetic material is not partitioned correctly, resulting in aneuploid daughter cells. Errors in chromosome segregation are established to cause pathologies, including cancer (Jallepalli and Lengauer 2001, Stallings 2007, Gisselsson 2008, Curtis, Ruda et al. 2020). Regulators of cell division and chromosome distribution are essential for the development of anticancer drugs. Therefore, discovering the new target genes potentially involved in the regulation of chromosome segregation and mitosis is expected to lead to new

anticancer drugs. Traditional genetic studies that led to the phenotypic discovery of many genes involved in chromosome segregation have recently been extended using systematic high-throughput approaches. The identification of entire gene sets required for chromosome segregation, on the other hand, is far from complete. The redundancy of gene functions and embryonic lethality is blamed for the lack of mutants in genes that mediate chromosome segregation.

A recent study on identifying genes required for proliferative signaling in cancer cells conducted a Genome-wide CRISPR screen across 342 different cancer cell lines (Meyers, Bryan et al. 2017). This genome wide CRISPR screen was a powerful tool and identified a repertoire of essential genes required for complex cellular signaling networks of cancer proliferation. We used the data from 278 cell lines and their Bayes factor (BF) scores from this study to evaluate cancer dependencies of our genes of interest, including *banp* (Meyers, Bryan et al. 2017, Mair, Tomic et al. 2019). The BF score is a confidence measure of whether a gene is required for fitness in a pooled CRISPR screen. A High BF score corresponds to increased essentiality of the corresponding gene of interest and vice versa. **Figure 4-3** shows the essentiality of selected genes across 278 cancer cells. Hence out of curiosity we selected to plot a set of known tumor suppressor genes, oncogenes, and genes involved in mitotic spindle regulation along with *banp*. The selected genes were clustered to place similar responding genes close to each other. This clustering has grouped the gene *banp* towards the right side of the heat map together with *bub1, spdl1, cenpe, cenpc, cenpt, cenpp braca1, braca2, ddx1, ddx5, Kras*, and *cdk6* (**Figure 4-3,** black arrow). Interestingly many of these genes are involved in specific functions during mitosis. Additionally, the highly essential genes for cell cycle regulation, such as *pcna*, *rpa1*, *ncapg*, are grouped into a cluster to the rightmost side, signifying high essentiality. Similarly, many known tumor suppressors such as *tp53* are grouped to the left side of the heatmap, showing the least essential gene sets. In conclusion, this research shows that Banp is one of the critical genes essential for the cell cycle, most likely engaged in mitotic regulation (Mair, Tomic et al. 2019, Grand, Burger et al. 2021). However, this result contrasts with the belief that Banp is a tumor suppressor (Rampalli, Pavithra et al. 2005, Pavithra, Singh et al. 2009, Singh, Sinha et al. 2009, Bhagat, Jadhav et al. 2018). A possible reason for such a difference is revealed by Grand et. al. Regulation by Banp depends on methylation status its targets, i.e., Banp can have differential functions dependent on cancer cell types due to their aberrant methylation status of chromatin (Grand, Burger et al. 2021). In summary, considering the pleotropic functions of Banp as summarized above and in chapter 1, this chapter compiles our effort to identify possible functions of Banp in regulating cell cycle under physiological conditions.

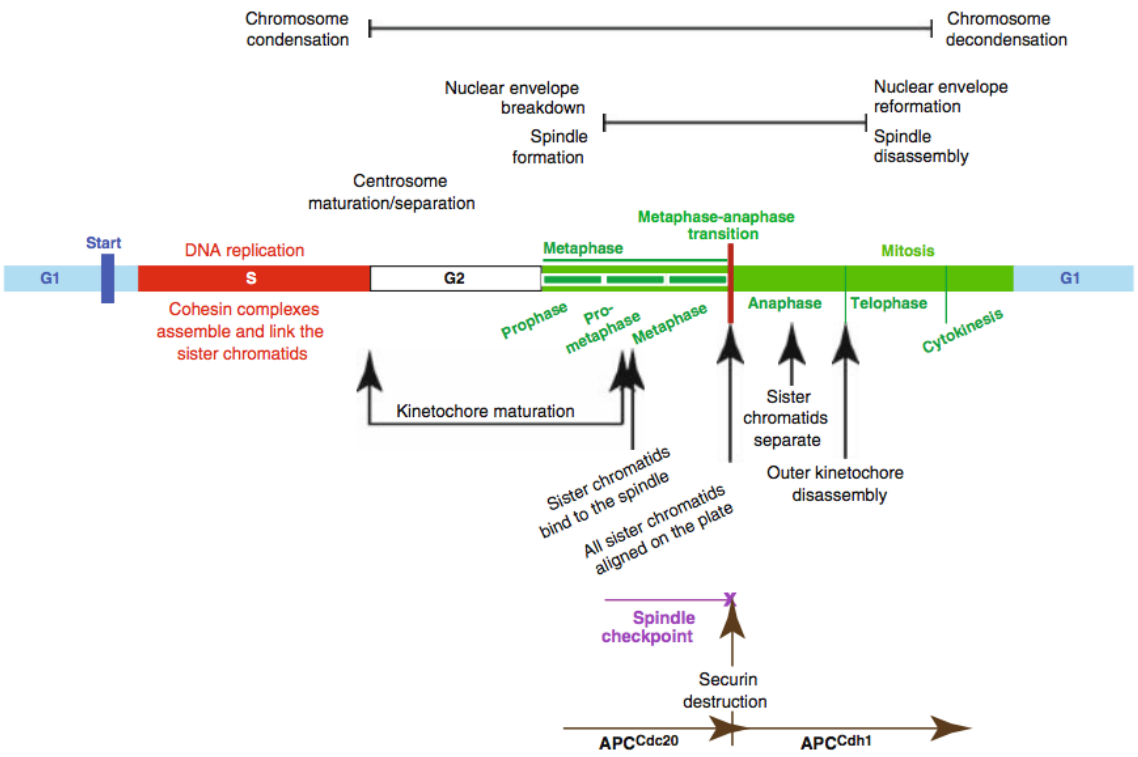

Figure 4-1: The state/activity of chromosomes, the spindle, kinetochores, and sister chromatids are shown schematically in the cell cycle stages.
The anaphase-promoting complex (APC) and the mitotic spindle checkpoint (MSC) functions are depicted in pink and brown. (G1: blue, S-phase: red, G2: white, M-phase (mitosis): green). Image adapted from (Yanagida 2005)

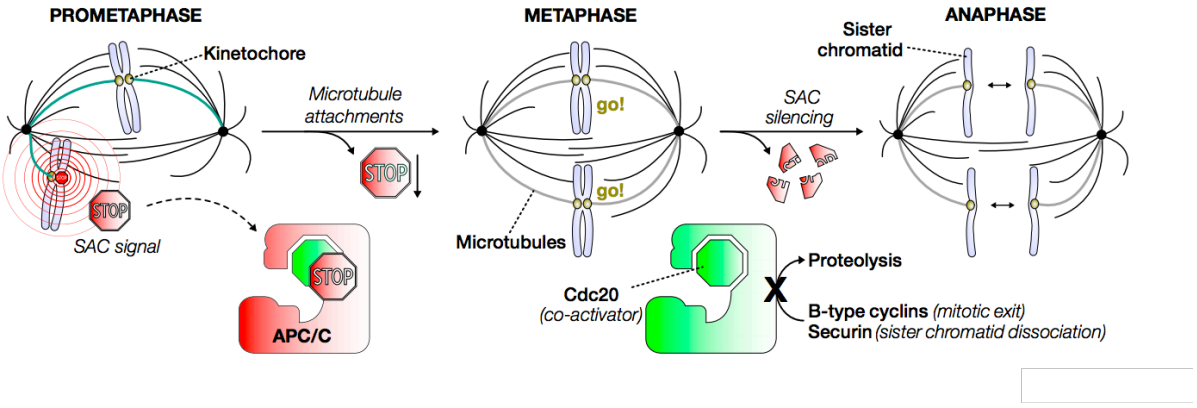

Figure 4-2: Function of spindle assembly checkpoint (SAC) during mitosis.
Image adapted from (Kops, Snel et al. 2020)

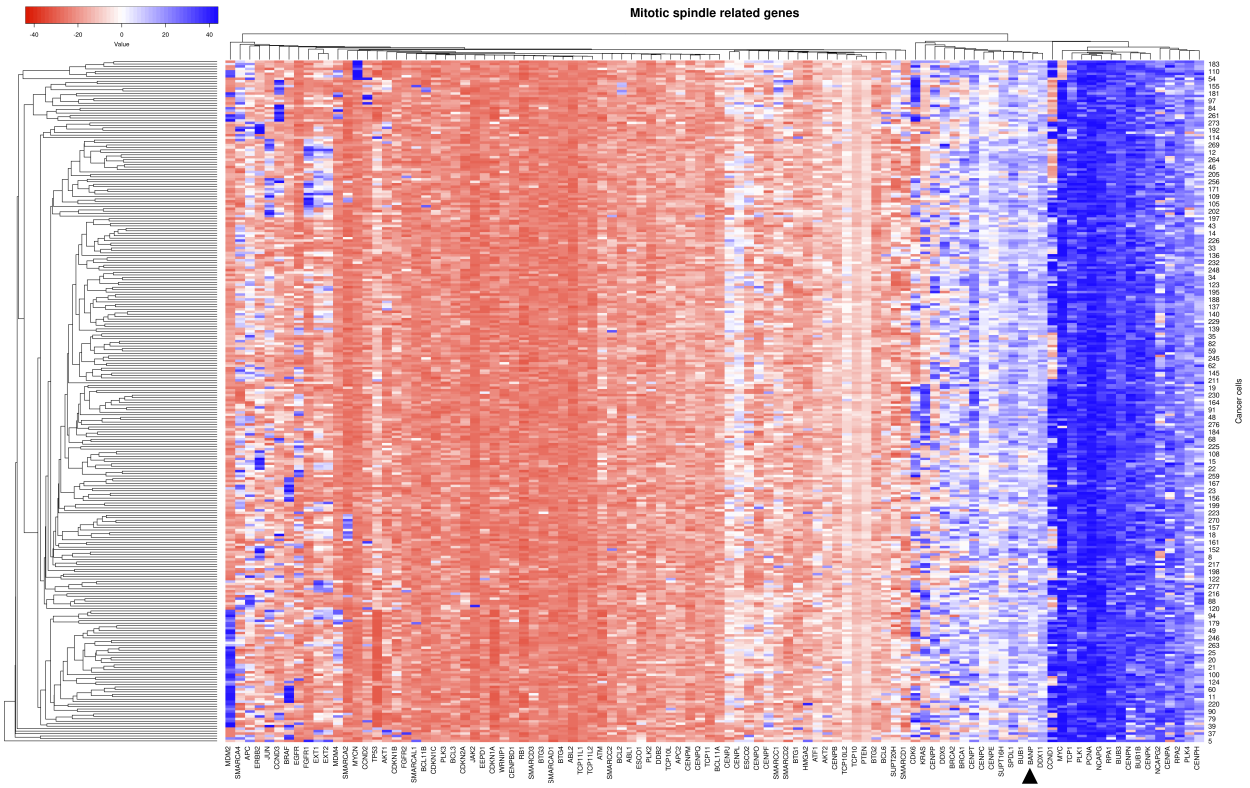

Figure 4-3: Essentiality of given genes in 278 cancer cell lines.
Heat map of Bayes factor (BF). A High BF score corresponds to increased essentiality of the corresponding gene of interest. Data adapted from (Mair, Tomic et al. 2019) and replotted.

4.2 Materials methods

4.2.1 Whole-mount immunostaining for γ-H2AX labeling

Protocol for whole-mount immunostaining to label γ-H2AX was adapted and modified from Diez et al. (Fernandez-Diez, Gonzalez-Rojo et al. 2018). Embryos were genotyped using AO and fixed overnight in 4% paraformaldehyde (in PBS) at 4°C. The next day embryos were washed three times in 1X PBS and permeabilized with 100% methanol for 2 hours at −20°C. Then, they were incubated with 2 N HCl for 1 hour at RT to denature the DNA. Then the embryos were washed twice with PDT [1× PBST (0.1% Tween 20 in PBS 1×), 0.3% Triton, and 1% DMSO] for 20 minutes at RT. After that, they were incubated in blocking solution (10% Goat serum in PBST) for 1 hour at RT and transferred to 1% blocking solution with diluted rabbit monoclonal γ-H2AX for 2 days at 4°C. Then, they were washed with PDT solution and then incubated with fluorescent conjugated secondary antibodies in a 1% blocking solution. Embryos were incubated in the dark with secondary antibodies for 2 days at 4°C. Next, all samples were washed in PDT (X3 times) followed by glycerol storage at 4ºC until imaging. The samples were Imaged with a confocal microscope LSM 710 (Zeiss) followed by image analysis using zen software (Zeiss) or IMARIS. Cell numbers were calculated using IMARIS, and the percentage area of signals was calculated using zen software (Zeiss).

4.2.2 Mitotic spindle labeling

Whole-mount immunostaining to label α-tubulin to label mitotic spindle was performed as follows. Embryos were genotyped using AO and fixed overnight in 2% trichloroacetic acid (TCA) (in MilliQ water) at RT for 2-3 hours. Then embryos were washed three times in 1X PBST (PBS, 0.1 % tritonx100) and left the tubes on ice for 5 minutes. Then, they were incubated in 0.2% trypsin for 4 minutes at 4ºC. Then the embryos were rinsed thrice with PBS. Next, they were fixed using 4% PFA for 5 minutes at 4ºC. After that, they were incubated in blocking solution (10% Goat serum in PBST) for 1 hour at RT and transferred to 1% blocking solution with diluted primary antibody for 2 days at 4°C. Then they were washed with PBST solution and then incubated with fluorescent conjugated secondary antibodies in a 1% blocking solution. Embryos were incubated in the dark with secondary antibodies for 2 days at 4°C. Next, all samples were washed in PBST (X3 times) and glycerol stored at 4ºC until imaging. The samples were imaged with a confocal microscope LSM 880 (Zeiss) followed by image analysis using IMARIS. α-tubulin antibody (Sigma-Aldrich #T5168) stained the fine structures of the mitotic spindle. However, the anti-α-tubulin antibody (GTX124303) did not label the fine structures of the mitotic spindle.

4.2.3 Morpholino injection

ATG morpholino (MO) was used to knock down *banp* and *tp53*. Embryos at the one-cell stage were used for injections. banp-MO was standardized for concentration which showed a similar phenotype to *banp*^{rw337} genetic mutant. 1mMol banp-MO (5'-CCACTAAATCTTGCTCTGACATCAT-3') were used for injections and compared with 5 mismatch banp-MO (5'-CCtCaAAATgTTcCTCTcACATCAT-3') as control. When 1mMol tp53 (5'-GCGCCATTGCTTTGCAAGAATTG-3') was injected, standard-MO (STD-MO) was used as control. To knock down Δ*113tp53*, MO6-*tp53* (5'-GCAAGTTTTTGCCAGCTGACAGAAG-3') was used. STD-MO (5'-CCTCTTACCTCAGTTACAATTTATA-3').

4.2.4 qRT-PCR

RNA isolation and cDNA synthesis were done as described in section 3.2.3 (Chapter 3, Materials and Methods). Primers used for real-time PCR are listed below.
cenpt Forward: tcatgaggagattgtggaagatg, *cenpt* Reverse: ggtgagctctgcgagttatt
ncapg Forward: ctgatgtgagggagcctattt, *ncapg* Reverse: gagtctgtttggcctccatta
atm Forward: cctcaaggctgtggagaact, *atm* Reverse: aggggattttctttacaccactc
atr Forward: aggaacccaatctgccagt, *atr* Reverse: gatgtccagtgccagctctc

4.2.5 Live imaging of cell cycle at 2 dpf zebrafish retina

banp ATG morpholino was injected at the single-cell stage of *Tg [h2afv: GFP; EF1α: mCherry-zGem]* embryos to knock down *banp.* 5-mismatch *banp* ATG morpholino was used as a control. At 2 dpf**,** live embryos were anesthetized using 5% (v/v) tricaine (3-amino benzoic acid- ethyl ester) and mounted laterally using a 1% low melting agarose on top of a depression slide to image retina without left or right preference. The confocal laser scanning microscope Zeiss LSM710 (40X0.8 /1.0 W Plane Apochromat) was used for live imaging. Time-series were obtained after every 1.1 minutes. Data were analyzed using IMARIS software for calculating the time taken to complete each cell division.

4.3 Results

4.3.1 *banp*^{rw337} mutants show DNA damage accumulation

RNA-sequencing analysis revealed upregulation of DNA damage response markers, including *tp53* pathway components and *exo5* (Ali, Zhang et al. 2020) in *banp*^{rw337} mutants (Figure 3-1 B, C). Quantitative RT-PCR revealed that sensors for DNA replication stress and damage, *atm* and atr (Williams and Zhang 2021), are elevated in *banp*^{rw337} mutants (Figure 4-4). Masai lab previously showed that replication stress induces *atr/atm-chk2-tp53* DNA damage pathway and retinal apoptosis in zebrafish (Yamaguchi, Fujimori-Tonou et al. 2008). To examine whether replicative DNA damage is increased due to loss of function of Banp, we labeled 48 hpf *banp*^{rw337} mutant retinas with anti-γ-H2AX antibody, which marks DNA double-strand breaks and replication fork stalling (Rogakou, Pilch et al. 1998, Mah, El-Osta et al. 2010). Whole-mount labeling of 48 hpf embryos using γ-H2AX antibody revealed that *banp* morphant and *banp*^{rw337} mutant embryos show accumulation of γ-H2AX, confirming the occurrence of DNA damage (Figure 4-5 A and Figure 4-6 A, D). These γ-H2AX signals revealed that the loss of function of Banp causes an accumulation of DNA strand breakage in zebrafish embryos. These results imply that Banp is required during zebrafish embryo development to prevent the accumulation of DNA strand breaks in rapidly proliferating tissues such as retina.

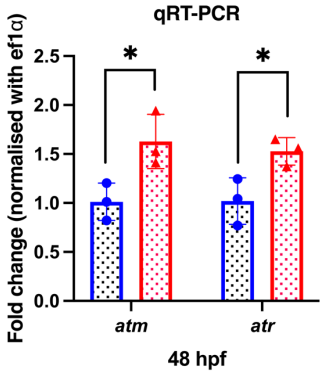

Figure 4-4: Relative mRNA expression levels for *atm*, *atr* in wild type and *banp*^{rw337} mutants.
qRT-PCR confirmed up-regulation of *atm* and *atr* in *banp*^{rw337} mutants at 48 hpf. Unpaired t-test (two-tailed) [n=3, $p < 0.05$ (*)]. Blue and red graph represent wildtype and *banp*^{rw337} mutants respectively.

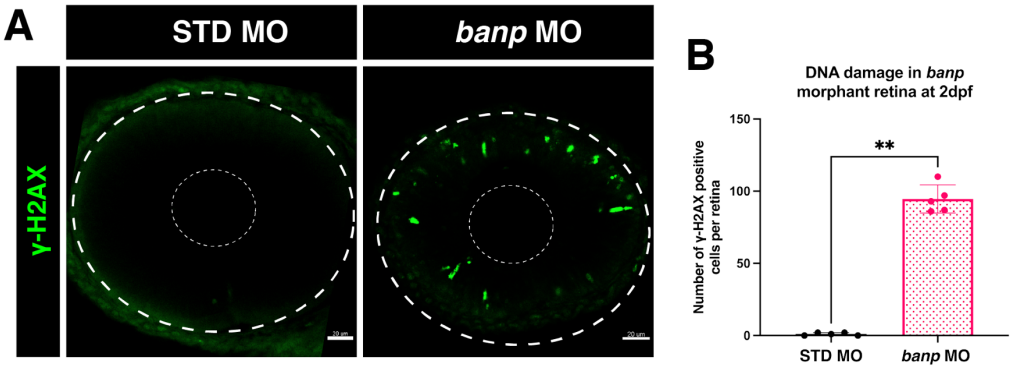

Figure 4-5: Loss of function of Banp accumulate γ-H2AX, corresponding to DNA damage.
(A) Whole-mount immunofluorescence labeling using γ-H2AX antibody at 48 hpf of STD-MO and banp-MO injected retina. STD-MO injected retina showing no accumulation of γ-H2AX corresponding to no

DNA damage, whereas loss of function of Banp (banp-MO) shows an accumulation of γ-H2AX. (B)Statistical analysis of the number of γ-H2AX cells per retina shows a significant increase in the number of cells accumulated DNA damage in the *banp* morphant retina. Mann Whitney test [n=5, $p < 0.01$ (**)].

4.3.2 *banp*^{rw337} mutants show *tp53* independent DNA damage accumulation and mitotic arrest

We investigated whether *tp53* modulates DNA damage accumulation and mitotic defect in *banp*^{rw337} mutants. Because *tp53* and Δ*113tp53* were upregulated in *banp*^{rw337} mutants. We used morpholino to knock down *tp53* and Δ*113tp53* and assess cell death, DNA damage, and mitotic arrest. Compared with STD-MO injection (average n=120.8/section), the injection of FL tp53-MO significantly rescued the number of γ-H2AX-positive cells in *banp*^{rw337} mutant retinas (average n=55.9/section) at 48 hpf (Figure 4-6 A, D). However, the number of γ-H2AX-positive cells in *banp*^{rw337} mutant retinas injected with FL tp53-MO were still significantly higher than in wildtype control retinas injected with FL tp53-MO, so DNA damage accumulation in *banp*^{rw337} mutants is likely independent of *tp53*. We also confirmed that the injection of Δ113tp53-MO did not rescue the number of γ-H2AX-positive cells, although the number of γ-H2AX-positive cells were mildly decreased (average n=85.3/section) (Figure 4-6 A, D). We also investigated whether retinal apoptosis and mitotic defect in *banp*^{rw337} mutants depend on FL tp53-MO or Δ113tp53-MO. Compared with STD-MO injection control (average n=174.7/section), retinal apoptosis was completely inhibited by FL tp53-MO in *banp*^{rw337} mutant retinas (average n=0/section) at 48 hpf (Figure 4-6 A, B). However, inhibition of apoptosis in *banp*^{rw337} mutant retinas by Δ113tp53-MO was significant but not effective (average n=58.0/section) (Figure 4-6 A, B). This result is consistent with the previous reports proposing that Δ*113tp53* preferentially activates the transcription of target genes related to cell-cycle arrest for promoting DNA repair and cell survival, whereas FL tp53 preferentially activates the transcription of target genes apoptosis for eliminating severe DNA damaged cells (Gong, Gong et al. 2015, Gong, Pan et al. 2020).

Compared with STD-MO injection (average n=376.6/section), the number of pH3-positive cells in *banp*^{rw337} mutants was significantly decreased by FL tp53-MO (average n=262.4/section) (Figure 4-6 A, C). However, the number of pH3-positive cells was still significantly higher in *banp*^{rw337} mutant retinas injected with FL tp53-MO than in wildtype control retinas injected with FL tp53-MO, so mitotic defect is likely independent of tp53. We confirmed that the injection of Δ113tp53-MO did not rescue mitotic arrest, even though the number of pH3-positive cells was very mildly decreased (average n=303.8/section) (Figure 4-6 A, C). Since FL tp53-MO inhibits the function of FL *tp53* and Δ*113tp53*, Δ*113tp53* may partially mediate mitotic cell accumulation in *banp*^{rw337} mutants together with FL *tp53*. These data suggest that the tp53-independent mechanism mainly mediates mitotic defect and accumulation of DNA damage in *banp*^{rw337} mutants.

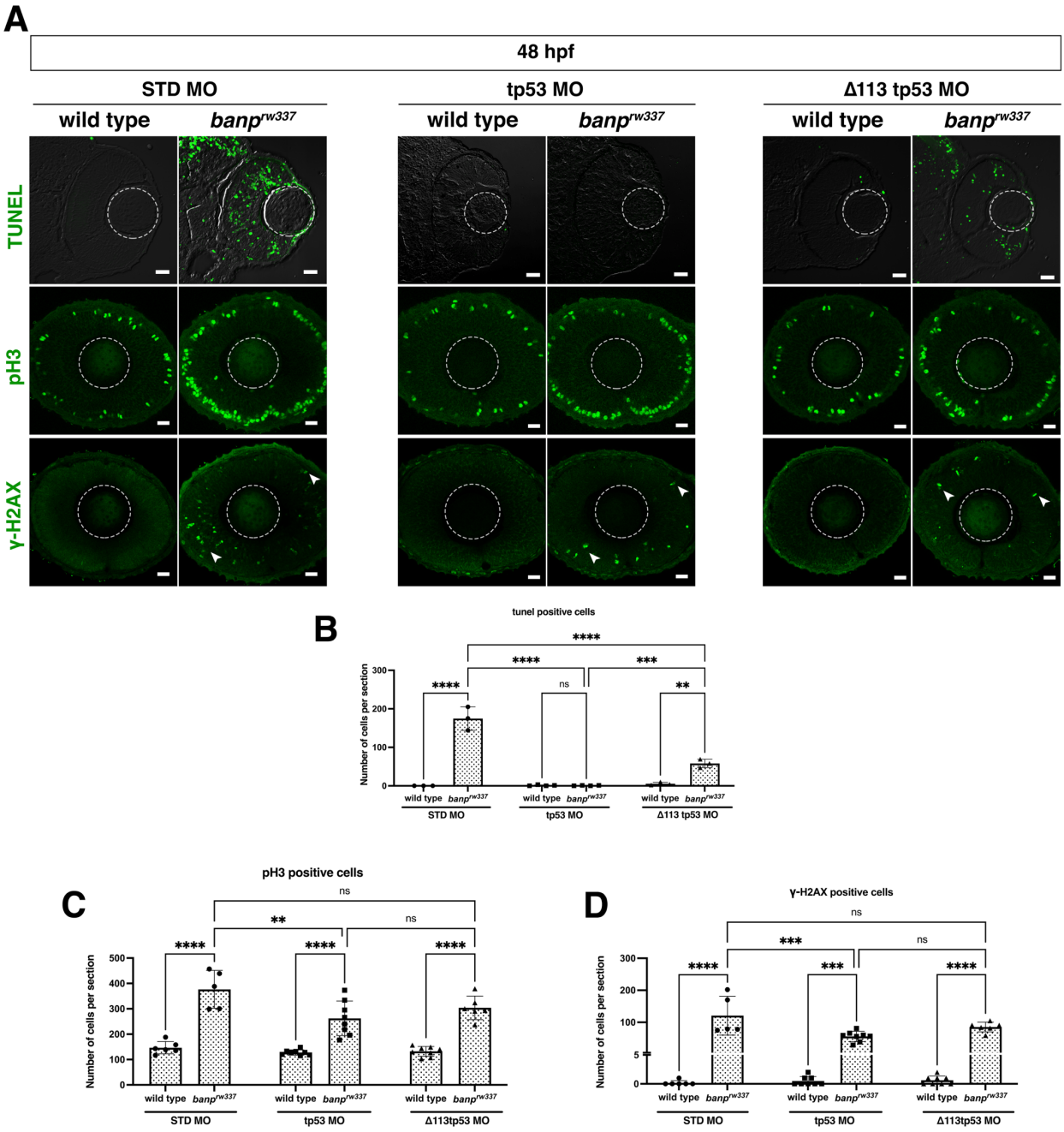

Figure 4-6: *banp*^{rw337} mutant shows activation *tp53* independent mitotic defect and DNA damage response at 48 hpf.

(A) TUNEL, pH3, and γ-H2AX antibody labeling in *banp*^{rw337} mutant and wildtype retinas in response to *tp53* and Δ*113tp53* knockdown using morpholinos. tp53-MO knockdown show rescue of cell death in *banp*^{rw337} mutant retinas. However, Δ113tp53-MO knockdown only partially rescues cell death. Both *tp53* and Δ*113tp53* knockdown did not rescue mitotic defect and accumulation of γ-H2AX cells (white arrow) in *banp*^{rw337} mutant retinas. AO- acridine orange stain represents cell death. Scale bars: 20 μm.

(B-D) Histogram of the number of TUNEL-positive cells (B), pH3-positive cells (C), and γ -H2AX-positive cells (D) per retinal section in wild-type and *banp*^{rw337} mutants injected with STD-MO, tp53-MO, and Δ113tp5- MO. Two-way ANOVA with Tukey's multiple comparisons test, [n= in graph, $p < 0.05$ (*), $p < 0.01$ (**), $p < 0.001$ (***), $p < 0.0001$ (****), NS (not significant)].

Next, to elucidate how DNA damage is introduced during retinal neurogenesis in *banp*^{rw337} mutants, we examined the fraction of S-phase cells, mitotic cells, and post-mitotic neurons in γ-H2AX-labeled retinal cells in *banp*^{rw337} mutants at 48 hpf. First, wild-type and *banp*^{rw337} mutant retinas carrying the transgene *Tg[ath5:EGFP]* were labeled with anti-BrdU and anti-γ-H2AX antibodies (Figure 4-7 A). The fraction of γ-H2AX+ cells increased in *banp*^{rw337} mutant retinas, whereas the fraction was almost zero in wild-type sibling retinas (Figure 4-7 B). Next, we compared the fraction of BrdU+ cells between the total retinal cells and γ-H2AX+ retinal cells in *banp*^{rw337} mutants (Figure 4-7 C, D). The BrdU+ fraction was significantly higher in γ-H2AX+ cells than in the total retinal cells (Figure 4-7 C, D) indicating that S-phase fraction is 4.3 fold higher in DNA damaged retinal cells than in the total retinal cells, in *banp*^{rw337} mutants. Thus, DNA double-strand breaks are abnormally induced or fail to be repaired in retinal progenitor cells undergoing S phase. Next, we examined the fraction of ath5:EGFP+ cells (Figure 4-7 E, F). There was no significant difference in ath5:EGFP+ cell fraction between the total retinal cells and γ-H2AX+ retinal cells in *banp*^{rw337} mutants (Figure 4-7 F). Finally, we determined the fraction of mitotic cells by labeling with anti-pH3 and anti-γ-H2AX antibodies in *banp*^{rw337} mutant retinas at 48 hpf (Figure 4-7 G, H). There is no significant difference in pH3+ cell fraction between the total retinal cells and γ-H2AX+ retinal cells (Figure 4-7 H). Although DNA damage may occur in post mitotic neurons and mitotic cells in *banp*^{rw337} mutants, it is likely that most DNA damage is introduced in S-phase of retinal progenitor cells in the absence of Banp. During S-phase DNA replication, rapidly dividing progenitor cells can generate intrinsic DNA strand breakage (Thompson and Schild 2002). In this circumstance, an effective damage repair mechanism is necessary. Furthermore, Banp is known to play a role in DNA damage repair (Chaudhary, Nakka et al. 2014). Thus, the loss of function of Banp may cause accumulation of intrinsic replicative DNA damage during S-phase, eventually leading to DNA replication stress in *banp*^{rw337} mutants. Additionally, the significant fraction of mitotic defect and DNA damage accumulation is independent of *tp53* in *banp*^{rw337} mutant retinas, so it is likely that Banp normally suppresses DNA replication stress and promotes DNA damage repair upstream of or independent of *tp53* (Figure 4-8).

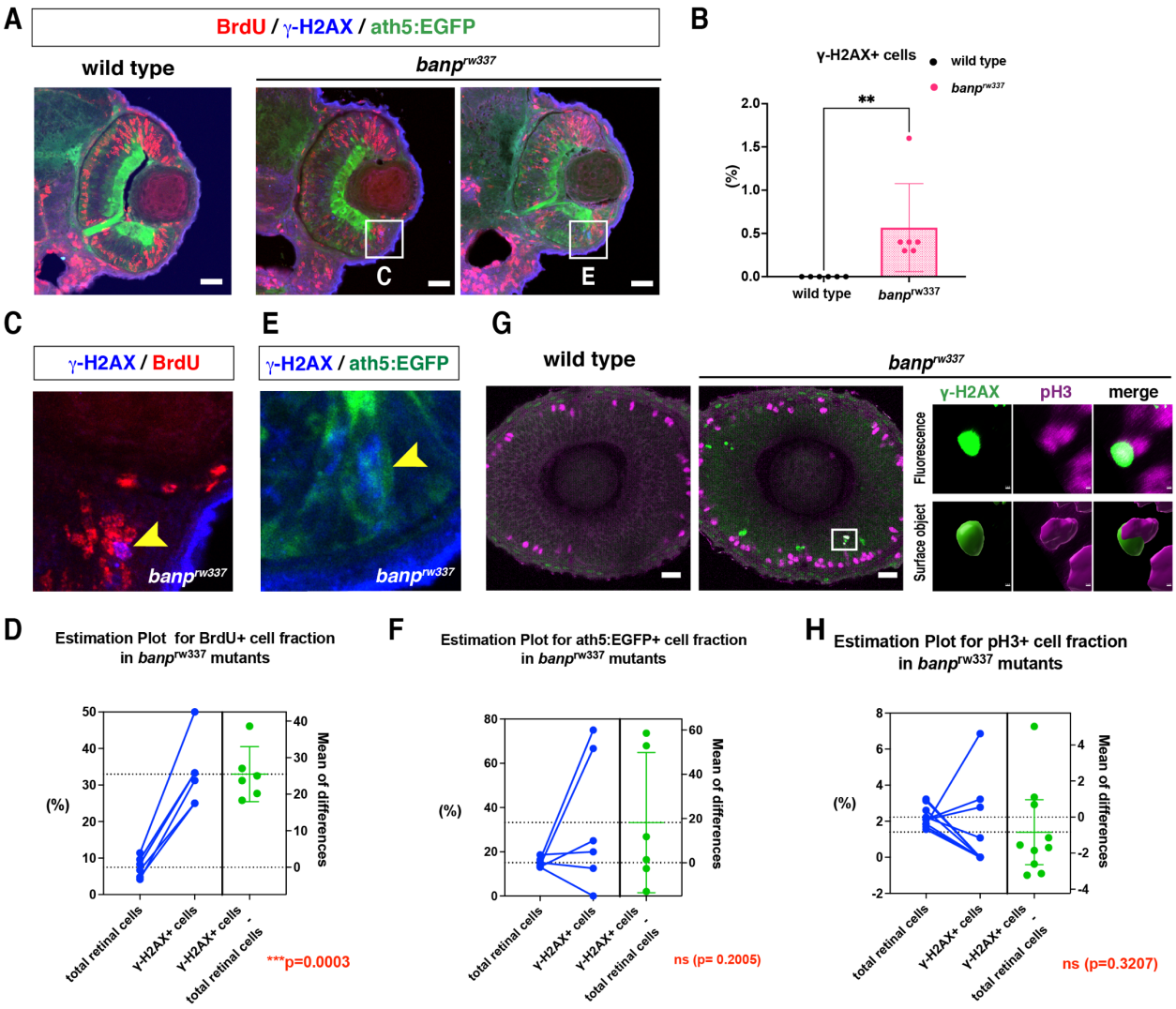

Figure 4-7: Characterization of DNA damage

(A) Labeling of 48 hpf wild-type and *banp*^{rw337} mutant retinas with anti-BrdU antibody (red), anti-γ-H2AX antibody (blue), and ath5:EGFP transgene (green). Two independent *banp*^{rw337} mutant retinas are shown. Scale bars: 20 μm.

(B) The fraction of γ-H2AX-positive cells in the total retinal area in wild-type and *banp*^{rw337} mutants. Mann Whitney test, Mean ± SD. [n=6, p <**0.01].

(C) Double labeling of retinal CMZ in *banp*^{rw337} mutants with anti-BrdU antibody (red), anti-γ-H2AX antibody (blue). Higher magnification images of square in *banp*^{rw337} mutant retinas shown in (A).

(D) The fraction of BrdU-positive cells in the total retinal cells and γ-H2AX-positive cells in *banp*^{rw337} mutants. Mean of difference between the total retinal cells and γ-H2AX-positive cells is shown in the right side. The fraction is significantly higher in γ-H2AX-positive cells than in the total retinal cells. Paired t-test. [n=6, p <***0.001].

(E) Double labeling of retinal CMZ in *banp*^{rw337} mutants with ath5:EGFP transgene (green), anti-γ-H2AX antibody (blue). Higher magnification images of square in *banp*^{rw337} mutant retinas shown in (A).

(F) The fraction of ath5:EGFP-positive cells in the total retinal cells and γ-H2AX-positive cells in *banp*^{rw337} mutants. Mean of difference between the total retinal cells and γ-H2AX-positive cells is shown in the right side. There is no significant difference between the total retinal cells and γ-H2AX-positive cells. Paired t-test. [n=6, ns].

(G) Labeling of 48 hpf wild-type and *banp*^{rw337} mutant retinas with anti-pH3 antibody (magenta), anti-γ-H2AX antibody (green). Top and bottom right-side panels of *banp*^{rw337} mutant retinas indicate original fluorescent images and their IMARIS surface-rendered images, respectively. Scale bars: 20 μm.

(H) The fraction of pH3-positive cells in the total retinal cells and γ-H2AX-positive cells in *banp*^{rw337} mutants. Mean of difference between the total retinal cells and γ-H2AX-positive cells is shown in the right side. There is no significant difference between the total retinal cells and γ-H2AX-positive cells. Paired t-test [n=10, ns].

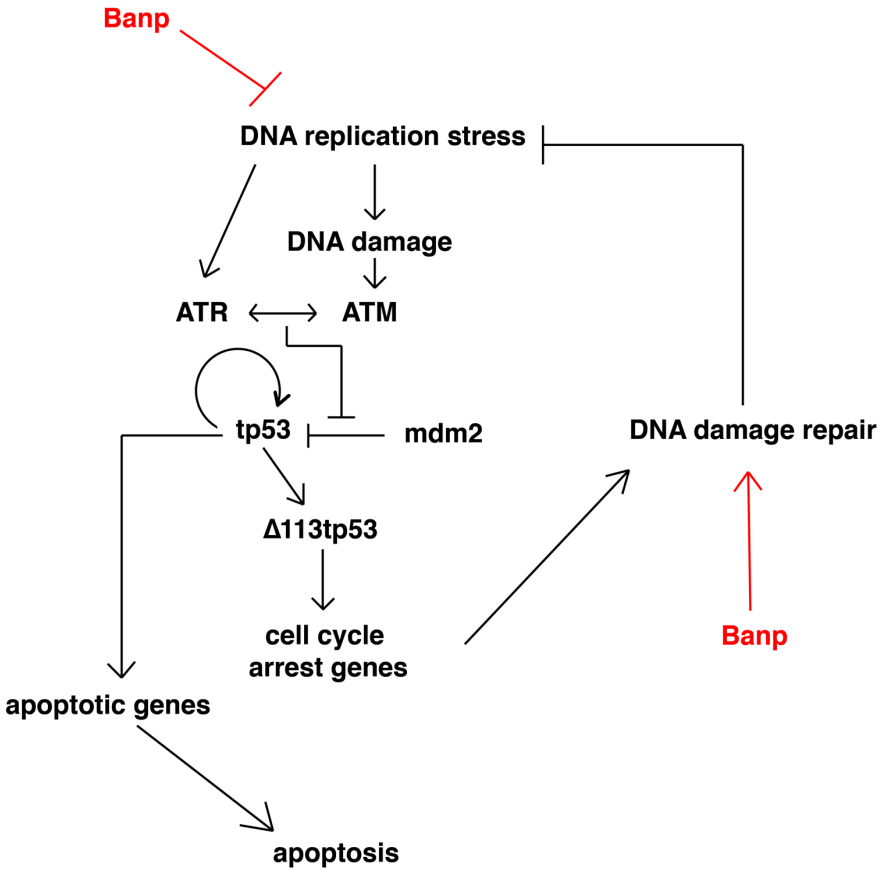

Figure 4-8: Possible role of Banp in tp53-mediated DNA damage pathway.
DNA replication stress and subsequent DNA damage activate *atr* and *atm*, respectively, which subsequently phosphorylate H2AX and inhibit Mdm2-mediated Tp53 degradation. Stabilized Tp53 mainly promotes the transcription of the *Δ113tp53* isoform, which activates cell-cycle arrest genes and promotes DNA damage repair. Chronic activation of *tp53* in turn activates apoptotic genes to induce apoptosis. Thus under normal conditions in highly proliferating cells like RPCs, Banp may suppress DNA replication stress and also promote DNA damage repair.

4.3.3 *cenpt* and *ncapg* are specifically downregulated in *banp*^{rw337} mutants.

Mitotic defect and accumulation of DNA damage in *banp*^{rw337} mutants occure independent of *tp53*. RNA-seq analysis revealed that two chromosomal segregation regulators, *cenpt* and *ncapg*, are downregulated in *banp*^{rw337} mutants at 48 hpf (Figure 3-1 C). Cenpt and Ncapg are essential for chromatin segregation (Seipold, Priller et al. 2009, Hung, Volkmar et al. 2017, Zhang, Su et al. 2018). Quantitative RT-PCR validation confirmed their downregulation in *banp*^{rw337} mutants and *banp* morphants, suggesting functional Banp is necessary for the expression of *cenpt* and *ncapg* (Figure 4-9 A, C). Furthermore, ATAC-seq analysis revealed decreased chromatin accessibility near the transcription start site (TSS) of both genes in *banp*^{rw337} mutants, revealing reduced transcription activity (Figure 4-9 B, D). These results show that Banp is required for transcriptional activation of *cenpt* and *ncapg* in zebrafish. Interestingly, two independent ChIP-sequencing studies using Banp (smar1) antibody revealed a specific binding site within 100bp from TSS at *cenpt* and *ncapg* gene in mice and humans (Mathai, Mittal et al. 2016, Grand, Burger et al. 2021), suggesting that the requirement of Banp for the transcription of *cenpt* and *ncapg* is likely conserved in zebrafish, mice, and human.

Additionally, our *de-novo* motif enrichment study using homer discovered TCTCGCGAGA (Banp motif) as the most enriched motif in the closed chromatin region of *banp*^{rw337} mutants (Table 3-3). Through this hitherto orphan Banp motif, a recent study establishes Banp as a transcription factor, demonstrating that Banp is required for the activity of numerous essential genes and adequate and autonomous for substantial gene activation in chromatin (Grand, Burger et al. 2021). Furthermore, we discovered a Banp motif upstream of the TSS in both the *cenpt* and *ncapg* genes in zebrafish, mice, and humans (Figure 4-10). The Banp motif, unlike standard core promoter elements, is not located at a constant distance from TSSs, but rather between 20 and 70 nucleotides upstream on both strands (Mahpour, Scruggs et al. 2018). Taken together, our findings reveal that in zebrafish, *cenpt* and *ncapg* are two of the gene targets for which Banp plays a significant role in transcription activation likely via the activation of its Banp motif.

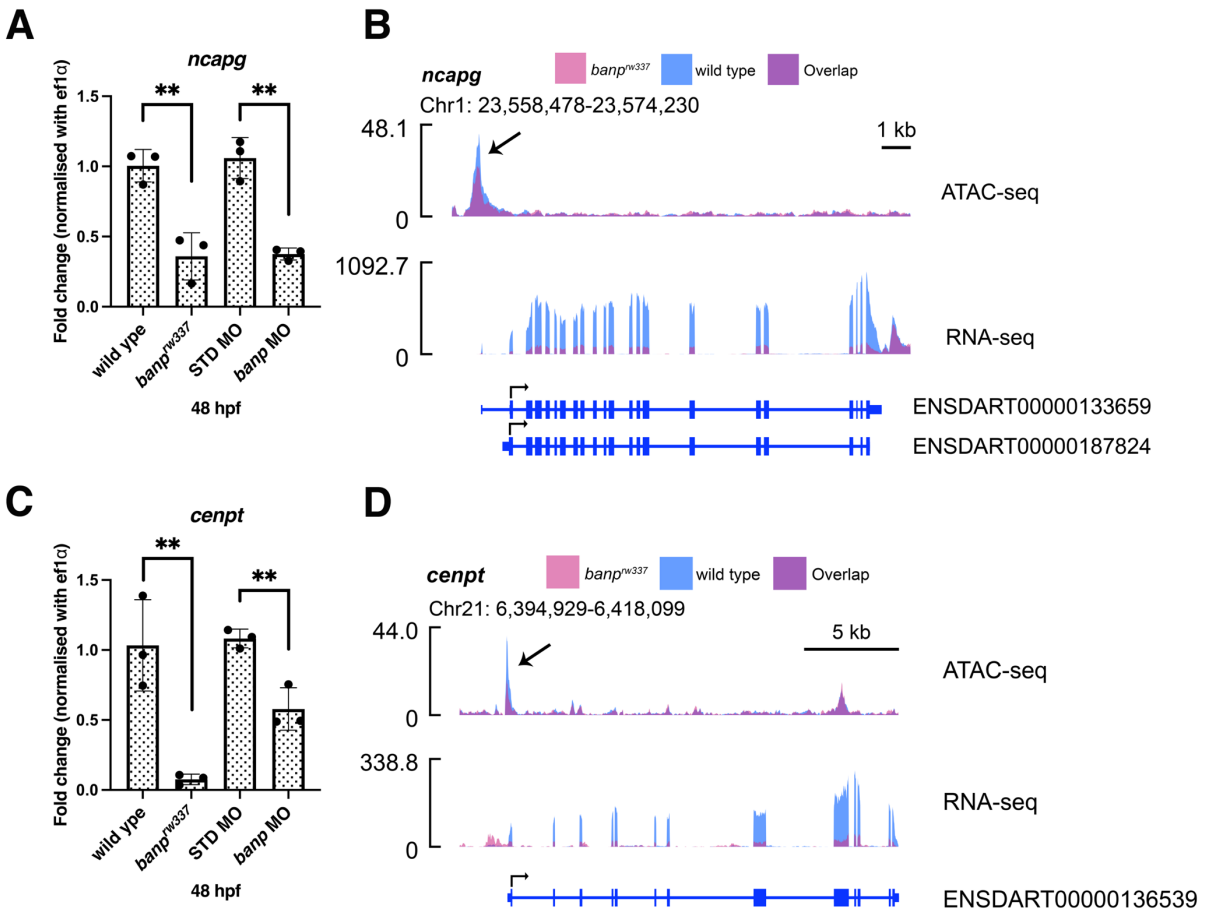

Figure 4-9: Loss of function of Banp cause reduced transcription of chromatin segregation genes.
(A) qRT-PCR based validation of *ncapg* expression at 48 hpf. qRT-PCR showing downregulation of *ncapg* in *banp*^{rw337} mutants and morphants in comparison to control. Unpaired t-test (two-tailed) [n=3, $p < 0.01$ (**)].
(B) The differential expression of *ncapg* is illustrated using data from ATAC-seq and RNA-seq. *banp*^{rw337} mutants show reduced transcription activity at TSS (ATAC-seq) and reduced transcript expression (RNA seq).
(C) qRT-PCR based validation of *cenpt* expression at 48 hpf. qRT-PCR showing downregulation of *ncapg* in *banp*^{rw337} mutants and morphants in comparison to control. Unpaired t-test (two-tailed) [n=3, $p < 0.01$ (**)].
(D) The differential expression of *cenpt* is illustrated using data from ATAC-seq and RNA-seq. *banp*^{rw337} mutants show reduced transcription activity at TSS (ATAC-seq) and reduced transcript expression (RNA seq).
The black arrow represents TSS.

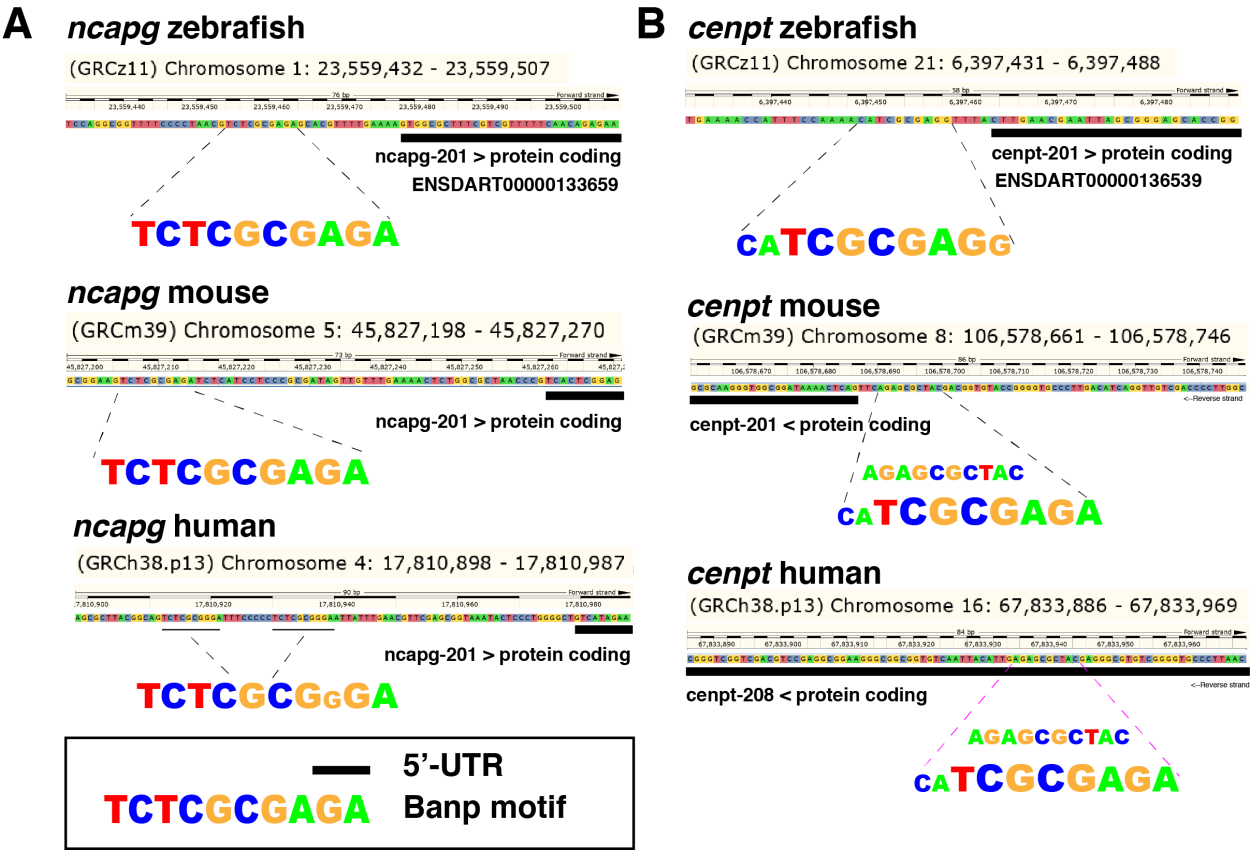

Figure 4-10: Banp motif is conserved in *cenpt* and *ncapg*
(A) and (B) indicates a putative Banp motif with a conserved CGCG element upstream of the 5' UTR of *cenpt* and *ncapg* in zebrafish, mice, and humans. We identified the Banp motif (TCTCGCGAGA) enriched regions with reduced chromatin accessibility in the *banp*^{rw337} mutants. Suggesting Banp specific targets are transcriptionally repressed in *banp*^{rw337} mutants.

4.3.4 Knocking down *banp* causes chromatin segregation defect

Knockdown of Cenpt and Ncapg causes defects in chromosomal segregation during mitosis in zebrafish (Seipold, Priller et al. 2009, Hung, Volkmar et al. 2017). Next, we did live imaging to monitor how cell cycle progression occurs in the absence of *banp*. We performed a live cell cycle analysis at 2 dpf using *Tg [h2afv: GFP; EF1α: mCherry-zGem]* fish line, which helps distinguish different cell cycle phases (Mochizuki, Suzuki et al. 2014). Time-lapse of cell division was obtained and compared between *banp* morphant and control embryos. *banp* was knocked down using ATG morpholino and 5-mismatch morpholino as control wildtype. *banp* ATG morpholino showed a similar phenotype to *banp*^{rw337} mutants (Figure 2-5 D, H) and inhibits protein expression explicitly from banp-EGFP mRNA (Figure 2-7 B, C), confirming the specificity of banp-MO for gene *banp*. Embryos were mounted laterally, and time-lapse of the retina was obtained for 1 to 2 hours at the developmental time point between 48 to 54 hpf. It is a time when most cells in the neural retina still undergo cell division (Xu, Tang et al. 2020). The cells that underwent a complete division during our recording were evaluated. The time required to complete mitotic division is calculated.

From the live cell division analysis, *banp* morphant embryos showed a marked increase in time taken for cell division with an average of 49.2± 17.0 minutes. However, the control embryos only took an average of 22.9±5.8 minutes to divide (Figure 4-11 B). Furthermore, the cells

entered mitosis in *banp* morphants showed evident chromatin segregation defect. Instead of proceeding through the cell cycle from metaphase (Figure 4-11, A t=21) to telophase (Figure 4-11, A t=26) as observed in control cells, morphant cells show segregation defect by reentering to dispersed chromatin phase (Figure 4-11, A t=41) after metaphase (Figure 4-11, A t=36) then again to metaphase like arrangement (Figure 4-11, A t=46) before finally moving to telophase and cytokinesis. We have observed 28 morphant divisions and 23 control cell divisions from at least 3 different embryos. All the observed divisions ended in cytokinesis. Thus, chromosomal segregation is abnormal during mitosis in the absence of Banp. This live imaging also suggest that the increased accumulation of mitotic cells that we are observing in *banp*^{rw337} mutants are likely due to delayed mitosis rather than mitotic arrest. Although we thought it would be a mitotic arrest in chapter 2 and chapter 3.

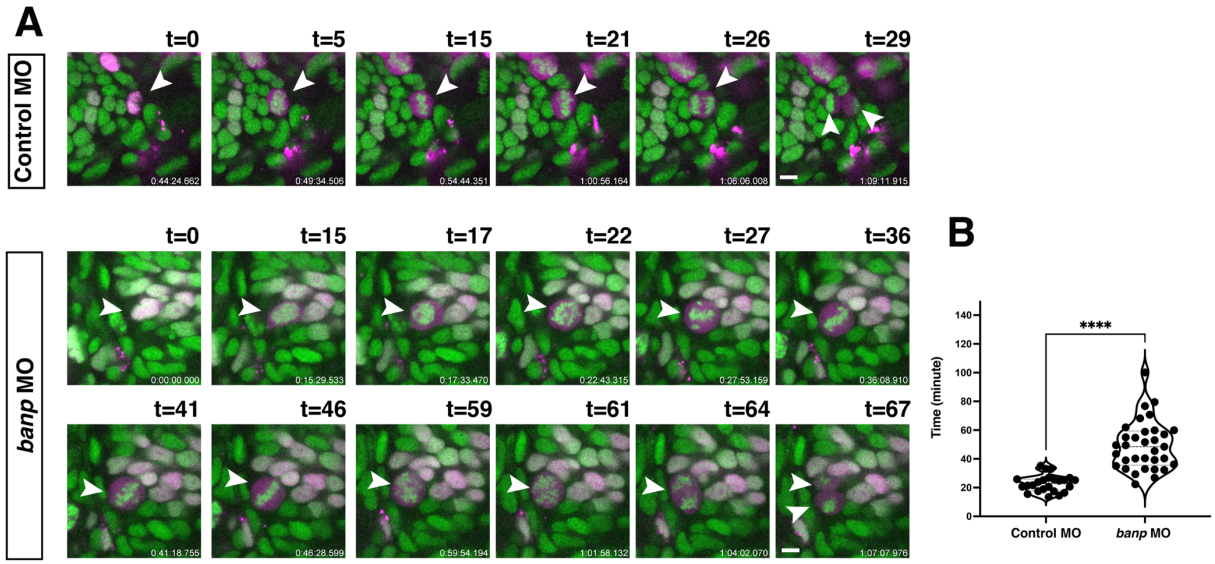

Figure 4-11: Time-lapse images of a cell division at 2 dpf using *Tg [h2afv: GFP; EF1α: mCherry-zGem]* zebrafish.

(A) Time-lapse images of cell division of retinal cells injected with *banp* 5-mismatch-MO (control-MO, upper) and banp-MO (lower) at 2 dpf using *Tg [h2afv: GFP; EF1α: mCherry-zGem]* transgenic zebrafish. In the control-MO, the cell proceeds sequentially from prophase (t=5~15), metaphase (t=21), anaphase (t=26), and telophase (t=29). In the banp-MO, cell division takes about one hour to divide, significantly longer than that of the control-MO. Prophase-like chromosome arrangement abnormally appeared (t=59) after several metaphase like alignment (t=36 and 46), followed by anaphase (t=64) and telophase. Scale bar: 5μm. (B) Violin plot represents the time taken for cell division in control and *banp* morphant zebrafish retina. Morphant cell division is significantly longer than the control. Mann Whitney test, [n=3, $p < 0.0001$ (****)]

4.3.5 *banp*^{rw337} mutants show mitotic spindle attachment defect

To validate the presence of mitotic chromosome segregation defect in *banp*^{rw337} mutants, we labeled 48 hpf embryos with anti-α-tubulin and pH3 antibodies to visualize mitotic spindle and mitosis, respectively. A proper attachment of mitotic spindle to chromosome is necessary for the accurate segregation of chromosomes during mitosis (section 4.1.1). Defective spindle attachments have often been reported to cause chromosome defects during mitosis (Mitchison and Salmon 2001, Pease and Tirnauer 2011). In *banp*^{rw337} mutants, we observed mitotic spindles are irregularly attached to less condensed and misaligned chromosome when compared to wild

type (Figure 4-12 A). The percentage of cells with abnormal mitosis was significantly higher in *banp*^{rw337} mutant retinas than those of wild type (Figure 4-12 B). These data suggest that the interaction between chromosomes and mitotic spindles is compromised in the absence of Banp, probably due to kinetochore attachment defects caused by lack of function its target gene such as Cenpt and Ncapg. Thus, Banp regulates chromosomal segregation during mitosis.

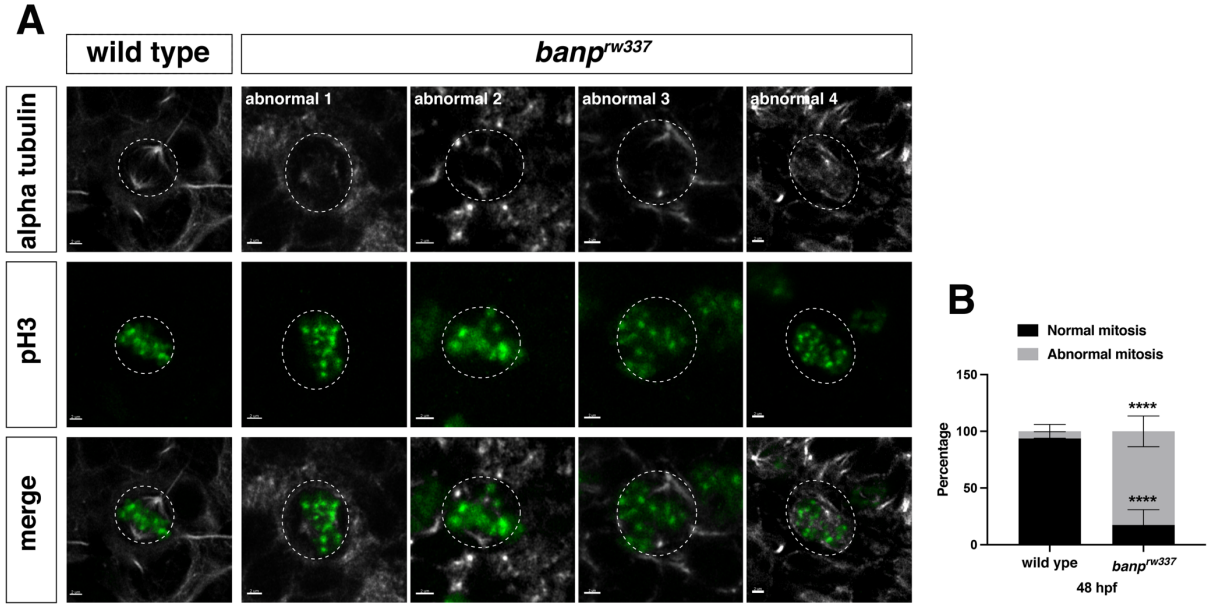

Figure 4-12: High-resolution images of metaphase cells from wild type and *banp*^{rw337} mutant zebrafish retina at 48 hpf.

(A) High-resolution images of metaphase cells in zebrafish retinas at 48 hpf. The mitotic spindle is labeled with anti-α-tubulin antibody (alpha tubulin), whereas metaphase chromosomes are labeled with anti-pH3 antibody. The mitotic spindle is correctly attached to metaphase chromosomes in wildtype retinal cells (left panel). Mitotic cells in *banp*^{rw337} mutants exhibit inefficient mitotic spindle attachment and poorly orientated metaphase chromosomes (right panel). Dotted circles indicate the outline of metaphase cells. Scale bar: 2 μm.

(B) The percentage of cells with normal and abnormal spindle attachment in wildtype and *banp*^{rw337} mutant embryos are shown in this graph. 2way ANOVA with Šídák's multiple comparisons test [n=3, $p < 0.0001$ (****)].

4.3.6 Direct transcription targets of Banp via Banp motif in zebrafish

In this section, we uncovered the gene targets with Banp motif that are potential transcription targets of Banp. Using the "findMotifs.pl" function of the Homer package, we scanned all significant differentially expressed genes in *banp*^{rw337} mutants for the presence of a Banp motif (Figure 4-13 A). Surprisingly, the Banp motif was found in 31 of the 80 downregulated genes (38%); however, none of the upregulated genes had Banp motif (Table 4-1). The Banp motif was exclusively found in downregulated targets suggests that Banp is a transcription activator and that activation of Banp motifs by Banp is required for the transcriptional activation of 38 percent of downregulated genes in the *banp*^{rw337} mutants. Interestingly, the Banp motif is found in several copies upstream of the TSS in most target genes (Table 4-1). The frequency of the Banp motif upstream of the TSS is reported to impact the subsequent transcriptional rate of target genes (Mahpour, Scruggs et al. 2018). In summary, loss of function of Banp leads to loss of function of its target genes. Furthermore, in *banp*^{rw337} mutants, loss of function of *cenpt*, *ncapg*, *spdl1*, *smrc1a* together may contribute to mitotic segregation defects and loss of function Banp protein itself and along with replication factors such as *wrnip1* is likely responsible for replication stress (Figure 4-13 B, C). Additionally, Table 4-1 shows a list of genes in developing zebrafish that are most likely transcriptionally regulated by Banp via the Banp motif. We also compared the genes that contain the Banp motif in zebrafish, mouse, and human. In comparison to published Banp motif containing genes in mouse and human, a venn diagram showing overlap of Banp motif containing genes in downregulated ATAC sequencing datasets of *banp*^{rw337} mutant zebrafish relative to wild-type reveals the potential candidate genes regulated by Banp in vertebrates (Figure 4-14).

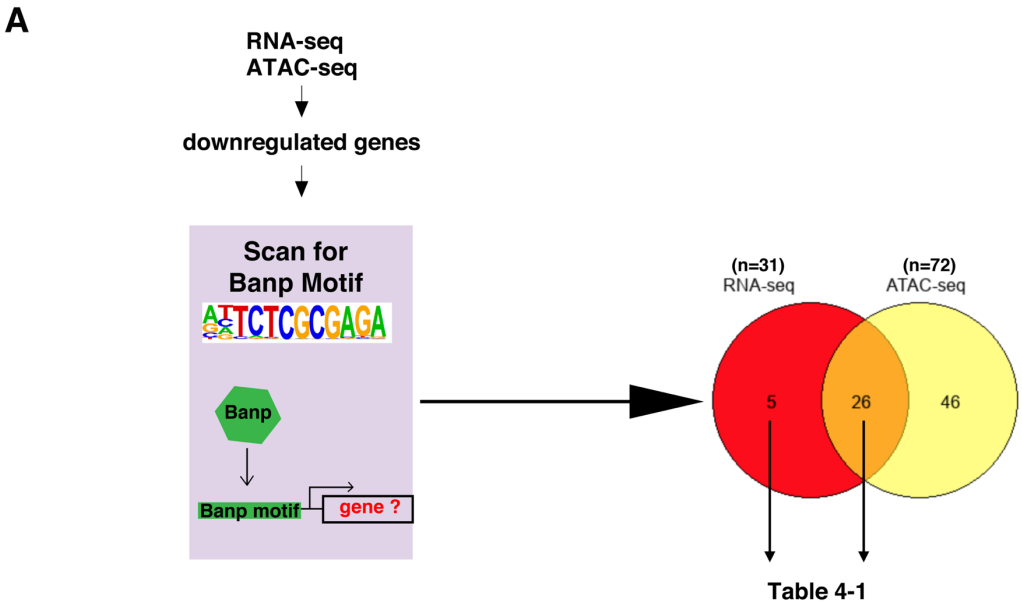

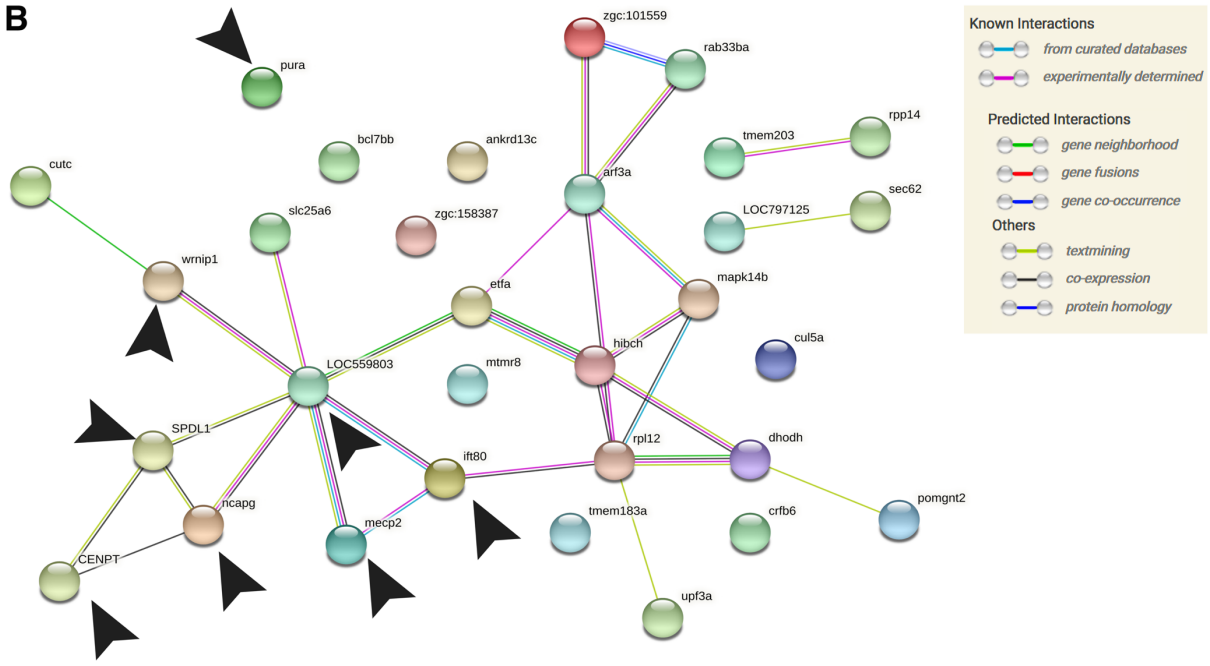

C

Gene Ontology (pathway)	downregulated genes with Banp motif (RNA-seq)	Gene names
cell cycle	**26 % (8/31)**	**Ncapg, Cenpt, Spdl1, Smarca1(LOC559803), Wrnip1, Ift80, Mecp2, Puraa.**

Figure 4-13: Direct transcription targets of Banp in zebrafish
(A) A schematic diagram representing the flow of RNA-sequencing combined with ATAC-sequencing to find candidates for zebrafish Banp direct target genes. HOMER was used to scan for Banp motifs in downregulated candidate genes, from RNA- and ATAC-sequencing in *banp*^{rw337} mutants. RNA

sequencing yielded 31 candidates, whereas ATAC sequencing yielded 72, with 26 target genes consistent in both. These 26 candidate genes are the most likely to be target genes of Banp.
(B) STRING interactome analysis showing the interaction of Banp motif-containing genes downregulated in RNA sequencing. Black arrows specify genes related to cell-cycle regulation.
(C) Banp target candidate genes related to cell-cycle regulation. Gene ontology (GO) analysis was applied to 31 Banp motif-containing genes downregulated in RNA sequencing. 26% of these genes are engaged in the cell-cycle regulation. Others participate in a variety of non-categorized pathways.

offset	Banp motif	Strand	Motif Score	Ensembl ID	Gene Name
-87	CTTCTCGCGAGA	+	13.16405	ENSDARG00000054867	hibch
-74	TCTCGCGAGATT	-	13.853252	ENSDARG00000054867	hibch
-9	ATTCCCGCGAGA	+	11.266745	ENSDARG00000069297	upf3a
4	TCCCGCGAGAGT	-	10.324241	ENSDARG00000069297	upf3a
-49	AATATCGCGAGA	+	11.239795	ENSDARG00000005853	slc25a6
-36	TATCGCGAGATG	-	9.757198	ENSDARG00000005853	slc25a6
-23	CCTCTCGCGATA	+	9.843419	ENSDARG00000003257	zgc:101559
-10	TCTCGCGATAAT	-	11.911384	ENSDARG00000003257	zgc:101559
-164	GCTCTCGCGAGA	+	13.204889	ENSDARG00000014218	mecp2
-116	CCTCTCGCGAGA	+	12.578682	ENSDARG00000014218	mecp2
-103	TCTCGCGAGATC	-	13.118668	ENSDARG00000014218	mecp2
-151	TCTCGCGAGAAC	-	13.790258	ENSDARG00000014218	mecp2
6	GTTCTCGCGAGA	+	13.790258	ENSDARG00000051889	dhodh
19	TCTCGCGAGAGT	-	13.939474	ENSDARG00000051889	dhodh
-94	GGTCTCGCGATA	+	10.015154	ENSDARG00000104996	tmem203
-81	TCTCGCGATATT	-	11.239795	ENSDARG00000104996	tmem203
-240	TCTCGCGATAAG	-	10.550592	ENSDARG00000067795	ifngr2
-52	GTTCTCGCGATA	+	11.054995	ENSDARG00000006691	rpl12
-39	TCTCGCGATACT	-	10.871543	ENSDARG00000006691	rpl12
-9	CTTCTCGCGATA	+	10.428787	ENSDARG00000008592	mtmr8
4	TCTCGCGATATT	-	11.239795	ENSDARG00000008592	mtmr8
-199	AATATCGCGAGA	+	11.239795	ENSDARG00000012776	smarca1
-149	AATCTCGCGAGA	+	13.853252	ENSDARG00000012776	smarca1
-136	TCTCGCGAGATT	-	13.853252	ENSDARG00000012776	smarca1
-186	TATCGCGAGATT	-	11.11799	ENSDARG00000012776	smarca1
-41	ACTCTCGCGAGA	+	13.939474	ENSDARG00000101631	etfa
-28	TCTCGCGAGAAC	-	13.790258	ENSDARG00000101631	etfa
-76	AATATCGCGAGA	+	11.239795	ENSDARG00000070539	arf3a
-23	TATCGCGAGAGC	-	10.469626	ENSDARG00000070539	arf3a
-63	TATCGCGAGATC	-	10.383405	ENSDARG00000070539	arf3a
-70	AGTGTCGCGAGA	+	10.280675	ENSDARG00000011152	rpp14
-21	ATTGTCGCGAGA	+	11.320516	ENSDARG00000011152	rpp14
-8	TGTCGCGAGATT	-	10.641066	ENSDARG00000011152	rpp14
-57	TGTCGCGAGAAT	-	11.312655	ENSDARG00000011152	rpp14
-70	GATCTCGCGAGA	+	13.118668	ENSDARG00000067591	puraa
-57	TCTCGCGAGAGC	-	13.204889	ENSDARG00000067591	puraa
-8	AATATCGCGAGA	+	11.239795	ENSDARG00000019951	sec62

5	TATCGCGAGAGT	-	11.204211	ENSDARG00000019951	sec62
-57	GATATCGCGAGA	+	10.50521	ENSDARG00000005218	**wrnip1**
-44	TATCGCGAGACG	-	9.388946	ENSDARG00000005218	**wrnip1**
-48	AGTCTCGCGAGA	+	13.485001	ENSDARG00000040396	bcl7bb
-35	TCTCGCGAGACC	-	12.750417	ENSDARG00000040396	bcl7bb
-60	TCTCGCGATAAC	-	11.1768	ENSDARG00000010941	pomgnt2
-23	AATCTCGCGAGA	+	13.853252	ENSDARG00000088764	lyplal1
-10	TCTCGCGAGACA	-	11.267272	ENSDARG00000088764	lyplal1
-24	AATCTCGCGAGA	+	13.853252	ENSDARG00000069742	cul5a
-11	TCTCGCGAGACC	-	12.750417	ENSDARG00000069742	cul5a
-59	AATCTCGCGAGA	+	13.853252	ENSDARG00000038879	ift80
-20	GTTCTCGCGAGA	+	13.790258	ENSDARG00000038879	ift80
-7	TCTCGCGAGACG	-	12.124209	ENSDARG00000038879	ift80
-46	TCTCGCGAGAAG	-	13.16405	ENSDARG00000038879	ift80
-14	CTTCTCGCGAGA	+	13.16405	ENSDARG00000052290	rab33ba
-1	TCTCGCGAGATT	-	13.853252	ENSDARG00000052290	rab33ba
-51	TTTCTCGCGAGA	+	12.307113	ENSDARG00000103996	spdl1
-38	TCTCGCGAGATG	-	12.49246	ENSDARG00000103996	spdl1
-29	ATTATCGCGAGA	+	11.911384	ENSDARG00000033364	mgst3b
-16	TATCGCGAGAGT	-	11.204211	ENSDARG00000033364	mgst3b
-61	AATCTCGCGAGA	+	13.853252	ENSDARG00000077306	cutc
-17	AATATCGCGAGA	+	11.239795	ENSDARG00000077306	cutc
-4	TATCGCGAGAGT	-	11.204211	ENSDARG00000077306	cutc
-48	TCTCGCGAGAGT	-	13.939474	ENSDARG00000077306	cutc
-196	ACTCTCGCGAGA	+	13.939474	ENSDARG00000103831	ankrd13c
-156	CGTCTCGCGAGA	+	12.124209	ENSDARG00000103831	ankrd13c
-109	ATTCTCGCGAGA	+	14.524842	ENSDARG00000103831	ankrd13c
-66	GTTCTCGCGAGA	+	13.790258	ENSDARG00000103831	ankrd13c
-53	TCTCGCGAGAGC	-	13.204889	ENSDARG00000103831	ankrd13c
-96	TCTCGCGAGACT	-	13.485001	ENSDARG00000103831	ankrd13c
-143	TCTCGCGAGAAT	-	14.524842	ENSDARG00000103831	ankrd13c
-183	TCTCGCGAGACT	-	13.485001	ENSDARG00000103831	ankrd13c
-33	ACTCTCGCGAGA	+	13.939474	ENSDARG00000044899	tmem183a
-20	TCTCGCGAGAAT	-	14.524842	ENSDARG00000044899	tmem183a
-69	GTTCTCGCGAGA	+	13.790258	ENSDARG00000028721	mapk14b
-56	TCTCGCGAGATT	-	13.853252	ENSDARG00000028721	mapk14b

Table 4-1: Downregulated genes (RNA seq) with Banp motif in *banp*^{rw337} mutants at 48 hpf.

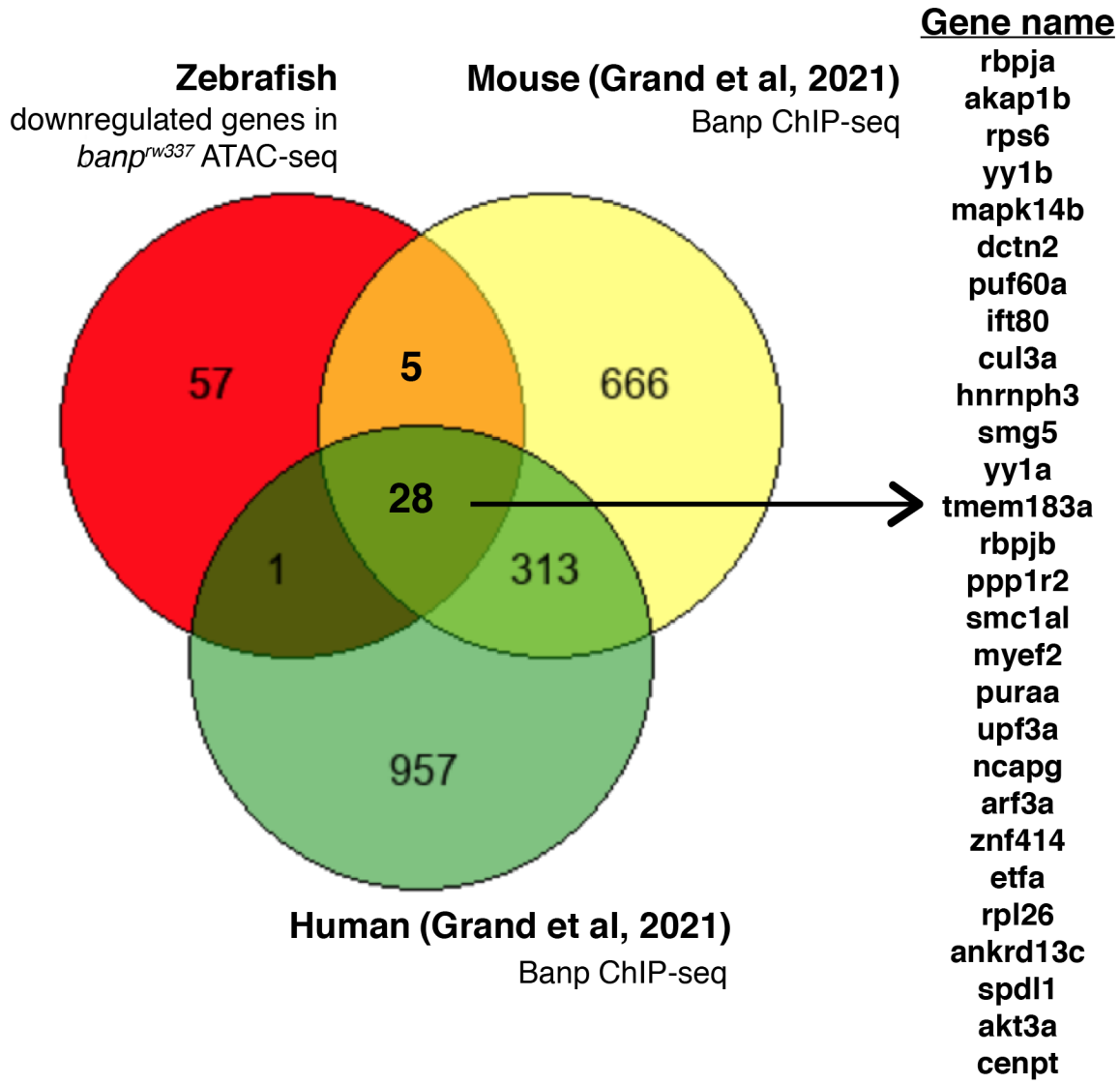

Figure 4-14: Overlapping Banp targets genes in zebrafish, mouse and human
A Venn diagram revealing overlap of Banp Motif containing genes in downregulated ATAC sequencing datasets of *banp*^{rw337} mutant zebrafish relative to wild-type in comparison to published Banp motif containing genes in mouse and human. The Banp motifs with Chip-seq signal published by Grand et al were annotated using HOMER to identify Banp target genes in mouse and human (GSE155603, (Grand, Burger et al. 2021)). 28 genes were identified to be common in zebrafish, mouse and human.

4.4 Discussion

In this section we attempted to identify the primary cause of cellular defects (cell cycle defect and apoptosis) in *banp*^{rw337} mutants. In search of the potential candidate genes responsible for the cellular defect, the last chapter revealed activation of *tp53* and its downstream targets as the most probable candidate. However, knocking down *tp53* only partially rescues cell death. Additionally, we identified molecular signatures of DNA damage (*exo5*, Δ*113tp53*) in *banp*^{rw337} mutants.

First, we examined DNA damage in *banp*^{rw337} mutants. We confirmed that morphant and mutant embryos show accumulation of γ-H2AX positive cells corresponding to DNA damage (Figure 4-5 and Figure 4-6 A, D). Developing embryos under normal conditions have characteristic rapid cell cycle. During development, lack of cell cycle regulatory factors often causes replication stress associated with DNA damage (Bellelli, Borel et al. 2018, Kermi, Aze et al. 2019). Rapid proliferation and differentiation during development also can cause intrinsic DNA damage, which is often repaired by surveillance mechanisms of damage repair (Lindahl and Barnes 2000, Miermont, Antolovic et al. 2019). Defects in such surveillance mechanisms also cause DNA damage in developing embryos (Liu, Howlett et al. 2003, Bladen, Lam et al. 2005, Bladen, Navarre et al. 2007, Hu, Holzschuh et al. 2015). Loss of function of Banp causing replicative DNA damage suggests that Banp is necessary to safeguard developing zebrafish embryos from accumulating DNA damage in rapidly proliferating cells.

Next, we looked at the role of *tp53* in mitotic cell accumulation and DNA damage accumulation in *banp*^{rw337} mutants based on the above findings. *tp53* is well known for regulating cell fate upon DNA damage and regulating surveillance mechanisms during cell division. Upon mild DNA damage, *tp53* evokes cell cycle arrest to activate DNA damage repair. However, severe DNA damage can also promote cell death (Chen 2016). In *banp*^{rw337} mutants, we see the stabilization of FL *tp53* and the transcription activation of the Δ*113tp53* transcript variant. This FL *tp53* activation is indeed responsible for the cell death observed in *banp*^{rw337} mutants during early development. It was confirmed by our *tp53* knockdown experiment where depleting FL *tp53* caused cell death rescue to return similar to wildtype at 48 hpf in *banp*^{rw337} mutant retina (Figure 4-6 A, B). However, loss of *banp* activates *tp53* independent damage response and mitotic defect (Figure 4-6 A, C, D). We speculate that the absence of Banp evokes both *tp53* dependent and independent DNA damage response pathways suggesting its potential function in *tp53* dependent and independent surveillance mechanisms.

In search of candidate genes responsible for the accumulation of mitotic defect, our ATAC-sequencing demonstrated decreased transcription of *cenpt* and *ncapg* in the *banp*^{rw337} mutants. Cenpt and Ncapg are necessary factors during mitosis chromosome segregation of the cell cycle. Our qRT-PCR confirmed the downregulation of *cenpt* and *ncapg* with loss of function of Banp (Figure 4-9 A, C). Additionally, we discovered that the Banp motif is conserved in zebrafish (Table 3-3). Interestingly, the putative Banp motif was identified in both *cenpt* and *ncapg* in human mice and zebrafish upstream of the 5'UTR (Figure 4-10). Further, two independent ChIP-sequencing utilizing Banp antibody also validated specific peaks at TSS of *cenpt* and *ncapg* (Mathai, Mittal et al. 2016, Grand, Burger et al. 2021). This ChIP-seq studies together with our physiological validation in zebrafish, suggests that Banp is necessary for the transcription activation of *cenpt* and *ncapg,* and its function is likely conserved in human mice and zebrafish. Reduced expression of *cenpt* and *ncapg* causes chromosome segregation defects in zebrafish (Seipold, Priller et al. 2009, Hung, Volkmar et al. 2017, Zhang, Su et al. 2018). As expected, loss of function of Banp also caused chromatin segregation defects in zebrafish

(Figure 4-11 A and Figure 4-12 A). Taken together, these results imply that in zebrafish, *banp* is required for transcription of factors necessary for chromatin segregation and has a protective role in developing retinal cells from accumulation of replicative DNA damage.

Chromatin segregation defect is often known to cause mild to severe DNA damage (Naim, Wilhelm et al. 2013). When chromatic segregation defects cause DNA damage, it is possible to detect γ-H2AX signals during mitosis. Depending on the extent of damage, a cell might repair the damage if it is mild or undergo cell death if severe (Surova and Zhivotovsky 2013, Liebl and Hofmann 2019). In *banp*^{rw337} mutants, an average of ~1 percent of DNA damage is observed in mitotic cells, although there is no significant difference in pH3+ cell fraction between the total retinal cells and γ-H2AX+ retinal cells (Figure 4-7 G, H). The rest of the DNA damage signals were from non-mitotic cells. The mitotic γ-H2AX signal suggests that chromosome segregation defects likely cause DNA damage in mutants. However, DNA damage during mitosis is not always repaired. It is often carried over to daughter cells followed by DNA repair during the S-phase of the corresponding damaged daughter cells (Pedersen, Karemore et al. 2016), which can likely show DNA damage response in non-mitotic cells *banp*^{rw337} mutants.

In order to detect the fraction of DNA damage during S-phase, we compared the fraction of BrdU+ cells between the total retinal cells and γ-H2AX+ retinal cells in *banp*^{rw337} mutants (Figure 4-7 C, D). The BrdU+ fraction was significantly higher in γ-H2AX+ cells than in the total retinal cells (Figure 4-7 D), indicating that S-phase fraction is 4.3 fold higher in DNA damaged retinal cells than in the total retinal cells, in *banp*^{rw337} mutants. Thus, DNA double-strand breaks are abnormally induced or fail to be repaired in retinal progenitor cells undergoing S phase. Next, we examined the fraction of ath5:EGFP+ cells (Figure 4-7 E, F). There was no significant difference in ath5:EGFP+ cell fraction between the total retinal cells and γ-H2AX+ retinal cells in *banp*^{rw337} mutants (Figure 4-7 F). Taken together it is implying that DNA damage accumulates during DNA replication and differentiation, respectively. However, it is likely that most DNA damage is introduced in S-phase of retinal progenitor cells in the absence of Banp.

In other words, sporadic DNA damage during S-phase in *banp*^{rw337} mutant is feasible during DNA replication because Banp reportedly plays a protective role during DNA damage repair (Chaudhary, Nakka et al. 2014). Furthermore, loss of function of Banp may also compromise the expression of target genes such as *wrnip1* and could induce replication stress (Table 4-1, highlighted in bold). DNA damage is likely to happen during mitosis due to segregation defects, while non-mitotic DNA damage signals could be sporadic (replicative DNA damage) or come from daughter cells whose parent cell had faulty chromatin segregation.

In summary, we have seen that a lack of Banp activity causes chromatin segregation defects during mitosis and replicative DNA damage during the S-phase of the cell cycle. However, it is unclear whether the segregation defect causes DNA damage carried over to subsequent cell cycle phases or whether replication stress causes DNA damage carried over to subsequent cell cycle phases; the tools to distinguish these are limited, especially in physiological settings. It is known that either outcome is possible because it is a vicious cycle that is poorly understood (Pedersen, Karemore et al. 2016).

The best method for elucidating the molecular mechanisms of Banp under physiological settings is to create animal models with mutations in the gene. We therefore reveal that our *banp*^{rw337} mutant is a good model for studying the function of the Banp under physiological conditions and during development, especially since we discovered that the Banp motif is conserved in zebrafish, like mice and humans. In conclusion, we uncovered that *banp* plays a vital role in the survival of zebrafish retinal neurons by controlling replication stress in RPCs. Banp is essential for the transcription of chromatin segregation genes like *cenpt* and *ncapg*. In

the absence of *cenpt* and *ncapg*, chromatin segregation is disrupted. Replication stress along with mitotic chromatin segregation defect results in activation of *tp53* independent DNA damage response. leveraging embryonic zebrafish retina, the regulatory role of Banp in RPC survival and transcription of chromatin segregation genes is elucidated under physiological settings for the first time (Figure 4-15). Lastly, we identified 26 candidates of Banp direct target genes, including *ncapg* and *cenpt*, which carry the Banp motifs near their TSSs, and show markedly decreased chromatin accessibility and transcription in the absence of Banp. This gene list will provide a useful starting point to investigate the Banp-mediated transcriptional network.

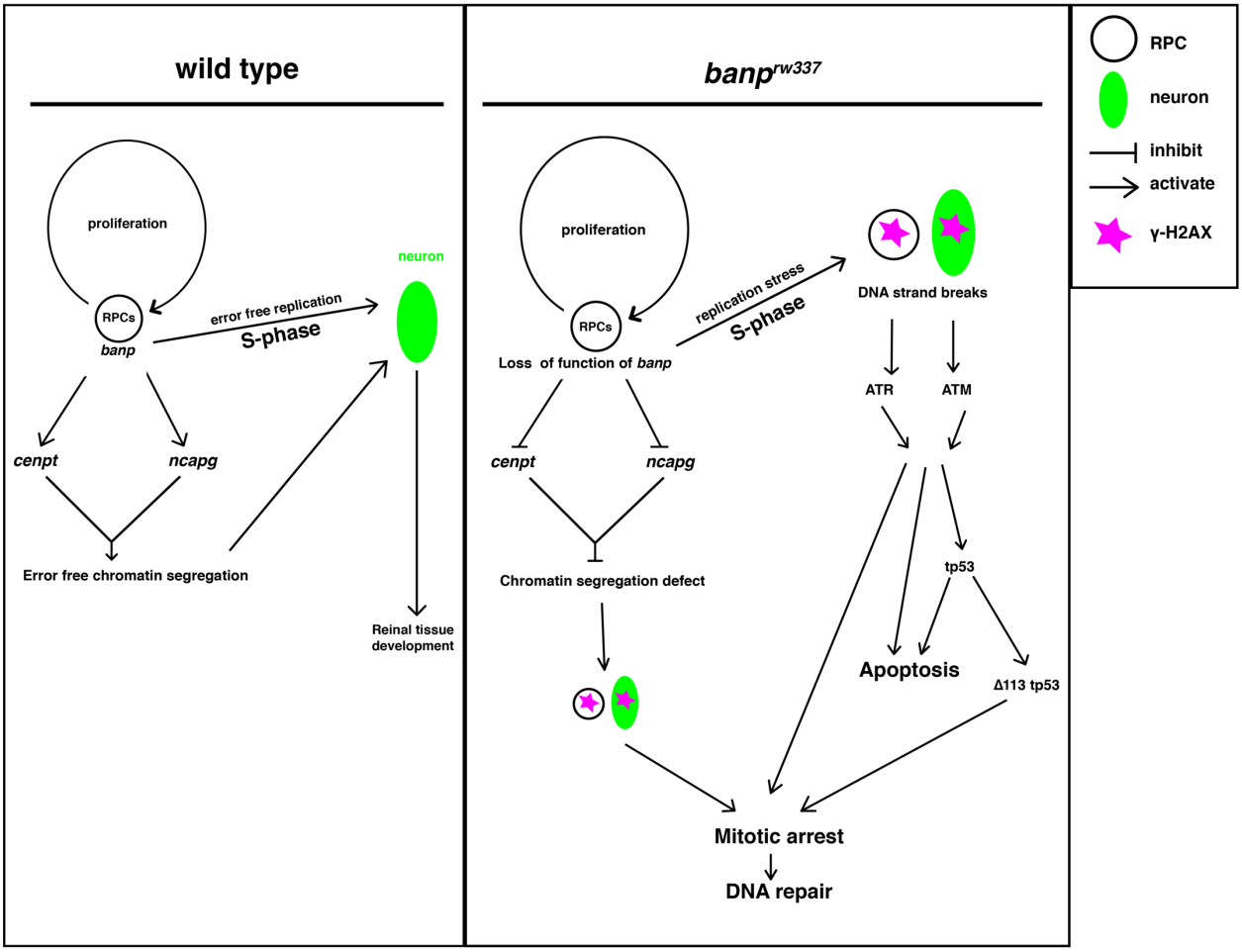

Figure 4-15: Summary of retinal phenotypes in zebrafish *banp* mutants.
In zebrafish, Banp is essential for the survival of RPCs and retinal neurogenesis. We show that the loss of function of Banp in *banp*^{rw337} primarily affects RPCs. In RPCs, loss of Banp causes 1) an accumulation of DNA strand breaks during replication, presumably generating replication stress in *banp*^{rw337} mutant embryos 2) Reduce *cenpt* and *ncapg* transcription, resulting in chromatin segregation defects. Replication stress, chromatin segregation defects activate the *tp53*-dependent and *tp53*-independent surveillance mechanisms, which can activate mitotic delay/arrest to repair the DNA damage and activate cell death upon irreparable damage.

4.5 Future perspectives

In terms of future research, we see a few intriguing areas that could be investigated further, such as the role of Banp in photoreceptor differentiation. We discovered that photoreceptors in *banp*^{rw337} mutants are poorly differentiated (**Figure 2-12** H). Given that Banp is a chromatin modulator (Sinha, Malonia et al. 2012, Grand, Burger et al. 2021) and that photoreceptor differentiation requires specific chromatin remodeling (Hughes, Enright et al. 2017), it will be interesting to see if Banp is involved in chromatin regulation in photoreceptor differentiation. Creating conditional Banp knockouts in photoreceptors will most likely offer the necessary insights. Additionally, Banp mRNA was only expressed in lateral lines at later larval stages (Figure 2-10 LL). It is also intriguing to look at the role of the specific expression Banp in lateral lines. Banp may have tissue or cell type-specific functions, during development although this remains elusive.

Furthermore, we discovered a set of novel physiological transcription targets for Banp. A ChIP-sequencing experiment can confirm the physical binding of Banp. However, obtaining a ChIP-sequencing grade antibody for zebrafish Banp may be challenging since our attempt to generate a custom antibody was unsuccessful. Future research could focus on figuring out how Banp regulates additional targets reported in our study (Table 4-1 and Figure 4-14) and how well their regulation is conserved across species.

Scope of Banp in cancer research:

- It is generally accepted that DNA methylation of essential genes is altered in cancer cells (Baylin, Esteller et al. 2001), which is expected to modify a pattern of gene transcription through Banp motifs (Grand, Burger et al. 2021). It will be interesting to investigate how Banp mediated transcription profile is changed in cancer models of zebrafish by combining zebrafish *banp* mutants. Such approach may provide more in-depth understanding on the effect of loss of function of Banp in cancer growth and metastasis as well as a new insight on therapy development of tumors in human.
- *tp53* is already being used as a therapeutic target for malignancies (Levine 2019). However, we see the emergence of a diversity of *tp53* mutations in recent tumors (Rivlin, Brosh et al. 2011, Muller and Vousden 2014). In this situation, it is becoming a challenge to target emerging *tp53* mutations for therapy. Here lies the importance of potential *tp53* independent gene targets responsible for regulating the cell cycle, genomic integrity, and DNA damage response. Finding genes that may activate cell death or DNA damage without relying on *tp53* will help induce cell death in *tp53* mutant malignancies. Our current evidence proposes that *banp* can be one such promising candidate. According to our findings, loss of *banp* causes DNA damage accumulation followed by cell death independent of *tp53*. The necessity of Banp in regulating DNA damage response pathways is demonstrated by the *tp53* independent stimulation of DNA damage and mitotic defect with loss of function of Banp. It is intriguing to check whether targeted knockdown of Banp in *tp53* mutant malignancies may sensitize malignant cells towards cell death.

Interesting experimental evidence of Banp activation in Glioblastomas is reported by Lee et al. (Lee, Seo et al. 2020). Glioblastoma is usually associated with the *tp53* mutation, which has been related to a poor prognosis and responsiveness to standard treatments such as chemoradiotherapy (Cancer Genome Atlas Research 2008). Tumor-treating fields (TTFields) is an emerging treatment method for glioblastoma that can be applied directly to the tumor, resulting in local tumor death (Swanson, Lok et al. 2016). Lee et al. identified the critical gene

signatures and pathways in response to TTFields in four glioblastoma cell lines varying in *tp53* mutation, using gene profiling and functional annotation to understand the influence of *tp53* mutations on the effectiveness of TTFields. Interestingly, Banp was strongly induced (>1.5 fold) in response to TTFields in all three *tp53* mutant glioblastoma cell lines, but not in a glioblastoma cell line with wildtype *tp53* (Supplementary Dataset 2, cell cycle (Lee, Seo et al. 2020). This result is a shred of experimental evidence that Banp is activated in glioblastomas in response to treatments like TTFields in a *tp53*-independent manner (Lee, Seo et al. 2020). However, the significance of Banp upregulation, in this case, is not known. The purpose of this study was to identify genes such as Banp differentially expressed following TTFields in varied cellular responses and to provide insights for creating combinatorial therapies or clinical techniques to maximize successful cancer treatment. Interestingly, our study showed that loss of *banp* causes DNA damage accumulation followed by cell death independent of *tp53*. Hence, it will be interesting to see if the targeted knockdown of Banp in *tp53* mutant glioblastomas may sensitize them more towards TTFields. By providing physiological insights, our study advanced Banp as a potential target for future targeted combinatorial therapies.

CHAPTER 5

Concluding remarks

5.1.1 Banp is a fundamental transcription factor

One of the most fundamental mechanisms responsible for inducible or tissue-specific transcription is the interaction between a transcription factor and its binding sites in gene promoters. As a result, determining the functional elements of a gene promoter enables the prediction of gene expression in various tissues and under varied environmental situations. With the consensus sequence TATAA, the TATA box is the most well-known promoter element that mediates the beginning of transcription of protein-coding genes (Sandelin, Carninci et al. 2007). This element is often found 25–34 base pairs upstream of transcription start sites (TSS). Many human promoters, including those that control housekeeping genes, do not have a TATA box. A tandem CGCG-element containing motif (TCTCGCGAGA) was a frequent DNA regulatory element in human TATA-less promoters. A significant number of promoters of cell cycle genes, including cyclins and transcription regulators, chromatin structure modulators, translation initiation, and ribosomal protein genes, have this TCTCGCGAGA motif. This motif is found in approximately 5% of human gene promoters (Wyrwicz, Gaj et al. 2007). Later, it was discovered that these TCTCGCGAGA elements are evolutionarily conserved in vertebrates, and they can activate gene expression via RNA Pol II (Mahpour, Scruggs et al. 2018). Through divergent start sites, it can also activate bidirectional transcription. TCTCGCGAGA elements appear in multiple copies in a tiny fraction of promoters, in contrast to other known promoter elements that activate transcription, which normally occur once in most promoters. This phenomenon presumably modulates RNA polymerase recruitment and subsequent transcriptional rates. The TCTCGCGAGA element, unlike standard core promoter elements, is not located at a constant distance from TSSs, but rather between 20 and 70 nucleotides upstream on both strands (Mahpour, Scruggs et al. 2018).

Banp was discovered to be the only interaction factor with the CGCG element containing TCTCGCGAGA motif, and it was named as Banp motif (Grand, Burger et al. 2021). Banp revealed a high activation of Banp motifs and corresponding essential metabolic genes in pluripotent stem and terminally differentiated neural cells. I.e., a set of essential gene targets contain a Banp motif, and Banp is the only known factor involved in the transcription regulation of such genes. However, the transcription regulation by Banp depends on the methylation status of Banp motifs. Banp opens chromatin and phases nucleosomes when it binds to an unmethylated motif (Grand, Burger et al. 2021). Banp binding is inhibited *in vitro* and *in vivo* by DNA methylation of its motif, which epigenetically restricts most binding to its motifs. Additionally, due to aberrant methylation of cancer cells, differential binding of Banp at aberrantly methylated promoters in cancer cells is the consequence (Grand, Burger et al. 2021). Aberrant binding of Banp in transformed cells restricts us from understanding the physiological gene targets of Banp. In other words, the regulation by Banp in cancer cells could be very different from physiological conditions. Such differences should be carefully considered while extrapolating findings regarding regulation by Banp from cancer cells to physiological conditions. Hence it is necessary to evaluate the function of Banp in a physiological setting such

as a knock out animal model. However, previous attempts to develop a Banp knockout animal model were unsuccessful (Chemmannur, Badhwar et al. 2015, Grand, Burger et al. 2021).

5.1.2 Summary of findings

In the present study, we report the first genetic mutation in the fundamental transcription factor Banp and its physiological role in a vertebrate model. We successfully characterize a *banp* genetic mutation and its phenotypic and molecular effects in developing zebrafish retina (Figure 2-5, Figure 4-15). We discovered that the Banp motif (TCTCGCGAGA) is conserved in zebrafish (**Table 3-3**, rank 1). Loss of function of Banp compromises transcription of crucial cell cycle genes such *cenpt* and *ncapg*, along with an accumulation of DNA damage in developing embryos and activation of the *tp53*-dependent and independent DNA damage response, which leads to cell death. Our current findings shedding light on the physiological function of Banp are critical for a comprehensive understanding of the molecular basis of health and disease.

First, we studied *banp* mRNA expression throughout zebrafish embryonic and early larval stages to understand its function by identifying spatial and temporal expression. *banp* mRNA was maternally expressed according to our whole-mount in situ hybridization (**Figure 2-10**). As a result, maternal transcript may compensate for the loss of function of Banp in the *banp*^{rw337} mutants during early development and potentially repair developmental abnormalities during cleavage, gastrulation, and somitogenesis. In zebrafish, zygotic *banp* mRNA expression was ubiquitous (**Figure 2-10**). Later, it became progressively restricted to the CNS towards 48 dpf. This distribution of *banp* mRNA in CNS suggested that the *banp* might play a role in CNS development. Interestingly, *banp*^{rw337} mutants showed cell death in the CNS at 48 dpf (**Figure 2-20**). Cell death in the CNS due to loss of function of Banp demonstrates that *banp* is required for cell survival in developing CNS. Additionally, frontal sections show that mRNA is expressed in neural retina at 24 hpf, but restricted in the CMZ at 48 hpf, suggesting that RPCs express *banp* mRNA implying its function in RPC maintenance (Figure 2-10 C).

Next, we evaluated the developing neural retina of *banp*^{rw337} mutants to examine the cellular function of *banp* in neuronal development. Our TUNEL staining indicated that cell death initiates in the *banp*^{rw337} mutants from 48 hpf during its development from 24 to 101 hpf (**Figure 2-17** and **Figure 2-18**). Further, immunofluorescence labeling for mitotic cells (pH3) revealed a significant increase in the number of mitotic cells from 48 hpf (**Figure 2-18** E, F). At 48 hpf, the cells accumulated at the mitotic phase are located towards the apical side of the retina. However, the apoptotic cells are spatially separated and distributed towards the central retina suggesting progenitor cells are likely undergoing apoptosis (**Figure 2-18** G). Furthermore, at 77 and 101 hpf, apoptotic cells accumulate at the interface between the CMZ and the neural retina (**Figure 2-17**, white open arrow); however, the mitotic accumulation was at the CMZ once again spatially separated (**Figure 2-17**, yellow open arrow). The apical retina at 48 dpf and CMZ consist of RPCs (Xu, Tang et al. 2020). This result suggests that mitotic cell accumulation is associated with RPCs. To further confirm the results, whole-mount co-labeling of proapoptotic marker caspase 3 with neuronal markers (HuC/D; mature neurons and ath5:EGFP; post-mitotic neurons) were used. There was no significant association of caspase3 signals with neuronal markers (**Figure 2-17** K). Although 8 percent of caspase3 signals were accumulated in ath5:EGFP positive neurons, it was insignificant (**Figure 2-17** I). Taken together, our results confirmed that the mitotic cell accumulation and apoptosis in *banp*^{rw337} mutants are associated with RPCs or differentiating neurons (**Figure 2-17** L).

The nuclear localization (**Figure 2-8**) and BEN domain (**Figure 2-9**) are conserved in zebrafish. We speculated that the transcription regulation is likely conserved as well. Hence, to determine the molecular basis of cellular defect, we performed RNA and ATAC sequencing to identify the differentially transcribed gene targets at 48 hpf. Our RNA sequencing revealed activation *tp53* pathway (**Figure 3-1** C*) and upregulation of *atm* and *atr* in *banp*^{rw337} mutants (Figure 4-4). Additionally, the *banp*^{rw337} mutant embryos had lower expression of exons 1 to 4 of the *tp53* transcript, which corresponds to the full-length *tp53*, and higher transcription of an alternate exon within intron 4 correlates to the 5′ untranslated region (UTR) of an alternate isoform Δ*113p53* (**Figure 3-7**). The zebrafish isoform Δ*113p53* is orthologous to the human isoform Δ*133p53,* thoroughly studied (Joruiz and Bourdon 2016). This variant functions as a *tp53*-response gene. It lacks the first 113 amino acids (133 in humans) from the N-terminal region of the protein, which includes the trans-activation, *mdm2*-binding, and part of the DNA-binding domains (Joruiz and Bourdon 2016). Activation of *atm*, *atr* corresponds to replication stress (Yamaguchi, Fujimori-Tonou et al. 2008), and Δ*133p53, exo5* corresponds to DNA damage response (Chen and Peng 2009, Gong, Gong et al. 2015, Khan, Stephen et al. 2019, Ali, Zhang et al. 2020, Joruiz, Beck et al. 2020). These results suggested activation of replication stress, DNA damage, and *tp53* dependent surveillance mechanism in *banp*^{rw337} mutants. Our whole-mount labeling for DNA damage response marker γ-H2AX confirmed the accumulation of DNA damage in *banp* morphants (Figure 4-5) and mutants (Figure 4-6).

Depleting *tp53* would allow us to determine the contribution of *tp53* to the cellular defects in *banp*^{rw337} mutants. Hence, we used morpholino to knock down FL *tp53* and Δ*113tp53* to evaluate cell death, mitotic arrest, and DNA damage *banp*^{rw337} mutants. Knocking down *tp53* eliminates cell death in *banp*^{rw337} mutant retinas at 48 hpf, implying that activation of *tp53* contributes to induce cell death in mutants (Figure 4-6). However, cell death reappears in tp53-MO injected mutants by 72 hpf (Figure 3-10). It shows that *banp*^{rw337} mutants have *tp53*-independent abnormalities. Knocking down Δ*113tp53* alone did not prevent cell death in *banp*^{rw337} mutant retinas (Figure 4-6). Additionally, knocking down *tp53* or Δ*113tp53* could only mildly rescue mitotic cell accumulation and accumulation of DNA damage (Figure 4-6). Taken together, the results suggest that although *tp53* partially contributes to cellular defects such as apoptosis, the mitotic defect and DNA damage occur due to molecular defects upstream or that bypass *tp53*.

Further, our motif enrichment analysis of ATAC-sequencing data revealed that in *banp*^{rw337} mutants, the Banp motif is enriched in downregulated peaks (**Table 3-3**). This result reveals that loss of function of Banp reduces the transcription of its targets gene with Banp motif in zebrafish (Table 4-1). Our data corroborates with the finding of Grand et al., where they discovered Banp motif in mice and humans (Grand, Burger et al. 2021). Furthermore, our ATAC-sequencing demonstrated a significant decrease in transcription of *cenpt* and *ncapg* in mutants (Figure 4-9). The Banp motif was found in both *cenpt* and *ncapg* in human mice and zebrafish upstream of the 5' UTR (Figure 4-10). ChIP sequencing utilizing Banp antibody also validated *cenpt* and *ncapg* TSS peaks (Mathai, Mittal et al. 2016, Grand, Burger et al. 2021). This ChIP seq studies and our physiological validation suggest that Banp is necessary for the transcription activation of *cenpt* and *ncapg,* and its function is likely conserved in human mice and zebrafish. Reduced expression of *cenpt* and *ncapg* causes segregation defects (Seipold, Priller et al. 2009, Hung, Volkmar et al. 2017, Zhang, Su et al. 2018). Interestingly, *banp* morphants show prolonged mitosis, chromosome segregation defects (Figure 4-11), and *banp*^{rw337} mutants reveal the abnormal mitotic distribution of chromosomes (Figure 4-12). These results show that reduced function of *cenpt* and *ncapg* in *banp*^{rw337} mutants leads to abnormal chromosome segregation and corresponding mitotic cell accumulation. This live imaging also suggest that

the increased accumulation of mitotic cells that we are observing in *banp*^{rw337} mutants are likely due to delayed mitosis rather than mitotic arrest. Although we thought it would be mitotic arrest in chapter 2 and chapter 3.

Two primary sources of DNA damage and genomic instability in proliferating cells are DNA replication stress and abnormal chromosomal separation (Pedersen, Karemore et al. 2016). In *banp*^{rw337} mutants, we show evidence for replication stress (Figure 4-4 and Figure 4-7 C) and chromatin segregation defect (Figure 4-11, Figure 4-12). Reduced transcription of replication factors such as *wrnip1* (Table 4-1, bold) or loss of function of Banp protein itself is likely to contribute to sporadic DNA damage and replication stress in *banp*^{rw337} mutants because Banp reportedly plays a direct protective role during DNA damage repair (Chaudhary, Nakka et al. 2014, Socha, Yang et al. 2020). The mitotic γ-H2AX signal suggests that chromosome segregation defects may cause DNA damage in mutants. However, DNA damage during mitosis is not always repaired. It is often carried over to daughter cells followed by DNA repair during the S-phase of the corresponding damaged daughter cells (Pedersen, Karemore et al. 2016), which is also likely to show most DNA damage response in non-mitotic cells *banp*^{rw337} mutants. In other words, DNA damage may happen during mitosis, while non-mitotic DNA damage signals could be sporadic or come from daughter cells whose parent cell had faulty chromatin segregation. We show that a lack of Banp activity causes chromatin segregation defects and DNA damage in the S-phase of the cell cycle. However, it is unclear whether the chromosome segregation defect causes DNA damage that is carried over to subsequent cell cycle phases or whether replication stress causes DNA damage that is carried over to subsequent cell cycle phases; the tools to distinguish these are limited, especially in physiological settings. It is known that either outcome is possible because it is a vicious cycle that is yet poorly understood (Pedersen, Karemore et al. 2016). Under physiological conditions, cells either perish in mitosis via apoptosis or exit mitosis without dying after a prolonged mitotic arrest, carrying DNA damage (Pedersen, Karemore et al. 2016, Thompson, Gatenby et al. 2019, Godinez, Kabbara et al. 2020). It is unknown what determines the balance between these two fates, but recent research reveals crucial components that influence mitotic cell fate (Pedersen, Karemore et al. 2016, Thompson, Gatenby et al. 2019, Godinez, Kabbara et al. 2020). Banp, we believe, maybe one of many such potential factors. The balance between apoptosis and survival can be pushed in favor of death by knocking down Banp. As a result, by utilizing methods such as targeted silencing of Banp, new possibilities for sensitizing cancer cells to anti-mitotic drugs may open. Loss of function of Banp induces *tp53*-independent cell death, which is particularly useful in *tp53* mutant malignancies. Considering the understanding of the damage response network is still limited (Pedersen, Karemore et al. 2016, Blackford and Stucki 2020), our current evidence suggesting the participation of Banp is substantial, although exact mechanism remains elusive.

The best method for elucidating the molecular mechanisms of Banp under physiological settings is to create animal models with mutations in the gene. We reveal that our *banp*^{rw337} mutant is a good model for studying the function of the Banp under physiological conditions and during development, especially since we discovered that the Banp motif is conserved in zebrafish, similar to mice and humans. In conclusion, we uncovered that *banp* plays a vital role in the survival of zebrafish retinal neurons by controlling replication stress in RPCs. Banp is essential for the transcription of chromatin segregation genes like *cenpt* and *ncapg*. In the absence of *cenpt* and *ncapg*, chromatin segregation is disrupted. Replication stress along with mitotic chromatin segregation defect results in activation of *tp53* independent DNA damage response. For the first time, leveraging embryonic zebrafish retina, the regulatory role of Banp in RPC

survival and transcription of chromatin segregation genes is elucidated under physiological settings (Figure 5-1).

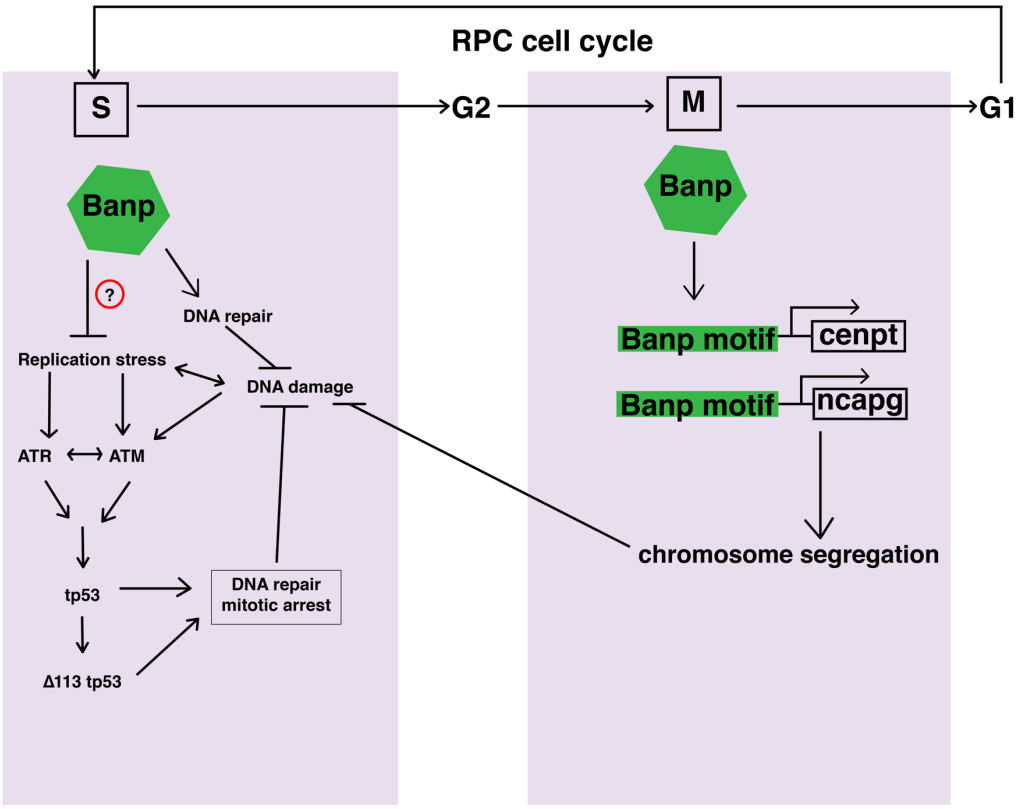

Figure 5-1: The key findings are summarized in this diagram.
Our study reveals two novel roles of Banp in cell-cycle regulation of retinal progenitor cells. First, Banp suppresses DNA replication stress and promotes DNA damage repair. In the absence of Banp, a DNA replication stress sensor, *atr*, is activated, as result of accumulation of DNA double-strand breaks, which activate *atm* and the tp53-mediated DNA damage response pathway. tp53 activates the apoptotic pathway and promotes transcription of Δ113tp53, both of which promote cell-cycle delay/arrest and DNA repair. Second, Banp is required for chromosome segregation during mitosis by promoting transcription of two mitotic regulators, *cenpt* and *ncapg*. Since a Banp motif is found near the TSSs of these genes, it is likely that *cenpt* and *ncapg* are direct targets of Banp.

REFERENCE:

Abhiman, S., L. M. Iyer and L. Aravind (2008). "BEN: a novel domain in chromatin factors and DNA viral proteins." Bioinformatics **24**(4): 458-461.

Ackermann, A. and L. Kaestner. (2019). "**UPDATED** ATAC-seq Protocol." from https://www.med.upenn.edu/kaestnerlab/protocols.html.

Adhikary, A., S. Chakraborty, M. Mazumdar, S. Ghosh, S. Mukherjee, A. Manna, S. Mohanty, K. K. Nakka, S. Joshi, A. De, S. Chattopadhyay, G. Sa and T. Das (2014). "Inhibition of epithelial to mesenchymal transition by E-cadherin up-regulation via repression of slug transcription and inhibition of E-cadherin degradation: dual role of scaffold/matrix attachment region-binding protein 1 (SMAR1) in breast cancer cells." J Biol Chem **289**(37): 25431-25444.

Ahnen, D. J. (1996). "Stalking the guardian of the genome: p53 in colorectal carcinogenesis." Am J Gastroenterol **91**(1): 3-6.

Ali, S., Y. L. Zhang, M. Zhou, H. Z. Li, W. W. Jin, L. Zheng, X. C. Yu, J. M. Stark, J. N. Weitzel and B. H. Shen (2020). "Functional deficiency of DNA repair gene EXO5 results in androgen-induced genomic instability and prostate tumorigenesis." Oncogene **39**(6): 1246-1259.

Anders, S., A. Reyes and W. Huber (2012). "Detecting differential usage of exons from RNA-seq data." Genome Research **22**(10): 2008-2017.

Andrews, S. (2010). "FastQC: A Quality Control Tool for High Throughput Sequence Data." from http://www.bioinformatics.babraham.ac.uk/projects/fastqc/.

Barak, Y., T. Juven, R. Haffner and M. Oren (1993). "Mdm2 Expression Is Induced by Wild Type-P53 Activity." Embo Journal **12**(2): 461-468.

Bartkova, J., J. Lukas, M. Strauss and J. Bartek (1995). "Cyclin D1 Oncoprotein Aberrantly Accumulates in Malignancies of Diverse Histogenesis." Oncogene **10**(4): 775-778.

Baye, L. M. and B. A. Link (2007). "Interkinetic nuclear migration and the selection of neurogenic cell divisions during vertebrate retinogenesis." J Neurosci **27**(38): 10143-10152.

Baylin, S. B., M. Esteller, M. R. Rountree, K. E. Bachman, K. Schuebel and J. G. Herman (2001). "Aberrant patterns of DNA methylation, chromatin formation and gene expression in cancer." Hum Mol Genet **10**(7): 687-692.

Bellelli, R., V. Borel, C. Logan, J. Svendsen, D. E. Cox, E. Nye, K. Metcalfe, S. M. O'Connell, G. Stamp, H. R. Flynn, A. P. Snijders, F. Lassailly, A. Jackson and S. J. Boulton (2018). "Polepsilon Instability Drives Replication Stress, Abnormal Development, and Tumorigenesis." Mol Cell **70**(4): 707-721 e707.

Benchimol, S. (2001). "p53-dependent pathways of apoptosis." Cell Death Differ **8**(11): 1049-1051.

Bhagat, P. N., S. H. Jadhav, S. Chattopadhyay and K. M. Paknikar (2018). "Carbon nanospheres mediated nuclear delivery of SMAR1 protein (DNA binding domain) controls breast tumor in mice model." Nanomedicine (Lond) **13**(4): 353-372.

Biehlmaier, O., S. C. Neuhauss and K. Kohler (2001). "Onset and time course of apoptosis in the developing zebrafish retina." Cell Tissue Res **306**(2): 199-207.

Birot, A., L. Duret, L. Bartholin, B. Santalucia, I. Tigaud, J. Magaud and J. Rouault (2000). "Identification and molecular analysis of BANP." Gene **253**(2): 189-196.

Blackford, A. N. and S. P. Jackson (2017). "ATM, ATR, and DNA-PK: The Trinity at the Heart of the DNA Damage Response." Mol Cell **66**(6): 801-817.

Blackford, A. N. and M. Stucki (2020). "How Cells Respond to DNA Breaks in Mitosis." Trends in Biochemical Sciences **45**(4): 321-331.
Bladen, C. L., W. K. Lam, W. S. Dynan and D. J. Kozlowski (2005). "DNA damage response and Ku80 function in the vertebrate embryo." Nucleic Acids Res **33**(9): 3002-3010.
Bladen, C. L., S. Navarre, W. S. Dynan and D. J. Kozlowski (2007). "Expression of the Ku70 subunit (XRCC6) and protection from low dose ionizing radiation during zebrafish embryogenesis." Neurosci Lett **422**(2): 97-102.
Blasquez, V. C., A. O. Sperry, P. N. Cockerill and W. T. Garrard (1989). "Protein - DNA Interactions at Chromosomal Loop Attachment Sites." Genome **31**(2): 503-509.
Blighe, K., S. Rana and M. Lewis. (2018). "EnhancedVolcano: Publication-ready volcano plots with enhanced colouring and labeling." from https://github.com/kevinblighe/EnhancedVolcano.
Cancer Genome Atlas Research, N. (2008). "Comprehensive genomic characterization defines human glioblastoma genes and core pathways." Nature **455**(7216): 1061-1068.
Chakraborty, S., A. Adhikary, M. Mazumdar, S. Mukherjee, P. Bhattacharjee, D. Guha, T. Choudhuri, S. Chattopadhyay, G. Sa, A. Sen and T. Das (2014). "Capsaicin-induced activation of p53-SMAR1 auto-regulatory loop down-regulates VEGF in non-small cell lung cancer to restrain angiogenesis." PLoS One **9**(6): e99743.
Chattopadhyay, S., R. Kaul, A. Charest, D. Housman and J. Z. Chen (2000). "SMAR1, a novel, alternatively spliced gene product, binds the scaffold/matrix-associated region at the T cell receptor beta locus." Genomics **68**(1): 93-96.
Chaudhary, N., K. K. Nakka, P. L. Chavali, J. Bhat, S. Chatterjee and S. Chattopadhyay (2014). "SMAR1 coordinates HDAC6-induced deacetylation of Ku70 and dictates cell fate upon irradiation." Cell Death Dis **5**: e1447.
Chavez, M. N., G. Aedo, F. A. Fierro, M. L. Allende and J. T. Egana (2016). "Zebrafish as an Emerging Model Organism to Study Angiogenesis in Development and Regeneration." Frontiers in Physiology **7**.
Chemmannur, S. V., A. J. Badhwar, B. Mirlekar, S. K. Malonia, M. Gupta, N. Wadhwa, R. Bopanna, U. Mabalirajan, S. Majumdar, B. Ghosh and S. Chattopadhyay (2015). "Nuclear matrix binding protein SMAR1 regulates T-cell differentiation and allergic airway disease." Mucosal Immunol **8**(6): 1201-1211.
Chemmannur, S. V., P. Bhagat, B. Mirlekar, K. M. Paknikar and S. Chattopadhyay (2016). "Carbon nanospheres mediated delivery of nuclear matrix protein SMAR1 to direct experimental autoimmune encephalomyelitis in mice." Int J Nanomedicine **11**: 2039-2051.
Chen, J. (2016). "The Cell-Cycle Arrest and Apoptotic Functions of p53 in Tumor Initiation and Progression." Cold Spring Harb Perspect Med **6**(3): a026104.
Chen, J., S. M. Ng, C. Chang, Z. Zhang, J.-C. Bourdon, D. P. Lane and J. Peng (2009). "p53 isoform delta113p53 is a p53 target gene that antagonizes p53 apoptotic activity via BclxL activation in zebrafish." Genes & development **23**(3): 278-290.
Chen, J., S. M. Ng, C. Chang, Z. Zhang, J. C. Bourdon, D. P. Lane and J. Peng (2009). "p53 isoform delta113p53 is a p53 target gene that antagonizes p53 apoptotic activity via BclxL activation in zebrafish." Genes Dev **23**(3): 278-290.
Chen, J. and J. Peng (2009). "p53 Isoform Delta113p53 in zebrafish." Zebrafish **6**(4): 389-395.
Chen, J., H. Ruan, S. M. Ng, C. Gao, H. M. Soo, W. Wu, Z. Zhang, Z. Wen, D. P. Lane and J. Peng (2005). "Loss of function of def selectively up-regulates Delta113p53 expression to arrest expansion growth of digestive organs in zebrafish." Genes Dev **19**(23): 2900-2911.
Chen, S. F., Y. Q. Zhou, Y. R. Chen and J. Gu (2018). "fastp: an ultra-fast all-in-one FASTQ preprocessor." Bioinformatics **34**(17): 884-890.

Chen, Y. C., S. Semenova, S. Rozov, M. Sundvik, J. L. Bonkowsky and P. Panula (2016). "A Novel Developmental Role for Dopaminergic Signaling to Specify Hypothalamic Neurotransmitter Identity." Journal of Biological Chemistry **291**(42): 21880-21892.
Cheung, H. W., G. S. Cowley, B. A. Weir, J. S. Boehm, S. Rusin, J. A. Scott, A. East, L. D. Ali, P. H. Lizotte, T. C. Wong, G. Z. Jiang, J. Hsiao, C. H. Mermel, G. Getz, J. Barretina, S. Gopal, P. Tamayo, J. Gould, A. Tsherniak, N. Stransky, B. A. Luo, Y. Ren, R. Drapkin, S. N. Bhatia, J. P. Mesirov, L. A. Garraway, M. Meyerson, E. S. Lander, D. E. Root and W. C. Hahn (2011). "Systematic investigation of genetic vulnerabilities across cancer cell lines reveals lineage-specific dependencies in ovarian cancer." Proceedings of the National Academy of Sciences of the United States of America **108**(30): 12372-12377.
Chin, C. F. and F. M. Yeong (2010). "Safeguarding Entry into Mitosis: the Antephase Checkpoint." Molecular and Cellular Biology **30**(1): 22-32.
Choksi, A., A. Parulekar, R. Pant, V. K. Shah, R. Nimma, P. Firmal, S. Singh, G. C. Kundu, S. Shukla and S. Chattopadhyay (2021). "Tumor suppressor SMAR1 regulates PKM alternative splicing by HDAC6-mediated deacetylation of PTBP1." Cancer Metab **9**(1): 16.
Choy, S. W., C. W. Cheng, S. T. Lee, V. W. T. Li, M. N. Y. Hui, C. C. Hui, D. Liu and S. H. Cheng (2010). "A Cascade of irx1a and irx2a Controls shh Expression During Retinogenesis." Developmental Dynamics **239**(12): 3204-3214.
Curtis, N. L., G. F. Ruda, P. Brennan and V. M. Bolanos-Garcia (2020). "Deregulation of Chromosome Segregation and Cancer." Annual Review of Cancer Biology, Vol 4 **4**: 257-278.
Danilova, N., E. Bibikova, T. M. Covey, D. Nathanson, E. Dimitrova, Y. Konto, A. Lindgren, B. Glader, C. G. Radu, K. M. Sakamoto and S. Lin (2014). "The role of the DNA damage response in zebrafish and cellular models of Diamond Blackfan anemia." Dis Model Mech **7**(7): 895-905.
Danilova, N., A. Kumagai and J. Lin (2010). "p53 Upregulation Is a Frequent Response to Deficiency of Cell-Essential Genes." Plos One **5**(12).
Del Bene, F., A. M. Wehman, B. A. Link and H. Baier (2008). "Regulation of neurogenesis by interkinetic nuclear migration through an apical-basal notch gradient." Cell **134**(6): 1055-1065.
Evans, T., E. T. Rosenthal, J. Youngblom, D. Distel and T. Hunt (1983). "Cyclin: a protein specified by maternal mRNA in sea urchin eggs that is destroyed at each cleavage division." Cell **33**(2): 389-396.
Fernandez-Diez, C., S. Gonzalez-Rojo, M. Lombo and M. P. Herraez (2018). "Tolerance to paternal genotoxic damage promotes survival during embryo development in zebrafish (Danio rerio)." Biology Open **7**(5).
Fischer, M. (2017). "Census and evaluation of p53 target genes." Oncogene **36**(28): 3943-3956.
Furnari, B., N. Rhind and P. Russell (1997). "Cdc25 mitotic inducer targeted by chk1 DNA damage checkpoint kinase." Science **277**(5331): 1495-1497.
Gaspar, J. M. (2019). "ATAC-seq Guidelines." from https://informatics.fas.harvard.edu/atac-seq-guidelines.html.
Gisselsson, D. (2008). "Classification of chromosome segregation errors in cancer." Chromosoma **117**(6): 511-519.
Godinez, V. G., S. Kabbara, A. Sherman, T. Wu, S. Cohen, X. D. Kong, J. L. Maravillas-Montero, Z. X. Shi, D. Preece, K. Yokomori and M. W. Berns (2020). "DNA damage induced during mitosis undergoes DNA repair synthesis." Plos One **15**(4).
Gong, L., H. Gong, X. Pan, C. Chang, Z. Ou, S. Ye, L. Yin, L. Yang, T. Tao, Z. Zhang, C. Liu, D. P. Lane, J. Peng and J. Chen (2015). "p53 isoform Delta113p53/Delta133p53 promotes DNA

double-strand break repair to protect cell from death and senescence in response to DNA damage." Cell Res **25**(3): 351-369.
Gong, L., H. J. Gong, X. Pan, C. Q. Chang, Z. Ou, S. F. Ye, L. Yin, L. N. Yang, T. Tao, Z. H. Zhang, C. Liu, D. P. Lane, J. R. Peng and J. Chen (2015). "p53 isoform Delta 113p53/Delta 133p53 promotes DNA double-strand break repair to protect cell from death and senescence in response to DNA damage." Cell Research **25**(3): 351-369.
Gong, L., X. Pan, G. K. Abali, J. B. Little and Z. M. Yuan (2020). "Functional interplay between p53 and Delta 133p53 in adaptive stress response." Cell Death and Differentiation **27**(5): 1618-1632.
Gramage, E., J. Li and P. Hitchcock (2014). "The expression and function of midkine in the vertebrate retina." British Journal of Pharmacology **171**(4): 913-923.
Grand, R. S., L. Burger, C. Grawe, A. K. Michael, L. Isbel, D. Hess, L. Hoerner, V. Iesmantavicius, S. Durdu, M. Pregnolato, A. R. Krebs, S. A. Smallwood, N. Thoma, M. Vermeulen and D. Schubeler (2021). "BANP opens chromatin and activates CpG-island-regulated genes." Nature.
Harris, W. A. (1997). "Cellular diversification in the vertebrate retina." Curr Opin Genet Dev **7**(5): 651-658.
Hart, C. M. and U. K. Laemmli (1998). "Facilitation of chromatin dynamics by SARs." Current Opinion in Genetics & Development **8**(5): 519-525.
Hart, T., M. Chandrashekhar, M. Aregger, Z. Steinhart, K. R. Brown, G. MacLeod, M. Mis, M. Zimmermann, A. Fradet-Turcotte, S. Sun, P. Mero, P. Dirks, S. Sidhu, F. P. Roth, O. S. Rissland, D. Durocher, S. Angers and J. Moffat (2015). "High-Resolution CRISPR Screens Reveal Fitness Genes and Genotype-Specific Cancer Liabilities." Cell **163**(6).
Heinz, S., C. Benner, N. Spann, E. Bertolino, Y. C. Lin, P. Laslo, J. X. Cheng, C. Murre, H. Singh and C. K. Glass (2010). "Simple combinations of lineage-determining transcription factors prime cis-regulatory elements required for macrophage and B cell identities." Mol Cell **38**(4): 576-589.
Henriksson, J., X. Chen, T. Gomes, U. Ullah, K. B. Meyer, R. Miragaia, G. Duddy, J. Pramanik, K. Yusa, R. Lahesmaa and S. A. Teichmann (2019). "Genome-wide CRISPR Screens in T Helper Cells Reveal Pervasive Crosstalk between Activation and Differentiation." Cell **176**(4): 882-+.
Hu, Z., J. Holzschuh and W. Driever (2015). "Loss of DDB1 Leads to Transcriptional p53 Pathway Activation in Proliferating Cells, Cell Cycle Deregulation, and Apoptosis in Zebrafish Embryos." PLoS One **10**(7): e0134299.
Hughes, A. E. O., J. M. Enright, C. A. Myers, S. Q. Shen and J. C. Corbo (2017). "Cell Type-Specific Epigenomic Analysis Reveals a Uniquely Closed Chromatin Architecture in Mouse Rod Photoreceptors." Scientific Reports **7**.
Hung, C. Y., B. Volkmar, J. D. Baker, J. W. Bauer, E. Gussoni, S. Hainzl, A. Klausegger, J. Lorenzo, I. Mihalek, O. Rittinger, M. Tekin, J. E. Dallman and O. A. Bodamer (2017). "A defect in the inner kinetochore protein CENPT causes a new syndrome of severe growth failure." PLoS One **12**(12): e0189324.
Imai, F., A. Yoshizawa, N. Fujimori-Tonou, K. Kawakami and I. Masai (2010). "The ubiquitin proteasome system is required for cell proliferation of the lens epithelium and for differentiation of lens fiber cells in zebrafish." Development **137**(19): 3257-3268.
Jallepalli, P. V. and C. Lengauer (2001). "Chromosome segregation and cancer: Cutting through the mystery." Nature Reviews Cancer **1**(2): 109-117.

Jalota-Badhwar, A., R. Kaul-Ghanekar, D. Mogare, R. Boppana, K. M. Paknikar and S. Chattopadhyay (2007). "SMAR1-derived P44 peptide retains its tumor suppressor function through modulation of p53." J Biol Chem **282**(13): 9902-9913.
Jegadesan, N. K. and D. Branzei (2021). "DDX11 loss causes replication stress and pharmacologically exploitable DNA repair defects." Proc Natl Acad Sci U S A **118**(17).
Joruiz, S. M., J. A. Beck, I. Horikawa and C. C. Harris (2020). "The Delta 133p53 Isoforms, Tuners of the p53 Pathway." Cancers **12**(11).
Joruiz, S. M. and J. C. Bourdon (2016). "p53 Isoforms: Key Regulators of the Cell Fate Decision." Cold Spring Harbor Perspectives in Medicine **6**(8).
Kaul, R., S. Mukherjee, F. Ahmed, M. K. Bhat, R. Chhipa, S. Galande and S. Chattopadhyay (2003). "Direct interaction with and activation of p53 by SMAR1 retards cell-cycle progression at G2/M phase and delays tumor growth in mice." Int J Cancer **103**(5): 606-615.
Kaul-Ghanekar, R., A. Jalota, L. Pavithra, P. Tucker and S. Chattopadhyay (2004). "SMAR1 and Cux/CDP modulate chromatin and act as negative regulators of the TCRbeta enhancer (Ebeta)." Nucleic Acids Res **32**(16): 4862-4875.
Kermi, C., A. Aze and D. Maiorano (2019). "Preserving Genome Integrity During the Early Embryonic DNA Replication Cycles." Genes (Basel) **10**(5).
Khan, F., T. Stephen, J. Friedman, D. Gao, M. Miller, M. Mehrotra, A. Hormigo, N. Tsankova, R. McBride and J. Houldsworth (2019). "The DNA Damage Repair Pathway Gene EXO5 Is Hypermethylated in Glioblastomas: Correlation with MGMT Hypermethylation, Genomic Alterations and Patient Outcome." Journal of Molecular Diagnostics **21**(6): 1220-1220.
Kim, D., J. M. Paggi, C. Park, C. Bennett and S. L. Salzberg (2019). "Graph-based genome alignment and genotyping with HISAT2 and HISAT-genotype." Nature Biotechnology **37**(8): 907-+.
Kops, G. J. P. L., B. Snel and E. C. Tromer (2020). "Evolutionary Dynamics of the Spindle Assembly Checkpoint in Eukaryotes." Current Biology **30**(10): R589-R602.
Kubbutat, M. H., S. N. Jones and K. H. Vousden (1997). "Regulation of p53 stability by Mdm2." Nature **387**(6630): 299-303.
Kurtenbach, S. and J. W. Harbour (2019). "SparK: A Publication-quality NGS Visualization Tool." bioRxiv.
Langheinrich, U., E. Hennen, G. Stott and G. Vacun (2002). "Zebrafish as a model organism for the identification and characterization of drugs and genes affecting p53 signaling." Current Biology **12**(23): 2023-2028.
Langmead, B. and S. L. Salzberg (2012). "Fast gapped-read alignment with Bowtie 2." Nature Methods **9**(4): 357-U354.
Lee, Y. J., H. W. Seo, J. H. Baek, S. H. Lim, S. G. Hwang and E. H. Kim (2020). "Gene expression profiling of glioblastoma cell lines depending on TP53 status after tumor-treating fields (TTFields) treatment." Sci Rep **10**(1): 12272.
Levine, A. J. (2019). "Targeting Therapies for the p53 Protein in Cancer Treatments." Annual Review of Cancer Biology, Vol 3 **3**: 21-34.
Li, H., B. Handsaker, A. Wysoker, T. Fennell, J. Ruan, N. Homer, G. Marth, G. Abecasis, R. Durbin and G. P. D. Proc (2009). "The Sequence Alignment/Map format and SAMtools." Bioinformatics **25**(16): 2078-2079.
Li, J. Z., F. Liu, Y. X. Lv, K. Sun, Y. T. Zhao, J. Reilly, Y. J. Zhang, J. Y. Tu, S. S. Yu, X. L. Liu, Y. Y. Qin, Y. W. Huang, P. Gao, D. N. Jia, X. Chen, Y. Q. Han, X. H. Shu, D. J. Luo, Z. H. Tang and M. G. Liu (2021). "Prpf31 is essential for the survival and differentiation of retinal progenitor cells by modulating alternative splicing." Nucleic Acids Research **49**(4): 2027-2043.

Li, Z., M. Hu, M. J. Ochocinska, N. M. Joseph and S. S. Easter, Jr. (2000). "Modulation of cell proliferation in the embryonic retina of zebrafish (Danio rerio)." Dev Dyn **219**(3): 391-401.
Liao, Y., G. K. Smyth and W. Shi (2014). "featureCounts: an efficient general purpose program for assigning sequence reads to genomic features." Bioinformatics **30**(7): 923-930.
Liao, Y., G. K. Smyth and W. Shi (2014). "featureCounts: an efficient general purpose program for assigning sequence reads to genomic features." Bioinformatics **30**(7): 923-930.
Liebl, M. C. and T. G. Hofmann (2019). "Cell Fate Regulation upon DNA Damage: p53 Serine 46 Kinases Pave the Cell Death Road." Bioessays **41**(12).
Lieschke, G. J. and P. D. Currie (2007). "Animal models of human disease: zebrafish swim into view." Nature Reviews Genetics **8**(5): 353-367.
Lindahl, T. and D. E. Barnes (2000). "Repair of endogenous DNA damage." Cold Spring Harb Symp Quant Biol **65**: 127-133.
Liu, H. C., F. Ma, Y. Shen, Y. Q. Hu and S. Pan (2014). "Overexpression of SMAR1 Enhances Radiosensitivity in Human Breast Cancer Cell Line MCF7 via Activation of p53 Signaling Pathway." Oncol Res **22**(5-6): 293-300.
Liu, M. and H. Y. Huang (2010). "Identification and validation of novel C/EBP beta-regulated genes in preadipocyte proliferation." Chinese Medical Journal **123**(9): 1190-1194.
Liu, T. X., N. G. Howlett, M. Deng, D. M. Langenau, K. Hsu, J. Rhodes, J. P. Kanki, A. D. D'Andrea and A. T. Look (2003). "Knockdown of zebrafish Fancd2 causes developmental abnormalities via p53-dependent apoptosis." Dev Cell **5**(6): 903-914.
Locker, M., M. Agathocleous, M. A. Amato, K. Parain, W. A. Harris and M. Perron (2006). "Hedgehog signaling and the retina: insights into the mechanisms controlling the proliferative properties of neural precursors." Genes Dev **20**(21): 3036-3048.
Lush, M. E., D. C. Diaz, N. Koenecke, S. Baek, H. Boldt, M. K. St Peter, T. Gaitan-Escudero, A. Romero-Carvajal, E. M. Busch-Nentwich, A. G. Perera, K. E. Hall, A. Peak, J. S. Haug and T. Piotrowski (2019). "scRNA-Seq reveals distinct stem cell populations that drive hair cell regeneration after loss of Fgf and Notch signaling." Elife **8**.
Magdalou, I., B. S. Lopez, P. Pasero and S. A. Lambert (2014). "The causes of replication stress and their consequences on genome stability and cell fate." Semin Cell Dev Biol **30**: 154-164.
Mah, L. J., A. El-Osta and T. C. Karagiannis (2010). "gamma H2AX: a sensitive molecular marker of DNA damage and repair." Leukemia **24**(4): 679-686.
Mahpour, A., B. S. Scruggs, D. Smiraglia, T. Ouchi and I. H. Gelman (2018). "A methyl-sensitive element induces bidirectional transcription in TATA-less CpG island-associated promoters." Plos One **13**(10).
Mair, B., J. Tomic, S. N. Masud, P. Tonge, A. Weiss, M. Usaj, A. H. Y. Tong, J. J. Kwan, K. R. Brown, E. Titus, M. Atkins, K. S. K. Chan, L. Munsie, A. Habsid, H. Han, M. Kennedy, B. Cohen, G. Keller and J. Moffat (2019). "Essential Gene Profiles for Human Pluripotent Stem Cells Identify Uncharacterized Genes and Substrate Dependencies." Cell Reports **27**(2): 599-+.
Malonia, S. K., S. Sinha, P. Lakshminarasimhan, K. Singh, A. Jalota-Badhwar, S. Rampalli, R. Kaul-Ghanekar and S. Chattopadhyay (2011). "Gene regulation by SMAR1: Role in cellular homeostasis and cancer." Biochim Biophys Acta **1815**(1): 1-12.
Malonia, S. K., B. Yadav, S. Sinha, G. Lazennec and S. Chattopadhyay (2014). "Chromatin remodeling protein SMAR1 regulates NF-kappaB dependent Interleukin-8 transcription in breast cancer." Int J Biochem Cell Biol **55**: 220-226.
Manfredi, J. J. (2009). "Insights from a novel p53 isoform in zebrafish want to reel us in, but will we take the bait?" Genes Dev **23**(3): 261-264.

Manfredi, J. J. (2010). "The Mdm2-p53 relationship evolves: Mdm2 swings both ways as an oncogene and a tumor suppressor (vol 24, pg 1580, 2010)." Genes & Development **24**(18): 2105-2105.
Martinez-Morales, J. R., F. Del Bene, G. Nica, M. Hammerschmidt, P. Bovolenta and J. Wittbrodt (2005). "Differentiation of the vertebrate retina is coordinated by an FGF signaling center." Dev Cell **8**(4): 565-574.
Masai, I., Z. Lele, M. Yamaguchi, A. Komori, A. Nakata, Y. Nishiwaki, H. Wada, H. Tanaka, Y. Nojima, M. Hammerschmidt, S. W. Wilson and H. Okamoto (2003). "N-cadherin mediates retinal lamination, maintenance of forebrain compartments and patterning of retinal neurites." Development **130**(11): 2479-2494.
Masai, I., D. L. Stemple, H. Okamoto and S. W. Wilson (2000). "Midline signals regulate retinal neurogenesis in zebrafish." Neuron **27**(2): 251-263.
Masai, I., M. Yamaguchi, N. Tonou-Fujimori, A. Komori and H. Okamoto (2005). "The hedgehog-PKA pathway regulates two distinct steps of the differentiation of retinal ganglion cells: the cell-cycle exit of retinoblasts and their neuronal maturation." Development **132**(7): 1539-1553.
Masai, I., M. Yamaguchi, N. Tonou-Fujimori, A. Komori and H. Okamoto (2005). "The hedgehog-PKA pathway regulates two distinct steps of the differentiation of retinal ganglion cells: the cell-cycle exit of retinoblasts and their neuronal maturation." Development **132**(7): 1539-1553.
Mathai, J., S. P. Mittal, A. Alam, P. Ranade, D. Mogare, S. Patel, S. Saxena, S. Ghorai, A. P. Kulkarni and S. Chattopadhyay (2016). "SMAR1 binds to T(C/G) repeat and inhibits tumor progression by regulating miR-371-373 cluster." Sci Rep **6**: 33779.
Matsuda, S., J. Rouault, J. Magaud and C. Berthet (2001). "In search of a function for the TIS21/PC3/BTG1/TOB family." FEBS Lett **497**(2-3): 67-72.
McCurley, A. T. and G. V. Callard (2008). "Characterization of housekeeping genes in zebrafish: male-female differences and effects of tissue type, developmental stage and chemical treatment." Bmc Molecular Biology **9**.
McElderry, J., B. Carrington, K. Bishop, E. Kim, W. H. Pei, Z. L. Chen, R. Ramanagoudr-Bhojappa, A. Prakash, S. M. Burgess, P. P. Liu and R. Sood (2019). "Splicing factor DHX15 affects tp53 and mdm2 expression via alternate splicing and promoter usage." Human Molecular Genetics **28**(24): 4174-4186.
Meek, D. W. (2009). "Tumour suppression by p53: a role for the DNA damage response?" Nat Rev Cancer **9**(10): 714-723.
Meyers, R. M., J. G. Bryan, J. M. McFarland, B. A. Weir, A. E. Sizemore, H. Xu, N. V. Dharia, P. G. Montgomery, G. S. Cowley, S. Pantel, A. Goodale, Y. Lee, L. D. Ali, G. Z. Jiang, R. Lubonja, W. F. Harrington, M. Strickland, T. Wu, D. C. Hawes, V. A. Zhivich, M. R. Wyatt, Z. Kalani, J. M. J. Chang, M. Okamoto, K. Stegmaier, T. R. Golub, J. S. Boehm, F. Vazquez, D. E. Root, W. C. Hahn and A. Tsherniak (2017). "Computational correction of copy number effect improves specificity of CRISPR-Cas9 essentiality screens in cancer cells." Nature Genetics **49**(12): 1779-+.
Miermont, A., V. Antolovic, T. Lenn, J. M. E. Nichols, L. J. Millward and J. R. Chubb (2019). "The fate of cells undergoing spontaneous DNA damage during development." Development **146**(12).
Mitchison and Salmon (2001). "Mitosis: a history of division. (vol 3, pg E17, 2001)." Nature Cell Biology **3**(5): 530-530.

Mochizuki, T., Y. J. Luo, H. F. Tsai, A. Hagiwara and I. Masai (2017). "Cell division and cadherin-mediated adhesion regulate lens epithelial cell movement in zebrafish." Development **144**(4): 708-719.
Mochizuki, T., S. Suzuki and I. Masai (2014). "Spatial pattern of cell geometry and cell-division orientation in zebrafish lens epithelium." Biol Open **3**(10): 982-994.
Muller, P. A. and K. H. Vousden (2014). "Mutant p53 in cancer: new functions and therapeutic opportunities." Cancer Cell **25**(3): 304-317.
Murga, M., S. Bunting, M. F. Montana, R. Soria, F. Mulero, M. Canamero, Y. Lee, P. J. McKinnon, A. Nussenzweig and O. Fernandez-Capetillo (2009). "A mouse model of ATR-Seckel shows embryonic replicative stress and accelerated aging." Nature Genetics **41**(8): 891-U846.
Musacchio, A. and E. D. Salmon (2007). "The spindle-assembly checkpoint in space and time." Nature Reviews Molecular Cell Biology **8**(5): 379-393.
Nag, S., J. Qin, K. S. Srivenugopal, M. Wang and R. Zhang (2013). "The MDM2-p53 pathway revisited." J Biomed Res **27**(4): 254-271.
Naim, V., T. Wilhelm, M. Debatisse and F. Rosselli (2013). "ERCC1 and MUS81-EME1 promote sister chromatid separation by processing late replication intermediates at common fragile sites during mitosis." Nature Cell Biology **15**(8): 1008-U1270.
Nakayama, N., G. Sakashita, T. Nagata, N. Kobayashi, H. Yoshida, S. Y. Park, Y. Nariai, H. Kato, E. Obayashi, K. Nakayama, S. Kyo and T. Urano (2020). "Nucleus Accumbens-Associated Protein 1 Binds DNA Directly through the BEN Domain in a Sequence-Specific Manner." Biomedicines **8**(12).
Nakka, K. K. and S. Chattopadhyay (2010). "Modulation of chromatin by MARs and MAR binding oncogenic transcription factor SMAR1." Mol Cell Biochem **336**(1-2): 75-84.
Nakka, K. K., N. Chaudhary, S. Joshi, J. Bhat, K. Singh, S. Chatterjee, R. Malhotra, A. De, M. K. Santra, F. J. Dilworth and S. Chattopadhyay (2015). "Nuclear matrix-associated protein SMAR1 regulates alternative splicing via HDAC6-mediated deacetylation of Sam68." Proc Natl Acad Sci U S A **112**(26): E3374-3383.
Neumann, C. J. and C. Nuesslein-Volhard (2000). "Patterning of the zebrafish retina by a wave of sonic hedgehog activity." Science **289**(5487): 2137-2139.
O'Connell, M. J., J. M. Raleigh, H. M. Verkade and P. Nurse (1997). "Chk1 is a wee1 kinase in the G2 DNA damage checkpoint inhibiting cdc2 by Y15 phosphorylation." EMBO J **16**(3): 545-554.
Oren, M. (1999). "Regulation of the p53 tumor suppressor protein." J Biol Chem **274**(51): 36031-36034.
Park, H. C., S. K. Hong, H. S. Kim, S. H. Kim, E. J. Yoon, C. H. Kim, N. Miki and T. L. Huh (2000). "Structural comparison of zebrafish elav/Hu and their differential expressions during neurogenesis." Neuroscience Letters **279**(2): 81-84.
Paul, D., S. Ghorai, U. S. Dinesh, P. Shetty, S. Chattopadhyay and M. K. Santra (2017). "Cdc20 directs proteasome-mediated degradation of the tumor suppressor SMAR1 in higher grades of cancer through the anaphase promoting complex." Cell Death Dis **8**(6): e2882.
Pavithra, L., S. Mukherjee, K. Sreenath, S. Kar, K. Sakaguchi, S. Roy and S. Chattopadhyay (2009). "SMAR1 forms a ternary complex with p53-MDM2 and negatively regulates p53-mediated transcription." J Mol Biol **388**(4): 691-702.
Pavithra, L., S. Rampalli, S. Sinha, K. Sreenath, R. G. Pestell and S. Chattopadhyay (2007). "Stabilization of SMAR1 mRNA by PGA2 involves a stem loop structure in the 5' UTR." Nucleic Acids Res **35**(18): 6004-6016.

Pavithra, L., S. Singh, K. Sreenath and S. Chattopadhyay (2009). "Tumor suppressor SMAR1 downregulates Cytokeratin 8 expression by displacing p53 from its cognate site." Int J Biochem Cell Biol **41**(4): 862-871.
Pease, J. C. and J. S. Tirnauer (2011). "Mitotic spindle misorientation in cancer - out of alignment and into the fire." Journal of Cell Science **124**(7): 1007-1016.
Pedersen, R. S., G. Karemore, T. Gudjonsson, M. B. Rask, B. Neumann, J. K. Heriche, R. Pepperkok, J. Ellenberg, D. W. Gerlich, J. Lukas and C. Lukas (2016). "Profiling DNA damage response following mitotic perturbations." Nature Communications **7**.
Rampalli, S., L. Pavithra, A. Bhatt, T. K. Kundu and S. Chattopadhyay (2005). "Tumor suppressor SMAR1 mediates cyclin D1 repression by recruitment of the SIN3/histone deacetylase 1 complex." Mol Cell Biol **25**(19): 8415-8429.
Riley, T., E. Sontag, P. Chen and A. Levine (2008). "Transcriptional control of human p53-regulated genes." Nat Rev Mol Cell Biol **9**(5): 402-412.
Rivlin, N., R. Brosh, M. Oren and V. Rotter (2011). "Mutations in the p53 Tumor Suppressor Gene: Important Milestones at the Various Steps of Tumorigenesis." Genes Cancer **2**(4): 466-474.
Robinson, M. D. and A. Oshlack (2010). "A scaling normalization method for differential expression analysis of RNA-seq data." Genome Biology **11**(3).
Rodrigues, P. M., P. Grigaravicius, M. Remus, G. R. Cavalheiro, A. L. Gomes, M. Rocha-Martins, L. Frappart, D. Reuss, P. J. McKinnon, A. von Deimling, R. A. Martins and P. O. Frappart (2013). "Nbn and atm cooperate in a tissue and developmental stage-specific manner to prevent double strand breaks and apoptosis in developing brain and eye." PLoS One **8**(7): e69209.
Rodriguez-Mari, A. and J. H. Postlethwait (2011). "The role of Fanconi anemia/BRCA genes in zebrafish sex determination." Methods Cell Biol **105**: 461-490.
Rogakou, E. P., D. R. Pilch, A. H. Orr, V. S. Ivanova and W. M. Bonner (1998). "DNA double-stranded breaks induce histone H2AX phosphorylation on serine 139." Journal of Biological Chemistry **273**(10): 5858-5868.
Sahin, U., V. Lallemand-Breitenbach and H. de The (2014). "PML nuclear bodies: regulation, function and therapeutic perspectives." J Pathol **234**(3): 289-291.
Sandelin, A., P. Carninci, B. Lenhard, J. Ponjavic, Y. Hayashizaki and D. A. Hume (2007). "Mammalian RNA polymerase II core promoters: insights from genome-wide studies." Nature Reviews Genetics **8**(6): 424-436.
Santaguida, S. and A. Musacchio (2009). "The life and miracles of kinetochores." Embo Journal **28**(17): 2511-2531.
Sasagawa, S., Y. Nishimura, T. Kon, Y. Yamanaka, S. Murakami, Y. Ashikawa, M. Yuge, S. Okabe, K. Kawaguchi, R. Kawase and T. Tanaka (2016). "DNA Damage Response Is Involved in the Developmental Toxicity of Mebendazole in Zebrafish Retina." Front Pharmacol **7**: 57.
Scheuermann, R. H. and W. T. Garrard (1999). "MARs of antigen receptor and co-receptor genes." Critical Reviews in Eukaryotic Gene Expression **9**(3-4): 295-310.
Schuler, M. and D. R. Green (2001). "Mechanisms of p53-dependent apoptosis." Biochem Soc Trans **29**(Pt 6): 684-688.
Schultz-Rogers, L. E., M. P. Almeida, W. A. Wierson, M. Kool and M. McGrail (2018). "Retinoblastoma binding protein 4 maintains cycling neural stem cells and prevents DNA damage and Tp53-dependent apoptosis in rb1 mutant neural progenitors." bioRxiv: 427344.

Seipold, S., F. C. Priller, P. Goldsmith, W. A. Harris, H. Baier and S. Abdelilah-Seyfried (2009). "Non-SMC condensin I complex proteins control chromosome segregation and survival of proliferating cells in the zebrafish neural retina." BMC Dev Biol **9**: 40.
Shen, Y. and E. White (2001). "p53-dependent apoptosis pathways." Adv Cancer Res **82**: 55-84.
Shiloh, Y. (2003). "ATM and related protein kinases: safeguarding genome integrity." Nat Rev Cancer **3**(3): 155-168.
Siefert, J. C., E. A. Clowdus and C. L. Sansam (2015). "Cell cycle control in the early embryonic development of aquatic animal species." Comp Biochem Physiol C Toxicol Pharmacol **178**: 8-15.
Singh, K., D. Mogare, R. O. Giridharagopalan, R. Gogiraju, G. Pande and S. Chattopadhyay (2007). "p53 target gene SMAR1 is dysregulated in breast cancer: its role in cancer cell migration and invasion." PLoS One **2**(7): e660.
Singh, K., S. Sinha, S. K. Malonia, P. Bist, V. Tergaonkar and S. Chattopadhyay (2009). "Tumor suppressor SMAR1 represses IkappaBalpha expression and inhibits p65 transactivation through matrix attachment regions." J Biol Chem **284**(2): 1267-1278.
Singh, K., S. Sinha, S. K. Malonia and S. Chattopadhyay (2010). "Tumor Necrosis Factor alpha (TNFalpha) regulates CD40 expression through SMAR1 phosphorylation." Biochem Biophys Res Commun **391**(2): 1255-1261.
Singh, S., V. Raina, P. L. Chavali, T. Dubash, S. Kadreppa, P. Parab and S. Chattopadhyay (2012). "Regulation of GAD65 expression by SMAR1 and p53 upon Streptozotocin treatment." BMC Mol Biol **13**: 28.
Sinha, S., S. K. Malonia, S. P. Mittal, J. Mathai, J. K. Pal and S. Chattopadhyay (2012). "Chromatin remodelling protein SMAR1 inhibits p53 dependent transactivation by regulating acetyl transferase p300." Int J Biochem Cell Biol **44**(1): 46-52.
Sinha, S., S. K. Malonia, S. P. Mittal, K. Singh, S. Kadreppa, R. Kamat, R. Mukhopadhyaya, J. K. Pal and S. Chattopadhyay (2010). "Coordinated regulation of p53 apoptotic targets BAX and PUMA by SMAR1 through an identical MAR element." EMBO J **29**(4): 830-842.
Skibbens, R. V. (2019). "Condensins and cohesins - one of these things is not like the other!" J Cell Sci **132**(3).
Socha, A., D. Yang, A. Bulsiewicz, K. Yaprianto, M. Kupculak, C. C. Liang, A. Hadjicharalambous, R. H. Wu, S. P. Gygi and M. A. Cohn (2020). "WRNIP1 Is Recruited to DNA Interstrand Crosslinks and Promotes Repair." Cell Reports **32**(1).
Sorrells, S., C. Toruno, R. A. Stewart and C. Jette (2013). "Analysis of Apoptosis in Zebrafish Embryos by Whole-mount Immunofluorescence to Detect Activated Caspase 3." Jove-Journal of Visualized Experiments(82).
Sreenath, K., L. Pavithra, S. Singh, S. Sinha, P. K. Dash, N. B. Siddappa, U. Ranga, D. Mitra and S. Chattopadhyay (2010). "Nuclear matrix protein SMAR1 represses HIV-1 LTR mediated transcription through chromatin remodeling." Virology **400**(1): 76-85.
Stallings, R. L. (2007). "Are chromosomal imbalances important in cancer?" Trends in Genetics **23**(6): 278-283.
Stark, R. and G. Brown (2021). "DiffBind: Differential binding analysis of ChIP- Seq peak data."
Stiff, T., T. C. Tena, M. O'Driscoll, P. A. Jeggo and M. Philipp (2016). "ATR promotes cilia signalling: links to developmental impacts." Human Molecular Genetics **25**(8): 1574-1587.
Surova, O. and B. Zhivotovsky (2013). "Various modes of cell death induced by DNA damage." Oncogene **32**(33): 3789-3797.

Swanson, K. D., E. Lok and E. T. Wong (2016). "An Overview of Alternating Electric Fields Therapy (NovoTTF Therapy) for the Treatment of Malignant Glioma." Curr Neurol Neurosci Rep **16**(1): 8.
Sykes, S. M., T. J. Stanek, A. Frank, M. E. Murphy and S. B. McMahon (2009). "Acetylation of the DNA binding domain regulates transcription-independent apoptosis by p53." J Biol Chem **284**(30): 20197-20205.
Tang, Y., J. Luo, W. Zhang and W. Gu (2006). "Tip60-dependent acetylation of p53 modulates the decision between cell-cycle arrest and apoptosis." Mol Cell **24**(6): 827-839.
Tao, T., H. Shi, Y. H. Guan, D. L. Huang, Y. Chen, D. P. Lane, J. Chen and J. R. Peng (2013). "Def defines a conserved nucleolar pathway that leads p53 to proteasome-independent degradation." Cell Research **23**(5): 620-634.
Tay, I. J. J. (2018). A Novel DNA Damage Quantification Platform Enables High Throughput Screening for Genes that Impact DNA Double Strand Breaks. Doctor of Philosophy, MASSACHUSETTS INSTITUTE OF TECHNOLOGY.
Taye, N., A. Alam, S. Ghorai, D. G. Chatterji, A. Parulekar, D. Mogare, S. Singh, P. Sengupta, S. Chatterjee, M. K. Bhat, M. K. Santra, P. B. Salunkhe, S. K. Finston and S. Chattopadhyay (2018). "SMAR1 inhibits Wnt/beta-catenin signaling and prevents colorectal cancer progression." Oncotarget **9**(30): 21322-21336.
Thompson, L. H. and D. Schild (2002). "Recombinational DNA repair and human disease." Mutat Res **509**(1-2): 49-78.
Thompson, R., R. Gatenby and S. Sidi (2019). "How Cells Handle DNA Breaks during Mitosis: Detection, Signaling, Repair, and Fate Choice." Cells **8**(9).
Tsuda, H., D. F. Callen, T. Fukutomi, Y. Nakamura and S. Hirohashi (1994). "Allele loss on chromosome 16q24.2-qter occurs frequently in breast cancers irrespectively of differences in phenotype and extent of spread." Cancer Res **54**(2): 513-517.
Wang, T., K. Birsoy, N. W. Hughes, K. M. Krupczak, Y. Post, J. J. Wei, E. S. Lander and D. M. Sabatini (2015). "Identification and characterization of essential genes in the human genome." Science **350**(6264): 1096-1101.
Wang, X., L. Gleich, Z. P. Pavelic, Y. Q. Li, N. Gale, S. Hunt, J. L. Gluckman and P. J. Stambrook (1999). "Cervical metastases of head and neck squamous cell carcinoma correlate with loss of heterozygosity on chromosome 16q." Int J Oncol **14**(3): 557-561.
Weber, I. P., A. P. Ramos, P. J. Strzyz, L. C. Leung, S. Young and C. Norden (2014). "Mitotic Position and Morphology of Committed Precursor Cells in the Zebrafish Retina Adapt to Architectural Changes upon Tissue Maturation." Cell Reports **7**(2): 386-397.
Westerfield, M. (1993). The zebrafish book : a guide for the laboratory use of zebrafish (Brachydanio rerio).
Wilkins, B. J., K. Lorent, R. P. Matthews and M. Pack (2013). "p53-Mediated Biliary Defects Caused by Knockdown of cirh1a, the Zebrafish Homolog of the Gene Responsible for North American Indian Childhood Cirrhosis." Plos One **8**(10).
Williams, R. M. and X. Zhang (2021). "Roles of ATM and ATR in DNA double strand breaks and replication stress." Prog Biophys Mol Biol **161**: 27-38.
Wyrwicz, L. S., P. Gaj, M. Hoffmann, L. Rychlewski and J. Ostrowski (2007). "A common cis-element in promoters of protein synthesis and cell cycle genes." Acta Biochimica Polonica **54**(1): 89-98.
Xu, B. J., X. Tang, M. M. Jin, H. Zhang, L. Du, S. G. Yu and J. He (2020). "Unifying developmental programs for embryonic and postembryonic neurogenesis in the zebrafish retina." Development **147**(12).

Xu, H., T. Liu, W. Li and Q. Yao (2021). "SMAR1 attenuates the stemness of osteosarcoma cells via through suppressing ABCG2 transcriptional activity." Environ Toxicol **36**(6): 1090-1098.
Xu, Q., N. Holder, R. Patient and S. W. Wilson (1994). "Spatially regulated expression of three receptor tyrosine kinase genes during gastrulation in the zebrafish." Development **120**(2): 287-299.
Yamaguchi, M., N. Fujimori-Tonou, Y. Yoshimura, T. Kishi, H. Okamoto and I. Masai (2008). "Mutation of DNA primase causes extensive apoptosis of retinal neurons through the activation of DNA damage checkpoint and tumor suppressor p53." Development **135**(7): 1247-1257.
Yamaguchi, M., N. Tonou-Fujimori, A. Komori, R. Maeda, Y. Nojima, H. Li, H. Okamoto and I. Masai (2005). "Histone deacetylase 1 regulates retinal neurogenesis in zebrafish by suppressing Wnt and Notch signaling pathways." Development **132**(13): 3027-3043.
Yan, F., D. R. Powell, D. J. Curtis and N. C. Wong (2020). "From reads to insight: a hitchhiker's guide to ATAC-seq data analysis." Genome Biology **21**(1).
Yanagida, M. (2005). "Basic mechanism of eukaryotic chromosome segregation." Philos Trans R Soc Lond B Biol Sci **360**(1455): 609-621.
Ye, S. F., T. Zhao, W. Zhang, Z. M. Tang, C. Gao, Z. P. Ma, J. W. Xiong, J. R. Peng, W. Q. Tan and J. Chen (2020). "p53 isoform Delta 113p53 promotes zebrafish heart regeneration by maintaining redox homeostasis." Cell Death & Disease **11**(7).
Yu, J. and L. Zhang (2005). "The transcriptional targets of p53 in apoptosis control." Biochemical and Biophysical Research Communications **331**(3): 851-858.
Zhang, Q., R. Su, C. Shan, C. Gao and P. Wu (2018). "Non-SMC Condensin I Complex, Subunit G (NCAPG) is a Novel Mitotic Gene Required for Hepatocellular Cancer Cell Proliferation and Migration." Oncol Res **26**(2): 269-276.
Zhao, T., S. Ye, Z. Tang, L. Guo, Z. Ma, Y. Zhang, C. Yang, J. Peng and J. Chen (2021). "Loss-of-function of p53 isoform Delta113p53 accelerates brain aging in zebrafish." Cell Death Dis **12**(2): 151.
Zhou, T., J. W. Chou, D. A. Simpson, Y. Zhou, T. E. Mullen, M. Medeiros, P. R. Bushel, R. S. Paules, X. Yang, P. Hurban, E. K. Lobenhofer and W. K. Kaufmann (2006). "Profiles of global gene expression in ionizing-radiation-damaged human diploid fibroblasts reveal synchronization behind the G1 checkpoint in a G0-like state of quiescence." Environ Health Perspect **114**(4): 553-559.